AIX-MARSEILLE UNIVERSITÉ
Faculté des Sciences de Luminy
Ecole doctorale des Sciences de la Vie et de la Santé

THESE DE DOCTORAT
Biologie spécialité immunologie

En vue d'obtenir le titre de
DOCTEUR DE L'UNIVERSITÉ D'AIX-MARSEILLE

Présentée et soutenue publiquement par

Cynthia Arroyo Portilla

18 Juin 2021

Phagocyte activation processes in Peyer's patches and development of a strategy to analyse the gut microbiota

Co-directeurs de thèse: Dr. Hugues Lelouard
Dr. Jean-Pierre Gorvel

Thèse soutenue devant le jury compose de:

Professeur	Frank Galland	Président	CIML, Marseille
Docteur	Corinne Grangette	Rapportrice	CIIL, Lille
Docteur	Fabienne Anjuère	Rapportrice	IPMC, Nice
Docteur	Hugues Lelouard	Co-directeur de thèse	CIML, Marseille
Docteur	Jean-Pierre Gorvel	Co-directeur de thèse	CIML, Marseille
Docteur	Tewfik Miloud	Examinateur	Beckman Coulter, Marseille

Thèse effectuée au Centre d'Immunologie de Marseille-Luminy, Aix-Marseille Université UM2, INSERM UMR S1104, CNRS UMR 7280

Table of contents

Acknowledgements

First, I would like to thank the Jury members for taking the time to evaluate my work. Also a special recognition to our collaborators in Beckman Coulter, Tewfik and Raphaelle, and in CSUR-IHU for their support.

I want to thank the Universidad de Costa Rica and all my colleagues for the trust they have placed in me by giving me the opportunity to pursue this doctorate. It will be an honor for me to be part of this excellent academic community; I will do my best to keep up with them.

Jean Pierre, thank you for lend me a hand in a time of need by opening the doors of your lab. For all the advices and your unvarnished honesty. You taught me a huge life lesson: “A veces hay que jugar a la ruleta rusa” jugué y sobreviví, gracias ;)

Hugues, thank you for letting me be part of your team, a group with a high scientific level but also with a big human side. For sharing your microscopy wisdom and for all the “pattes” processing, we manage always to have happy chimeras. And of course, thank you for all your work and corrections.

My godfather Rémi, thanks for all your advices. I know that at the end, I was very elusive but I always knew that you were there for me.

LysoDC team, the best team ever!! Not only a hard working one, but also the funniest and coolest. Thanks for all the philosophic, artistic, etymologic and, of course, scientific discussions. Also, for all the chocolate we shared. For teaching me all the protocols and after helping me with my huge and endless experiments, not without dancing and laughing. However, your help did not stop there, you helped me also to be a more diplomatic person and you always supported me when I was “au bout de ma vie”. Merci infiniment et muchas gracias muchachas.

Sylvie, thank you for showing me that passion for science can survive anything, you are really an example of resilience. For all the good advices for my projects, all the French cuisine experiences and your constant support.

JPG lab present and past members: thanks for your help (Stéphane, even during your holidays), council and for the great lab ambiance. It was always a pleasure to work with you. We enjoy endless “dégustations”, birthdays and Friday breakfasts (even if I was always late). I also want to apologize for being the trash/recycling police, but I know that some of you already think twice before using or trashing something, for me my most valuable legacy.

Thanks to all the CIML-platforms for their work and help. A special mention to Virginie for taking care of the mice (on a réussi a pas perdre les OTII), Romain for all his work with the single-cell analysis and Lionel for the cryostat cuts but specially for your positive energy.

In almost five years that I spend at the CIML, I encountered many nice people, it will be impossible for me to depict all the good moments we lived. Since day one I was very lucky to be in the same office with Clara, Le and Xing; my very first friends here in Marseille. I worked also with wonderful people: Momette (ma prof de raclette), Bubu (merci pour ta gentillesse), Ghita (compañera de

desaventuras) and Marcello (thanks for your friendly perseverance and for not giving up on me). I had also great conversations during the Friday night's scientific meetings; especially with Sethu, Daiki, Honza (always a fan of your shirts) and Marine (ma binôme pour tartiner le foie gras). A special thanks for Lisiena (my swimming partner) for all the social activities that the whole CIML enjoyed at your place.

A mi pequeña burbuja epidemiológica latinoamericana: (no podía faltar una alusión al Covid-19 en mi tesis) muchas gracias por las comilonas, bailadas, cantadas, noches de videos y juegos. Con ustedes reí hasta más no poder, pero más importante aún me sentí acompañada y apoyada.

Teresa et Mag, vous avez donné une touche d'art et de musique à ma vie. En plus vous m'avez gâté tout le temps avec une gastronomie des dieux, surtout à Noël (les dîners les plus longs de ma vie). Mais je vous remercie surtout pour votre compagnie et votre amitié.

Kiki, you were and are always there supporting me and advising me to think of myself first. We had so many adventures together and the best part is that they will continue, love you x3

María, Juan José y Mónica primero agradecerles por fiarse de mí, también agradecerles por el apoyo y el cariño incondicional. María mi confidente, gracias por todas las llamadas a media madrugada y por todos los regalos de cumpleaños que, junto con Andrés, me hicieron llegar (siempre llenaron mi corazoncito de ilusión). Andrés, gracias también por nuestras discusiones trascendentales sobre el séptimo arte e incluso por la colaboración gráfica incluida en esta tesis. Max, mi corazón, mi visitante asiduo, cada visita fue una maravillosa aventura. Manuel mi fuente de inspiración en los momentos más duros, lo admiro demasiado y lo quiero aún más. Carito, ya más de 30 años de amistad no hay mucho más que agregar, gracias por las perennes llamadas telefónicas y sueños compartidos.

A ma famille marseillaise, les mots ne seront jamais suffisants pour vous exprimer toute ma gratitude. Vous avez ouvert la porte de votre maison à une personne que vous ne connaissiez même pas et sans demander rien en retour. Michel, avec toi j'ai eu toujours des excellentes conversations politiques, économiques et anthropologiques mais surtout sur les chats et accompagnées toujours avec des superbes jeux de mots ; bien sûr avec un verre de vin à la main. Françoise « mi mamá marseillaise », dès le premier jour tu as veillé tout le temps sur moi. Tu m'as fait connaitre la culture française surtout provençale, on n'a pas mal visité ensemble et tu m'as toujours gâté avec les meilleurs repas. Tu es tout le temps en train d'aider les gens, n'importe qui et n'importe quand, pour moi tu es un exemple d'altruisme à suivre. En fin avec vous j'ai toujours bien rigolé et surtout vous m'avez fait grandir énormément en tant que personne. Un grand merci aussi au reste de la famille et aux amis, avec qui j'ai partagé des précieux moments. Je me suis toujours senti accueillie et aimée, pour cela vous serez toujours dans mon cœur.

Finalmente quiero agradecer a mi mami, no hubo un solo día sin al menos un mensaje de buenos días o buenas noches, me acompañaste cada día y en cada momento. A los pocos meses de estar acá vinieron, Lolo y vos, a ayudarme a instalarme como se debe en mi apartamento, reparación de horno incluida. Junto con Laura, Manuel y Daniel siempre estuvieron ahí para ayudarme con cada problema de jardinería, cocina, electrónico, de construcción y sobre todo informático. Esta experiencia me hizo independiente (más de lo que hubiera imaginado) pero me hizo comprender también que la independencia no vale de nada si no puedo compartirla con ustedes. Mi familia, todo lo que soy es gracias a ustedes, los amo con todo mi ser.

Abbreviations

AID: activation-induced cytidine deaminase

AMPs: antimicrobial peptides

BAFF: B-cell activating factor

BCR: B cell receptor

BM: bone marrow

CCR7: C-C chemokine receptor type 7

cDC: conventional dendritic cells

CDP: common dendritic cell precursor

Clec9a: C-type lectin domain family 9 member A

CSR: class switch recombination

CTL: cytotoxic T lymphocyte

CTLA-4: cytotoxic T-lymphocyte antigen 4

CV: coefficients of variation

DAV: dome-associated villus

DC: dendritic cells

DN: doble negative cDC2

DT: diphtheria toxin

DZ: dark zone

EpCAM: epithelial cell adhesion molecule

FAE: follicle-associated epithelium

FDC: follicular dendritic cells

FISH: fluorescence *in situ* hybridization

GALT: gut-associated lymphoid tissues

GC: germinal centers

HEV: high endothelial venules

IEL: intraepithelial lymphocyte

IFN: interferon

IFR: interfollicular region

ILC: innate lymphoid cells

ILF: isolated lymphoid follicles

JAM-A: junctional adhesion molecule-A

LN: lymph nodes

LP: lamina propria

LZ: light zone

MCM: M cell-derived microvesicles

MHC: major histocompatibility complex

MLN: mesenteric lymph nodes

MPS: mononuclear phagocyte system

Mϕ: macrophages

OTU: operational taxonomic units

pDC: plasmacytoid dendritic cells

PP: Peyer's patches

PRRs: pattern recognition receptor

RA: retinoic acid

SCFA: short-chain fatty acids

SED: subepithelial dome

SFB: segmented filamentous bacteria

SHM: somatic hypermutation

sIgA: secretory IgA

SILT: solitary intestinal lymphoid tissues

SIRPα: signal regulatory protein α

TBM: tingible-body macrophages

TCR: T-cell receptor

TD: T-dependent activation pathway

TFH: T follicular helper cells

TFR: T follicular regulatory cells

TGFβ: transforming growth factor beta

TI: T-independent activation pathway

TIM-4: T-cell immunoglobulin- and mucin-domain-containing molecule

TLR: Toll-like receptor

TMD: trans-M cell dendrites

TNF: tumor necrosis factor

Treg: regulatory T cells

XCR1: X-C motif chemokine receptor 1

Thesis project abstract

Phagocyte activation processes in Peyer's patches and development of a strategy to analyse the gut microbiota

Among secondary lymphoid organs, Peyer's patches (PP) have the unique property to combine both antigen sampling and adaptive immune initiation sites. PP phagocytes comprise conventional dendritic cells (cDC) and lysozyme expressing monocyte-derived cells. The latter include dendritic cells (DC) called LysoDC and macrophages termed LysoMac. We deciphered the transcriptional and spatiotemporal landscape of all PP phagocyte populations from their arrival in the tissue to their final maturation state at homeostasis and then compared it with two types of *in vivo* activation, involving the endosomal Toll-like receptors (TLR) 7 and 9. Use of specific agonists helped us to better understand the role of the different phagocytes in the initiation of the immune response. Furthermore, given that PP interfollicular region hosts both villus and subepithelial dome emigrated cDC, we studied their activation profile and showed that the initial residence site shapes their activation profile. These activation profiles were associated with a B and regulatory T cell response upon TLR7 stimulation whereas a strong CD8+ T cell response was elicited upon TLR9 stimulation. Altogether, our study underscores the importance of targeting not only the right phagocyte subset but also the right place at the right time with the right stimulus.

The microbiota is crucial for the development and homeostasis of the mucosal immune system. Furthermore, variations in the composition of the gut microbiota between and within individuals over time are associated with a range of health conditions. We designed a FISH-Flow multiparametric panel including nine specific probes that target the main phyla of the gut: Firmicutes, Bacteroidetes, Proteobacteria, Actinobacteria, and Verrucomicrobia. Once all the different conditions were standardized, we tested our panel in mouse fecal samples including vancomycin-treated animals. As expected, a majority of the fecal bacteria of non-treated mice belonged to Firmicutes and Bacteroidetes, whereas a decrease of both phyla and an important increase of Verrucomicrobia was observed after the antibiotic treatment. This method allowed us to know the fecal composition in a fast, semi-quantitative and cost-effective way. Therefore, it can be very useful to detect a microbiota dysregulation and potentially predict the development of non-communicable diseases.

Resumen del proyecto de tesis

Proceso de activación de fagocitos en las placas de Peyer y desarrollo de una estrategia para analizar la microbiota intestinal

Entre los órganos linfoides secundarios, las placas de Peyer (PP) tienen la peculiaridad de combinar al mismo tiempo el muestreo de antígenos y la inducción de la respuesta inmune adaptativa. Los fagocitos de las PP incluyen a las células dendríticas convencionales (cDC) y a las células derivadas de monocitos que expresan lisozima. Estas últimas comprenden a las células dendríticas (CD) llamadas LysoDC y a los macrófagos llamados LysoMac. En este trabajo, desciframos los perfiles transcripcionales y distribución espacio-temporal de todas las poblaciones de fagocitos de las PP desde el momento de su llegada al tejido hasta su estado final de madurez, durante la homeostasia. Luego los comparamos con dos tipos de activación *in vivo*, involucrando los receptores endosomales tipo-Toll (TLR) 7 y 9. La utilización de estos agonistas específicos nos permitió comprender el rol de los diferentes fagocitos en la inducción de la respuesta inmune. Además, dado que la región interfolicular de las PP hospeda a la vez cDC provenientes de las vellosidades y de los domos sub-epiteliales, estudiamos su perfil de activación y demostramos que el sitio de residencia inicial define su perfil de activación. Estos perfiles de activación se asociaron a una respuesta de linfocitos B y T reguladores luego de una estimulación del TLR7, mientras que una fuerte respuesta de linfocitos T $CD8^+$ es desencadenada luego de una estimulación del TLR9. En términos generales, nuestro estudio no solo resalta la importancia de dirigirse a la población apropiada de fagocitos sino también el momento y lugar correctos en combinación con el estímulo adecuado.

Por otro lado, la microbiota es crucial para el desarrollo y la homeostasia del sistema inmune de las mucosas. Variaciones en la composición de la microbiota intestinal entre individuos y dentro de un individuo a lo largo del tiempo se han asociado frecuentemente a diferentes problemas de salud. Diseñamos un panel multiparamétrico de FISH-Flow que incluye nueve sondas específicas que reconocen los principales filos presentes en el intestino: Firrmicutes, Bacteroidetes, Proteobacteria, Actinobacteria y Verrucomicrobia. Una vez estandarizadas las diferentes condiciones, pusimos a prueba nuestro panel con muestras fecales de ratón incluyendo individuos tratados con vancomicina. De acuerdo a lo esperado, la mayoría de las bacterias fecales de ratones no tratados pertenecieron a Firmicutes y Bacteroidetes, mientras que una disminución de ambos filos junto con un aumento significativo de Verrucomicrobia fueron observados tras el tratamiento antibiótico. Este método nos permitió conocer la composición bacteriana fecal de forma rápida, semi-cuantitativa y rentable; por lo que podría ser útil para predecir el desarrollo de enfermedades no transmisibles.

Résumé du projet de thèse

Processus d'activation des phagocytes des plaques de Peyer et élaboration d'une stratégie d'analyse du microbiote intestinal

Parmi les organes lymphoïdes secondaires, les plaques de Peyer (PP) ont la propriété unique de combiner à la fois l'échantillonnage d'antigènes et l'initiation de l'immunité adaptative. Les phagocytes des PP comprennent des cellules dendritiques conventionnelles (cDC) et des cellules dérivées de monocytes exprimant le lysozyme. Ces dernières comprennent des cellules dendritiques (CD) appelées LysoDC et des macrophages appelés LysoMac. Nous avons analysé les paysages transcriptionnel et spatio-temporel de toutes les populations de phagocytes des PP depuis leur arrivée dans le tissu jusqu'à leur état final de maturation à l'homéostasie, puis nous l'avons comparé à deux types d'activation in vivo, impliquant les récepteurs endosomiaux Toll-like (TLR) 7 et 9. L'utilisation d'agonistes spécifiques nous a permis de mieux comprendre le rôle des différents phagocytes dans l'initiation de la réponse immunitaire. De plus, étant donné que la région interfolliculaire des PP accueille à la fois des cDC émigrées des villosités et des dômes sous-épithéliaux, nous avons étudié leur profil d'activation et montré que le site de résidence initial façonne leur profil d'activation. Ces profils d'activation ont été associés à une réponse des lymphocytes B et T régulateurs lors de la stimulation par TLR7, tandis qu'une forte réponse des lymphocytes T CD8+ est déclenchée lors de la stimulation par TLR9. Dans l'ensemble, notre étude souligne l'importance de cibler non seulement la population de phagocytes adéquate mais aussi le bon endroit au bon moment avec le bon stimulus.

Le microbiote est crucial pour le développement et l'homéostasie du système immunitaire des muqueuses. En outre, les variations de la composition du microbiote intestinal entre les individus et au sein d'un même individu au fil du temps peuvent fréquemment être associées à des problèmes de santé. Nous avons conçu un panel de neuf sondes FISH pour la cytométrie qui ciblent spécifiquement les principaux phyla de l'intestin : Firmicutes, Bacteroidetes, Proteobacteria, Actinobacteria, et Verrucomicrobia. Une fois les différentes conditions standardisées, nous avons testé notre panel sur des échantillons fécaux de souris, dont certaines avaient été traitées avec l'antibiotique vancomycine. Comme prévu, la majorité des bactéries fécales des souris non traitées appartiennent aux Firmicutes et aux Bacteroidetes, alors qu'une diminution de ces deux phyla et une augmentation importante des Verrucomicrobia sont observées après le traitement antibiotique. Cette méthode nous a permis de connaître la composition fécale d'une manière rapide, semi-quantitative et économique. Elle peut donc être très utile pour détecter un dérèglement du microbiote et potentiellement prédire le développement de maladies non transmissibles.

INTRODUCTION

All living organisms on Earth are part of the biosphere, which is composed by different ecosystems. An ecosystem is considered as a community of living organisms in conjunction with their environment. The microorganisms that live in close association with plants and animals, form a community known as microbiota. In order to stay alive, both plants and animals, need to be able to metabolize compounds into energy, and to adapt in response to external changes. For this purpose, the exchange with the environment requires to be ensured but in a regulated and supervised manner. The barriers between the organism and its surroundings should be permeable but selective aiming to avoid the entrance of any potential pathogens. One example of these barriers is the mucosa that outlines body cavities in contact with the exterior. The mucosal immune system is then in charge of monitoring exchanges with the external environment and fight pathogens.

A-The intestinal immune system

A-I/ Introduction

A superficial layer of epithelial cells and a deeper layer of connective tissue called lamina propria (LP) composes the mucous membrane or mucosa. The term mucosa comes from the fact that the major substance secreted from this tissue is mucus. The mucosal surfaces are portals of entry present in the respiratory, middle ear, digestive, and urogenital tracts. They are surrounded mainly by the resident microbiota, antigens of food origin (gastrointestinal tract) or from inhaled air (airways) and xenobiotics. They prevent potential pathogens and non-desirable compounds from entering while allowing exchange and keeping underlying tissue moist.

The mucosal surface forms a physical barrier that constitutes the first line of defense of the body. The constant presence of environmental antigens results in the strategic distribution of numerous immune cells throughout the mucosa. The mucosal immune system forms the largest part of immune tissues, containing approximately three-quarters of all lymphocytes and producing the majority of immunoglobulins in healthy individuals. Moreover, myeloid cells of the mucosal immune system display the greater phenotypic and functional heterogeneity in the body (Russell *et al.*, 2015).

From an evolution point of view, the gut mucosal immune system may represent the origin of the vertebrate immune system. The hypothesis of a common origin for immunity and digestion is mainly based on the existence of shared components such as enzymes, receptors, signaling pathways and cellular processes. Thus, many of the enzymes involved in immunity play also a role in digestion (e.g., lysozymes and proteases), with specific contexts for which these functions cannot be distinguished, e.g., for animals that capture and feed on bacteria. Phagocytosis extended from the nutritional function into key roles in homeostasis, such as apoptotic cell removal, tissue remodeling and immune defense. The intestine has the only lymph producing tissue common to all forms of triploblastic animals. In addition, organized lymphoid tissues are first found in the gut of primitive cartilaginous fishes (Arroyo Portilla *et al*., 2021; Annex 1). Furthermore, two important central lymphoid organs derive from the embryonic intestine: the thymus and the avian bursa of Fabricius.

The intestinal immune system has evolved to discern between harmful pathogens and innocuous antigens, eliciting a meticulously regulated immune response. Thus, an active immune response against innocuous agents would be inappropriate and harmful. Indeed, dysfunctions, such as hypersensitivity responses against the wheat protein gluten or commensal bacteria, cause severe diseases, such as celiac disease and Crohn's disease, respectively (Sartor and Wu, 2017; Lebwohl *et al*., 2018). Therefore, the usual response to harmless gut antigens is the induction of local and systemic immunological tolerance, known as oral tolerance (Mowat and Agace, 2014; Anagnostou and Clark, 2016). The intestinal mucosal immune system has a pivotal role in host protection while preserving good neighborhood with a diversified microbiota. Indeed, the number of bacteria living in the human body is of the same order as the number of human cells. An estimate of 10^{13} -10^{14} bacteria was calculated per person, among which the vast majority reside in the colon (Sender *et al*., 2016). In addition, the human gastrointestinal tract represents one of the largest interfaces between the host and the microbiota. In consequence, the "gut microbiota" has been deeply studied in the last decades. The gut microbiota has co-evolved with the host over thousand years to form a symbiotic relationship through their crucial contribution to nutrient processing, pathogen colonization resistance and immune system development (Thursby and Juge, 2017).

In this thesis, we will focus on the intestinal immune system with a special focus on its inductive sites and then discuss the importance of the microbiota on shaping this immune system and how its composition may reflect host health.

1) Physiology of the gut

The intestine is the tubular part of the alimentary canal that extends from the stomach to the anus. The small intestine begins at the pylorus of the stomach and ends at the ileocaecal valve where large intestine starts. It is divided into three main segments: duodenum, jejunum and ileum (Fig. 1). The large intestine begins at the caecum, followed by the ascending (proximal) colon, the transverse colon, the descending (distal) colon and the rectum, terminating at the anus.

The principal function of the intestine is the absorption. Small intestine absorbs mainly nutrients and the large intestine mostly water and metabolites produced by the microbiota from undigested foodstuffs before their elimination.

A transverse cross section of the small intestine wall shows the different concentric layers present from the lumen to the periphery: mucosa, submucosa, muscularis and serosa (Fig. 2a). To increase the exchange surface necessary for the digestive functions and optimal uptake of nutrients, the mucosa and submucosa form circular folds (Fig. 2b). Then, the mucosa has finger-like projections extending into the lumen called villi (Fig. 2c). Finally, the apical membrane of the main population of small intestinal epithelial cells termed enterocytes has microscopic cellular membrane protrusions termed microvilli (Mescher, 2018). By contrast, the colon lacks villi and therefore displays reduced exchange surfaces as it has only minimal intrinsic digestive functions.

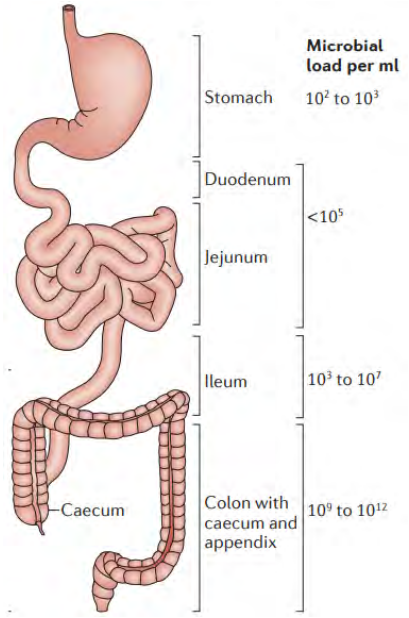

Figure 1: Distribution of microbiota along the length of the anatomical segments of the intestine. Adapted from Mowat and Agace, 2014.

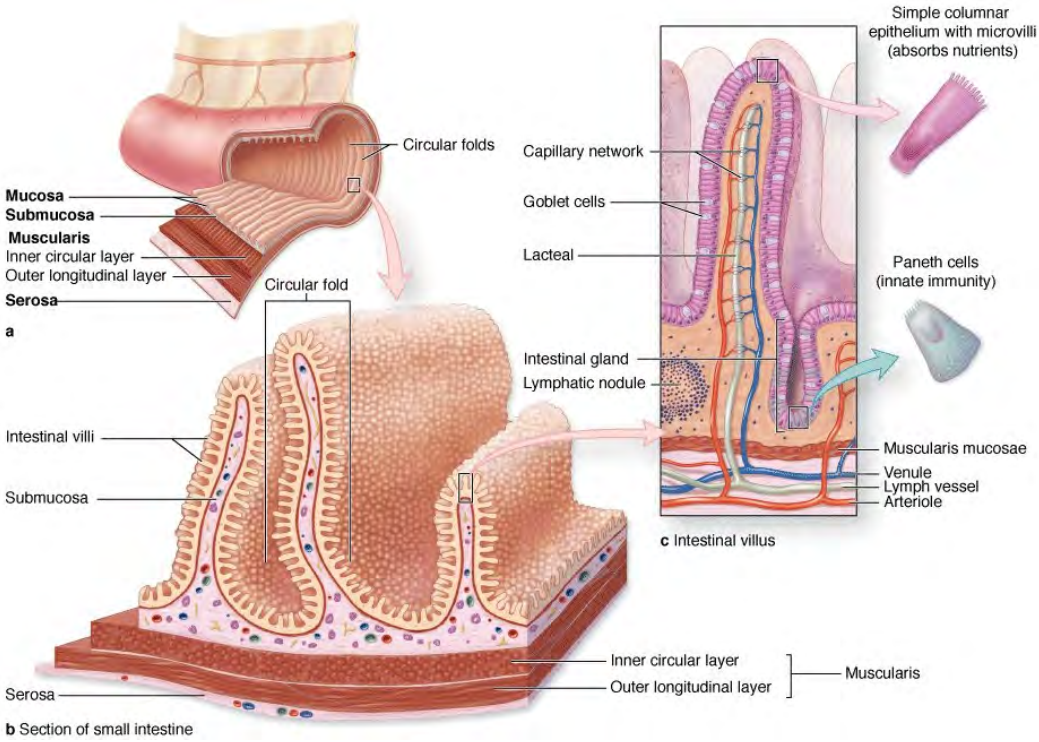

Figure 2: Absorptive surface of small intestine: a): The mucosa and submucosa are the inner two of the gut's four concentric layers. b): They form circular folds, which increase the absorptive area. c): They are lined by a dense covering of finger-like projections called villi. Adapted from Mescher, 2018.

2) Composition of the small intestinal epithelium

As previously stated, the intestinal mucosa is our first line of defense and, in addition to promoting nutrient uptake, its superficial layer of epithelial cells displays several mechanisms to protect itself and preserve its integrity (Peterson and Artis, 2014; Allaire *et al*., 2018). The epithelium is continuously renewed by immature cells arising from the intestinal epithelial stem cells located in invaginations known as crypts and contains several cell subsets (Fig. 3):

- **Enterocytes**: equipped with microvilli, their main function is to absorb nutrients but they are also capable of producing some antimicrobial peptides (AMPs), such as the C-type lectin regenerating islet-derived protein IIIγ (REGIIIγ), β-defensins and cathelicidins. Moreover, its apical membrane, enriched in ectoenzymes, is covered with acidic mucopolysaccharides and glycoproteins creating a meshwork known as glycocalyx. The glycocalyx acts as a physical barrier limiting bacterial access to the epithelium (Frey *et al*., 1996).

- **Paneth cells**: exclusively located at the bottom of the small intestine crypts, they are capable of secreting many additional AMPs, including α-defensins, phospholipases A2 and lysozyme. These AMPs target highly conserved and essential features of bacteria, such as cell wall peptidoglycans.
- **Goblet cells**: secrete mucins that crosslink to form a layer of mucus. The thickness of this layer and the frequency of goblet cells correlate with the amount of the microbiota (Fig. 1) and reach their highest levels in the colon. By contrast, mucus layer is looser in the small intestine. The mucus layer forms a physical barrier that prevents microorganisms to reach the epithelium. In addition, the mucus provides a matrix for AMPs and antibodies avoiding them to be rapidly washed out. Finally, it provides some anchors but also substrates to the microbiota.
- **Tuft cells**: chemosensory cells that play a key role in the defense against helminth parasites.
- **Neuroendocrine cells**: secrete hormones that regulate the digestive function.
- **M cells**: are specifically located in gut immune inductive sites such as Peyer's patches (PP) and are specialized in antigen uptake as detailed later.

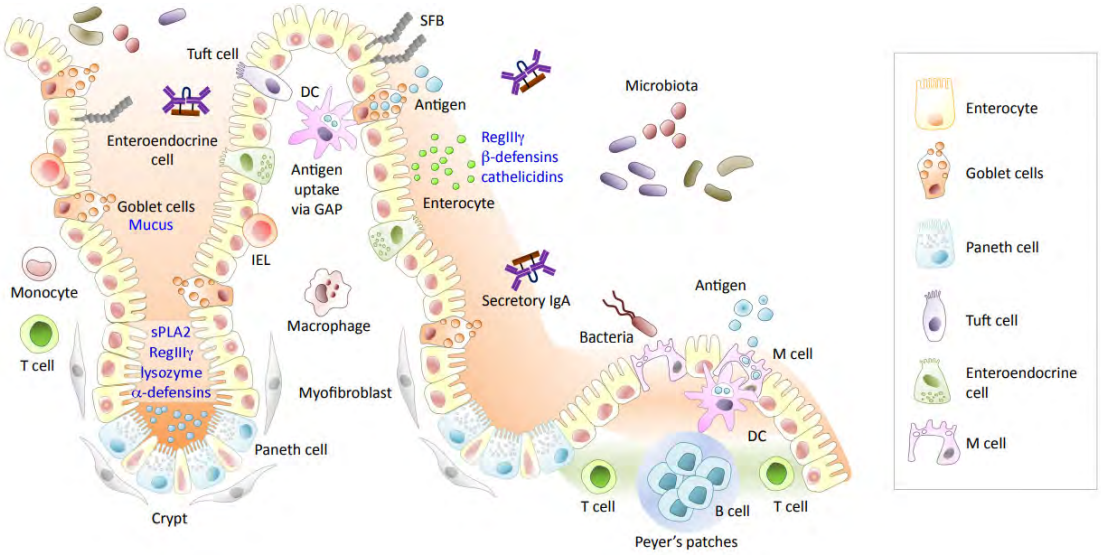

Figure 3. Representative composition of the small intestinal epithelium. Enterocytes are the main intestinal epithelial cell type. Goblet, Tuft and enteroendocrine cells are located along the whole crypt–villus axis whereas Paneth cells are located at the base of the crypts. M cells are mainly found in the follicle-associated epithelium of Peyer's patches where they transport antigens from the lumen to the subepithelial domes. Abbreviations: DC, dendritic cell; IEL, intraepithelial lymphocyte. Adapted from Allaire *et al.*, 2018.

In summary, epithelial cells create a physical and biochemical barrier to external antigens. However, it is not sufficient to prevent penetration of pathogens that have evolved strategies to circumvent these defense mechanisms. Therefore, a dedicated and adapted immune system lies below the epithelium in the LP to protect our body from such pathogens.

A-II/ Organization of the intestinal immune system

Immune cells work together to contain the vast onslaught of environmental antigens, without compromising the integrity of the mucosal barrier nor promoting an overstimulation of the immune system. Immune cells located mostly below the epithelium lining of the mucosa include myeloid and lymphoid cells. All together, they are the actors of the intestinal immune system, which can be divided into immune inductive and effector sites. Organized lymphoid tissues termed gut-associated lymphoid tissues (GALT) are the immune inductive sites of the gut that initiate the adaptive immune response together with the mesenteric lymph nodes (MLN). The MLN are a chain of several lymph nodes (LN) embedded in the mesenteric membranes where antigens are drained from the intestine to promote tolerance or immune response (Houston *et al*., 2016; Esterhazy *et al*., 2019).

Immune effector sites are made up of all immune cells scattered throughout the LP of the small intestine and colon outside of the GALT. Most of the scattered lymphocytes are activated by antigens and comprise mainly effector T cells and plasma cells secreting IgAs. Most intraepithelial lymphocytes (IEL) are memory $CD8^+$ T cells. Conversely, in LP effector and memory $CD4^+$ T cells predominate. The presence of such large numbers of effector cells is more often the consequence of a local tolerogenic response to innocuous antigens normally present at mucosal surfaces and involves regulatory T cells (Treg) that are crucial to prevent inflammation. However, when necessary, this tolerogenic response can be refocused to produce a full adaptive immune response to invading pathogens (Boyaka and Fujihashi, 2019). LP also contains innate lymphoid cells (ILC), mast cells and a diversified mononuclear phagocyte system (MPS). The MPS includes two large families of cells distinguishable by their origin: the common dendritic cell precursor (CDP)-derived conventional dendritic cells (cDC) or plasmacytoid dendritic cells (pDC) and the embryo or monocyte-derived macrophages (Mϕ). CDP-derived cells are FMS like tyrosine kinase ligand (Flt3L)-dependent whereas monocyte-derived cells are colony stimulating factor 1/2 (CSF-1/2)-dependent (Bogunovic *et al*., 2009; Varol *et al*, 2009).

On one hand, CDP give rise to pDC and to pre-DCs in the bone marrow (BM). pDC have a plasma cell-like morphology and produce massive amounts of type I interferons (IFNα and IFNβ) in response to

Toll-like Receptor (TLR) stimulation during viral infection. This response regulates antiviral genes and activate effector cells. Conventional dendritic cells (cDC) differentiate from pre-DCs and express the zinc finger and BTB domain containing 46 (Zbtb46) transcription factor (Satpathy *et al*., 2012; Meredith *et al*., 2012). cDC comprise two major subsets: cDC1 and cDC2, which can be defined in mice and humans by expression of X-C motif chemokine receptor 1 (XCR1) and signal regulatory protein α (SIRPα/CD172a), respectively (Becker *et al*., 2014; Guilliams *et al*., 2016). cDC1 are specialized in cross presentation of antigens to naive $CD8^+$ T cells in a major histocompatibility complex I (MHCI) context. Conversely, cDC2 excel at the presentation of antigens to naive $CD4^+$ T cells in a MHCII context (Merad *et al*., 2013; Sichien *et al*., 2017). cDC2 comprise the majority of cDC in the small intestinal LP (Sun *et al*., 2020). They have a lifespan in the tissue of only a few days, and have the capacity to migrate in afferent lymph to the MLN, where they can prime naive T cells (Joeris *et al*., 2017). In mice, cDC1 are $CD103^+CD11b^–$, whereas cDC2 comprise $CD103^–CD11b^+$ and $CD103^+CD11b^+$ cells (Becker *et al*., 2014). Equivalent cDC populations are present in the human intestine and are often identified based on expression of CD103 in conjunction with XCR1 (cDC1) or SIRPα and CD1c (cDC2) rather than CD11b (Stagg, 2018). $CD103^+$ DCs are potent inducers of gut homing receptors (CCR9 and the α4β7 integrin) in T and IgA^+ B cells. $CD103^–CD11b^+$ cDC2 give rise to $CD103^+CD11b^+$ cells under the influence of the transforming growth factor beta (TGFβ) (Bain *et al*., 2017). Following antigen encounter in the LP and maturation, cDC2 and cDC1 express C-C chemokine receptor type 7 (CCR7) to migrate to the MLN and induce gut-tropic Treg, underlying the long-recognized phenomenon of oral tolerance (Welty *et al*., 2013; Mowat, 2018). cDC constitutively traffic out the intestinal LP and deliver antigens derived from food, commensal bacteria and apoptotic epithelial cells to the MLN (Huang *et al*., 2000; Macpherson and Uhr, 2004; Cerovic *et al*., 2013; Cerovic *et al*., 2015). The ability of these cDC to generate Treg is dependent on their expression of the integrin αvβ8, which activates latent TGFβ (Worthington *et al*., 2011; Païdassi *et al*., 2011), and is enhanced by their production of retinoic acid (RA) (Sun *et al*., 2007; Coombes *et al*., 2007). cDC1 and $CD103^+CD11b^+$ cDC2 are mutually redundant in maintaining Treg numbers in the small intestinal LP in vivo (Sun *et al*., 2020).

On the other hand, monocytes egress from the BM into the blood in a CCR2-dependent manner (Serbina and Pamer, 2006) to give rise to $CX3CR1^{hi}$ (fractalkine receptor) Mϕ in the gut (Bogunovic *et al*., 2009; Bain *et al*., 2014). However, caution has to been taken when using CX3CR1 alone to identify Mϕ since CX3CR1 is also express although at lower levels by a subset of CD103- cDC2 in both the small intestine and the colon (Scott *et al*., 2015). Therefore, it is recommended to use it in combination with other specific Mϕ markers such as F4/80, CD64 or MerTK to distinguish Mϕ from cDC. Mϕ are by far the major mononuclear phagocyte population in the intestinal LP. They play a wide variety of roles to maintain

intestinal homeostasis (Arroyo Portilla *et al*., 2021; Annex 1). They are involved in tissue repair and remodeling of the epithelium and vasculature, clearance of apoptotic or senescent cells, and elimination of penetrating bacteria. These non-migratory Mϕ can even sample antigens directly from the lumen via trans-epithelial paracellular processes (Niess *et al*., 2005; Chieppa *et al*., 2006). Then, they can transfer soluble antigens to $CD103^+$ cDC2 through a membrane transfer system called trogocytosis, where gap-junctions are formed between these cells (Mazzini *et al*., 2014). This cooperative process may compensate for the poor phagocytic activity of $CD103^+$ cDC2 (Tezuka and Ohteki, 2019). They also contribute to the oral tolerance development by supporting Treg primed in the MLN, and assuring their local maintenance in the mucosa by producing the anti-inflammatory cytokines IL-10 and TGFβ (Hadis *et al*., 2011; Bain and Schridde, 2018). As well as Treg, other effector T cells are locally controlled by regulatory Mϕ through their anti-inflammatory cytokines (Stagg, 2018). Importantly, monocytes have the dual capacity to differentiate into regulatory or inflammatory populations depending on the local environmental conditions. In the LP, under inflammatory conditions, the recruitment of inflammatory monocytes massively increases (Rivollier *et al*., 2012; Bain *et al*., 2013; Tamoutounour *et al*., 2012). They massively infiltrate the LP and play pro-inflammatory functions by producing IL-12, IL-23, inducible nitric oxide synthase (iNOS), and tumor necrosis factor (TNF).

Interestingly, at steady state, MPS of the LP strongly differ from the one of GALT. This is likely due to the unique microenvironment at each mucosal site. Indeed, as we will see below, contact with pathogens is favored in GALT as compared to villi and a pro-rather than anti-inflammatory/tolerogenic response must be ready to be generated, likely reminiscent of that obtained in the small intestine and colon under inflammatory conditions.

A-III/ Peyer's patches, main organized gut-associated lymphoid tissues of the small intestine

1) The GALT, immune inductive sites of the gut

The GALT encompasses the solitary intestinal lymphoid tissues (SILT) and the macroscopic patches that are named according to their anatomical position: caecal patches, colonic patches or, for the small intestine, Peyer's patches (Russell *et al.*, 2015; Buettner and Lochner, 2016).

SILT have been described in humans (Moghaddami *et al*., 1998; Fenton *et al*., 2020) and in mice (Hamada *et al*., 2002) along the small and large intestine. SILT develop strictly after birth and consist of a dynamic continuum of structures ranging from small cryptopatches to large, mature isolated lymphoid follicles (ILF) (Buettner and Lochner, 2016). This development occurs in response to dietary products and colonization with specific bacteria such as segmented filamentous bacteria (SFB) or to imbalance in the luminal microbial communities, suggesting that ILF provide an expandable reservoir of compensatory inductive sites (Knoop and Newberry, 2012).

Unlike SILT, Peyer's, caecal and colonic patches develop in an embryonic-programed fashion. Colonic patches are equivalents of small intestine PP, but they are smaller lying deep in folds of colonic tissue (Bennett *et al*., 2016). In mice, there are between 6 and 12 PP depending on individuals and strains but only two to five colonic patches (Agace and McCoy, 2017). PP are primary sites of the small intestinal humoral immune response initiation whereas caecal, colonic patches and colonic ILF are rather involved in the colonic humoral immune response, underlying the regionalization of the intestinal immune system (Craig and Cebra, 1971; Masahata *et al*., 2014; Fenton *et al*., 2020).

2) Distribution and structure of Peyer's patches

In humans, PP are primarily located in the terminal ileum. Their number increases from 100 at birth to 200 in puberty, and then the number diminishes around 100 between 70 and 96 years of age (Cornes, 1965). PP consist of two or more large B cell follicles forming domes at the surface of the mucosa and separated by T cell areas termed interfollicular region (IFR) underneath dome-associated villi (DAV) (Fig. 4) (Jung *et al*., 2010). Unlike other secondary lymphoid organs, PP follicles contain permanent germinal centers (GC) where activated B cells proliferate and differentiate into antigen-specific IgA-secreting cells. This indicates that a constant influx of antigens occurs in PP, despite the lack of afferent lymphatics that brings antigens in all other secondary lymphoid organs. This permanent sampling of luminal antigens occurs thanks to their well-adapted follicle-associated epithelium (FAE) that contains the specialized epithelial cell termed M cell. Indeed, the FAE lacks goblet cells and is mainly composed of enterocytes that display lower levels of digestive enzymes than villus enterocytes and do not express the polymeric IgR that normally allows the secretion of IgA in the gut lumen. Accordingly, FAE secretes lower levels of antibodies and mucus, making it easier for antigens to reach its surface.

M cells are specialized in the transport of these antigens from the lumen to the underlying subepithelial dome (SED). Scattered through the FAE, M cells comprise 10% of the total FAE in mouse and human PP (Ohno, 2016). They lack microvilli and offer a flattened luminal surface with a reduced glycocalyx enabling luminal antigens to easily bind their apical surface. The basolateral membrane is deeply invaginated, allowing lymphocytes, Mϕ and DC to migrate into intraepithelial microdomains termed "M-cell pockets" (Gebert *et al*., 1996; Kobayashi *et al*., 2019). These microdomains reduce the distance from the apical to basolateral surface, accelerating the transfer of luminal antigens to immune cells (Mowat and Agace, 2014).

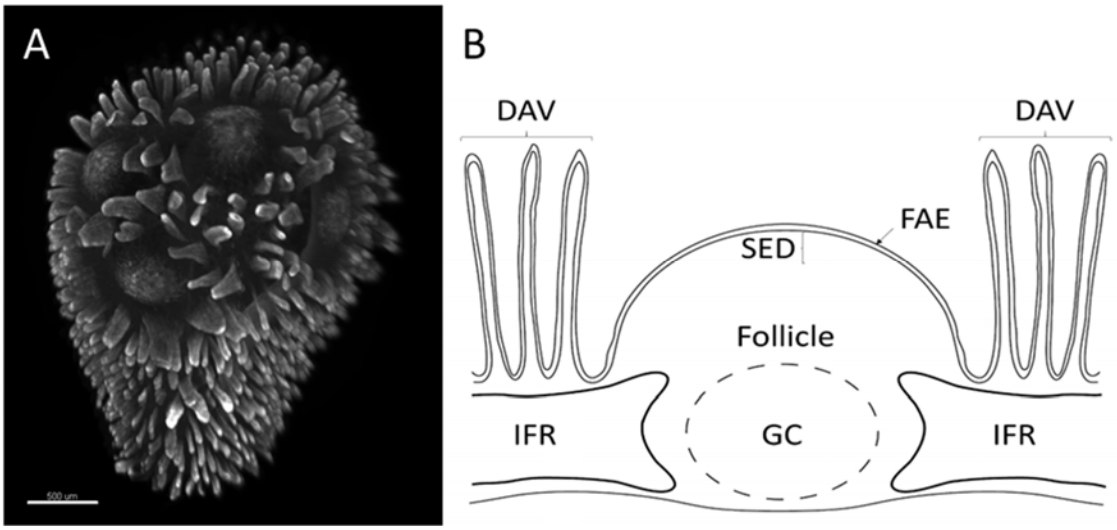

Figure 4: A: Light sheet microscopy view of one Peyer's patch comprising four domes and stained for its reticular network (white: Collagen IV). B: Diagram of a transversal cut through the dome showing the different Peyer's patch regions. Abbreviations: DAV, dome-associated villus; FAE, follicle-associated epithelium; GC, germinal center; IFR, interfollicular region; SED, subepithelial dome.

The overall structural organization of PP is made possible by the presence of specific fibroblastic reticular networks and the secretion of specific chemokines by stromal cells of these networks in each region (Fig. 5) (Prados *et al*., 2021). Thus, the SED is enriched in RANKL-expressing stromal cells, necessary for the differentiation of M cells, and for the production of the chemokine CCL20 by the FAE (Knoop *et al.*, 2009; Nagashima *et al*., 2017). CCL20 together with CCL9, another chemokine expressed by M cells, are secreted in the SED where they attract CCR6 and CCR1-expressing phagocytes, respectively (Iwasaki *et al*., 2000; Zhao *et al*., 2003; Da Silva *et al*., 2017).

Moreover, the stromal cells of the follicle and of the IFR produce the chemokines CXCL13 or CCL21 and CCL19, respectively (Fig. 5). These chemokines attract and interact with the specific receptors CXCR5 or CCR7 expressed on B and T lymphocytes, respectively. This allows their segregation into their specific B and T cell zone. Immune cells enter PP from the bloodstream via high endothelial venules (HEV). Most HEV are in the IFR but some HEV can be found within follicles. PP HEV strongly express the mucosal addressin cell adhesion molecule 1 (MAdCAM-1), which is the ligand for L selectin (also known as CD62L) and for the integrin α4β7. This integrin is more abundantly expressed by naive B cells than by naive T cells, which could explain the more efficient entry of B cells than T cells into PP. Finally, the chemokine CXCL12 is involved in the attachment of lymphocytes to the endothelium favoring diapedesis (Cyster and von Andrian, 2004). In summary, PP regions possess a highly organized microarchitecture necessary for the compartmentalization of numerous cellular interactions and therefore provide the optimal environment for the initiation of immune responses (Cyster and von Andrian, 2004).

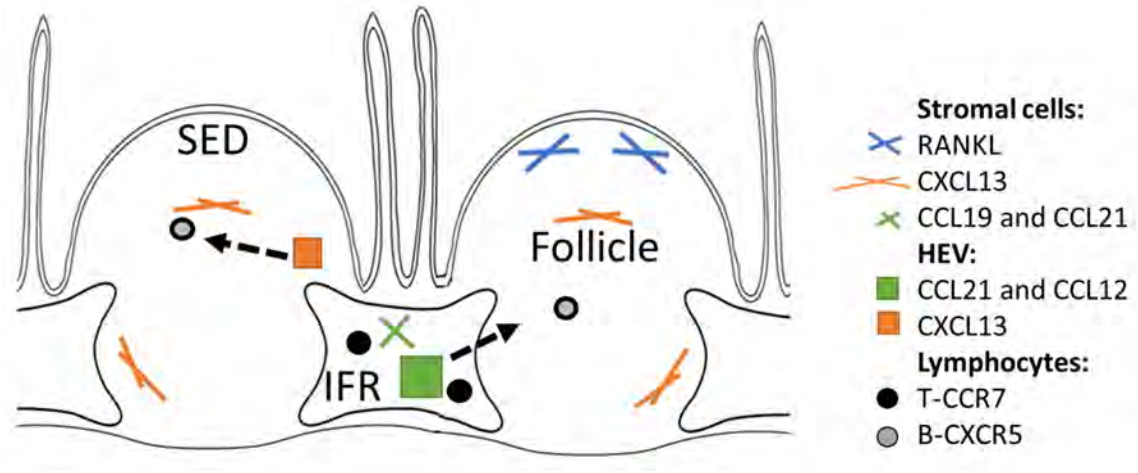

Figure 5: Lymphocyte trafficking in Peyer patches. Abbreviations: HEV, high endothelial venules; IFR, interfollicular region; SED, subepithelial dome.

Recruited B and T cells patrol randomly inside the follicle and the IFR, in search for intact antigens or MHC-peptide complexes, respectively. The transit time of B cells through PP, between half-an-hour and 10 hours, is shorter than through LN (Reboldi and Cyster, 2016). B- and T-cell egress from PP are dependent on sphingosine-1-phosphate receptor-1 (S1PR1), which allows the egress to the MLN. Sphingosine-1-phosphate (S1P) concentrations are high in the blood and the lymph compared with the interstitial fluid of lymphoid organs. Naive lymphocytes produce S1PR1 abundantly; much of it reaches the surface, while some form a complex that is retained intracellularly with the transmembrane protein CD69. After antigen

recognition, lymphocytes need to remain in the PP to undergo clonal expansion and receive instructive signals before exiting as effector cells. To accomplish this, activated lymphocytes increase the expression of CD69 causing S1PR1 removal from their surface avoiding egress from PP (Cyster and Schwab, 2012).

Although not related to leukocytes, stromal cells associated with the follicles are termed follicular dendritic cells (FDC) (Suzuki *et al*., 2010; Prados *et al*., 2021). FDC have a stellate shape, with long dendrites that form intercellular connections between them building the scaffolding of the GC where every single B cell is in contact with several dendritic processes. Outside the GC, the number of FDC decreases and only a limited number of B cells are in direct contact with them (Sobhon, 1971). FDC express high levels of complement receptor 1 (CR1) and 2 (CR2), which binds to various fragments of C3. They also express Fc binding receptors, such as FcγRIIB, which bind immune complexes (Batista and Harwood, 2009). This antigen-retaining capacity allows close contact with antigen-specific B cells. Moreover, FDC participate to the selection of B cells in the GC by probing the affinity of the B cell receptor (BCR) for its antigen, allowing the survival of the most affine clone (Suzuki *et al*., 2010; Aguzzi *et al*., 2014).

3) Adaptive immune response initiated in Peyer's patches

- T cell activation

In the IFR, naïve T cells encompass around 65% of $CD4^+$ T cells and 35% of $CD8^+$ T cells (Boyaka and Fujihashi, 2019). Naïve T cells encounter antigens that are presented by DC. The interaction between a naive $CD4^+$ T cell with a DC defines the cell fate decision to become a TFH, TFR, Th1, Th2, Treg or Th17 cells (Choi *et al*., 2011; DiToro *et al*., 2018). Naive T cells express high levels of CD62L but after antigen encounter, CD69 is rapidly induced (Cyster and Schwab, 2012). CD44 is also upregulated early after T-cell receptor (TCR) engagement and is a marker for antigen-experienced effector and memory T cells (Baaten *et al*., 2012). T follicular helper cells (TFH) primed by DC migrate to the T–B border upon downregulation of CCR7 expression and upregulation of CXCR5, which directs TFH cells to the follicle via gradients of CXCL13 expressed by FDC (Haynes *et al*., 2007). They also express the inhibitory receptor PD1 that inhibits the expression of CXCR3, which is important for a proper localization inside the follicles (Shi *et al*., 2018). Most other effector T cells egress from PP to seed the LP. They down-regulate CD62L limiting their ability to home to PP (Mueller *et al*., 2013). In the small intestine LP, $Foxp3^+$ Treg and $ROR\gamma t^+$ Th17 cell populations are the most abundant (Fagarasan *et al*., 2010). Cytotoxic T lymphocyte (CTL) precursors also migrate to

the gut. These precursors do not develop a cytotoxic function until they encounter their antigen in a MHC-class I context presented by target cells. It is possible that this mechanism protects the common mucosal immune system network from inadvertent cytotoxic inflammatory events (Boyaka and Fujihashi, 2019).

- B cell activation

B cells can recognize and respond to both soluble and membrane-associated antigens (Batista and Harwood, 2009). Small molecules are mainly delivered to the SED via M cells (Ohno, 2015; Nakamura *et al*., 2018; Kobayashi *et al*., 2019). Direct encounter between antigens and lymphocytes present in the pockets of M cells has been observed by electron microscopy (Owen, 1977). Subepithelial B cells can indeed encounter antigens without any $CD11c^+$ phagocyte help via close contact with M cells before migrating towards the GC (Komban *et al*., 2019).

Alternatively, antigens can be presented intact on the surface of phagocytes via complement receptors or IgA binding molecules, such a Dectin-1 or Siglec-F (Rochereau *et al*., 2013). B cells can also recognize membrane-associated antigens that are retained by the FDC (Batista and Harwood, 2009). Indeed, FDC in LN primary follicles display antigen for encounter by recirculating naive B cells (Heesters *et al*, 2014); whether it is the same in PP is not known but seems likely (Reboldi and Cyster, 2016). Hence, during their subepithelial and follicular journey B cells can encounter specific antigens by different ways and become activated.

- IgA switching

Naive B cell precursors expressing IgM and IgD are induced to switch to the IgA isotype in the presence of certain factors that are constitutively present in the gut microenvironment. The precise signals that direct class-switching differ during T-dependent (TD) or T-independent (TI) pathways of activation. In all cases, BCR antigen stimulation is necessary to induce the expression of activation-induced cytidine deaminase (AID). AID promotes class switch recombination (CSR) and affinity maturation through somatic hypermutation (SHM) (Muramatzu *et al*., 2000). On one hand, CSR is a process during which DNA is deleted from the antibody heavy chain constant region to allow the IgM region to be exchanged for downstream regions, while keeping the antigen-binding variable region (Bemark *et al*., 2012). Thus, CSR alters the effector function of antibodies without changing their antigen-binding specificity. In PP, CSR mainly lead

the production of IgA isotype (Fagarasan *et al*., 2010). On the other hand, SHM creates random mutations in the variable region changing the affinity of the antibody for the antigen. This process termed affinity maturation requires interactions between B cells, antigens on FDC, and TFH in the GC (Bemark *et al*., 2012) and leads to the selection of B cells bearing BCR that bind antigen with high affinity (Stebegg *et al*., 2018). BCR selection and affinity maturation in PP GC occur even under homeostasis conditions (Chen *et al*., 2020).

The preferential switching to IgA in PP is explained by several extrinsic molecular factors (Fig. 6). PP DC and epithelial cells are an important source of a proliferation inducing ligand (APRIL). Mice deficient in APRIL and some humans with mutations in its receptor are characterized by a reduced IgA production (Castigli *et al*., 2004; Castigli and Geha, 2007). PP FDC are conditioned by the bacterial and food-derived products present in the gut, such as lipopolysaccharides (LPS) and retinoic acid (RA). FDC produce matrix metalloproteases that facilitate the activation of TGFβ, and secrete large amounts of B-cell activating factor (BAFF) (Suzuki *et al*., 2010). These two essential cytokines allow CSR to IgA and survival of recently switched IgA^+ B cells, respectively (Cazac and Roes, 2000; Mackay and Browning, 2002). One key source of TGFβ is the B cells themselves (Gros *et al*., 2008), but T cells, FDC, and DC may also produce this cytokine in the PP (Fagarasan *et al*., 2010). TFH likely promote IgA-producing cells generation through two mechanisms: by contributing signals that induce IgA CSR, and by promoting expansion of B cells that have already completed CSR (Reboldi and Cyster, 2016).

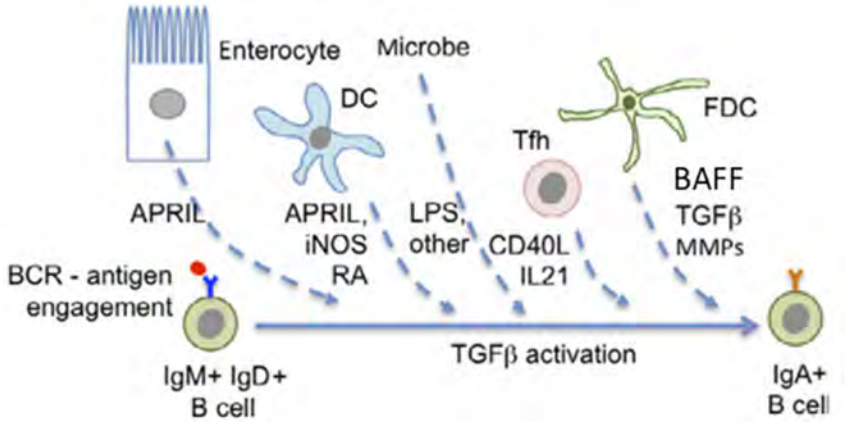

Figure 6: Factors promoting IgA switching in Peyer's patches. Abbreviations: APRIL, a proliferation inducing ligand; BCR, B cell receptor; DC, dendritic cell; FDC, follicular DC; LPS, lipopolysaccharide; MMPs, matrix metalloproteases; RA, retinoic acid; Tfh, T follicular helper cell. Adapted from Reboldi and Cyster, 2016.

As stated before, in PP CSR takes place predominantly in the SED (Biram *et al*., 2019). B cell enter into the SED where the necessary signals for CSR to the IgA isotype are provided (Reboldi *et al*., 2016). CSR to IgA requires natural thymus-derived Treg and probably T follicular regulatory cells (TFR), these cells are located in the border between the IFR and the follicles (T–B border) where they express a latent form of TGFβ (Gribonika *et al*., 2019). The major triggers for CSR are CD40 (in TD pathway), extensive BCR cross-linking, TLR stimulation or binding of APRIL or BAFF to transmembrane activator and calcium modulator and cyclophilin ligand interactor (TACI) (Bemark *et al*., 2012). The SED also contains scattered RORγt$^+$ ILC3, which are an important source of LTα1β2 and IL-22. The lack of ILC3 induces an impaired ability to undergo IgA class switching and an increased propensity to switch to IgG1 (Reboldi *et al*., 2016).

After initiating CSR, B cells migrate back to the follicle where they can differentiate through either TD or TI pathways (Fig. 7). Antigen-specific B cells are not subjected to affinity-based competition in the SED. TFH-like cells can promote B cell expansion without clonal selection in the SED but B cell affinity-based competition is ensued during or immediately after GC infiltration and interaction with proper TFH. Thus in PP, IgA CSR can occur outside the GC and T-independently, whereas SHM require GC environment and T cells (Bergqvist *et al*., 2006). Analysis of SHM distribution and of T cell-deficient mice indicates that the gut IgA$^+$ cell repertoire is a mixture of TI and TD specificities. In young mice and humans, 75% of IgAs are mutated and likely of TD origin (Bunker and Bendelac, 2018). Given that the majority of IgA antibodies, including those against commensals, are somatically hypermutated, it seems likely that T cells are normally involved in the induction of antibody responses toward many commensals (Benckert *et al*., 2011).

- T-dependent pathway

Permanent GC in the PP are the consequence of the continual exposure to microbiota-derived molecules. After CSR to IgA, B cells can infiltrate these preformed GC (Bergqvist *et al*., 2013; Reboldi *et al*., 2016) where they interact with CD4$^+$ T cells to generate IgAs with higher specificities for antigens. The two major kinds of CD4$^+$ T cells located inside GC are TFH and TFR. In PP TFH and TFR can differentiate either from RORγt$^+$ Th17 cells (Hirota *et al*., 2013) or from Foxp3$^+$ Treg, respectively (Tsuji *et al*., 2009). In PP GC, there is an increased TFH/TFR ratio as compared to LN GC (Kato *et al*., 2014). This favors a quick generation of diverse low-affinity antibodies in response to microbial antigens (Reboldi and Cyster, 2016).

GC are organized into light zone (LZ) and dark zone (DZ), B cells proliferate extensively and turn on the SHM machinery in the DZ and are selected in the LZ (Biram *et al*., 2019). Selection occurs through

BCR recognition of antigens in immune complexes on FDC, internalization and presentation of the antigen in MHCII complexes to TFH. B cells that do not receive TFH help die. Upon receiving survival signals from TFH, B cells re-enter the DZ for further rounds of proliferation and SHM after which they exit the GC as memory B cells or high-affinity antibody-secreting plasma cells (Victora and Nussenzweig, 2010; Stebegg *et al*., 2018). TFR of the LZ control the output of the GC response by regulating these TFH-B cell interactions (Chung *et al*., 2011).

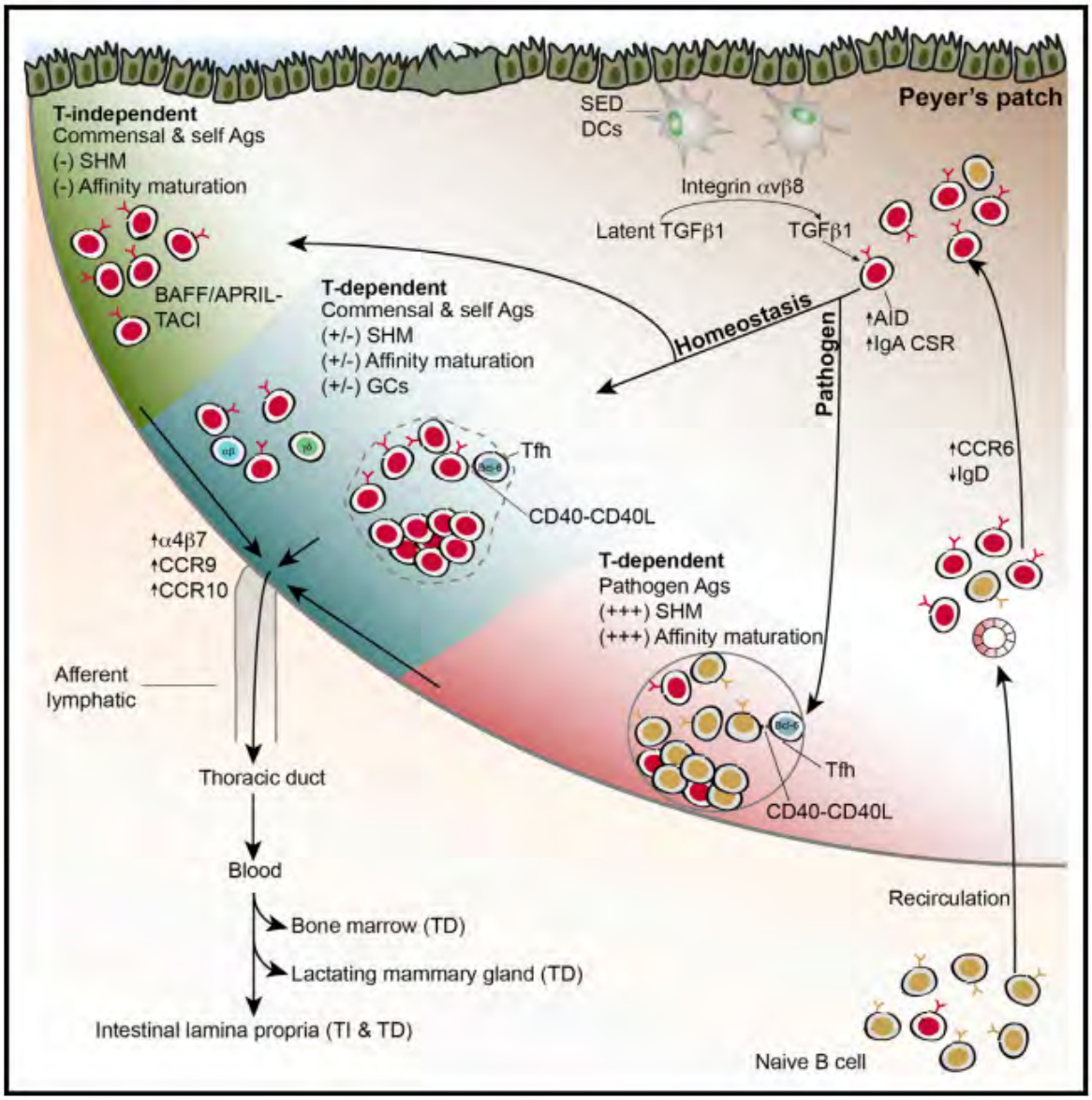

Figure 7: Mechanisms of IgA Selection in Peyer's Patches. Abbreviations: Ags, antigens; AID, activation-induced cytidine deaminase; CSR, class switch recombination; DC, dendritic cell; GC, germinal center; SED, subepithelial dome; SHM, somatic hypermutation; TFH, T follicular helper cells. Adapted from Bunker and Bendelac, 2018.

- T-independent pathway

In some cases, when signaling via co-receptors such as TLR is strong, the need for T cell help may be overcome. Alternatively, highly multivalent antigens alone may trigger sufficiently strong BCR signaling for B cells to enter into expansion. TI pathway involves rapid cellular differentiation with little SHM (Bunker and Bendelac, 2018). TI responses are capable of generating IgA that bind many commensals. It will be therefore crucial to determine the relative contribution of TD versus TI IgA responses to gut bacteria and other antigens in animals able to mount both types of response (Reboldi and Cyster, 2016).

Bunker and Bendelac recently proposed a model that summarizes the two distinct types of humoral immunity that coexist in the gastrointestinal mucosa (Fig. 7). The first—a homeostatic response to commensals—involves natural polyreactive specificities that differentiate largely in the absence of T cell help with little somatic hypermutation or affinity maturation. The second—a protective response to pathogens—involves the production of high-affinity and specific antibodies generated in germinal centers by mechanisms that resemble systemic responses (Bunker and Bendelac, 2018).

- Egress of activated immune effector cells from PP

The majority of lymphocytes leave the PP via the draining lymphatics, pass through the MLN to enter the thoracic duct and the bloodstream, which facilitates their migration to mucosal effector sites such as the intestinal LP. Effector cells are imprinted for gut homing by expression of the integrin α4β7 and the chemokine receptor CCR9 (small intestine addressing) or CCR10 (colon addressing). Under normal circumstances, only lymphocytes that encounter antigen in GALT or MLN are induced to express gut homing receptors and integrins (Fagarasan *et al*., 2010; Bunker and Bendelac, 2018). α4β7, CCR9, and CCR10 bind to their intestinal ligands MAdCAM-1, CCL25, and CCL27 or CCL28, respectively. B cells fully differentiate into IgA-producing plasma cells only once they have returned to the LP. As a result, plasma cells are rarely found in PP. This is also true for effector T cells, which fully differentiate only after arrival in the mucosa. Plasma cells secrete IgA in a dimeric form linked by a small polypeptide called J chain. The polymeric Ig receptor pIgR expressed on the basolateral surface of intestinal epithelial cells binds selectively to polymeric IgA and IgM and transport them to the apical surface of the epithelial cell, where proteolytic cleavage releases the antibody bound to a highly glycosylated 80 kDa fragment of the pIgR known as secretory component (Kaetzel, 2005). The complex of dimeric IgA, J chain, and the secretory component is referred to as secretory IgA (sIgA) (Bunker and Bendelac, 2018).

Few effector cells remain in the PP as first line of defense. The FAE produces CXCL16 and this may have a role in recruiting CXCR6-expressing activated or effector T cells to the SED (Hase et al., 2006). CCR6 is upregulated on activated B cells but is minimal on naive B cells. Memory B cells in PP display high amounts of CCR6, and have privileged access to the SED, perhaps facilitating a faster exposure to newly arriving antigens (Reboldi *et al*., 2016). Thus, M cell pockets contain a dense population of memory (IgD–) B cells that may originate from the underlying B cell follicles (Biram *et al*., 2019). M cell pocket memory B cells are thought to be actively engaged in sampling luminal antigens and presenting them to adjacent T cells. Activated T cells that express CD40L may, in turn, induce CD40+ memory B cell survival and proliferation (Neutra *et al*., 2001).

A-IV/ The Peyer's patch mononuclear phagocyte system

1) Phenotype, location and specificity of the PP MPS

The origin and main location of phagocytes composing the MPS of the PP are shown in figure 8. Like LP MPS, PP MPS include the CDP-derived cells pDC, cDC1 and cDC2. cDC2 comprise two subsets historically termed double negative (DN) and $CD11b^+$ cDC. The DN cDC2 are actually immature cDC2 that undergo a developmental continuum leading to the $CD11b^+$ mature stage (Bonnardel *et al*., 2017). The SED contains few cDC, mainly immature (DN) cDC2 that are rather located in its lower part. By contrast, the IFR is enriched in pDC, cDC1 and mature cDC2 (Da Silva *et al*., 2017). PP pDC recruitment is conditioned to type I IFN/STAT1 signaling which could favor the production of the inflammatory cytokines IL-6, IL-23, and TNF instead of type I IFNs (Li *et al*., 2011).

In PP, lysozyme expression is a hallmark of monocyte-derived phagocytes that include the DC called LysoDC and the Mϕ termed LysoMac (Bonnardel *et al*., 2015). These cells represent two-third of SED phagocytes with increasing ratio in the upper part of the dome.

LysoDC are specific of PP, and maybe of ILF, in several species including humans (Lelouard *et al*., 2010; Wagner *et al*., 2020). They are short-lived, weakly autofluorescent and express very high levels of MHCII, but no CD4 (Bonnardel *et al*., 2015). Morphologically, they are large stellate motile cells (Lelouard *et al*., 2010; Lelouard *et al*., 2012). LysoDC comprise four subsets characterized by the progressive acquisition of a DC gene signature (Wagner *et al*., 2020). Thus, immature LysoDC are the precursors of follicular and subepithelial intermediate and mature LysoDC (Fig. 8). Follicular LysoDC are scattered

through the upper part of the follicle where they can have a potential role in providing support for B cells. Other LysoDC are located mainly in the SED. Mature LysoDC gene signature seems to correspond to the minimal requirement to exert DC functions (Wagner *et al.*, 2020). LysoDC are in comparable proportions among total phagocytes in conventional and germ-free mice, which are devoid of any microbiota induced stimulus. Thus, LysoDC recruitment is independent from the microbiota (Bonnardel *et al.*, 2015).

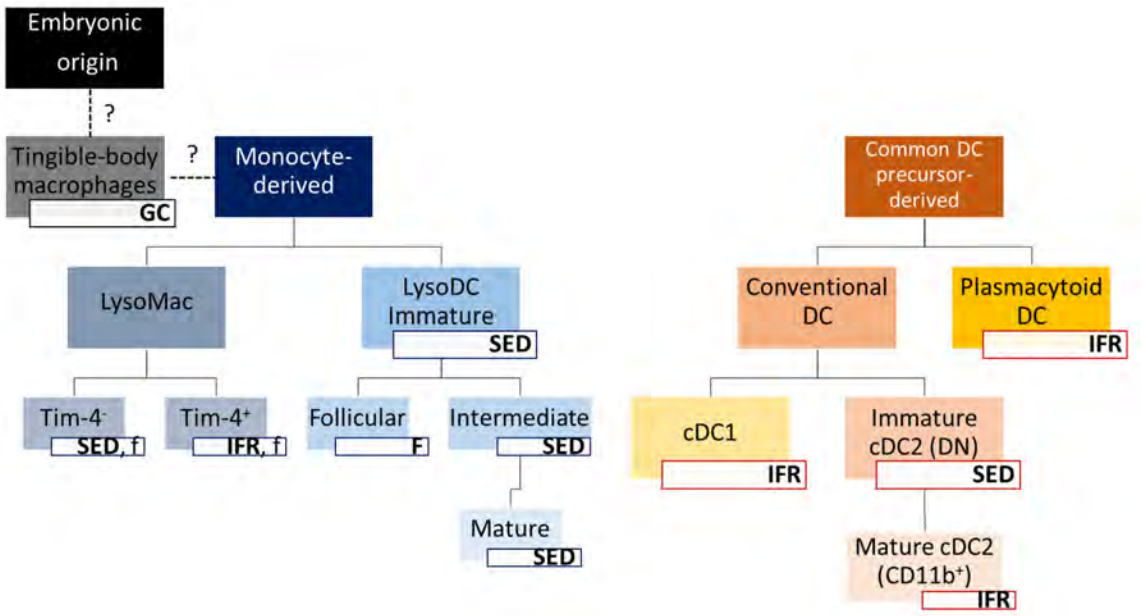

Figure 8: The Peyer's patch mononuclear phagocyte system. The origin of different phagocytes composing the PP MPS is shown, either common DC precursor-derived or monocyte-derived. The origin of the tingible-body macrophages is still unknown. The small squares indicate the main location of each phagocyte subset in the Peyer's patch. Abbreviations: DC, dendritic cell; F, follicle; GC, germinal center; IFR, interfollicular region; SED, subepithelial dome. Adapted from Da Silva *et al.*, 2017 and Wagner *et al.*, 2020.

LysoMac are strongly autofluorescent large long-lived cells, which like LysoDC depend on the growth factor M-CSF to develop (Bonnardel, 2015). Unlike LysoDC, they express CD4 and only very low levels of MHCII. Unlike other gut Mϕ LysoMac do not express IL-10 even after stimulation and lack the expression of classic Mϕ markers such as F4/80 (EMR1), sialoadhesin (Siglec1/CD169), Mannose Macrophage Receptor (MMR/CD206), or Fc Gamma Receptor I (FcGRI/CD64) (Wagner *et al.*, 2018). Depending on their location, LysoMac express or not the T-cell immunoglobulin- and mucin-domain-containing molecule (TIM-4) a phosphatidyl serine receptor involved in efferocytosis (Miyanishi *et al.*, 2007; Lemke, 2019). Thus, LysoMac express TIM-4 in the IFR but not in the SED (Bonnardel *et al.*, 2015).

In the germinal center, PP also contain tingible-body macrophages expressing CX3CR1 and lysozyme (TBM), whose origin is still unknown (either monocyte or embryonic) (Bonnardel *et al*., 2015). Finally, PP contain also a layer of poorly described TIM-4^{+} serosal / muscularis Mϕ, which express CD169 at the base of the IFR but not of the follicle (Bonnardel *et al*., 2015; Wagner *et al*., 2018).

Identification of each phagocyte subset is crucial to assess its contribution to the main functions of PP; i.e. the sampling of luminal antigens and the initiation of an antigen-dependent intestinal immune response that disseminates to the rest of the gastrointestinal mucosa (Reboldi and Cyster, 2016; Da Silva *et al*., 2017). The main markers expressed by each subset of the intestinal MPS are summarized in Table 1. The differential expression of these markers allows the identification by microscopy and flow cytometry of each subset. Thus, the cDC2 and Mϕ present in the small intestinal villi including the DAV, can be distinguished from PP cDC2 and monocyte-derived cells by the expression of CD101 and F4/80, respectively. Until now a marker to distinguish cDC1 in the DAV from those of the IFR has not been reported (Da Silva *et al*., 2017).

Table 1: Main phenotypic markers expressed by the intestinal monocyte phagocytic system.

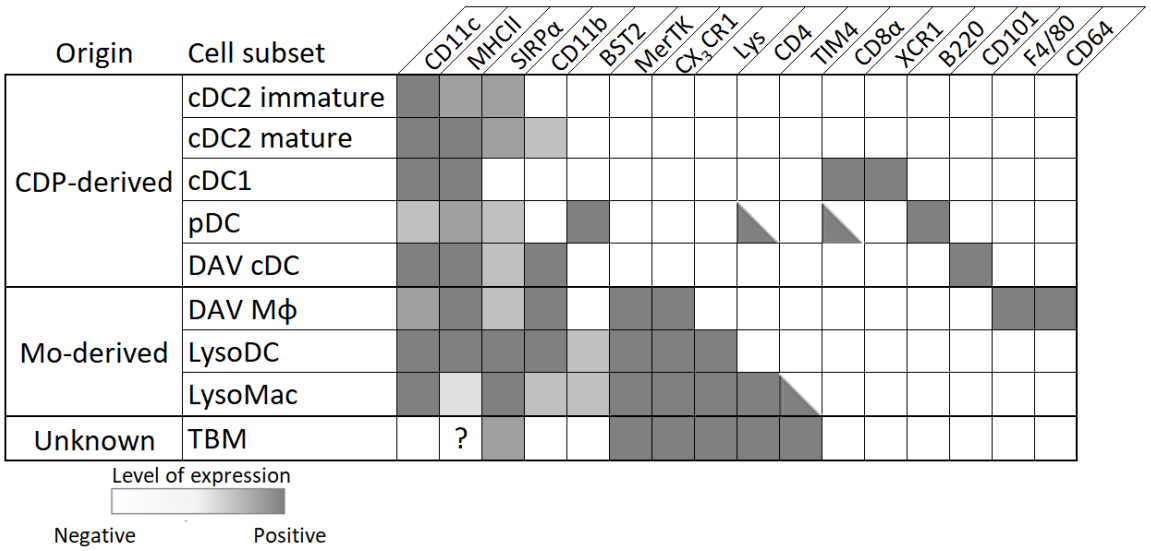

Abbreviations: CDP, common DC precursor; cDC, conventional dendritic cell; DAV, dome-associated villus; DN cDC2, double-negative cDC2; Lys, lysozyme; Mo, monocyte; Mϕ, macrophages; TBM, tingible-body macrophages; question marks indicate missing information.

2) Functions of Peyer's patch mononuclear phagocyte subsets

- Antigen sampling

LysoDC and LysoMac support the accessibility of luminal antigens to the FAE through release of IL-22BP, a protein that inhibits IL-22, the cytokine that stimulates the production of AMPs and mucins by the epithelium (Jinnohara *et al.*, 2017; Da Silva *et al.*, 2017). Therefore, its inhibition favors the access of luminal particulate antigens and bacteria to the FAE. Then, antigen uptake can occur through at least four distinct routes, which all involve M cells (Fig. 9).

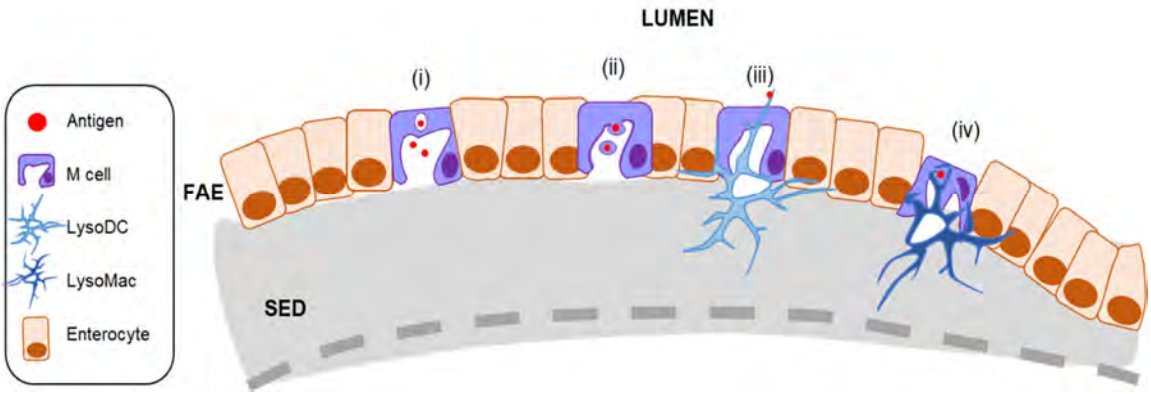

Figure 9: Distinct routes of antigen uptake in PP. (i) M cell-mediated transcytosis, (ii) M cell microvesicle shedding (MCM), (iii) Trans-M cell dendrites (TMD), and (iv) Dying M cell phagocytosis.

i. M cell-mediated transcytosis: uptake of luminal antigens can involve specific apical surface receptors expressed by M cells such as glycoprotein-2 (GP2), cellular prion protein (PrP^C), and β1-integrin (Ohno, 2015; Kobayashi *et al.*, 2019). Thus, microorganisms can be delivered intact and alive to underlying phagocytes but the machinery used for apical-to-basolateral transport has not been clearly identified. Moreover, it is not clear whether the same mechanisms are used for all types of cargo (Nakamura *et al.*, 2018). M cells express on their surface Dectin-1 and Siglec-F, which can serve as sIgA receptors for sIgA-opsonized luminal antigen transcytosis (Rochereau *et al.*, 2013). In the SED these sIgA-coated antigens are taken up by $CX3CR1^+$ cells, i.e., LysoDC and/or LysoMac (Rochereau *et al.*, 2013).

ii. M cell microvesicle shedding: M cell-derived microvesicles (MCM) containing cytoplasmic content are constitutively shed into the SED (Sakhon *et al.*, 2015). Thus, MCM are likely more important for delivering soluble antigens entering the M cell cytoplasmic compartment. Once released by M

cells, MCM are taken up by CX3CR1^{+}CD11b^{+}CD11c^{+} cells, i.e., LysoDC and/or LysoMac (Sakhon *et al*., 2015).

iii. Trans-M cell dendrites: The mucosal immune system can be aware of the presence of pathogens before they manage to penetrate the epithelial barrier through an early sampling mechanism. Protected by their antiviral and antibacterial profile, LysoDC indeed extend dendrites through M cell–specific transcellular pores to capture luminal antigens (Lelouard *et al*., 2012). This sampling mechanism involved the redistribution of the M cell adhesion molecules such as junctional adhesion molecule-A (JAM-A) and epithelial cell adhesion molecule (EpCAM) from the lateral borders to the site of transcellular migration without disturbing the tight junctions, thereby preserving the integrity of the epithelial barrier. Trans-M cell dendrites (TMD) recruit filamentous actin, which makes them highly motile facilitating an efficient scan of the M cell apical surface and of the gut luminal content. After antigen uptake, LysoDC retract back to the SED to encounter other actors of the immune response initiation. The accessibility to the M cell apical surface by TMD complement the transcytosis route and offer a quick and safe way of sampling (Lelouard *et al*., 2012).

iv. Dying M cell phagocytosis: During apoptosis, the cells expose PS on their surface as an 'eat me' signal for phagocytes. Dying M cells are indeed engulfed by LysoDC and LysoMac (Lelouard *et al*., 2010). The engulfment of M cell remnants could notably allow the capture of antigens previously sampled by M cells.

Interestingly, like LysoDC immature cDC2 can penetrate the FAE and strongly interact with M cells (Bonnardel *et al*., 2017; Kolesnikov *et al*., 2020). Therefore, immature cDC2 may also phagocyte antigens transferred by M cells. However, both *in vitro* and *in vivo* microparticle uptake assays showed a much more efficient phagocytic activity of LysoDC and LysoMac as compared to immature cDC2 (Lelouard *et al*., 2010; Bonnardel *et al*., 2015; Wagner *et al*., 2020). In addition, LysoDC and TIM-4^{-} LysoMac are involved in FAE apoptotic cell removal (Lelouard *et al*., 2010), uptake of MCM (Sakhon *et al*., 2015) and are the main cells involved in the uptake of pathogenic bacteria (Lelouard *et al.*, 2010; Disson *et al.*, 2018). They are both enriched in the SED and are the main phagocytes involved in the uptake of luminal particulate materials (Lelouard *et al*., 2010; Bonnardel *et al*., 2015; Wagner *et al*., 2020).

Overall, at steady state, luminal antigen uptake by PP occurs predominantly via M cells (Ohno, 2015; Nakamura *et al*., 2018; Kobayashi *et al*., 2019). Moreover, released antigens are then taken up mostly by LysoDC and LysoMac, which are both enriched in the SED and equally effective at internalizing particulate antigens (Lelouard *et al*., 2010; Bonnardel *et al*., 2015; Wagner *et al*., 2020). Degradation and presentation of these antigens by these or other phagocytes are then the initial crucial steps of the intestinal mucosal immune response initiation (Da Silva *et al*., 2017).

- Innate defense function

Whereas the FAE is permissive to pathogen entry, a strong protection is provided just below these entry points in the SED. This is highlighted by the strong expression of the antibacterial agent lysozyme by LysoDC and LysoMac. In addition, they express the virus restriction factor BST2 (Bone marrow stromal antigen 2) and their transcriptional profile shows a strong antibacterial and antiviral gene signature contrary to cDC profile (Bonnardel *et al*., 2015). Thus, LysoDC and LysoMac express several types of pattern recognition receptor (PRRs) genes. PRRs either recognize simple molecules known as pathogen-associated molecular patterns (PAMPs) or detect cellular damage signals also known as damage-associated molecular patterns (DAMPs). PAMPs are microbial elements that have been conserved during evolution, making them excellent targets for recognition. Some of these PRRs are transmembrane proteins, such as TLR and C-type lectin receptors (CLR), but other PRRs are cytoplasmic proteins, such as RIG-I-like receptors (RLR), ZBP1, STING and NOD-like receptors (NLR) (Murphy and Weaver, 2017). Among the latter, LysoDC express *Naip1*, *Naip2*, and *Naip5* coding receptors for the needle and inner rod proteins of the type III secretion system and for flagellin of pathogenic bacteria such as *Salmonella* Typhimurium, respectively (Vance, 2015; Da Silva *et al*., 2017). Upon recognition of their ligands, NAIP proteins form an inflammasome complex and recruit and activate caspase-1, resulting in cleavage and activation of the pro-inflammatory cytokines of IL-1β and IL-18 (Vance, 2015). In addition, detection of microbiota species by the CLR Mincle/Clec4e, which is mainly expressed by LysoDCs and LysoMacs, promotes their production of IL-23, followed by activation of ILC3s, leading to IL-22 production, barrier integrity strengthening and microbial translocation limitation (Martinez-Lopez *et al.*, 2019).

Most often, the first event that occurs upon pathogen detection is an increase of the sampling activity by recruitment in the FAE of $CD11c^+$ phagocytes, likely LysoDC and immature cDC2, and by formation of TMD (Chabot *et al.*, 2006, Chabot *et al.,* 2008; Anosova *et al.*, 2008, Lelouard *et al.*, 2012). Then, these phagocytes are thought to either prime B cells and induce their class switching in the SED

(Reboldi *et al.*, 2016) or migrate from the SED to the IFR in order to prime naive T cells (Wagner *et al*., 2020), as detailed below.

- Priming of B Cells

Even though, pDC can efficiently promote *in vitro* IgA class switch recombination independently of any T-cell or microbial stimulus, pDC depletion showed that pDC are dispensable for intestinal IgA production *in vivo* (Moro-Sibilot *et al*., 2016). B cells use the chemokine receptor CCR6 to access the SED and interact with subepithelial $CD11c^+CD11b^+$phagocytes, i.e. either cDC2 or LysoDC (Reboldi *et al*., 2016). The integrin αvβ8 expression by these phagocytes activates the TGFβ required for IgA class switching. Furthermore, these phagocytes express the lymphotoxin beta receptor (LTβR) and are maintained in the SED by the LTα1β2 provided locally by ILC. The SED is therefore a niche supporting phagocyte–B cell interactions needed for TGFβ activation and induction of mucosal IgA responses. However, the mechanisms leading to IgA class switching in the SED are just starting to be deciphered and their elucidation will require further investigation.

- Priming of T Cells

cDC have been long recognized as the most efficient professional antigen-presenting cells to initiate an antigen-specific immune response through the priming of naive T cells. Upon activation, cDC initiate a complex transformation process leading to migration to T cell zones, antigen presentation and naive T cell priming (Sichien *et al*., 2017). However, even without overt stimulation cDC mature and can upregulate the chemokine receptor CCR7 to migrate in the T cell zone. This steady state migration of non-stimulated mature cDC is believed to favor polarization of T cells toward tolerance profile. In PP most dome cDC already reside in the IFR, where naive T cells are. IFR contain mainly cDC1 and $CD11b^+$ cDC2 but also some $TIM\text{-}4^+$ LysoMac. It has been proposed that immature cDC2 are the main subset migrating from the SED to the IFR at steady state. Immature cDC2 may indeed acquire antigens either directly or by transfer from LysoDC or $Tim\text{-}4^-$ LysoMac and shortly after upregulate CCR7 and downregulate CCR6 to migrate from the SED to the IFR and become mature $CD11b^+$ (Bonnardel *et al*., 2017). This steady state migration of cDC2 could explain the underrepresentation of cDC2 in the upper part of the SED. By contrast, LysoDC seems not migrate in the IFR at steady state. Therefore, in absence of stimulation, they may be unable to

mount an adaptive immune response. This could help to protect the body from unwanted and/or excessive inflammation while maintaining the possibility of responding to important threats (Wagner *et al*., 2020).

In vitro, unlike LysoMac, both dome cDC and LysoDC are able to induce naive antigen-specific T helper cell proliferation. Both cDC1 and LysoDC prime naive antigen-specific T helper cells for IFNγ production. LysoDC also induce the production of IL-6, a property shared with cDC2 (Bonnardel *et al*., 2015). Only mature LysoDC are able to efficiently prime naive T cells *in vitro.* However, *in vivo* they require additional signals, such as those provided by TLR ligands, to undergo an activation process that leads to their migration from the SED to the peripheral region of the IFR, where they can encounter naïve T cells and where proliferation of helper T cells preferentially occurs upon stimulation (Wagner *et al*., 2020). Since TLR7 is strongly enriched in LysoDC and LysoMac as compared to cDC, its agonist R848 has been used to better understand their activation and their role in the initiation of this immune response (Bonnardel *et al*., 2017; Wagner *et al*., 2020). Upon R848 stimulation *in vitro*, unlike LysoMac, LysoDC increase the expression of MHCII, CD40 and CD86 and secrete IL-6 and TNF (Bonnardel *et al*., 2015). They also significantly increase their ability to prime naive T cells, inducing their proliferation and polarization toward a Th1 immune response.

Interestingly, 4h only after R848 stimulation *in vivo*, cDC2 of the DAV and of the SED start to express CCR7 (Fig. 10) (Wagner *et al*., 2020). This activation is indirect and depends on the production of TNF, likely by LysoDC, LysoMac and pDC (Bonnardel *et al*., 2017). $CCR7^{+}$ cDC2 from the DAV and the SED are thus massively recruited in the IFR, probably carrying sampled antigens. In parallel, like cDC1, they increase their MHCII and decrease their CD11c surface expression. Both also strongly increase their CD83, CD49d, CCL22 and CD86 expression in the IFR. At 8h post R848 stimulation *in vivo*, activated mature LysoDC in turn start to express CCR7 and to migrate from the SED to the IFR periphery. Moreover, they begin to express also CCL22, CD40, IL-12 p40 involved in attraction, co-stimulation and polarization of T cells, respectively. Indeed, activated migratory LysoDC strongly interact with T cells, some of which starting to proliferate and to express CD69, suggesting a role of LysoDC in T cell priming *in vivo* (Wagner *et al*., 2020).

Detection of some microbiota species by Mincle/Clec4e by LysoDCs fosters their IL-6 production and their ability to generate Th17 cells, thereby promoting the production of IL-17 and IL-22 known to contribute to intestinal barrier integrity (Martinez-Lopez *et al*., 2019). However, LysoDC migratory activity under such stimulation conditions has not been studied, yet and other phagocytes, such as cDC2 that express minimal levels of Mincle, may be involved as well.

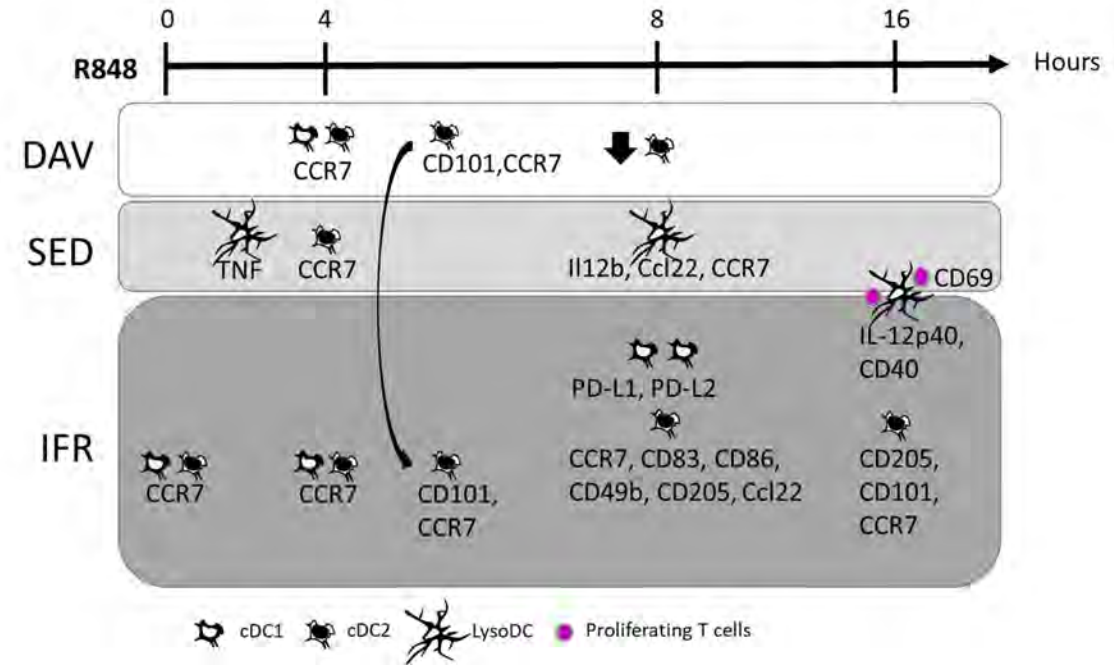

Figure 10: Upon R848 treatment, TLR7-activated LysoDC produce TNF that induces activation of cDC2 in the SED after 4h. One hour after, DAV cDC2 migrate to the IFR. At 9h in the IFR, cDC1 number increase and express PD-L1, PD-L2. CD11b^{+}cDC2 upregulate CD205, CCR7, Cd49b, CCL22, MHCII, CD83 and CD86. In the SED, LysoDC express CCR7, Il12p40 and Ccl22. At 16h, activated LysoDC migrate from the SED to the IFR periphery. In the IFR but not at the IFR periphery, cDC continue to express CD205, CD101, and CCR7. Abbreviations: DAV, dome-associated villus; FAE, follicle-associated epithelium; IFR, interfollicular region; SED, subepithelial dome. From Bonnardel *et al*., 2015; 2017; Wagner *et al*., 2020.

- Regulation of the adaptive immune response

The majority of B cells generated in the GC reaction do not achieve higher antigen affinity during the selection process and undergo cell death through apoptosis. These cells are cleared by the highly specialized TBM, which are the only phagocytes of the GC (Sobhon, 1971; Lelouard *et al*., 2010). A PS-binding protein known as milk fat globule epidermal growth factor 8 (MFG-E8) acts as a bridging molecule between the apoptotic cell and the TBM (Hanayama *et al*., 2006). The FDC produce large quantities of MFG-E8, which accumulate around their dendrites and drench the GC B cells, ensuring an instantaneous opsonization of dying B cells exposing PS on their surface. TBM scavenging function requires the expression of the apoptotic receptors MerTK and TIM-4. This clearance process is highly efficient and in healthy individuals, apoptotic cells within the GC can only be detected inside TBM (Aguzzi *et al*., 2014). The origin and lifespan of PP TBM remain unknown (Wagner *et al*., 2018).

In PP, both TIM-4$^+$ TBM and TIM-4$^+$ LysoMac could play a critical role in adaptive immune response regulation at the level of GC and IFR, respectively. Indeed, the IFR contains mainly TIM-4$^+$ LysoMac, some of which surrounding the IFR, forming border guards of the T cell zone (Bonnardel *et al*., 2015). TIM-4$^+$ LysoMac are located in a region of effector cell priming where they could participate to the clearance of dying T cells, like TBM participate in the clearance of dying B cells. TIM-4 contributes indeed to the control of the adaptive immune response and to tolerance through the removal of antigen-specific cells and its deficiency leads not only to hyperactivity of B cell but also of T cell (Rodriguez-Manzanet *et al*., 2010).

A-V/ Conclusions

The different subsets of the MPS present in the PP play different roles necessary to fulfill the initiation and regulation of the adaptive immune response. Their functions correlate with their anatomical localization. Figure 11 summarizes the origin, localization and microscopic shape of all phagocytes subsets with pie charts indicating the distribution of phagocyte subsets in the different regions of PP at steady state. However, a similar schema in inflammatory conditions is still lacking. Indeed, whereas the effect of a PP stimulation by a TLR7 ligand *in vivo* on the distribution and activation of these phagocytes has begun to be revealed, whether other conditions of stimulation give similar activation patterns remains unknown as well as the consequences of such activation of PP phagocytes on PP effector cells *in vivo*. Moreover, although PP are colonized with a specific microbiota termed Lymphoid-Tissue-Resident Commensal Bacteria (Obata *et al*., 2010; Sonnenberg and Artis, 2012) and although microbiota play a critical role in the development and education of the gut immune response (see second part below), very little is known about its influence on PP phagocytes. Influence of stimuli and microbiota on PP phagocytes are however critical points to understand for the design of therapeutic strategies aiming at: (i) developing efficient immune protection against enteropathogens, while avoiding deleterious inflammatory responses; (ii) correcting any imbalance in the microbiota/immune system relationship that could lead to diseases. During my thesis I worked on the characterization of the PP phagocyte response to two stimuli of the endosomal TLR7 and TLR9 pathways and develop a tool to study microbiota composition in different conditions.

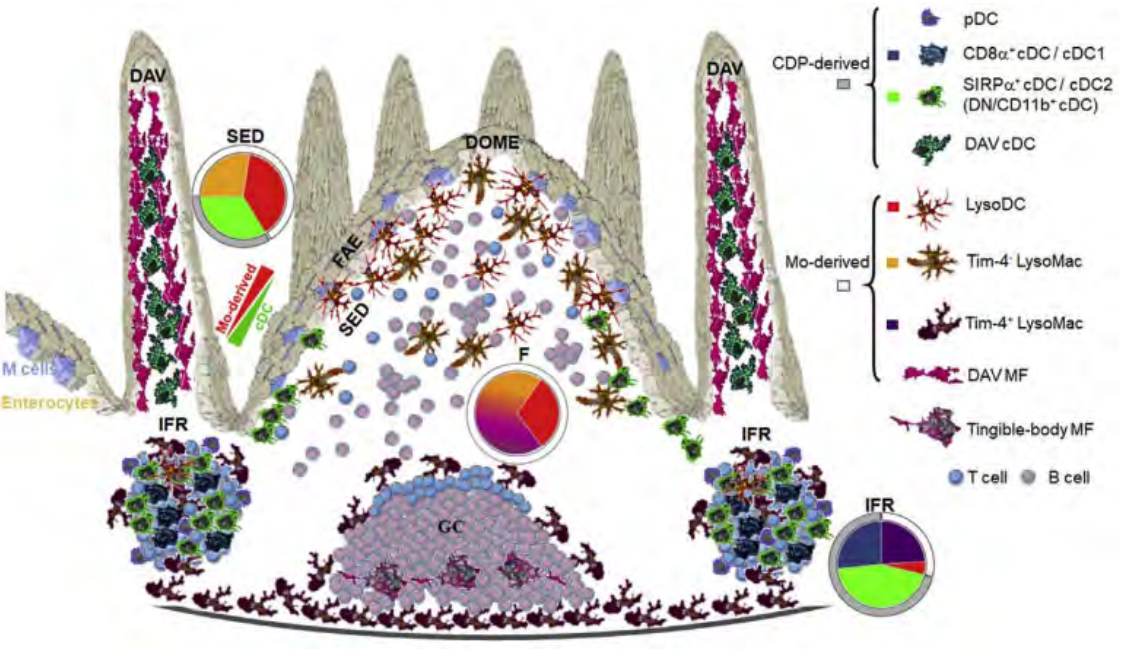

Figure 11: Anatomic localization of PP phagocyte subsets. Origin and shape of each PP phagocyte subset is displayed on the right. Color codes correspond to colors displayed in pie charts. The latter show in each region of the dome the distribution of PP phagocyte subsets. Abbreviations: CDP, common DC precursor; DAV, dome-associated villus; DN, double negative; F, follicle; FAE, follicle-associated epithelium; GC, germinal center; IFR, interfollicular region; MF, macrophages; Mo, monocyte; SED, subepithelial dome. From Wagner *et al*., 2018.

B-The microbiota and its influence on the intestinal immune system

Microbiome or microbiota is defined as “the ecological community of commensal, symbiotic, and pathogenic microorganisms that literally share our body space” (Lederberg and McCray, 2001). It is important to keep in mind that microbiome can also refer specifically to the genetic elements of the microbiota. The microbiota includes not only bacteria but also archaea, protists, fungi and viruses (DeLong and Pace, 2001). However, through this manuscript we will only focus on bacteria.

Education of our mucosal immune system early in life strongly influences adult health and the risk of developing non-communicable diseases such as allergies, asthma, obesity and inflammatory bowel diseases. This education strongly relies on mucosal surface colonization by the microbiota.

The mucosal immune system interacts with the microbiota continuously and in a bidirectional manner. The mucosal immune system has evolved to discriminate between noxious and harmless

environmental antigens. It can differentiate food and symbiotic microbiota from dangerous pathogens or toxins in order to mount an appropriate immune response (Russell *et al.*, 2015).

B-I/ Gut Microbiota composition

Hugon and collaborators identified 2172 species of bacteria from the whole body human microbiota (Hugon *et al*., 2015). These species are classified into 12 different phyla, of which 93.5% belonged to Proteobacteria, Firmicutes, Actinobacteria and Bacteroidetes (Fig. 12). Three of the 12 identified phyla contained only one species, including two intestinal species:

a) *Akkermansia muciniphila*, the only known representative of the Verrucomicrobia phylum.

b) *Victivallis vadensis*, which belongs to the Lentisphaerae phylum.

In addition, 386 of the identified species are strictly anaerobic, belonging mostly to the phylum Firmicutes and generally found in mucosal regions such as the oral cavity and the gut (Hugon *et al*., 2015).

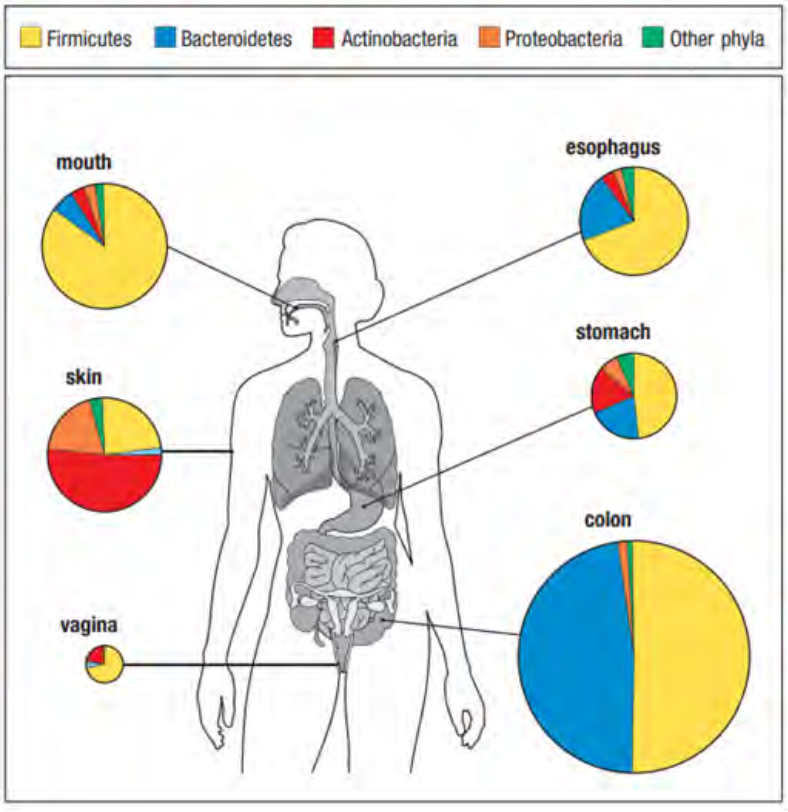

Figure 12: Composition of the microbiota at different mucosal surfaces in healthy humans. The different sizes of the pie charts for different sites reflect the number of distinct bacterial species typically present at those sites. Modified from Murphy and Weaver, 2017.

The gut is the most important reservoir of microorganisms in the human body and, despite extensive culturing and sequencing efforts, the bacterial repertoire of the human gut microbiota remains incomplete. However, the gut microbiota is not as diverse as the microbial communities from the rest of the body. In addition, the gut microbiota reveals a high degree of functional redundancy meaning that microbiota with different composition can share the same functionalities given by similar expressed genes, protein and metabolite profiles (Moya and Ferrer, 2016; Thursby and Juge, 2017).

The vast majority of the gut microbial community is composed of only five phyla: Bacteroidetes, Firmicutes, Actinobacteria, Proteobacteria and Verrucomicrobia. There is however an important diversity at the genus level. Key members of Firmicutes include the genera *Clostridium, Lactobacillus* and *Ruminococcus*, as well as the butyrate producers *Eubacterium, Faecalibacterium* and *Roseburia*. Members of Bacteroidetes include the genera *Bacteroides, Prevotella* and *Xylanibacter*, known to be efficient degraders of dietary fiber. *Bifidobacterium,* largely used as probiotic, is a major genus within Actinobacteria. Proteobacteria includes *Escherichia* and *Desulfovibrio*, whereas Verrucomicrobia so far includes only the mucus-degrading genus *Akkermansia* (Schroeder and Bäckhed, 2016).

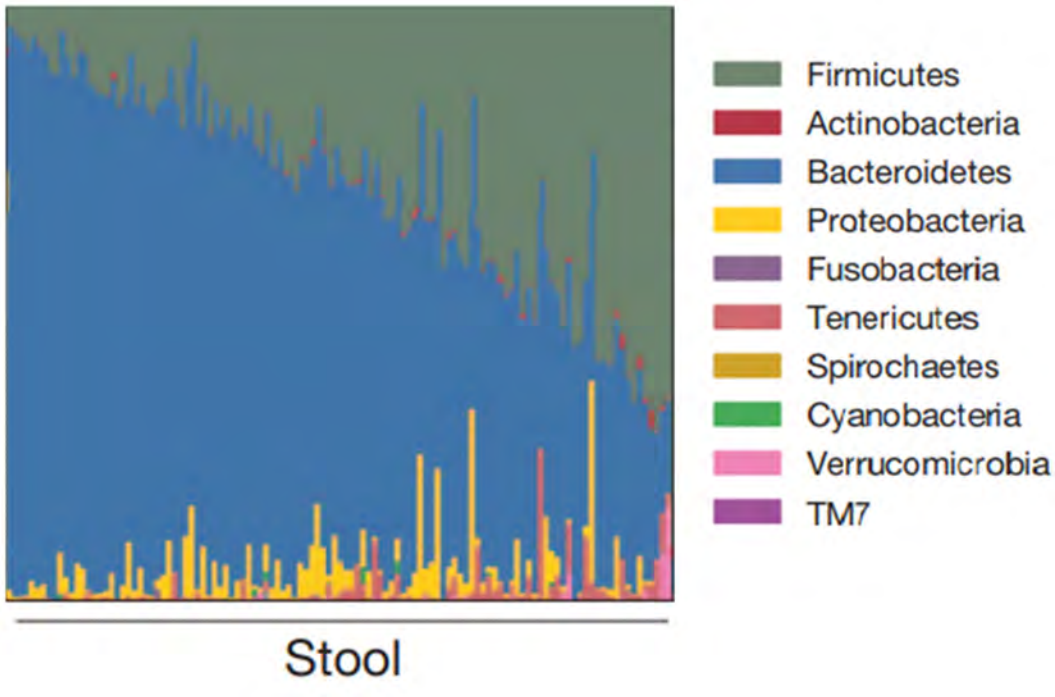

Figure 13: Composition of microbial taxa varies within a healthy population. HMP, 2012.

The Human Microbiome Project (HMP) is the largest study accounting 242 healthy individuals allowing to determinate different parameters of the diversity of the microbiota. The beta diversity corresponds to the differences between samples, e.g. intestinal bacteria shared or not by different people. The gut has an intermediate beta diversity in comparison to other mucosa such as oral cavity and vagina. In general, all the individuals present a majority of species from the phyla Firmicutes, Bacteroidetes, Proteobacteria, Verrucomicrobia and Actinobacteria but to different degree (Fig. 13). The uniqueness of each individual's microbiota seems to be stable over time, which seems specifically associated with health condition (The Human Microbiome Project Consortium, 2012). This stability is an important step in enabling prediction of disease states and developing therapies to correct dysbiosis.

In addition to the HMP, the Metagenomics of the Human Intestinal Tract (MetaHIT) (MetaHIT Consortium *et al*., 2010; MetaHIT Consortium *et al*., 2014) and the Human Gastrointestinal Bacteria Genome Collection (HGG) (Forster *et al*., 2019) have provided the most comprehensive view of the gut microbiota repertoire to date (Almeida *et al*., 2019). These extensive and well-characterized collections of reference genomes comprise samples mostly from healthy but also from patients suffering from inflammatory bowel disease (IBD), obesity and diabetes.

B-II/ Regulation of the gut microbiota by the mucosal immune system

The gut microbiota composition changes on both a transverse and longitudinal axis reflecting the physiological properties of each region (Tropini *et al*., 2017). These properties include chemical, nutritional and immunological gradients and have dynamic mutually reinforcing interactions. In a longitudinal level, the small intestine has typically high levels of acids, oxygen and antimicrobial compounds, and a short transit time as compared to colon. This hostile environment limits bacterial growth, meaning that only rapidly growing, facultative anaerobes that are able to adhere and form a biofilm with the epithelia or mucus can survive. In contrast, colonic conditions support a dense and diverse community of bacteria, mainly anaerobes that are able to metabolize the complex carbohydrates of undigested foodstuffs (Donaldson *et al*., 2016; Martinez-Guryn *et al*., 2019).

The intestinal immune response can also shape transversally the composition of the microbiota, mainly by the stratification and compartmentalization. As previously detailed, the physicochemical barrier avoids opportunistic invasion of host tissues. It includes mainly the production of mucus, AMPs and sIgA. The mucus composed by mucins creates a viscous gel-like layer that helps with the stratification. Mucus

can be also a source of nutrients for mucus-degrading microbiota species, such as *A. muciniphila*, found in the all the intestinal tract especially in the colon (Derrien *et al*., 2008; Geerlings *et al*., 2018). The AMPs are localized in the mucus layer and kill bacteria through disruption of the bacterial cell wall or inner membrane via enzymatic activity.

sIgA is secreted into the intestinal lumen at the rate of several grams per day. This isotype acts both to prevent infections and to maintain homeostasis of the commensal microbiota. Mucosal IgA preferentially targets surface antigens of intact bacteria, unlike systemic antibody responses that target both cytosolic and surface antigens. In general, the mucosal exposure trigger responses with a reduced B cell repertoire diversity as compared with systemic exposure (Li *et al*., 2020). sIgA can prevent or promote bacterial colonization, depending on the type and context of the interaction. The mechanisms by which sIgA can provide both positive and negative selection of the microbiota are not fully understood (Huus *et al*, 2021). Slow-growing bacteria form smaller clumps; these small aggregates could thus more successfully resist peristaltic flow and immune exclusion. Conversely, fast-growing bacteria quickly form large clumps that are unable to interact with the epithelium and are generally subject to immune exclusion. sIgA enhances aggregation and biofilm formation in bacteria forming “clonally enchained” clumps but it can also form mixed-species “random” clumps (Hoces *et al*., 2020).

Most commensals elicit strong TI responses, atypical commensals such as SFB evade TI responses and elicit TD IgA. Under homeostatic conditions, most small intestinal bacteria are IgA^+ while only 20% of colonic bacteria are IgA^+ (Bunker *et al*., 2015). IgA also targets immunogenic or invasive commensal fecal bacteria that can lead to intestinal disease or undernutrition (Palm *et al*., 2014; Kau *et al*., 2015). IgA regulates commensal community composition and gene expression, which is required for gut homeostasis and health. For example, $Foxp3^+$ T cells repress inflammation, regulate the IgA selection in GC and contribute to diversification of gut microbiota. On its side, the diversified and balanced microbiota facilitate the expansion of $Foxp3^+$ T cells creating a symbiotic regulatory loop (Kawamoto *et al*., 2014).

Many affinity-matured microbiota-reactive IgA clones bind to microbial structures shared across diverse bacterial taxa explaining cross-species reactivity. These surface structures; such as LPS, teichoic acid and extracellular capsules are rich in repetitive glycan motifs, offering significant potential for cross-species reactivity (Sterlin *et al*., 2019). It is important to keep in mind that cross-species reactivity is not associated with antibody polyreactivity (Pabst and Slack, 2020; Huus *et al*., 2021). For example, in both mice and humans, IgA binds to *Bacteriodetes thetaiotaomicron* via glycan–glycan interactions and enhances their association with host mucus. Mucus-associated bacteria induce Mucus-Associated

Functional Factor (MAFF) system expression and enhances its metabolic activity. MAFF system facilitates symbiosis with other members of the phylum Firmicutes and promotes protection from a chemically induced model of colitis (Nakajima *et al*., 2018).

Despite this protective barrier, even at homeostasis, some bacterial species from the microbiota are able to reach the intestinal epithelium. In healthy humans and mice, a core microbiota has been described for crypts and mucosa (Saffarian *et al*., 2019). Detected in the terminal part of the ileum of several species, SFB attach to epithelial cells of the PP FAE and of the tip of villi (Flannigan and Denning, 2018), thereby strongly influencing intestinal immunity as described below.

B-III/ Microbiota shapes the immune system and the host metabolism

One of the most appreciated benefits to the host of the gut microbiota comes from bacterial metabolites, which are important for both systemic and intestinal development of the host. Anaerobic bacterial fermentation produces several metabolites including bile acids, lipids, amino acids, vitamins, and short-chain fatty acids (SCFA). SCFA-producing colonic bacteria and certain types of colonic Clostridia, as well as ileal SFB, are critical in shaping the host immune balance in mice (Kasubuchi *et al*., 2015). For example, SCFA especially butyric acid, facilitate the induction and expansion of $Foxp3^+$ T cells in gut (Arpaia *et al*., 2013).

Apart from their metabolic role, the microbiota is important for immune response induction and homeostasis. In germ-free mice, GALT presents abnormalities, such as fewer and smaller PP and no formation of ILF. In addition, numbers of villus effector cells are decreased, including the $CD8^+$ IEL, the LP $CD4^+$ T cells (both Th17 and Treg) (Niess *et al*., 2008). Additionally, germ-free mice have a low secretion of AMPs, decreased mucus thickness, extremely reduced activation of germinal centers in PP and thus very limited production and secretion of IgA (Parker *et al*., 2018). The absence of gut microbiota leads also to functional alterations in immune and intestinal epithelial cells, which express less TLR and MHC II molecules for antigen presentation (Spiljar *et al*., 2017). Commensal bacteria can influence ILC development and functional potential indirectly through myeloid or epithelial cell populations. In addition, signals derived from commensal bacteria may substantially impact the function of ILC, such as NK cell cytolytic and IFNγ responses. However, more studies are required to clarify the mechanisms by which commensal microbiota influences ILC responses (Sonenberg and Artis, 2012).

Intestinal colonization induces a range of T cell functions and simultaneously stimulates T cells of Th17 but also Th1, Th2, and regulatory cell phenotype. These phenotypes can be induced by SFB (Gaboriau-Routhiau *et al*., 2009). So, SFB trigger Th17 cell differentiation and its accumulation in the LP and correlate with increased expression of genes associated with inflammation and anti-microbial defenses, resulting in enhanced resistance to the intestinal pathogen (Ivanov *et al*., 2009). This bacterium is also a potent inducer of mucosal IgA by stimulating the development of GC. In absence of PP, SFB stimulate the development of ILF allowing the induction of intestinal IgA and SFB-specific Th17 responses (Lécuyer *et al*., 2014). Furthermore, SFB through differentiation and egress of PP TFH cells into systemic sites exacerbate arthritis. This is an example of how gut microbiota remotely regulated a systemic disease (Teng *et al*., 2016). *Alcaligenes* species, specifically inhabit PP and ILF and affect the development and maturation of the host mucosal immune system. Specific IgA may play a critical role in the PP tissue colonization by these bacteria. They are also known to express nitric oxide (NO) reductase and reduce NO, which was reported to up-regulate IgA class-switch recombination (Obata *et al*., 2010).

Interestingly, exposure to microbes during a temporal window appears critical for the development of a balanced immune system. A growing literature demonstrates that bacteria and their products modulate the development of the immune system during the neonatal period by a succession of non-redundant phases, with long-term consequences on immune reactivity and immunopathology (Hornef and Torow, 2019). This period termed as “window of opportunity” allows an important host-microbe cross-talk. For instance, mice treated with antibiotics or inhibitors of antigen transcytosis through the epithelium before weaning, but not after, and GF mice colonized with microbiota after weaning but not before, develop increased susceptibility to allergy and IBD in adulthood (Nabhani and Eberl, 2020). This ‘‘weaning reaction’’ allows intestinal microbiota to induce the generation of RORγt^{+} regulatory T cells which require bacterial and dietary metabolites (RA and SCFA) and are essential to prevent pathological imprinting (Nabhani *et al*., 2019).

B-IV/ Disease and dysbiosis

A broad spectrum of human diseases has been related to gut microbiota ranging from intestinal immune-mediated disease to neuropsychiatric and metabolic disorders. Gastrointestinal dysbiosis might be a secondary consequence of gastrointestinal inflammation or it might directly contribute to the

pathogenesis (Nagao-Kitamoto *et al*. 2016). The causal or consequence link remains debatable due to lack of direct evidence and mechanistic details (Kho and Lal, 2018). Different dysbiosis have being associated for each disease, table 2 summarizes the changes in the composition of the gut microbiota.

Table 2: Gut Microbiota associated human diseases and their respective dysbiotic features.

Category	Disease	Changes in microbiota	Reference
Immune mediated disease	Inflammatory bowel disease	Bacteroidetes ↓ Firmicutes ↓ Proteobacteria ↑ Actinobacteria ↑	Spor *et al*., 2011 Peterson *et al*., 2008
	Type 1 Diabetes*	Bacteroidetes ↑ Firmicutes ↓ Actinobacteria ↓ F/B ↓	Leiva-Gea *et al*., 2018 Murri *et al*., 2013
Metabolic disease	Obesity	Bacteroidetes ↓ F/B ↑	Ley *et al*., 2005
	Type 2 Diabetes	Firmicutes ↓ Bacteroidetes ↑ Proteobacteria ↑	Larsen *et al*., 2010
	Hypertension	F/B ↑	Yang *et al*., 2015
Infectious disease	Clostridium difficile associated disease	Bacteroidetes ↓ Firmicutes ↓	Khoruts et al., 2010
Neuro-psychiatric disease	Autism spectrum disorder*	Bacteroidetes ↑ Proteobacteria ↑ Actinobacteria ↑ F/B ↑	Iglesias-Vázquez *et al*., 2020
Other	Necrotizing enterocolitis*	Firmicutes ↓ Proteobacteria ↑	Spor *et al*., 2011 Wang *et al*., 2009
	Chronic kidney disease	Firmicutes ↑ Proteobacteria ↑ Actinobacteria ↑	Vaziri *et al*., 2013

*Studies perform in a pediatric population; F/B, Firmicutes to Bacteriodetes ratio.

The *Firmicutes* to *Bacteroidetes* ratio is considered of great importance for human gut microbiota composition analysis. An increase in the ratio of Firmicutes to Bacteroidetes (F/B) has been reported to be

associated with various pathological states but this ratio can be also affected by age or a vegetarian diet (Liang *et al*., 2018). In addition, the most consistent and robust ecological pattern observed during gut dysbiosis is an expansion of facultative anaerobic bacteria belonging to the phylum Proteobacteria (Shin *et al*., 2015). This expansion of facultative anaerobic bacteria is driven by an increase of oxygen availability during intestinal inflammation due to endothelial dysfunction (Litvak *et al*., 2017). It has been proposed that an increased prevalence of Proteobacteria is a potential diagnostic signature of dysbiosis and risk of disease (Shin *et al*., 2015).

Transplantation of a foreign gut microbiota has proven to be a valuable tool in the treatment of certain diseases by restoring a healthy microbial community (Khoruts *et al*., 2010). Fecal transplantation is considered to be the best available treatment for recurrent *Clostridium difficile* infection (Schroeder and Bäckhed, 2016). These transplant experiments support the hypothesis that changes in the microbiota are a driving force in disease progression (Clemente *et al*., 2012).

Probiotics and prebiotics have also been used as treatment or prophylaxis for dysbiosis. Probiotics are live microorganisms that can confer a health benefit on the host; e.g. lactobacilli, bifidobacteria, and other lactic acid-producing bacteria. Prebiotics are substrates selectively used by microbiota conferring a health benefit. They may also assist to correct compositional imbalance through promoting the growth of under-represented species (Cunningham *et al*., 2021).

B-V/ Conclusion

Our understanding of gut microbiota regulation is still at a very preliminary stage. However, this is of critical importance given its role in the health status of individuals and in the development of non-communicable diseases. More large-scale longitudinal studies are necessary to better assess subject-specific variations of microbiota. Methodological limitations, such as difficulties to reliably identify bacteria and recognize new species diversity but also to isolate and cultivate organisms by conventional microbiological methods, are a hindrance to increase this knowledge. Future applications of microbiota-based disease diagnosis, prognosis, monitoring, prophylaxis and treatments could potentiate and revolutionize the current measures in disease management and treatment (Kho and Lal, 2018). Thus, analysis of fecal microbiota composition is a valuable tool and could serve as a biomarker for several diseases.

RESULTS

A) Analysis of maturation and activation of Peyer's patch phagocytes *in vivo*

A-I/ Introduction

As previously described, PP are major sentinel and immune inductive in the small intestine. Sampling of antigens and the initiation of an appropriate immune response rely mostly on the mononuclear phagocytes that encompass several cell populations with different but complementary roles (Da Silva *et al*., 2017). Thus, cDC2, LysoDC and LysoMac are all located in the SED but the latter two alone represent two-third of SED phagocytes with increasing ratio in the upper part of the dome where most of the antigen sampling occurs. Moreover, they display the highest phagocytic activity among PP phagocytes and, due to strong innate defense mechanisms, represent the first line of defense below the FAE (Bonnardel *et al*., 2015).

At steady state, whereas cDC2 migrate continuously from the SED to the IFR during their maturation process, LysoDC reside mostly in the SED and therefore do not encounter naïve T cell from the IFR. However, upon stimulation with TLR7 ligand R848 they start to express CCR7 and migrate in the IFR where the T cell priming occurs (Wagner *et al*., 2020). Therefore, it is crucial to study the transcriptional profile of PP phagocytes in vivo at steady state but also after activation with different stimuli to fully understand their role in inducing the immune response in different contexts.

Although the transcriptional profile of LysoDC has been recently obtained at the single cell level (Wagner *et al*., 2020), a similar high-resolution view of the whole PP MPS is still lacking at steady state. Since TLR7 is strongly enriched in LysoDC and LysoMac as compared to cDC, its agonist R848 has been used to better understand their functions and activation profile (Bonnardel *et al*., 2017; Wagner *et al*., 2020) but a complete transcriptional profile of all R848-activated phagocytes is lacking. Moreover, the consequences of PP stimulation by other stimuli have not been characterized so far, as well as the consequences of such activation of PP phagocytes on PP effector cells *in vivo*. For these reasons, we characterized in this study the transcriptional profiles of cDC1, cDC2, LysoDC and LysoMac at steady state and after stimulation with R848 and CpG, a TLR9 ligand with broad expression in phagocytes. Additionally, we evaluated the B and T cell responses in each context to better understand the role of phagocytes in the initiation of the adaptive immune response.

Analysis of maturation and activation of Peyer's patch phagocytes *in vivo*

Cynthia Arroyo Portilla[1,2], Romain Fenouil[1], Cécilia Luciani[1], Camille Wagner[1], Margaux Lagier[1], Fanny Hidalgo[1], Julie Tomas[1], Lionel Spinelli[1], Jean-Pierre Gorvel[1] and Hugues Lelouard [1]

1 Aix Marseille Univ, CNRS, INSERM, CIML, Marseille, France.

2 Departamento de Análisis Clínicos, Facultad de Microbiología, Universidad de Costa Rica, 11501-2060 San José, Costa Rica.

Contact: Hugues Lelouard, Centre d'Immunologie de Marseille-Luminy, Marseille, 13288, France. Phone: + 33 4 91 26 94 16; Fax: + 33 4 91 26 94 30; e-mail: lelouard@ciml.univ-mrs.fr

Running title: Activation profile of Peyer's patch phagocytes

Among secondary lymphoid organs, Peyer's patches (PP) have the unique property to combine both antigen sampling and adaptive immune response sites. They therefore offer the opportunity to study the whole phagocyte differentiation and activation processes in a single tissue. Here, we deciphered the transcriptional and spatiotemporal landscape of all PP phagocyte populations from their arrival in the tissue to their final maturation state at homeostasis and with two types of *in vivo* activation, involving the endosomal TLR 7 and 9. As expected, stimulus type and subset identity imprint the activation profile of dendritic cells (DC), thus orientating the immune response. We showed that the activation profile of the monocyte-derived dendritic cells termed LysoDC diverge even more from that of macrophages upon activation with upregulation of typical cDC molecules such as CCR7 and downregulation of typical monocyte-derived cells molecules such as CX_3CR1. We determined sets of genes that distinguish cDC from monocyte-derived DC in all tested conditions and disqualified others. Finally, taking advantage of the Peyer's patch interfollicular region ability to host both villus and subepithelial dome emigrated cDC, we showed that the initial residence site of cDC shapes their future activation profile. Altogether, our study underscores the importance of targeting not only the right phagocyte subset but also the right place at the right time to orientate the immune response.

Introduction

Peyer's patches (PPs) are the main immune inductive sites of mammal small intestine (Jung et al., 2010). Comprising several B cell follicles forming domes at the surface of the mucosa interspersed with dome-associated villi (DAV) above interfollicular regions (IFRs) enriched in naïve T cells, PPs excel in the generation of the antigen-specific IgA-secreting cells that populate the villus lamina propria (Craig and Cebra, 1971; Reboldi and Cyster, 2016). Notably, PPs have to distinguish pathogens from the vast majority of innocuous antigens derived from food and microbiota. This specific detection of pathogens and the initiation of an appropriate immune response rely on a complex network of specific mononuclear phagocytes that encompass several cell populations with different but complementary roles (Da Silva et al., 2017). Like in most other tissues, three main families of phagocytes have been documented in PPs: plasmacytoid dendritic cells (pDCs), conventional DCs (cDCs) and monocyte-derived phagocytes. However, each of these families seems to possess specificities that are unique to PPs. Thus, the pDCs mainly located in the IFRs of PPs lack the typical type I interferon production ability of pDCs (Contractor et al., 2007; Da Silva et al., 2017). Among cDCs, the type 1 cDCs (cDC1s) that express CD8a, XCR1 and Clec9A are mainly located in the IFRs (Becker et al., 2014) whereas type 2 cDCs (cDC2s) are located both in the IFRs and in the lower parts of the subepithelial dome (SED) (Bonnardel et al., 2017; Da Silva et al., 2017). Importantly, all cDC2s express SIRPα but form a very complex and heterogeneous population, likely due to both their differentiation state and their dual location. Thus, immature cDC2s lack CD11b expression but express the chemokine receptor CCR6 that favors their addressing to the SED whereas mature cDC2s express CD11b, increase the surface expression of major histocompatibility complex of class II (MHCII) and of the chemokine receptor CCR7 that promotes their migration to the IFRs (Bonnardel et al., 2017). In addition, half of the PP $CD11b^{+}$

cDC2s express lysozyme M, normally expressed by monocyte-derived phagocytes (Bonnardel et al., 2017). The latter comprise both macrophages termed LysoMacs and dendritic cells termed LysoDCs (Bonnardel et al., 2015b). LysoDCs are mainly located in the SED whereas LysoMacs are present both in the SED and in the IFR. Additionally, LysoDCs and LysoMacs are the only phagocyte subsets present in the follicles. LysoDCs and LysoMacs share many functional properties, such as high phagocytic activities and strong innate defense mechanisms (Bonnardel et al., 2015a). Thus, they represent the first line of defense below the follicle-associated epithelium (FAE) that contains the specialized epithelial cells termed M cells in charge of transporting antigens from the lumen to the SED. Interestingly, LysoDCs cooperate with M cells to perform their antigen sampling function by extending dendrites through M cell-specific transcellular pores (Lelouard et al., 2012). Moreover, unlike subepithelial LysoMacs, LysoDCs are able to express CCR7, to migrate in the IFR and to prime naïve helper T cells upon stimulation (Wagner et al., 2020). Importantly, only fully mature LysoDCs prime naïve helper T cells but only when activated are they able to express CCR7 and to migrate in the IFRs where naïve T cells reside, indicating that the priming activity of LysoDCs is tightly regulated *in vivo* and rely on the sensing of a stimulating agent (Wagner et al., 2020). In addition, when stimulated by the complement fragment C5a, LysoDC can cross-present antigens to elicit an antigen-specific $CD8^+$ T cell response (Kim et al., 2021).

In addition to the cDCs and monocyte-derived phagocytes located in SED, follicle and IFRs, there are cDCs and macrophages residing in DAVs that strongly resemble those of conventional villi (Da Silva et al., 2017). For simplicity, all phagocytes located in the SED, follicle or IFR will be referred to as dome phagocytes as opposed to phagocytes located in the DAVs. Interestingly, the activation kinetics of LysoDC and cDCs *in vivo* are different, indicating that the immune response in PP is initiated by a well-orchestrated succession of events operated in precise time windows

(Wagner et al., 2020). However, only TLR7 stimulation of PP has been performed so far and the process of activation of all PP phagocyte populations in different stimulation conditions and how this could lead to different responses has not been determined. Here, we investigated the transcriptional profiles of the different PP phagocyte populations at homeostasis and upon stimulation *in vivo* with ligands of the two endosomal TLRs TLR7 and TLR9.

Results

Steady state scRNAseq analysis of Peyer's patch CD11c^{hi} phagocytes identifies the minimal gene signature that distinguishes mouse monocyte-derived DCs from cDCs.

Although the transcriptional profile of LysoDCs has been recently obtained at the single cell level (Wagner et al., 2020), a similar high-resolution view of the whole CD11c^{hi}MHCII^{+} phagocyte system of Peyer's patch is still lacking. We sought to isolate PP CD11c^{hi}MHCII^{+} phagocytes and used single cell mRNA sequencing (scRNAseq) to analyze their transcriptional profiles. Since SIRPα^{+} cDC2s represent about 60% of PP phagocytes (Bonnardel et al., 2017), we decided to discard half of them (see figure S1A and Table S1) to allow a good representativeness of other subsets (cDC1s, LysoDCs and LysoMacs).

On the uniform manifold approximation and projection (UMAP) embedding of the data, a small isolated cluster and three groups of several clusters were identified (Figure 1A). The first group consisted of monocyte-derived cells and expressed specifically *Mafb*, *Cx3cr1*, *Mertk* and *Msr1* (Figure 1B). In line with previous reports (Bonnardel et al., 2017; Wagner et al., 2020), monocyte-derived cells represented 28% of total PP phagocytes. They globally expressed less ribosomal protein genes but more genes and transcripts than the other groups (Figure 1A). As expected from the atypical nature of PP monocyte-derived cells and from their lack of Fcγ receptor I/CD64

expression (Wagner et al., 2018), *Fcgr1* was not detected in any cluster but another Fcγ receptor gene *Fcgr3* was strongly expressed by all monocyte-derived cells (Figure S1B). PP monocyte-derived cells are also known for their strong expression of lysozyme and Bst2 (Bonnardel et al., 2015a), which genes (*Lyz1*, *Lyz2* and *Bst2*) were indeed strongly enriched in this group although expressed by the other phagocytes (Figure 1B and S1B). PP monocyte-derived cells also strongly expressed *Csf1r,* encoding the receptor for the cytokine CSF1 involved in monocyte-derived cell differentiation and survival (Figure 1B). In line with their key role in particulate antigen phagocytosis (Bonnardel et al., 2015a; Lelouard et al., 2012; Lelouard et al., 2010; Wagner et al., 2020), monocyte-derived cells specifically expressed the gene involved in the phagocytic cup formation *Gas7* (Hanawa-Suetsugu et al., 2019) (Figure S1C). Moreover, they were strikingly enriched for lysosomal machinery genes, such as those encoding the lysosomal-associated membrane proteins LAMP1 and LAMP2 and the lysosomal proteases involved in antigen degradation, cathepsin A, B, C, D, F, L, S and X (Figure S1C). Finally, the gene encoding cystatin F (*Cst7*), a regulator of cysteine cathepsin activity, especially cathepsins L, S and X, was upregulated in monocyte-derived cells (Figure S1C).

Monocyte-derived cells consisted of two main clusters corresponding to LysoDCs and LysoMacs. As expected, LysoDCs expressed much higher levels of MHCII presentation pathway encoding genes (e.g. *H2-Ab1* and *H2-DMb2*) whereas LysoMacs specifically expressed *Cd4* (Figure 1C). LysoMacs have been shown to strongly express some complement machinery genes as compared to LysoDCs (Bonnardel et al., 2015a). Among PP phagocytes, LysoMacs indeed specifically expressed *C2* and *C3* (Figure 1C). As previously reported (Wagner et al., 2020), unlike LysoMacs, most LysoDCs expressed *Emb* encoding for embigin (Figure 1C). Moreover, LysoDCs were enriched in *Ccr2* expression (Figure 1C), the chemokine receptor known to be crucial for their

recruitment in PP (Bonnardel et al., 2015a). As previously suspected (Da Silva et al., 2017), LysoDCs but also part of LysoMacs, were also the main producer of *Il22ra2* (Figure 1C) that encodes for IL-22BP, an inhibitor of IL-22 signaling that promotes antigen uptake in PP (Jinnohara et al., 2017).

The two other groups and the small cluster of cells consisted of cDC subsets and were characterized by specific expression of *Zbtb46*, *Flt3*, *Btla*, *Kit, Anpep, Kmo* and *Spint2* although *Btla* and *Kit* were only weakly or not expressed in the small cluster (Figure 1D). Many genes of the "so-called" cDC gene signature (Miller et al., 2012), such as *Amica1, Ass1, Bri3bp, Cbfa2t3, Cnn2, Pstpip1*, *Traf1* and genes of the MHCII presentation pathways, were enriched in cDCs but also expressed by LysoDCs, the closest monocyte-derived phagocytes to cDCs in mice (Figure S1D). Other genes of this signature, such as *Adam19*, *Adgrg5*, *Dpp4, Fgl2, Gpr68, H2-Q6, Napsa, Runx3* and *Tbc1d8*, even failed to discriminate cDCs from all monocyte-derived cells (Figure S1D). Actually, we could confirm by flow cytometry that the recently proposed cDC specific marker CD26 (Bosteels et al., 2020; Scott et al., 2015) encoded by *Dpp4* was expressed by both LysoDCs and LysoMacs in addition to cDCs (Figure S1E). Therefore, CD26 is unable to distinguish cDCs from monocyte-derived cells in PPs and should not be considered anymore as a specific cDC marker, at least in PPs. Finally, of the initial cDC signature, only *Anpep, Ap1s3, Bcl11a, Btla*, *Ccr7, Flt3*, *Gpr82*, *Gpr132*, *Hmgn3*, *Kit, Klri1, Kmo*, *P2ry10*, *Rab30*, *Sept6, Spint2* and *Zbtb46*, showed a strict specificity for cDCs in PPs, among which only *Anpep*, *Flt3*, and *Spint2* displayed an almost equal distribution among all cDC clusters (Figure 1D and S1D). However, although absent from PP monocyte-derived cells, CD13 encoded by *Anpep* is known to be expressed by monocyte-derived cells in other tissues, especially under inflammatory conditions.

The prominent cDC group and the small isolated cluster, representing altogether 65% of total PP phagocytes, shared many genes with monocyte-derived cells, such as *Sirpa* and *Csf1r*, indicating

that they were cDC2s (Figure 1B and 1E). As expected from previous studies (Bonnardel et al., 2015a; Bonnardel et al., 2017; Wagner et al., 2020), they also shared *Emb*, *Clec4a4* and *F11r* expression with LysoDCs but not LysoMacs (Figure 1B and 1E). However, gene expression of the recently described PP cDC2 marker EpCAM (Bonnardel et al., 2017) was specific of all cDC2 clusters but one and was not shared with any other PP phagocyte clusters (Figure 1E). Unexpectedly, we also found that the gene encoding S100a4, a protein involved in M cell maturation initially thought to be expressed mainly by PP LysoDCs, LysoMacs and type 3 innate lymphoid cells (Kunimura et al., 2019), was mostly expressed by the prominent cDC2 cluster (Figure 1E). In line with previously published flow cytometry and microscopy results (Bonnardel et al., 2017), the CD11b gene *Itgam* was expressed at very low levels by few cDC2s of the prominent cDC2 group as compared to LysoDCs, suggesting a very transient expression of this integrin in PP cDC2s. However, *Itgam* was expressed at high levels by cDC2s of the small isolated cDC2 cluster. Since CD11b is known to be strongly expressed by both LysoDCs and DAV cDC2s as compared to SED and IFR cDC2s (Bonnardel et al., 2017), we hypothesized that this small isolated cluster consisted of DAV cDC2s. The latter but not dome cDC2s are known to express CD101 (Bonnardel et al., 2017). *Cd101* was indeed specifically expressed by the small isolated cluster, confirming that it was made up of DAV cDC2s.

The minor cDC group (7 % of total PP phagocytes) consisted of cDC1s expressing typical marker genes, such as *Xcr1*, *Clec9a*, *Cd8a*, *Cadm1*, *Tlr3* and *Clec12a* (Figure 1F). The transcription factor involved in cDC1 commitment, *Irf8*, was also enriched in this group, but expressed by monocyte-derived cells, too.

Transcriptional profile and differentiation pathways of dome cDC2 *in vivo*.

We next perform subclustering of each group of phagocytes to study in further details their transcriptional profile and differentiation pathways as previously done for LysoDCs (Wagner et al., 2020). Dome cDC2s were split into 5 clusters whereas DAV cDC2s were represented by only one small cluster (8.6 % of total cDC2; Figure 2A). In addition to *Cd101*, the latter was notably distinguished from dome cDC2 clusters by its expression of *Apol10b*, *Cd209b*, *Cxx1b, Gp2*, *Mgl2*, *Siglecf* and of the transcription factor *Runx1* (Figure 2B and S2A). We could indeed demonstrate by flow cytometry the specific expression of CD209b (SIGNR1) by nearly half of small intestinal villus CD101$^+$ cDC2s but not by dome cDC2s, further confirming the identity of this cluster as DAV cDC2s (Figure 2C). By contrast, all dome cDC2 clusters but not DAV cDC2s expressed *S100a4*, suggesting that the latter could represent the first specific reliable marker of dome cDC2s (Figure 2D). We could indeed confirm by microscopy the specific expression at the protein level of S100a4 by both SED and IFR cDC2s (CD11c$^+$SIRPα$^+$CX3CR1$^-$ phagocytes) but not or weakly by DAV cDC2s or monocyte-derived cells (CD11c$^+$SIRPα$^+$CX3CR1$^+$ phagocytes) (Figure 2E and S2B). In line with their role in M cell maturation (Kunimura et al., 2019), subepithelial S100a4$^+$ cDC2s were enriched in the crypts and at the base of the dome where immature M cells lies (Figure 2E). Moreover, they interacted with and penetrated the FAE specifically at this location. Nevertheless, their number rapidly decreased in the upper part of the SED where monocyte-derived cells became largely predominant (Figure 2E). We next sought to identify mature cDC2s based on the expression of typical cDC maturation marker genes, such as *Ccr7*, and found that they represented 16.5 % of total cDC2s (Figure 2A and 2F). Interestingly, some genes, such as *Socs2* and *Nudt17*, were likely late maturation markers as they were restricted to a small distal area of the mature cDC2 cluster whereas others, such as *Ccr7*, *Cd83* and *Gadd45b*, were likely early maturation markers and showed a more diffuse expression pattern with a gradient expression that

probably reflected the maturation path of cDC2s (Figure 2F and S2C). The proliferative cDC2 cluster defined by expression of typical proliferation marker genes, such as *Mki67*, *Birc5*, *Ccne1*, *Ccnb2* and *Mcm7* was located in the UMAP at the exact opposite to mature cDC2s and represented 5.4 % of total cDC2s (Figure 2A, 2G and S2D). We previously showed that surface expression of CD24 decreased while that of JAM-A increased upon maturation of dome cDC2s (Bonnardel et al., 2017). *F11r* encoding JAM-A was indeed expressed in the mature cDC2 cluster as well as by another nearby cluster, likely an intermediate state of maturation representing 27.7 % of total cDC2s (Figure 2A and 2H). By contrast, *Cd24a* was expressed by all cDC2s except mature ones (Figure 2H).

Recently, a cDC2 subset specific to cryptopatches and isolated lymphoid follicles (ILFs) was characterized by its expression of lysozyme M, IL22-BP and PLET1 (Guendel et al., 2020). We previously showed that half of $CD11b^+$ cDC2s actually express lysozyme M in PP (Bonnardel et al., 2017). Moreover, some dome cDC2s also express PLET1 (Wagner et al., 2020). To determine whether these lysozyme M-expressing $CD11b^+$ dome cDC2s are similar to those present in ILFs, we examined the expression of ILF cDC2 key genes in our dataset. We indeed found that the cDC2 cluster that expressed the highest levels of *Lyz2* encoding lysozyme M also expressed *Il22ra2* and *Plet1* and corresponded to the intermediate maturation cluster identified above (figure 2I). Moreover, this cluster was also enriched for genes specifically expressed by ILF and cryptopatch cDC2s, such as *Tgfbi*, *Mmp12*, *Il1rn*, and *Pla2g7* (Figure S2E), suggesting that the specific pattern of gene expression observed in cDC2s of ILFs and cryptopatches can actually be generalized to all gut-associated lymphoid tissues (GALTs). However, *Plet1* and *Pla2g7* were expressed at similar levels by DAV and dome cDC2s, suggesting that these two genes may not be fully specific of GALTs. Finally, we checked whether ILFs and cryptopatches cDC2s expressed the dome cDC2 specific marker S100a4. Indeed, we observed that many $CD11c^+$ cells of cryptopatches and ILFs

expressed S100a4 (Figure S2F), confirming the strong similarity between ILF/cryptopatch cDC2s and PP dome cDC2s, validating their common denomination as GALT-specific cDC2s expressing S100a4. Mature cDC2 genes showing diffuse expression pattern, i.e. *Ccr7*, *Cd83* and *Gadd45b*, started to be expressed in this GALT-specific cDC2 cluster whereas some GALT-specific cDC2 genes, such as *Il1rn*, *Pla2g7*, *IL22ra2* and *F11r* were expressed by mature cDC2s, indicating that the GALT-specific cDC2 gene signature represents and intermediate maturation state imprinted by the GALT microenvironment (Figure 2E, 2G, 2H and S2E). Interestingly, this signature shows high similarities with LysoDC transcriptional profile, including expression of *Csf1r*, *Lyz2*, *Il22ra2* but also of *Tgfbi* and *Pla2g7* (Figure S2E). However, expression of these genes was much higher in LysoDCs than in GALT-specific cDC2s (Figure 1B, 1C, S1B and S2G).

The proliferative cluster and part of its two closest neighbours expressed *Cd7*, a transient marker of pre-cDCs and pre-cDC2s (Schlitzer et al., 2015), and the transcription factor *Bcl11a* required for Flt3 expression in early cDC differentiation (Wu et al., 2013) (Figure 2J), which suggests that these clusters includes likely immature cDC2s. One these two clusters expressed specifically the cadherin gene *Cdh17*, normally expressed by the epithelium (Figure 2J). This cluster was also enriched for *Ccr6* expression, the chemokine receptor gene involved in the addressing to the SED (Figure 2J).

To strengthen these findings and determine dome cDC2 differentiation pathway, we used the RNA velocity-based algorithm scVelo (Bergen et al., 2020). Clusters of dome cDC2s showed a ratio of unspliced mRNA beween 22 and 27 % of total mRNA, validating this approach to infer cell fate trajectories (Figure 2K). Based on the dynamic mRNA velocity streamlines projected onto the cDC2 subclustering UMAP, the emission basins, i.e. the differentiation starting points of dome cDC2s, were located close to proliferative cDC2s (Figure 2K). Several intermediate basins with converging streamlines on one side and emerging streamlines on the other could be drawn, two of

which located in immature cDC2s closed to the intermediate cDC2 cluster, probably reflecting the beginning of this maturation process. Finally, three attraction basins, i.e. differentiation end points of dome cDC2s, were observed, suggesting that cDC2s may have different fate depending on the signals they receive from their microenvironment. Nevertheless, the transcriptional dynamics of cDC2s displayed as latent time UMAP highlighted the mature cDC2 cluster as the main terminal differentiation state of cDC2s (Figure 2K). Finally, the heatmap of top 150 likelihood-driver genes of cDC2 differentiation trajectories resolved along latent time showed a clear cut in the transcriptional cascade at the border between the mature cDC2 cluster and the other clusters, illustrating the profound change occurring during the maturation process (Figure 2L). Top driver genes of the dome cDC2 differentiation process included the transcription factors from the NF-kB family *Rel* and *Relb*, the transcription factors *Runx3*, *Stat1* and *Nr4a3*, the MHC-II related genes (*Ciita*, *Cd74*, *H2-DMb2*, *H2-Eb1* and *H2-Eb2*) but also the previously identified genes *Epcam*, *Il22ra2*, *Plet1*, *Pla2g7*, *Ccr6*, *Cdh17*, *Cd83*, *Gadd45*b and *Ccr7* (Figure 2L). The transcription factor *Runx3* was expressed early during the differentiation process of dome cDC2s, whereas the transcription factors *Stat1*, *Rel* and *Nr4a3* were induced at the maturation transition phase (Figure 2H). Velocity of *Il22ra2* (abundance of unspliced RNA) was maximum in the whole intermediate cluster. Finally, and as expected, *Ccr7* was induced in the intermediate cDC2 cluster, well before reaching its peak of expression in the mature cDC2 cluster, confirming the state of differentiation of both intermediate and mature dome cDC2 clusters (Figure 2L).

Transcriptional profile and differentiation pathway of dome cDC1 *in vivo*.

By subclustering the cDC1 group, 6 clusters were obtained (Figure 3A). One of these cluster representing 16.7% of total cDC1s segregate apart from the others and was therefore suspected to correspond to DAV cDC1s. Unlike other clusters, cells of this cluster lack expression of the

transcription factor *Jun*, of the mRNA-binding protein genes *Zfp36* (Tristetraprolin) and Zfp36l1, of the long non coding RNA *Neat1*, and of *Clec12a*. However, like DAV cDC2s, they were enriched for *Mgl2* and *Cxx1b* (Figure3B and 3C), suggesting that these two genes tags villus cDCs at steady state independently of the subset they belong to. In addition, putative DAV cDC1s were enriched for *Dapk2* and *Ctla2b*, which together with *Cxx1b*, was also expressed by another small cluster (9.2 % of total cDC1s) that showed some hybrid characteristics between dome and DAV cDC1s. The latter cluster was enriched for *Stt3b* expression.

Like cDC2s, mature cDC1s identified by their *Ccr7* expression and representing 17.4 % of total cDC1 were located in the UMAP at the exact opposite to the proliferative cDC1 cluster identified by *Mcm7* expression and representing 5.0% of total cDC1s (Figure 3D). Like cDC2s, the expression pattern of *Ccr7* and *Cd83* was broader than that of *Nudt17* and *Socs2*, confirming their status of early and late maturation markers, respectively. Other maturation markers, such as *Aldh1a2*, *Gliprl2*, and *Il12b* involved in retinoic acid production, autophagy regulation and T cell polarization, respectively, were enriched in mature cDC1s as compared to mature cDC2s (Figure 3E). Surprisingly, *Aldh1a2* was also enriched in DAV cDC1. On their side, mature cDC2s but not cDC1s were enriched in the lipid-binding protein coding genes *Fabp5* and *Gpr183* (Figure 3F).

The proliferative cDC1 cluster and one of its closest neighbour expressed the early cDC marker *Bcl11a* and *Ccr2*, a transient marker of pre-cDCs and pre-cDC1s (Schlitzer et al., 2015), suggesting that this cluster is likely constituted of immature cDC1s, representing 27.8 % of total cDC1s (Figure 3G). Finally, the cluster in between immature and mature cDC1s, assumed to be intermediate cDC1s, was enriched for *Notch2* expression (Figure 3H).

As with cDC2s, scVelo confirmed cDC1 differentiation trajectories and identified driver genes along them (Figure 3I). Although numbers of cDC1s did not allow to reach an as good dynamical resolution of RNA velocities as compared to cDC2s, individual cell velocities follow streams that

fitted with our differentiation model. For instance, the mature cDC1 cluster was clearly identified as final differentiation state by the latent time UMAP. As with cDC2s, there was a clear cut in the transcriptional cascade of the top 150 likelihood-driver genes at the level of the mature cDC1 cluster. Among cDC1 maturation driver genes, *Cd40* was induced in immature and intermediate cDC1s well before reaching its peak of expression in the mature cDC1 cluster whereas *Aldh1a2* dynamic behaviour was representative of late maturation markers and entirely restrained to the mature cDC1 cluster. Finally, the chronology of maturation marker expression obtained for both cDC1s and cDC2s identified: (i) common early maturation markers including *Cd274* encoding the immunoregulatory molecule PD-L1 and the transcription factors *Rel* and *Nr4a3*; (ii) intermediate maturation markers such as *Ccr7, Marcks*, *Traf1* and the mRNA regulator *Zfp36l1*; and (iii) late maturation markers including the gene expression repressor *Pcgf5* and the transmembrane proteins *Tspan3* and *Gpr132* (Figure 2L and 3I).

Transcriptional profile and differentiation pathway of monocyte-derived phagocytes *in vivo*. By subclustering the monocyte-derived group, LysoMacs were split into two clusters expressing or not *Timd4*, thus representing TIM4^{-} and TIM4^{+} LysoMacs, whereas LysoDC were subdivided into seven clusters (Figure S3A). However, the two minor LysoDC clusters located at the periphery of other LysoDC clusters and representing only 3 and 4.2% of total monocyte-derived cells showed weird gene enrichments, suggesting that they could correspond to doublets due to tight interaction with or phagocytosis of other cell types as already observed by microscopy (Bonnardel et al., 2017; Lelouard et al., 2010; Wagner et al., 2020). For instance, many cells of one these two clusters express *Flt3* (Figure S3B), which is never expressed by LysoDCs but by cDC2s that can strongly interact with LysoDCs in the SED and in the FAE (Bonnardel et al., 2017). We therefore decided to remove these small clusters from the following analyses (Figure 4). Filtered LysoDCs accounted

for 64.3 % of monocyte-derived cells. Around 6% of monocyte-derived cells were in proliferation, most of which were LysoDCs (*Cd4*$^{-}$ cells expressing strong levels of MHCII-related genes) (Figure 4A). Therefore, both short-lived LysoDCs and cDCs but not long-lived LysoMacs showed marked proliferative activities representing 5 to 9 % of their total number. Like cDCs, mature LysoDCs, revealed by their *Plet1*, *Cd9* and *Ifitm1* expression (Wagner et al., 2020) and representing 20% of total LysoDCs, were located in the UMAP at the opposite of proliferative LysoDCs (Figure 4B). As expected from our previous study (Wagner et al., 2020), mature LysoDCs were also enriched for *Il1b*, *F11r* and *Cd24* expression whereas follicular LysoDCs lack *Emb* expression (Figure 4B). In addition to *Cd4*, LysoMac were enriched for *Tspan 10* expression and Tim4+ LysoMac expressed more *Wfdc17* than TIM4- LysoMac.

As previously shown (Wagner et al., 2020), scVelo identified 2 attractions basins in the mature LysoDC cluster and one attraction basin in the follicular LysoDC cluster (Figure 4C). By contrast, most LysoMacs converge towards a single attraction basin at the edge of TIM4^{+} LysoMacs (Figure 4C).

Stimulation of Peyer's patch phagocytes *in vivo* following different administration route of TLR 7 and 9 ligands

We next sought to investigate PP phagocyte activation processes following TLR ligand stimulation *in vivo*. We previously showed that the TLR7 ligand R848 was a powerful direct activator of monocyte-derived cells as well as an indirect activator of cDCs through a TNF-dependant pathway (Bonnardel et al., 2017; Wagner et al., 2020). In addition to TLR7, we decided to study the activation of PP phagocytes by another endosomal TLR with broad expression in phagocytes, TLR9. Unfortunately, the TLR9 ligand CpG failed to induce noticeable stimulation of PP cDCs following oral administration (Figure S4A). However, CpG induced their stimulation when

administrated intraperitoneally (Figure S4A). Moreover, PP phagocytes stimulated with the TLR7 ligand R848 via oral or peritoneal route showed similar pattern of activation. Thus, cDC surface expression of MHC-II increased whereas CD11c one decreased in similar proportion (Figure S4A) and CD40, CD86 and CD205 surface expression increased with similar amplitude (Figure S4B). We therefore decided to pursue our study using intraperitoneal injection for both TLR ligands.

scRNAseq analysis of R848 and CpG stimulated PP phagocytes

Given that LysoDC migration from the SED starts 8h after R848 stimulation (Wagner et al., 2020), we decided to perform scRNAseq analysis of PP phagocytes 9h after stimulation to study fully activated LysoDCs but also some that are still in the process of activation. In line with published results (Bonnardel et al., 2017), we obtained two times more cDC1s upon R848 stimulation, but the most striking difference was obtained with CpG stimulation for which three times more cDC1s but also 1.5 times more cDC2s were obtained. Thus, cDCs represented around 90% of total phagocytes after CpG stimulation. Based on these phagocyte ratios, we decided to discard half of R848-stimulated cDC2s like at steady state but also 2/3 of CpG-stimulated cDC2s and half of CpG-stimulated cDC1s before preparation of scRNAseq libraries (Table S1).

As in steady state, the 3 groups of cDC1s, cDC2s and monocyte-derived cells were clearly separated on the UMAP of R848 and CpG-activated phagocytes (Figure 5A). Among monocyte-derived cells, the separation between LysoDCs and LysoMacs was more pronounced than at steady state, thus reinforcing their lineage distinction. Activation by both ligands led to a complete loss of *Itgax* (encoding CD11c) expression in most cDCs but not in monocyte-derived cells (Figure 5B). The key PP monocyte-derived markers *Bst2*, *Lyz1*, *Lyz2* as well as the genes encoding Gas7 and the lysosomal machinery (Lamp1, Lamp2, Cystatin F and cathepsin genes) were also conserved upon activation (Figure 5B and S5A), in line with the preserved ability of LysoDC to phagocytose

after R848 stimulation *in vitro* (Wagner et al., 2020). However, with the notable exception of *Mertk*, key genes of the monocytic lineage including *Csf1r*, *Cx3cr1*, *Mafb*, and *Msr1* were typically dowregulated in the most activated LysoDCs forming a small peripheral cluster in R848-treated mice (see Figure S5B and the subclustering of activated monocyte-derived phagocytes in Figure 8). Expression of genes encoding MHC-II molecules was maintained in all LysoDCs but decreased in part of activated cDCs and not induced in LysoMacs (Figure 5C and S5C). *Ccr2* and *Il22ra2* expression was also retained in LysoDCs (Figure 5C). Finally, specific expression of *Cd4* and *C3* by LysoMacs was retained upon activation.

As expected, in both conditions of activation, cDCs express strong levels of *Ccr7*, with the notable exception of one cDC2 cluster, likely representing newly recruited cDC2s (Figure 5D). As expected, the most activated LysoDCs also expressed *Ccr7*. Expression of cDC marker genes that were equally distributed among cDC clusters at steady state, i.e., *Anpep*, *Flt3*, and *Spint2* were relatively preserved upon activation, with the exception of *Anpep* in cDC1s (Figure 5D). Moreover, cDC marker genes that were enriched in mature cDCs (i.e., *Ccr7*, *Gpr132*, *Hmg3* and *P2ry10*), the closest differentiation state to activated cDCs at homeostasis, were also highly expressed upon activation.

Most of the previously identified cDC2 markers, including *Sirpa*, *Epcam* and the GALT-specific cDC2 markers *Plet1*, *Il22ra2* and *Lyz2* were repressed upon activation, except in the *Ccr7*-negative cluster (Figure 5C, 5E, S5A and S5D). Nevertheless, expression of the GALT-specific cDC2 marker *S100a4* was retained upon activation in all cDC2 clusters but one. By contrast, the latter was positive for the DAVcDC2 marker gene *Apol10b* (Figure 5E). Therefore, *S100a4* and *Apol10b* are general markers of GALT cDC2 and villus cDC2, respectively, both at steady state and upon activation.

Like cDC2s, most cDC1s typical marker genes were repressed upon activation with the notable exception of *Cd8a* and *Clec12a* for R848 stimulation and of *Irf8* for both stimuli (Figure 5F). Under stimulation conditions, *Irf8* was actually expressed by all activated PP phagocyte subsets. Interestingly, *Il12b*, which was mainly expressed by mature cDC1s at homeostasis, was repressed in activated cDC1s in both stimulation conditions but induced in R848-activated LysoDCs and CpG-induced cDC2s (Figure 5F).

Following cDC2 subclustering, we identified each cluster from stimulated PPs thanks to the previous identified markers *S100a4*, *Apol10b*, *Ccr7*, *Ccr6*, *Il22ra2*, *Cdh17*, *Runx1* and *Runx3* (Figure 6A and 6B). Thus, *Ccr7*-negative non activated cDC2 encompassed immature *Ccr6*$^{+}$ cDC2s that expressed *Runx3* and could be separated in two distinct groups based on *Cdh17* and *Il22ra2* expression. In addition, R848- but not CpG-stimulated PP contained a small *Ccr7* and *Ccr6* double negative cluster of immature DAV cDC2 that expressed *Runx1* but not *S100a4*. Instead, in CpG-stimulated PP all *S100a4*-negative cDC2 clusters were *Ccr7*$^{+}$ and thus activated. However, as expected *Apol10b* expression was anti-correlated with that of *S100a4* in all conditions, providing the position of DAV cDC2s. We then studied the profile of activation of dome cDC2s and DAV cDC2s, which both migrate in the IFR upon activation (Bonnardel et al., 2017; Wagner et al., 2020). Interestingly, unlike DAV cDC2s, activated dome cDC2s expressed the transcription factor *Tcf7*, the ICOS ligand *Icosl* and for the most activated ones *Il12b*. *Il6* expression was also restrained to dome cDC2s in R848 but not in CpG-stimulated mice for which *Il6* expression was extended to all activated DAV cDC2s. By contrast, *Ccl17* and *Ido1* expression were mostly confined to DAV cDC2s.

Following cDC1 subclustering, a small proliferative (*Birc5* expression) and an immature/early activated cluster that still express the cDC1 markers *Xcr1* and *Clec9a* (Figure 7A and 7B) were identified for both stimulation conditions. Other clusters expressed strong levels of *Ccr7* and were

globally divided in two branches, likely corresponding to activated dome and DAV cDC1s. Since activation induced a loss of all DAV cDC1 markers, we analysed genes that were expressed only by dome but not DAV cDC1s at steady state. We found that *Jun, Neat1, Zfp36 and Zfp36l1* were not expressed by one of the two branches in each condition (Figure 7C). This was also true for other dome cDC1 markers, such as *Akap9*, *Akap13*, *Alkbh1* and *Arhgap31*. Therefore, even if, unlike DAV cDC2, DAV cDC1 lose their specific transcriptional identity upon activation and migration into PP IFRs, they never acquire the gene signature of dome cDC1 and they segregate apart from them.

Monocyte-derived cell subclustering allowed to identify two subsets of LysoMacs ($CD4^+$ cells) like in steady state (Figure 8A). However, these subsets did not segregate based on *Timd4* expression but rather based on their activation status that correlated with a loss of the monocyte-derived cell markers *Csf1r* and *Msr1* in R848- but not CpG-stimulated mice (Figure 8B). The most activated LysoMac expressed *Ccl3* and *Ccl4* in R848-treated mice and *Cxcl10* in CpG-treated mice. In addition, all monocyte-derived cells expressed strong levels of *Cxcl9* in R848-treated mice.

Subepithelial LysoDC were identified by their *Emb* expression (Figure 8C). They expressed the highest levels of *Ccr2* and *Il22ra2* among monocyte-derived cells (Figure 8C). Part of them also expressed *Cd9* and *Plet1*, suggesting that beside their activation process, subepithelial LysoDCs persisted in following the same differentiation path from immature ($Emb^+Plet1^-Cd9^-$) to mature ($Emb^+Plet1^+Cd9^+$) state. However, due to stimulation, *Ifitm1* expression expanded to the whole LysoDC population whereas *Cd24a* was repressed in R848-treated mice (data not shown).

The activation profile of follicular LysoDC was closer from LysoMac than from other LysoDC with upregulation of *Ccl3* and *Ccl4* (R848 stimulation) or Cxcl9 (CpG stimulation and *Cxcl10* expression (both stimulation; Figure 8B), as well as of *Ly6a* (R848 stimulation) or Ccl12 (CpG stimulation) and *Ifit1*, *Ifit2*, *Ifit3* and *Rsad2* (both stimulation, Figure 8D).

As expected from previous works (Bonnardel et al., 2015a; Wagner et al., 2020), fully R848-activated LysoDC expressed *Ccr7*, *Cd40*, *Il12b* and *Il6* (Figure 8E). Although not identified as a cluster on the global phagocyte UMAP, a small cluster of *Ccr7*-expressing LysoDC was detected in the subclustering UMAP of CpG-stimulated mice. They also expressed *Cd40* but not *Il12b* and weakly *Il6*.

Impact of R848 and CpG stimulation on the global PP immune response initiation

To determine what could be the consequences of R848 and CpG different activation profiles of phagocytes in immune response initiation, we analysed B and T cell numbers in PPs at different time after stimulation (see Figure S6 for the gating strategy). After a slight initial increase, the number of total and naïve B cells (IgD^+ B cells) dropped below basal levels from 3 days to one week after stimulation with both TLR ligands (Figure 9A). In addition, in CpG-treated mice, the numbers of both $CD4^+$ and $CD8^+$ naïve T cells were reduced from 48h onwards. These data suggest that stimulated B and T cells rapidly egress from PP to reach effector sites. Thus, we blocked sphingosine-1 phosphate dependent egress from PP using FTY720 to study activated B and T cell in PP when their number decreased 72 h after both stimulation. In CpG-treated mice, there was an increase of activated $CD8^+$ T cells (proliferative, early and late activated cytotoxic T cells; Figure 9B), in line with the increase of activated cDC1 numbers in this stimulation condition (Figure 5A). By contrast, only proliferative regulatory T cell numbers slightly increased in R848-treated mice (figure 9B). However, the latter showed an increase in IgA-producing B cells and more generally of proliferative B cells (Figure 9C). This increase was largely due to proliferation of $CCR6^+$ B cells (Figure 9D), known to be mainly located in the SED (Reboldi et al., 2016).

Discussion

In this study, we performed a single cell transcriptional analysis of PP phagocytes at steady state and upon R848 and CpG stimulation *in vivo* to decipher their maturation and activation pathways. To date, LysoDCs represent the closest monocyte-derived cells to cDCs in mice at steady state, providing an unparalleled tool for defining the specific genetic traits of cDCs and monocyte-derived DCs. Actually, of the initial cDC gene signature proposed by Miller *et al.* (Miller et al., 2012), 17 genes show specificity for cDCs as compared to LysoDCs, but only two genes, *Flt3* and *Spint2*, are specifically expressed by all PP cDC independently of their maturation and activation state. *Flt3* is undoubtedly a key cDC marker since it is not required for monocyte-derived cell differentiation whereas essential for steady state cDC development (Durai et al., 2018; Waskow et al., 2008). By contrast, the role in cDCs of *Spint2* encoding the serine protease inhibitor hepatocyte growth factor activator inhibitor-2 (HAI-2) is unknown. In the gut, HAI-2 expression by intestinal epithelial cells is required to inactivate the enzyme matriptase and thereby stabilize the epithelial cell adhesion molecule (EpCAM), avoid luminal bleeding, villous atrophy and loss of crypt architecture (Kawaguchi et al., 2019; Szabo et al., 2019). Whether HAI-2 expression in cDCs also helps in preventing degradation of cell adhesion molecules deserves further investigations. Surprisingly, CD26, one of the last identified cDC markers (Bosteels et al., 2020; Scott et al., 2015), fails to discriminate cDCs from monocyte-derived cells in PP, showing how delicate generalization can be and highlighting the importance of unbiased tissue-specific studies. As PP MF are distinct from villus and other tissue MF (Wagner et al., 2018), the transcriptional profile of dome cDCs is different from villus cDCs one. However, dome cDC2 transcriptional profile appears very similar to that of the recently described ILF and cryptopatch cDC2s (Guendel et al., 2020). Thus, we identified gene markers that distinguish dome cDC2s from DAV cDC2s that belong to the ILF and

cryptopatch cDC2 gene signature. Moreover, we showed that one of the key dome cDC2 marker S100A4 we have identified is also expressed by ILF cDC2s but not villus cDC2s, bringing GALT cDC2 together under a single banner. Interestingly, S100A4 is essential for the development of mature M cells that are fully able to transport antigens (Kunimura et al., 2019). In line with this, we found that subepithelial S100A4-expressing cDC2s are mainly located in the crypts and in the first half of SED height where they strongly interact and penetrate into the FAE and where M cell maturation is known to occur (Kimura et al., 2015). S100A4 expression was initially attributed to LysoDCs, LysoMacs and ILC3s (Kunimura et al., 2019). The strong phenotypic and genetic similarity between LysoDCs and cDC2s combined with the fact that LysoDCs do express minimal amounts of S100A4 (Figure 1E) probably account for the initial confusion between these two types of phagocytes. Regarding ILC3s, we indeed detect S100A4 expression by small CD11c$^-$SIRPα$^-$ CX$_3$CR1$^-$cells below the layer of subepithelial phagocytes but not in contact with the FAE, making their role in M-cell maturation unlikely but fully compatible with subepithelial dome cDC2s imprinting, as it occurs in ILFs and cryptopatches (Guendel et al., 2020). Indeed, in the latter CCR6$^+$ ILC3s control the differentiation of cDC2s via direct LTα1β2:LTβR signalling. Therefore, we can draw a model in which CCR6$^+$ ILC3s of the SED would program newly recruited CCR6$^+$ subepithelial cDC2s, which would in turn induce M cell maturation by expressing S100A4.

After their initial imprinting by the GALT microenvironment, both dome cDC1s and cDC2s follow a chronology of maturation that involves common features with an initial upregulation of genes encoding the transcription factors NF-kB (*Rel*) and NR4A3. The latter was indeed recently shown to be involved in CD103$^+$ cDC migration by promoting *Ccr7* expression (Park et al., 2016), which indeed belongs to the following genes in the cDC maturation chronology we established.

As expected, stimulation of PP with any of the two ligands induces a dramatic change in phagocyte transcriptional profiles close to but distinct from mature phagocytes. Thus, whereas mature cDC1s express *Il12b*, activated cDC1s do not. By contrast, R848-activated but not mature or CpG-activated LysoDC express *Il12b*. This is in line with an *in vitro* study showing the ability of R848-stimulated LysoDC to induce a Th1 polarization of naïve helper T cells (Bonnardel et al., 2015a). Globally, changes operating at the levels of monocyte-derived cells are less pronounced than that of cDCs. Thus, only a minor part of LysoDCs evolve toward a fully activated state whereas most cDCs do. Moreover, some typically downregulated key genes in activated cDCs, such as *Itgax*, *H2-Ab1* and *Sirpa*, are maintained in activated LysoDCs. Interestingly, distinction between LysoDCs and LysoMacs is reinforced upon activation. DAV activated cDCs remain also fully distinguishable from dome activated cDCs although they both migrate in the IFRs of PPs. Therefore, the site of initial residence is crucial for shaping the activation profile of cDCs and thus the orientation of the adaptive immune response. Since sampling of pathogens and noxius agents is favored in the FAE and SED as compared to villus epithelium (Da Silva et al., 2017; Jinnohara et al., 2017), this could help the immune system to locally distinguish innocuous from hazardous matter-derived antigens depending on the original location of cDCs, which in addition could provide either inflammatory (e.g., IL-6 and IL-12) or anti-inflammatory signals (retinoic acid via RALDH2 and kynurenines via IDO1) necessary to adequately polarize naïve T cells.

Finally, differences in phagocyte activation profile for each stimulus correlate with a different adaptive immune response, R848 leading to Treg and IgA-secreting B cell production and CpG leading to a CD8+ T cell response, in line with the strong recruitment of cDC1s in CpG-treated mice. The pathways of maturation and activation highlighted in this study should now pave the way to a better understanding of the mechanisms involved in these two types of adaptive immune response initiation.

Figure legends

Figure 1. Steady state scRNAseq analysis of Peyer's patch CD11c^{hi} phagocytes.

(A–F) Single-cell mRNA sequence analysis of 5013 PP CD11c^{hi} phagocytes extracted from 12 C57Bl/6 mice. (A) Uniform manifold approximation and projection (UMAP) embedding map colored by Seurat clustering showed three groups of clusters representing monocyte-derived cells (Mo-derived; yellow, orange and magenta clusters), cDC1s (shades of green) and cDC2s (shades of blue) together with an isolated cluster of cDC2s. Number of cells for each type of phagocytes is indicated in the middle column as well as the ratio it represents in the UMAP and among total phagocytes, taking into account that half of cDC2s were discarded. Histograms on the left show the ratio of ribosomal (r) and mitochondrial (mt) RNA as well as the number of genes and UMI detected in each cluster. (B-F) Expression of monocyte-derived cell (B), LysoDC and LysoMac (C), cDC (D), cDC2 (E) and cDC1 (F)-oriented marker genes in PP phagocyte UMAP shows the transcriptional specificities of each phagocyte type. See also Figure S1 for gating strategy and additional gene expression.

Figure 2. Transcriptional profile and differentiation pathways of dome cDC2 *in vivo*.

A) UMAP embedding map colored by Seurat clustering of 2406 cDC2s extracted from PPs shows a major group (2199 cells) of 5 dome cDC2 clusters and a small isolated cluster (207 cells) of DAV cDC2s. Color code and identification of each cluster based on gene expression with the number of cells and % of total cDC2s indicated in brackets are shown below the UMAP. (B and C) Expression of CD101 and CD209b genes (B) and proteins (C) in villus but not dome cDC2s. (D and E) Expression of S100a4 gene (D) and protein (E) in dome but not DAV cDC2s. (E) By spectral confocal microscopy, S100a4 expression (magenta) in the SED is mainly concentrated in SIRP□$^{+}$ (orange), CX$_3$CR1^{-} (green), CD11c^{+} (red) cDC2 of the first half of dome height whereas monocyte-derived cells (i;e., LysoDCs and LysoMacs, SIRP□$^{+}$CX$_3$CR1^{+}CD11c^{+} cells) are more evenly

distributed. S100a4 is also expressed by small CD11c$^-$Sirpa$^-$CX3CR1$^-$ cells, presumably ILC3s, located just below the subepithelial phagocyte layer (asterisks). (F to J) Expression of maturation (F), proliferation (G), differentially-expressed (H), GALT-specific (I) and immature (J) marker genes in cDC2 UMAP. (K and L) RNA velocity analysis of dome cDC2s. (K) Top panel: ratio of unspliced vs spliced mRNA in dome cDC2 clusters. Lower left: mRNA velocity streamlines projected onto cDC2 UMAP. Streamline emission basins are drawn in purple, intermediate basins are in mixed purple to red colours according to streamline orientation and streamline attraction basins are in red. Lower right: latent time UMAP highlighting the main terminal differentiation state of cDC2s in yellow. (L) Heatmap of top 150 likelihood-driver genes of cDC2 differentiation trajectories resolved along latent time. Velocity (abundance of unspliced RNA) and expression of four representative driver genes *Runx3*, *Il22ra2*, *Stat1* and *Ccr7* are shown on the right. See also Figure S2 for additional gene expression and location of S100A4-expressing cDC2 in the gut.

Figure 3. Transcriptional profile and differentiation pathways of dome cDC1 *in vivo*.

A) UMAP embedding map colored by Seurat clustering of 562 cDC1s extracted from PPs shows a major group (468 cells) of 5 dome cDC1 clusters and a small isolated cluster (94 cells) of DAV cDC1s. Color code and identification of each cluster based on gene expression with the number of cells and % of total cDC1s indicated in brackets are shown below the UMAP. (B and C) Expression of dome (B) vs DAV (C) cDC1-marker genes in the cDC1 UMAP. (D and E) Expression of the proliferation marker MCM7 (DNA replication licensing factor) and of cDC maturation marker genes in the cDC1 UMAP (D) and in the cDC1 and PP phagocyte UMAP (E). (F) Expression of the lipid-binding protein coding genes *Fabp5* and *Gpr183* in PP phagocyte UMAP shows enrichment in mature cDC2 but not cDC1. (G and H) Violin plots of the pre-cDC1 markers *Ccr2* and *Bcl11a* (G) and of *Notch2* (H) in the different cDC1 clusters. (I) RNA velocity analysis of dome cDC1s. Top left panel: ratio of unspliced vs spliced mRNA in dome cDC1 clusters. Bottom left:

individual cell mRNA velocity projected onto cDC1 UMAP. Major directions are indicated by arrows and emission, intermediate and attraction basins are drawn in purple, mixed purple to red colours and red. Bottom right: latent time UMAP highlighting the main terminal differentiation state of cDC1s in yellow. Right panel Heatmap of top 150 likelihood-driver genes of cDC1 differentiation trajectories resolved along latent time. Velocity (abundance of unspliced RNA) and expression of three representative driver genes *Spi1*, *Cd40* and *Aldh1a2* are shown on the right.

Figure 4. Transcriptional profile and differentiation pathway of monocyte-derived phagocytes *in vivo*.

A) UMAP embedding map colored by Seurat clustering of 1896 filtered monocyte-derived phagocytes extracted from PPs shows a major group (1784 cells) of 6 clusters and a small peripheral cluster (112 cells) mainly constituted of proliferative LysoDC. Color code and identification of each cluster based on gene expression with the number of cells and % of total monocyte-derived phagocytes indicated in brackets are shown below the UMAP. (B) Expression of genes differentially expressed between clusters. (C) RNA velocity analysis of monocyte-derived phagocytes. left: ratio of unspliced vs spliced mRNA in monocyte-derived phagocyte clusters. Right: mRNA velocity streamlines projected onto monocyte-derived phagocyte UMAP. Emission, intermediate and attraction basins are drawn in purple, mixed purple to red colours and red. See also Figure S3 for monocyte-derived phagocyte UMAP without filtering.

Figure 5: scRNAseq analysis of R848 and CpG stimulated PP phagocytes

(A–F) Single-cell mRNA sequence analysis of 4815 and 4822 PP CD11c^{hi} phagocytes extracted from 12 C57Bl/6 mice 9 hours after intraperitoneal injection of R848 or CpG, respectively. (A) Uniform manifold approximation and projection (UMAP) embedding map colored by Seurat clustering showed for each stimulation condition (R848 on the left; CpG on the right) three groups

of clusters representing monocyte-derived cells (Mo-derived; yellow, orange and magenta clusters), cDC1s (shades of green) and cDC2s (shades of blue). Number of cells for each type of phagocytes is indicated in the middle column as well as the ratio it represents in the UMAP and among total phagocytes, knowing that half of cDC2s were discarded for R848-treated mice and that only one third of cDC2s and half of cDC1s were retained for CpG-treated mice. (B-F) Expression of monocyte-derived cell (B), LysoDC and LysoMac (C), cDC (D), cDC2 (E) and cDC1 (F)-oriented marker genes in PP phagocyte UMAP from each stimulation condition (R848 on the left of the dotted line; CpG on the right) shows the transcriptional specificities of each phagocyte type.

Figure 6: scRNAseq analysis of R848 and CpG stimulated PP cDC2

A) UMAP embedding map colored by Seurat clustering of 1840 and 2467 cDC2s extracted from PPs of R848 and CpG-treated mice, respectively. Color code and identification of each cluster based on gene expression with the number of cells and % of total cDC2s indicated in brackets are shown on the right of each UMAP. In both conditions, two DAV cDC2 and three dome cDC2 clusters at different state of activation were obtained (dotted line). In both conditions, a cluster of likely newly recruited dome cDC2s was not activated (*Ccr7* negative) and represented more than 20% of total cDC2s. (B) Expression of genes differentially expressed between clusters in both conditions. *S100a4* and *Apol10b* allowed to distinguish DAV from dome cDC2s. (C and D) Expression of activation marker genes differentially expressed by dome cDC2s (C) and DAV cDC2s (D).

Figure 7: scRNAseq analysis of R848 and CpG stimulated PP cDC1

A) UMAP embedding map colored by Seurat clustering of 928 and 1076 cDC1s extracted from PPs of R848 and CpG-treated mice, respectively. Color code and identification of each cluster

based on gene expression with the number of cells and % of total cDC1s indicated in brackets are shown on the right of each UMAP. In both conditions, DAV cDC1 and dome cDC1 clusters at different state of activation were detected (dotted line). In both conditions, nearly all cDC1 were activated. (B and C) Expression of genes differentially expressed between clusters in both conditions.

Figure 8: scRNAseq analysis of R848 and CpG stimulated PP monocyte-derived phagocytes

A) UMAP embedding map colored by Seurat clustering of 2047 and 1279 monocyte-derived phagocytes extracted from PPs of R848 and CpG-treated mice, respectively. Color code and identification of each cluster based on gene expression with the number of cells and % of total monocyte-derived phagocytes indicated in brackets are shown on the right of each UMAP. (B to E) Expression of genes differentially expressed between clusters in both conditions.

Figure 9: Impact of R848 and CpG stimulation on the global PP immune response initiation

The effects of phagocyte stimulation with R848 (green) and CpG (red) in B and T cells responses were quantified by flow cytometry, non-stimulated condition was used as control (grey). Different populations of B and T cells were obtained using the gating strategy in Fig.S6. Only subsets that showed differences in at least one of the stimulation conditions are shown. A) Kinetics were made for both stimuli after IP injection, absolute numbers of naïve B and $CD4^+$ and $CD8^+$ T cells showed a significant loss from 48 h or 72 h onward. Data were obtained from 5 to 7 independent experiments depending on the time points. Impaired egress of lymphocytes was induced by sphingosine-1 phosphate receptor agonist FTY720 treatment 24 h after the stimulation. Absolute numbers of total (first row) and proliferative (second row) selected T cells (B) and proliferative B cells (C) at 72 hours after stimulation. Data were obtained from 3 independent experiments. D)

Based on the level of expression of Ki67 (proliferation marker) and CCR6 (SED marker) we differentiate B cells present in different zones: Subepithelial proliferative (SED), follicular (F) and proliferative outside SED (F+GC). Additionally, surface expression of GL-7 and IgD distinguished three populations of B cells in PP: Naive, Switched and GC. Flow cytometry quantification of each population absolute number per PP in each zone for the three conditions are shown, data were obtained from 3 independent experiments. Each point represents an individual mouse. *, $p<0.05$; **, $p<0.01$; ***, $p<0.001$, nonparametric Kruskal-Wallis with Dunn's multiple comparisons tests. F: follicle; GC: germinal center; SED: Subepithelial dome.

Supplementary data

Table S1: Number of sorted cells from each phagocyte subset that was used for scRNAseq in each condition.

Numbers in brackets indicate the total number of sorted cells from which only half of cDC2 (control and R848 treatment) or one third of cDC2 and half of cDC1 (CpG treatment) were retained.

	Control	R848	CpG
LysoDCs	5974	5841	4177
LysoMacs	3657	4123	2845
cDC1s	2556	4154	4020 (8040)
cDC2s	10774 (21548)	7177 (14354)	10694 (32082)

Supplementary figure legends:

Figure S1 related to Figure 1: Gating strategy of cell sorting and scRNAseq analysis of Peyer's patch CD11c^{hi} phagocytes at steady state. (A) Gating strategy of PP CD11c^{hi} phagocyte sorting for scRNAseq analysis. (B) Expression of monocyte-derived cell related genes in Peyer's patch CD11c^{hi} phagocytes. (C) Expression of genes involved in phagocytosis and lysosomal machinery in Peyer's patch CD11c^{hi} phagocytes. (D) Expression of the cDC gene signature by Peyer's patch

CD11c^{hi} phagocytes. Color of gene name depends on its cDC specificity in PP ranging from not specific in black to highly specific in red. Note that many highly cDC-specific genes were however weakly expressed by PP cDCs. (E) CD26 was expressed both at the gene (*Dpp4*) and protein levels by all CD11c^{hi} phagocytes, precluding its use as a cDC specific marker in PP. In grey, the FMO of each population.

Figure S2 related to Figure 2: scRNAseq analysis of Peyer's patch cDC2s at steady state and location of S100a4^{+} cDC2s in PP IFR and ILF. (A) Expression of DAV cDC2 related genes in PP cDC2. (B) Location of S100a4^{+} cDC2 (CD11c^{+}SIRPα^{+}CX$_3$CR1^{-} cells) in the IFR of PP. (C to E) Expression of activation (C), proliferation (D) and GALT-specific cDC2 (E) marker genes in PP cDC2s. (F) Location of S100a4^{+}CD11c^{+}LysM^{+} cDC2 in an immature ILF (RORγt-enriched region in orange) but not in adjacent villi. (F) Expression of the GALT-specific cDC2 marker genes *Pla2g7* and *Tgfbi* in Peyer's patch CD11c^{hi} phagocytes. Both are expressed at higher levels by monocyte-derived cells than by cDC2s. Note that *Pla2g7* is also expressed by DAV cDC2, suggesting that it may actually not be fully GALT cDC2 specific.

Figure S3 related to Figure 4: scRNAseq analysis of Peyer's patch monocyte-derived cells at steady state. (A) UMAP embedding map colored by Seurat clustering of 2045 monocyte-derived phagocytes extracted from PPs shows a major group (1784 cells) of 6 clusters and three peripheral clusters, among which one was made of proliferative LysoDC (112 cells) but the two other (87 and 62 cells) remained undetermined. Color code and identification of each cluster based on gene expression with the number of cells and % of total monocyte-derived phagocytes indicated in brackets are shown below the UMAP. (B) The two undefined LysoDC clusters expressed genes both related (first row) and unrelated to monocyte-derived cells (second and third rows).

Figure S4 related to Figure 5: Activation profile of PP phagocytes stimulated with the TLR ligands R848 (TLR7) and CpG (TLR9). (A and B) Comparison of gavage and intraperitoneal (IP) administration route of stimulation. CD11c and MHCII scatterplots (A) and CD40, CD86 and CD205 histograms (B) profiles showed that CpG activates cDCs only by IP injection whereas both routes are equally effective for R848. Percentage of gated cells are shown next to the gates (A) or on the upper right of each histogram (B). C) Quantification of CD40, CD86 and CD205 expressing cDC1, cDC2 and LysoDC at different time points after IP injection of R848 (green), CpG (red) or PBS-control (grey). Each point represents the number of cells per PP in three independent experiments. *, $p<0.05$, nonparametric Kruskal-Wallis with Dunn's multiple comparisons tests.

Figure S5 related to Figure 5: scRNAseq analysis of R848 and CpG stimulated PP phagocytes (A and B) Expression of genes related to monocyte-derived cells in phagocytes from R848 and CpG-treated mice. (C) Expression of genes from the MHCII presentation pathway in phagocytes from R848 and CpG-treated mice.

Figure S6 related to Figure 6: Gating strategies used to distinguish T (A) and B (B) cell populations. Ki67 staining was used to identify proliferative cells. (A) Live $CD45^+CD3^+$ T cells were split into $CD4^+$ and $CD8^+$ cells. In each population, naive cells were identified as $CD62L^+CD44^-$, early activated cells as $CD62L^-CD44^+CD69^+$ and activated as $CD62L^-CD44^+CD69^-$. Among $CD4^+$ T cells, TFH cells were $Bcl6^+PD1^+$ cells, Treg were $FoxP3^+$ and Th17 were $ROR\gamma t^+$. (B) Live $CD45^+lin^-$ (CD3/XCR1/Siglec-F) cells were separated into $GL\text{-}7^-IgD^+$ naive cells, $GL\text{-}7^+IgD^-$ GC cells and $GL7^-IgD^-$ cells that had switched (SW) to IgM and IgA-producing cells.

Figure 1

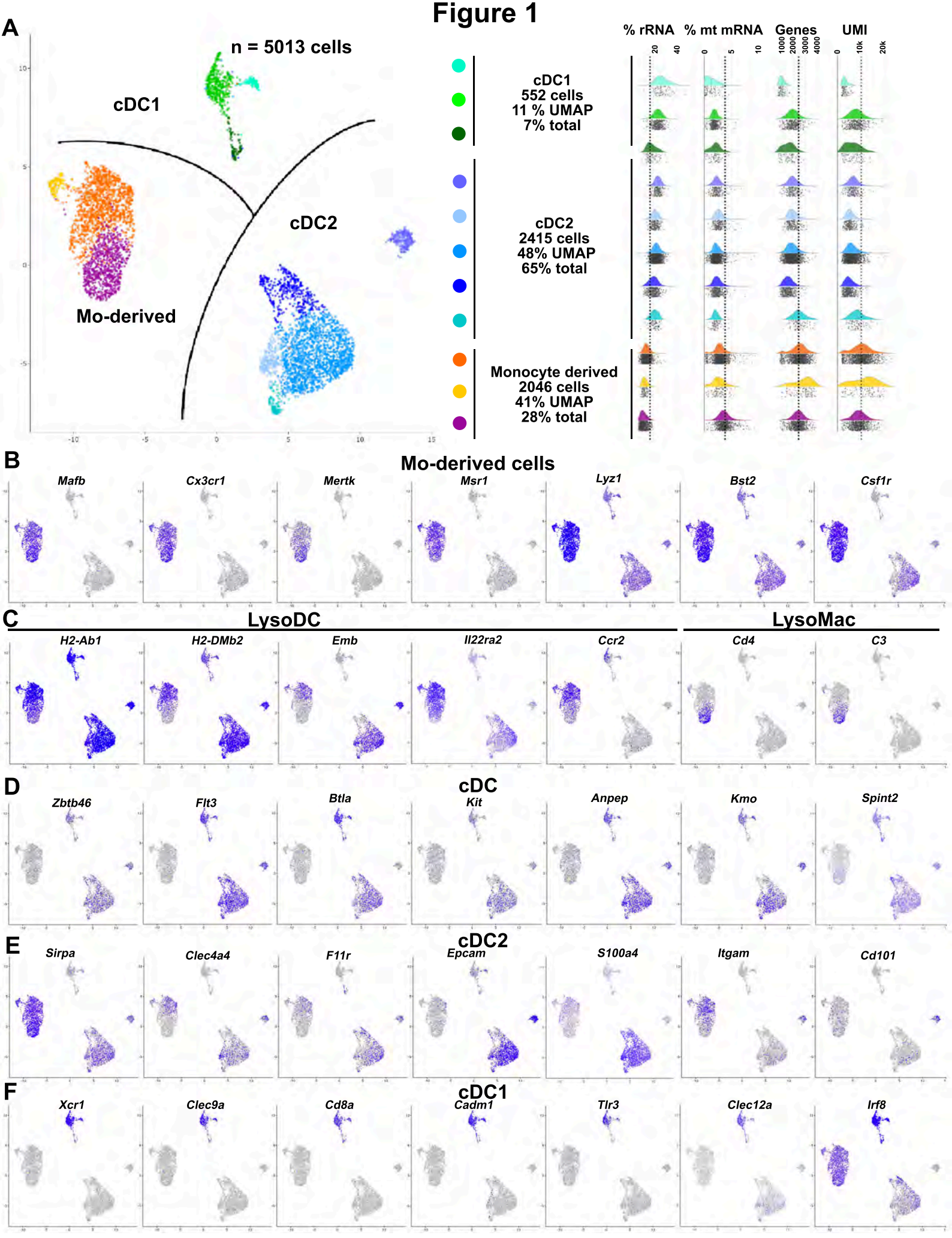
A
n = 5013 cells
cDC1
cDC2
Mo-derived
cDC1
552 cells
11 % UMAP
7% total
cDC2
2415 cells
48% UMAP
65% total
Monocyte derived
2046 cells
41% UMAP
28% total
% rRNA
% mt mRNA
Genes
UMI
B
Mo-derived cells
Mafb
Cx3cr1
Mertk
Msr1
Lyz1
Bst2
Csf1r
C
LysoDC
LysoMac
H2-Ab1
H2-DMb2
Emb
Il22ra2
Ccr2
Cd4
C3
D
cDC
Zbtb46
Flt3
Btla
Kit
Anpep
Kmo
Spint2
E
cDC2
Sirpa
Clec4a4
F11r
Epcam
S100a4
Itgam
Cd101
F
cDC1
Xcr1
Clec9a
Cd8a
Cadm1
Tlr3
Clec12a
Irf8

Figure 2

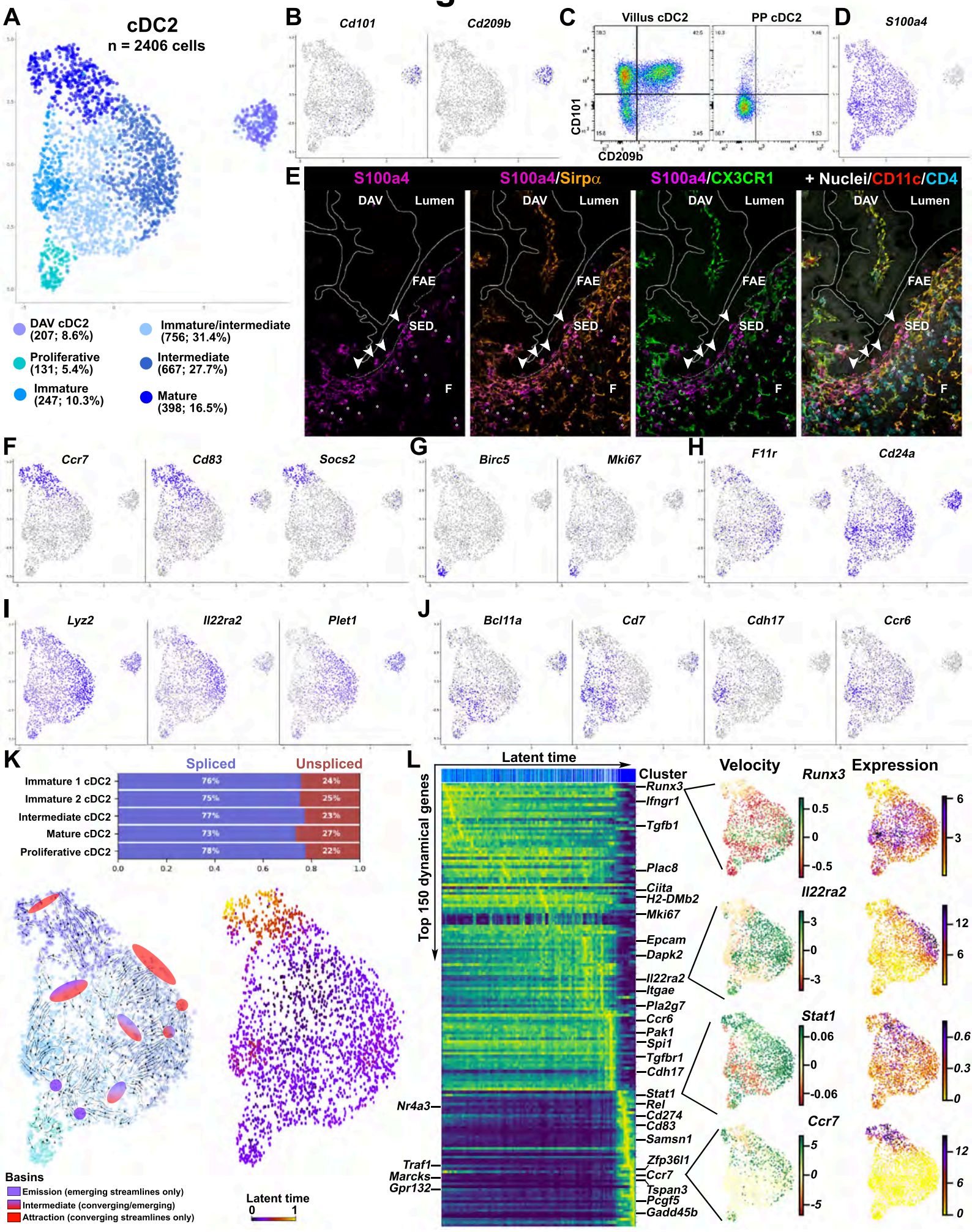
A
cDC2
n = 2406 cells
DAV cDC2 (207; 8.6%)
Immature/intermediate (756; 31.4%)
Proliferative (131; 5.4%)
Intermediate (667; 27.7%)
Immature (247; 10.3%)
Mature (398; 16.5%)
B
Cd101
Cd209b
C
Villus cDC2
PP cDC2
CD101
CD209b
D
S100a4
E
S100a4
S100a4/Sirpα
S100a4/CX3CR1
+ Nuclei/CD11c/CD4
DAV
Lumen
FAE
SED
F
F
Ccr7
Cd83
Socs2
G
Birc5
Mki67
H
F11r
Cd24a
I
Lyz2
Il22ra2
Plet1
J
Bcl11a
Cd7
Cdh17
Ccr6
K
Spliced
Unspliced
Immature 1 cDC2
Immature 2 cDC2
Intermediate cDC2
Mature cDC2
Proliferative cDC2
76%
24%
75%
25%
77%
23%
73%
27%
78%
22%
0.0
0.2
0.4
0.6
0.8
1.0
Basins
Emission (emerging streamlines only)
Intermediate (converging/emerging)
Attraction (converging streamlines only)
Latent time
0
1
L
Latent time
Top 150 dynamical genes
Cluster
Runx3
Ifngr1
Tgfb1
Plac8
Ciita
H2-DMb2
Mki67
Epcam
Dapk2
Il22ra2
Itgae
Pla2g7
Ccr6
Pak1
Spi1
Tgfbr1
Cdh17
Stat1
Rel
Cd274
Cd83
Samsn1
Zfp36l1
Ccr7
Tspan3
Pcgf5
Gadd45b
Nr4a3
Traf1
Marcks
Gpr132
Velocity
Expression
Runx3
0.5
0
-0.5
6
3
Il22ra2
3
0
-3
12
6
Stat1
0.06
0
-0.06
0.6
0.3
0
Ccr7
5
0
-5
12
6
0

Figure 3

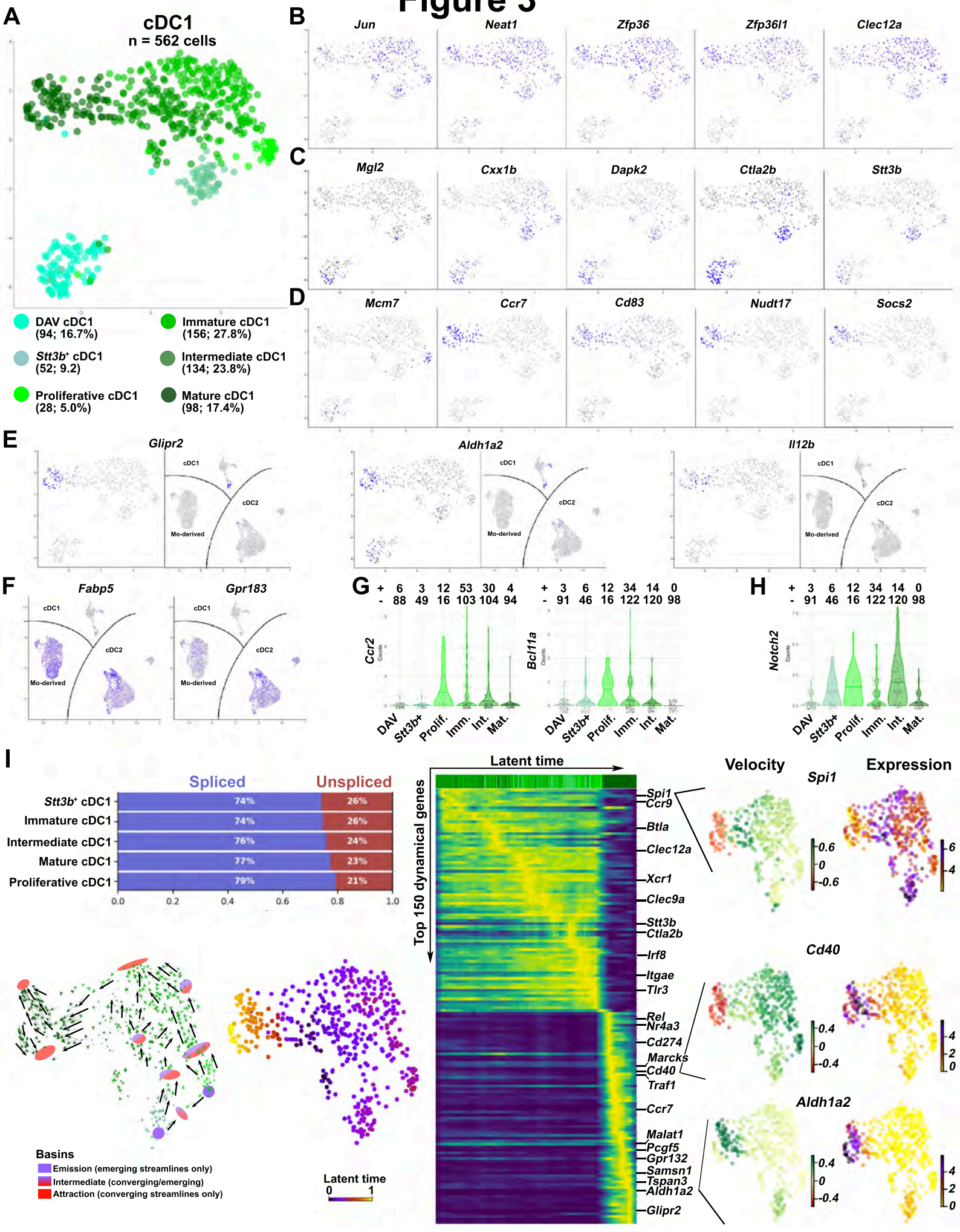
A
cDC1
n = 562 cells
DAV cDC1 (94; 16.7%)
Immature cDC1 (156; 27.8%)
Stt3b+ cDC1 (52; 9.2)
Intermediate cDC1 (134; 23.8%)
Proliferative cDC1 (28; 5.0%)
Mature cDC1 (98; 17.4%)
B
Jun
Neat1
Zfp36
Zfp36l1
Clec12a
C
Mgl2
Cxx1b
Dapk2
Ctla2b
Stt3b
D
Mcm7
Ccr7
Cd83
Nudt17
Socs2
E
Glipr2
Aldh1a2
Il12b
cDC1
cDC2
Mo-derived
F
Fabp5
Gpr183
G
+ 6 3 12 53 30 4
- 88 49 16 103 104 94
+ 3 6 12 34 14 0
- 91 46 16 122 120 98
Ccr2
Bcl11a
DAV
Stt3b+
Prolif.
Imm.
Int.
Mat.
H
Notch2
I
Spliced
Unspliced
Stt3b+ cDC1 74% 26%
Immature cDC1 74% 26%
Intermediate cDC1 76% 24%
Mature cDC1 77% 23%
Proliferative cDC1 79% 21%
0.0 0.2 0.4 0.6 0.8 1.0
Basins
Emission (emerging streamlines only)
Intermediate (converging/emerging)
Attraction (converging streamlines only)
Latent time
0 1
Latent time
Top 150 dynamical genes
Spi1
Ccr9
Btla
Clec12a
Xcr1
Clec9a
Stt3b
Ctla2b
Irf8
Itgae
Tlr3
Rel
Nr4a3
Cd274
Marcks
Cd40
Traf1
Ccr7
Malat1
Pcgf5
Gpr132
Samsn1
Tspan3
Aldh1a2
Glipr2
Velocity
Expression
Spi1
Cd40
Aldh1a2
0.6
0
-0.6
0.4
-0.4

Figure 4

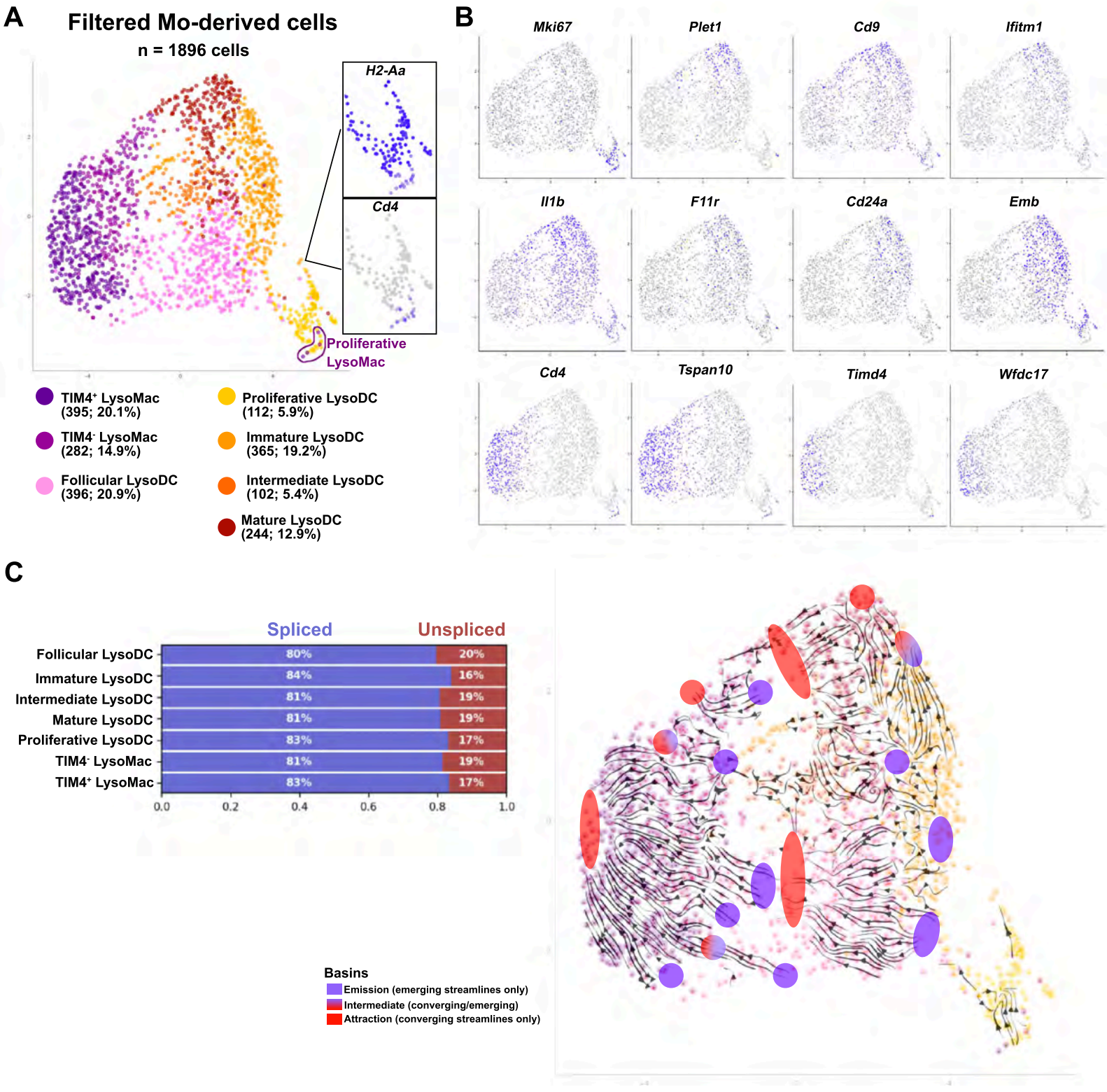
A
Filtered Mo-derived cells
n = 1896 cells
H2-Aa
Cd4
Proliferative LysoMac
TIM4+ LysoMac (395; 20.1%)
TIM4- LysoMac (282; 14.9%)
Follicular LysoDC (396; 20.9%)
Proliferative LysoDC (112; 5.9%)
Immature LysoDC (365; 19.2%)
Intermediate LysoDC (102; 5.4%)
Mature LysoDC (244; 12.9%)
B
Mki67
Plet1
Cd9
Ifitm1
Il1b
F11r
Cd24a
Emb
Cd4
Tspan10
Timd4
Wfdc17
C
Spliced
Unspliced
Follicular LysoDC 80% 20%
Immature LysoDC 84% 16%
Intermediate LysoDC 81% 19%
Mature LysoDC 81% 19%
Proliferative LysoDC 83% 17%
TIM4- LysoMac 81% 19%
TIM4+ LysoMac 83% 17%
0.0 0.2 0.4 0.6 0.8 1.0
Basins
Emission (emerging streamlines only)
Intermediate (converging/emerging)
Attraction (converging streamlines only)

Figure 5

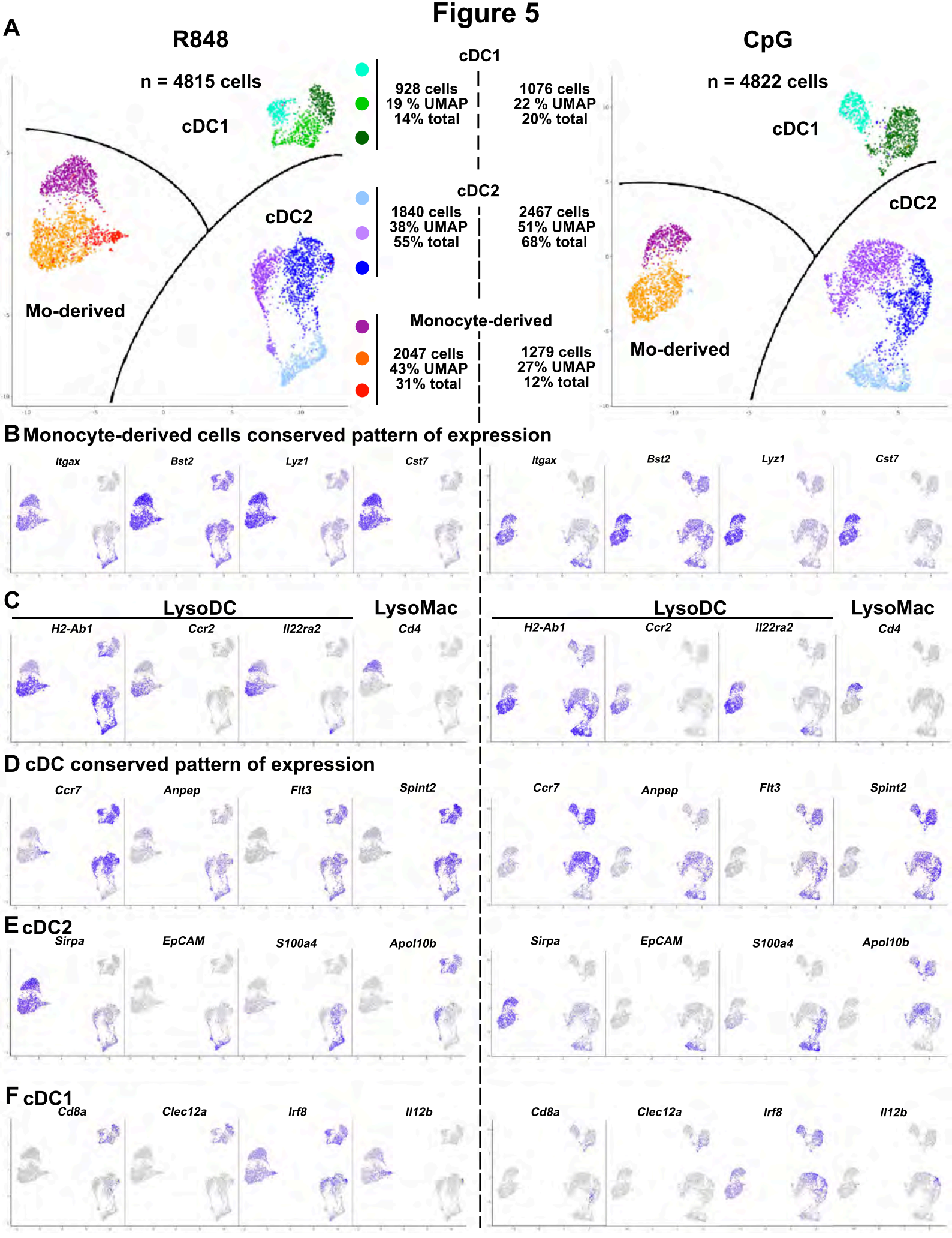
A
R848
n = 4815 cells
cDC1
cDC2
Mo-derived
cDC1
928 cells
19 % UMAP
14% total
1076 cells
22 % UMAP
20% total
cDC2
1840 cells
38% UMAP
55% total
2467 cells
51% UMAP
68% total
Monocyte-derived
2047 cells
43% UMAP
31% total
1279 cells
27% UMAP
12% total
CpG
n = 4822 cells
cDC1
cDC2
Mo-derived
B Monocyte-derived cells conserved pattern of expression
Itgax
Bst2
Lyz1
Cst7
C
LysoDC
LysoMac
H2-Ab1
Ccr2
Il22ra2
Cd4
D cDC conserved pattern of expression
Ccr7
Anpep
Flt3
Spint2
E cDC2
Sirpa
EpCAM
S100a4
Apol10b
F cDC1
Cd8a
Clec12a
Irf8
Il12b

Figure 6

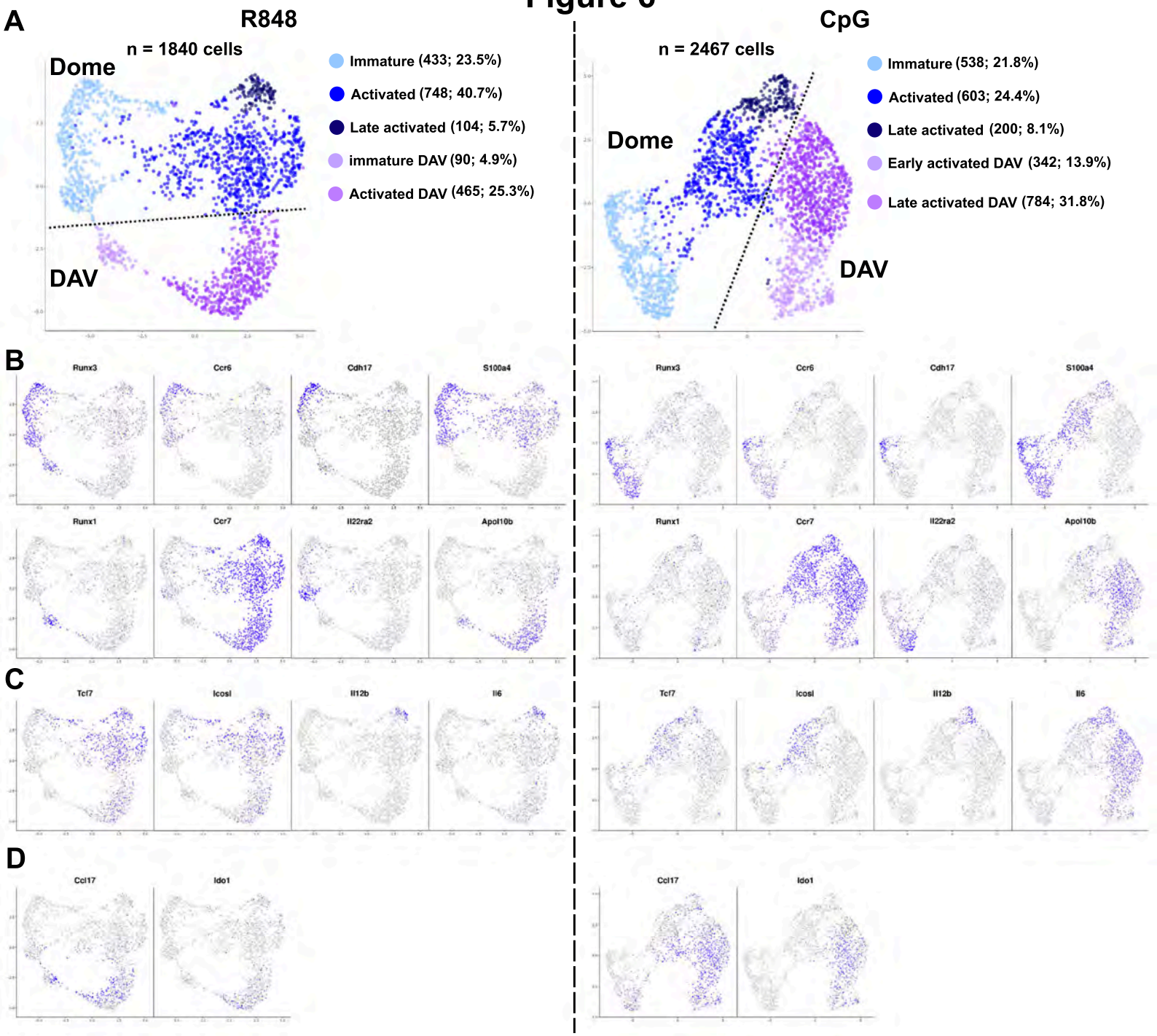
A
R848
n = 1840 cells
Dome
DAV
Immature (433; 23.5%)
Activated (748; 40.7%)
Late activated (104; 5.7%)
immature DAV (90; 4.9%)
Activated DAV (465; 25.3%)
CpG
n = 2467 cells
Dome
DAV
Immature (538; 21.8%)
Activated (603; 24.4%)
Late activated (200; 8.1%)
Early activated DAV (342; 13.9%)
Late activated DAV (784; 31.8%)
B
Runx3
Ccr6
Cdh17
S100a4
Runx1
Ccr7
Il22ra2
Apol10b
C
Tcf7
Icosl
Il12b
Il6
D
Ccl17
Ido1

Figure 7

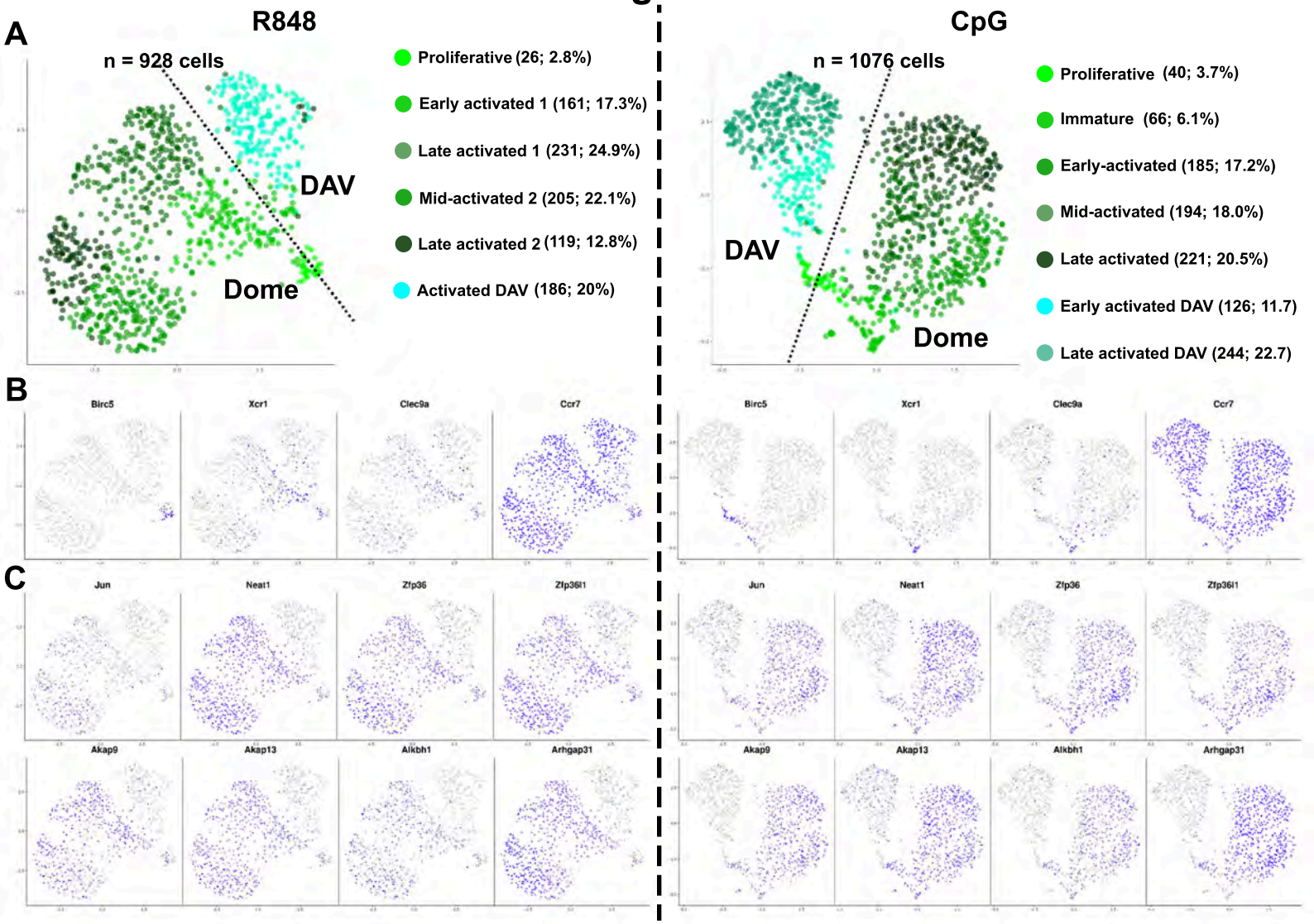
A
R848
n = 928 cells
DAV
Dome
Proliferative (26; 2.8%)
Early activated 1 (161; 17.3%)
Late activated 1 (231; 24.9%)
Mid-activated 2 (205; 22.1%)
Late activated 2 (119; 12.8%)
Activated DAV (186; 20%)
CpG
n = 1076 cells
DAV
Dome
Proliferative (40; 3.7%)
Immature (66; 6.1%)
Early-activated (185; 17.2%)
Mid-activated (194; 18.0%)
Late activated (221; 20.5%)
Early activated DAV (126; 11.7)
Late activated DAV (244; 22.7)
B
Birc5
Xcr1
Clec9a
Ccr7
C
Jun
Neat1
Zfp36
Zfp36l1
Akap9
Akap13
Alkbh1
Arhgap31

Figure 8

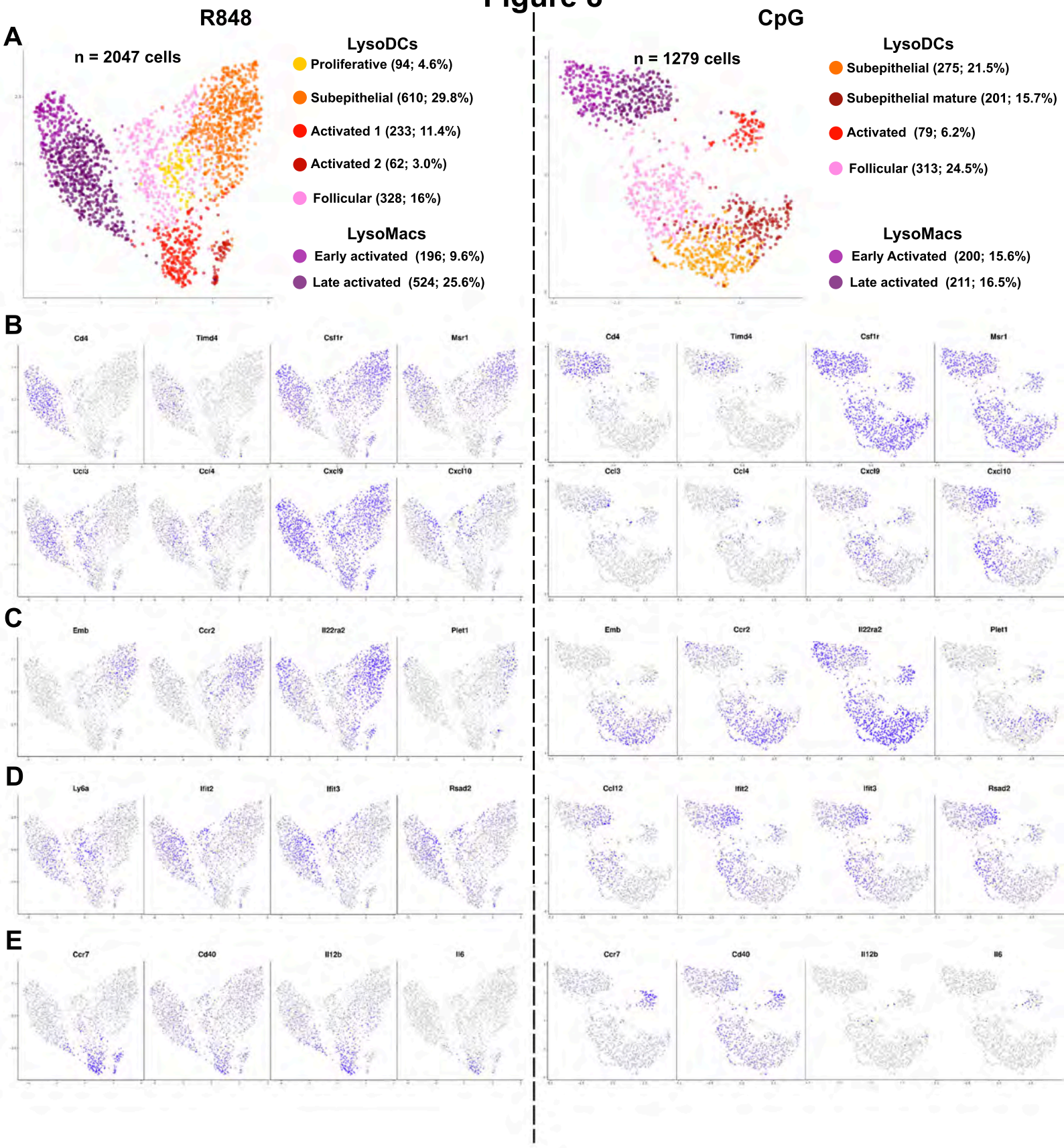
R848
CpG
A
n = 2047 cells
n = 1279 cells
LysoDCs
Proliferative (94; 4.6%)
Subepithelial (610; 29.8%)
Activated 1 (233; 11.4%)
Activated 2 (62; 3.0%)
Follicular (328; 16%)
LysoMacs
Early activated (196; 9.6%)
Late activated (524; 25.6%)
LysoDCs
Subepithelial (275; 21.5%)
Subepithelial mature (201; 15.7%)
Activated (79; 6.2%)
Follicular (313; 24.5%)
LysoMacs
Early Activated (200; 15.6%)
Late activated (211; 16.5%)
B
Cd4
Timd4
Csf1r
Msr1
Ccl3
Ccl4
Cxcl9
Cxcl10
C
Emb
Ccr2
Il22ra2
Plet1
D
Ly6a
Ifit2
Ifit3
Rsad2
Ccl12
E
Ccr7
Cd40
Il12b
Il6

Figure 9

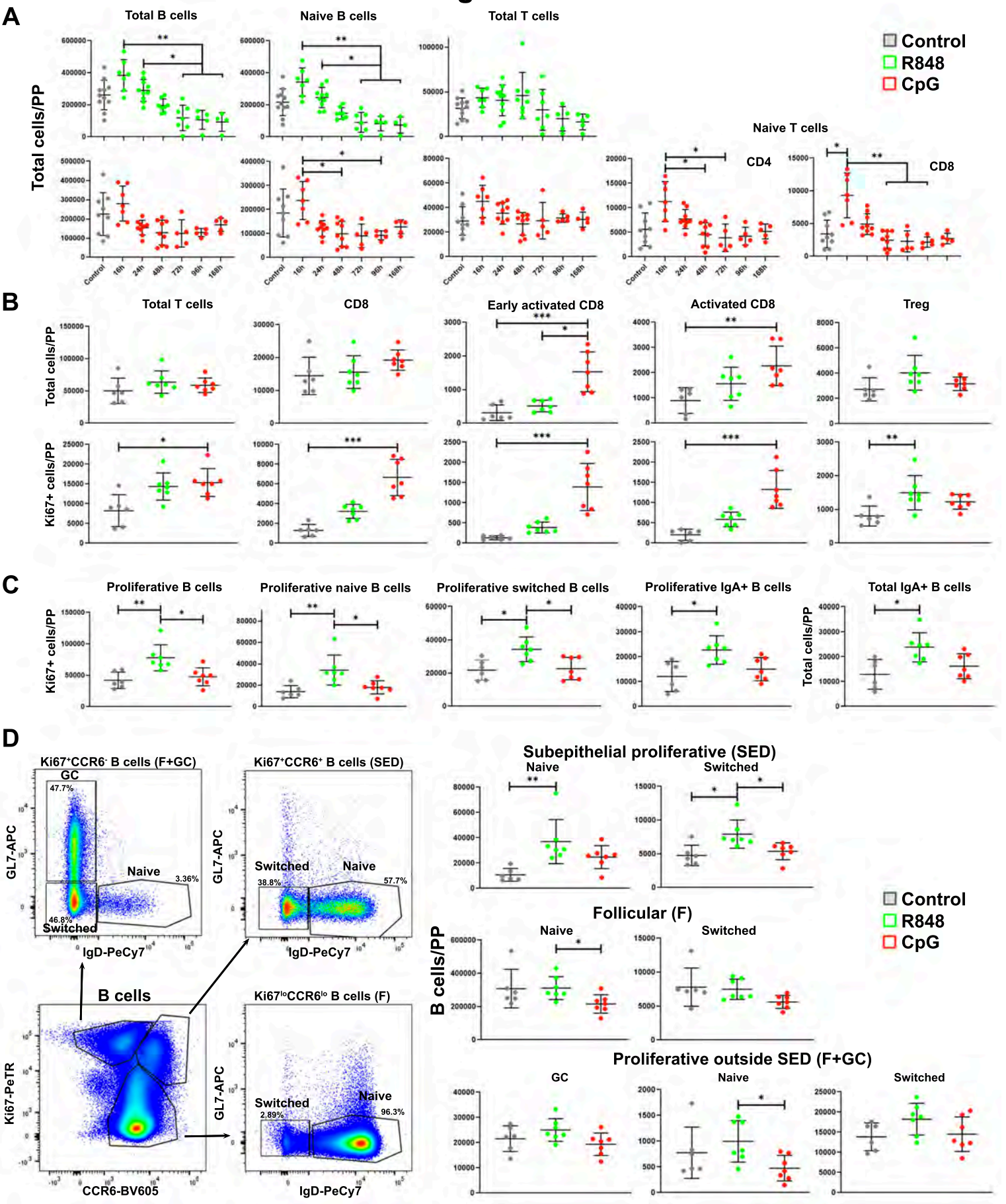
A
Total B cells
Naive B cells
Total T cells
Naive T cells
CD4
CD8
Total cells/PP
Control
R848
CpG
Control
16h
24h
48h
72h
96h
168h
B
Total T cells
CD8
Early activated CD8
Activated CD8
Treg
Total cells/PP
Ki67+ cells/PP
C
Proliferative B cells
Proliferative naive B cells
Proliferative switched B cells
Proliferative IgA+ B cells
Total IgA+ B cells
Ki67+ cells/PP
Total cells/PP
D
Ki67+CCR6- B cells (F+GC)
GC
47.7%
Naive
3.36%
46.8%
Switched
GL7-APC
IgD-PeCy7
Ki67+CCR6+ B cells (SED)
Switched
Naive
38.8%
57.7%
GL7-APC
IgD-PeCy7
B cells
Ki67-PeTR
CCR6-BV605
Ki67loCCR6lo B cells (F)
Switched
Naive
2.89%
96.3%
GL7-APC
IgD-PeCy7
Subepithelial proliferative (SED)
Naive
Switched
Follicular (F)
Naive
Switched
B cells/PP
Control
R848
CpG
Proliferative outside SED (F+GC)
GC
Naive
Switched

Figure S1

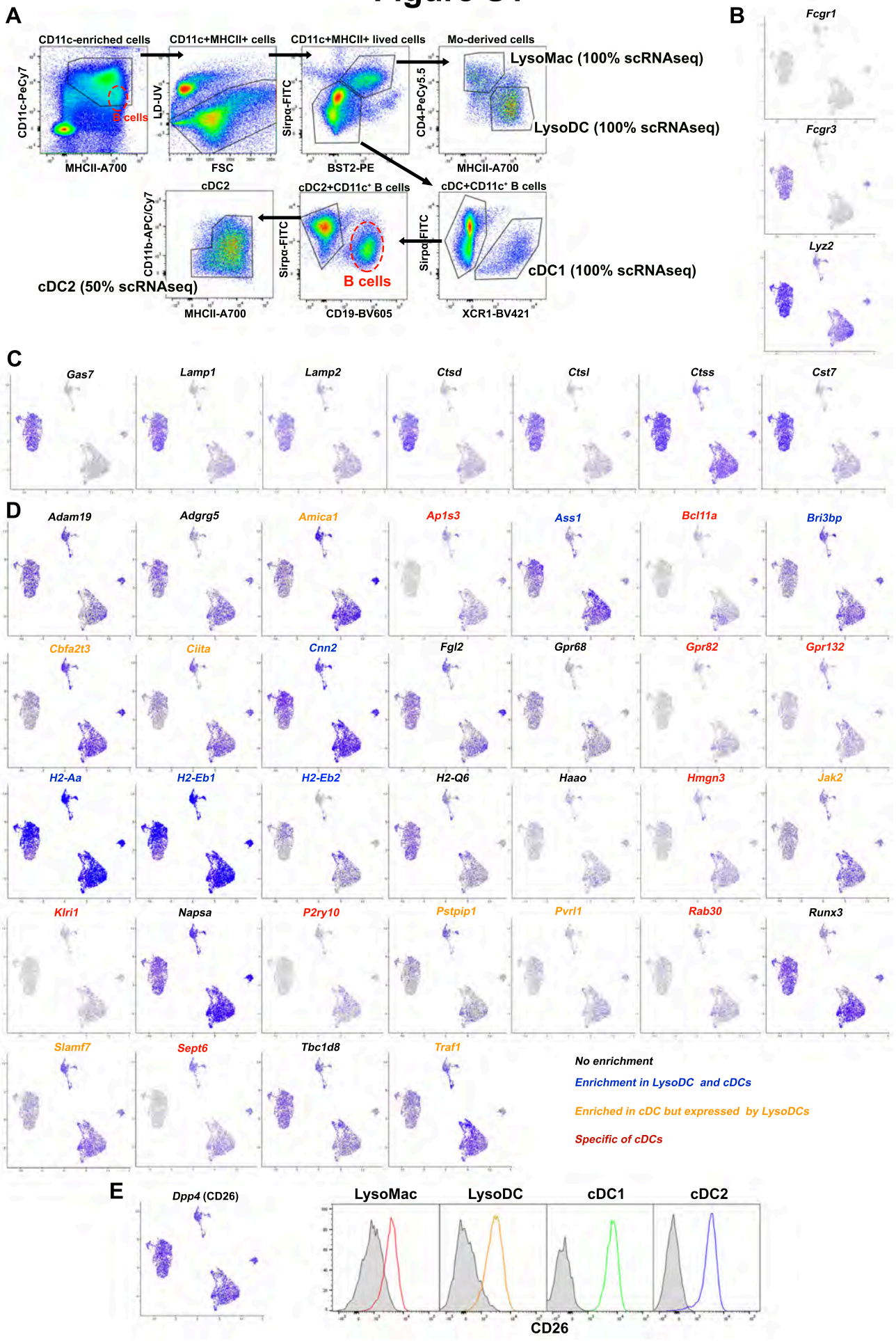
A
CD11c-enriched cells
CD11c+MHCII+ cells
CD11c+MHCII+ lived cells
Mo-derived cells
CD11c-PeCy7
B cells
MHCII-A700
LD-UV
FSC
Sirpα-FITC
BST2-PE
CD4-PeCy5.5
MHCII-A700
LysoMac (100% scRNAseq)
LysoDC (100% scRNAseq)
cDC2
cDC2+CD11c+ B cells
cDC+CD11c+ B cells
CD11b-APC/Cy7
Sirpα-FITC
Sirpα-FITC
B cells
MHCII-A700
CD19-BV605
XCR1-BV421
cDC2 (50% scRNAseq)
cDC1 (100% scRNAseq)
B
Fcgr1
Fcgr3
Lyz2
C
Gas7
Lamp1
Lamp2
Ctsd
Ctsl
Ctss
Cst7
D
Adam19
Adgrg5
Amica1
Ap1s3
Ass1
Bcl11a
Bri3bp
Cbfa2t3
Ciita
Cnn2
Fgl2
Gpr68
Gpr82
Gpr132
H2-Aa
H2-Eb1
H2-Eb2
H2-Q6
Haao
Hmgn3
Jak2
Klri1
Napsa
P2ry10
Pstpip1
Pvrl1
Rab30
Runx3
Slamf7
Sept6
Tbc1d8
Traf1
No enrichment
Enrichment in LysoDC and cDCs
Enriched in cDC but expressed by LysoDCs
Specific of cDCs
E
Dpp4 (CD26)
LysoMac
LysoDC
cDC1
cDC2
CD26

Figure S2

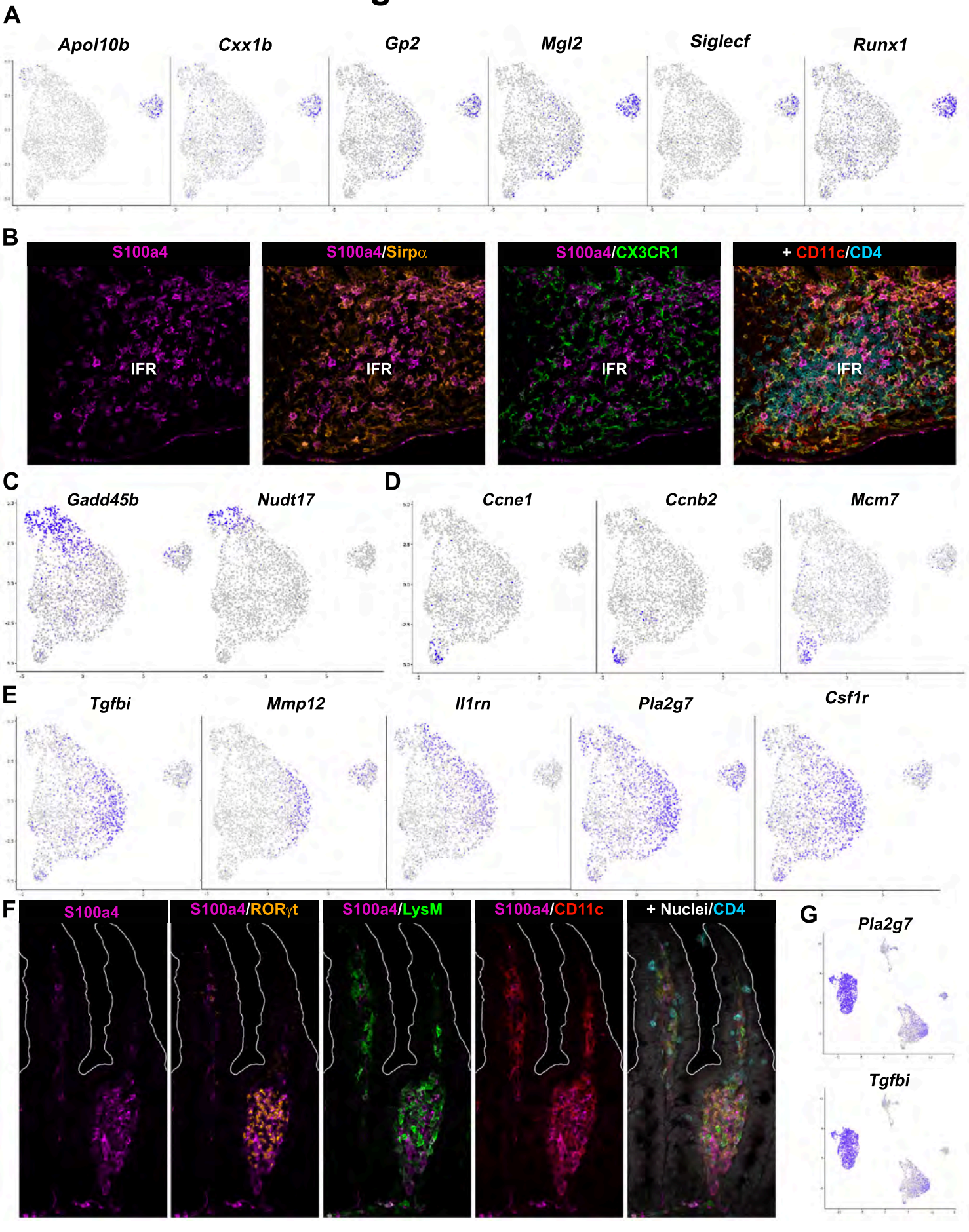
A
Apol10b
Cxx1b
Gp2
Mgl2
Siglecf
Runx1
B
S100a4
S100a4/Sirpα
S100a4/CX3CR1
+ CD11c/CD4
IFR
C
Gadd45b
Nudt17
D
Ccne1
Ccnb2
Mcm7
E
Tgfbi
Mmp12
Il1rn
Pla2g7
Csf1r
F
S100a4
S100a4/RORγt
S100a4/LysM
S100a4/CD11c
+ Nuclei/CD4
G
Pla2g7
Tgfbi

Figure S3

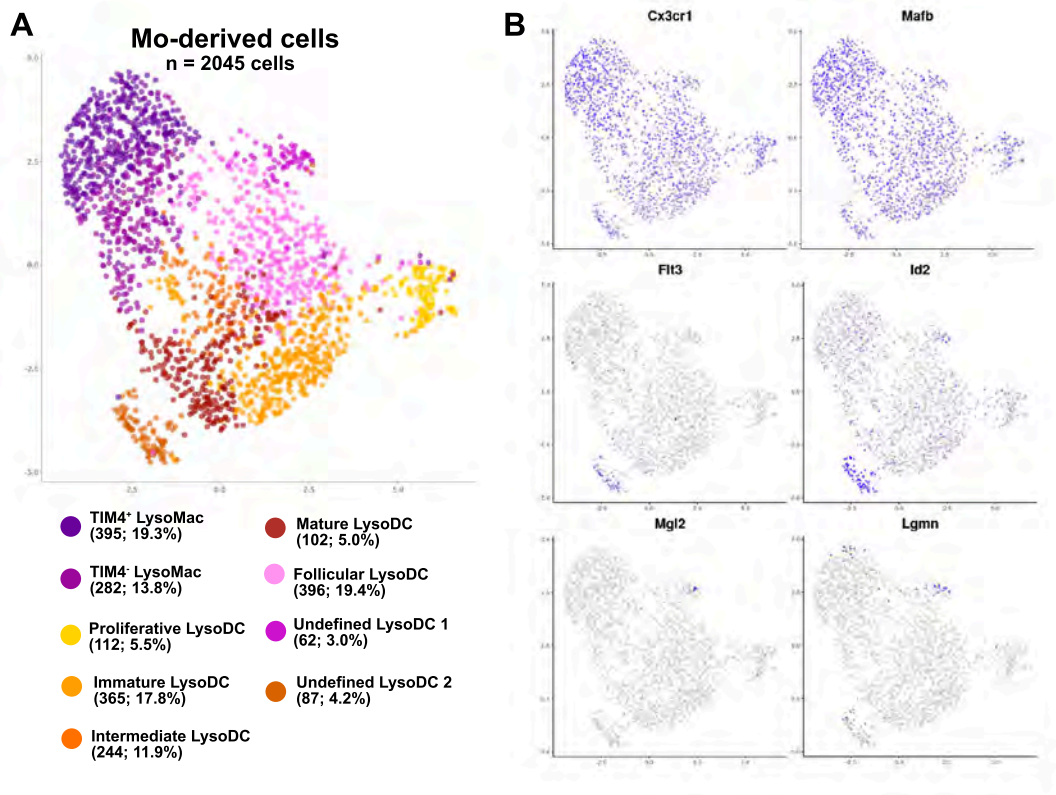

Figure S4

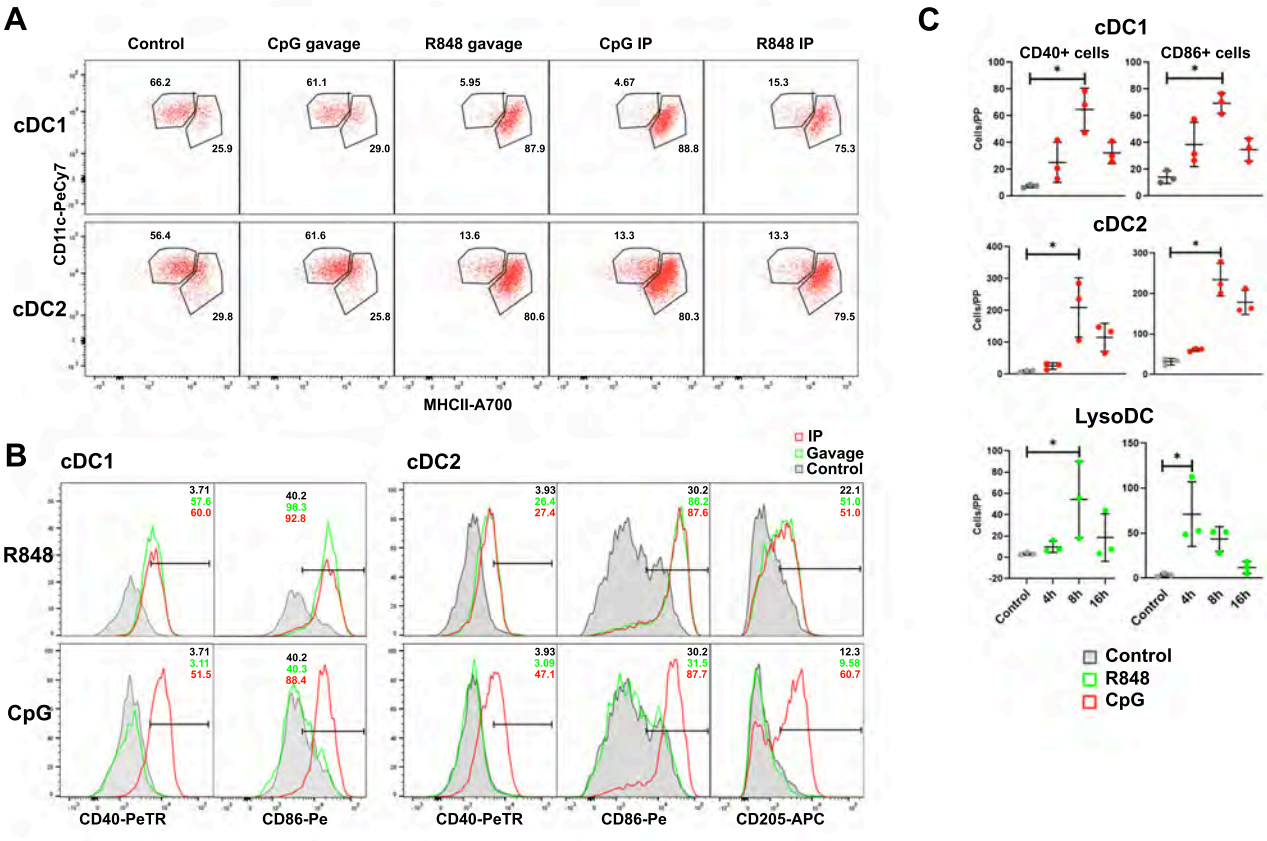

Figure S5


A
Lyz2
Gas7
Lamp1
Lamp2
Ctsd
Ctsl
Ctss
R848
CpG
B
Csf1r
Cx3cr1
Mafb
Msr1
MerTK
R848
CpG
C
Cd74
H2-Aa
H2-Eb1
H2-DMa
H2-DMb2
R848
CpG

Figure S6

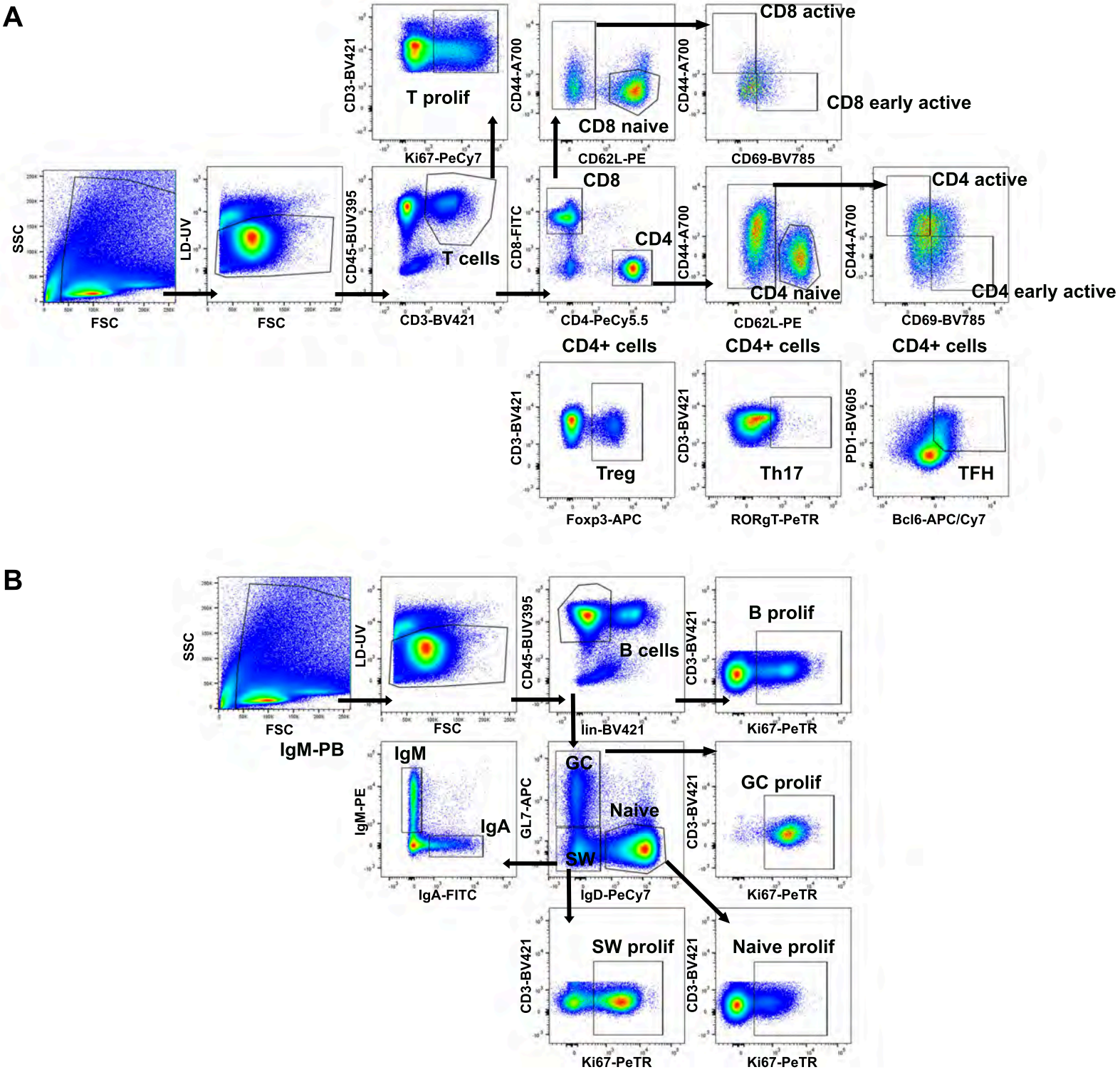
A
SSC
FSC
LD-UV
FSC
CD45-BUV395
CD3-BV421
T cells
CD3-BV421
Ki67-PeCy7
T prolif
CD8-FITC
CD4-PeCy5.5
CD8
CD4
CD44-A700
CD62L-PE
CD8 naive
CD44-A700
CD69-BV785
CD8 active
CD8 early active
CD44-A700
CD62L-PE
CD4 naive
CD44-A700
CD69-BV785
CD4 active
CD4 early active
CD4+ cells
CD3-BV421
Foxp3-APC
Treg
CD4+ cells
CD3-BV421
RORgT-PeTR
Th17
CD4+ cells
PD1-BV605
Bcl6-APC/Cy7
TFH
B
SSC
FSC
IgM-PB
LD-UV
FSC
CD45-BUV395
B cells
lin-BV421
CD3-BV421
Ki67-PeTR
B prolif
IgM-PE
IgA-FITC
IgM
IgA
GL7-APC
IgD-PeCy7
GC
Naive
SW
CD3-BV421
Ki67-PeTR
GC prolif
CD3-BV421
Ki67-PeTR
SW prolif
CD3-BV421
Ki67-PeTR
Naive prolif

Methods

Mice

7-10 weeks old C57Bl6/J males and females were obtained from Janvier Labs. CX3CR1-GFP and Lys-EGFP mice have been previously described (Faust et al., 2000; Jung et al., 2000). Mice were maintained at our animal house facility in ventilated cages under specific pathogen free conditions at an ambient temperature of 22°C with a 12h light/dark cycle. The French ethical committee approved all animal studies.

Antibodies

XCR1-BV421 (clone ZET), CD19-BV625 (clone 6D5), BST2-PE and-BV605 (clone 927), CD11c-PeCy7 (clone N418), CD11b-APC/Cy7 (clone M1/70), IgD-Pe/Cy7 (clone 11-26c.2a), CD8a-AF488 (clone 53-6.7), CD64-PE (clone X54-5/7.1), CD86-PE (clone GL1), CD40-biotin (clone 3/23), CD205-APC (clone NLCD-145) and CD19-BV605 (clone 6D5) were purchased from BioLegend. CD24-BV786 (clone M1/69), CD172a-FITC (clone P84), CD101-AF647 (clone 307707), CCR7-PE (clone 4B12), CCR6-BV605 (29-2L17), CD45-BUV395 (clone 30-F11), Siglec-F-BV421 (clone E50-2440), PD-1-BV605 (clone J43), CD62L-PE (clone MEL-14), B220-BV786 (clone RA3-6B2), CD26-BUV737 (clone H194-112), CD43-BUV737 (clone S7), CD69-BV786 (clone H1.2F3) and Bcl6-APC/Cy7 (clone K112-91) were purchased from BD Biosciences. CD4-eFluor450 (clone RM4-5), Ki-67-eFluor660 and –PE/Cy7 (clone SolA15), RORgt-Pe-eFluor610 (clone B2D), GL-7-eFluor660 (clone GL-7), CD3-eFluor450 (clone 17A2), CD4-PeCy5.5 (clone RM4-5), MHCII-A700 (clone M5/114.15.2), CD172a -biotin (clone P84), IgA-PE (clone mA-6E1), CD38-A700 (clone 90), IgM-biotin (clone II/41), FoxP3-APC (clone FJK-16S),

CD44-A700 (clone IM7) and CD209b-A488 (clone 22D1) were purchased from ThermoFisher Scientific.

Chicken anti-GFP (polyclonal) was from AvesLab. Armenian hamster anti CD11c (clone N418) was from Biolegend. Rat anti Sirpα was from BD Biosciences. Rat anti RORgt was from ThermoFisher Scientific. Rabbit anti S100a4 was from Bio-Techne. Donkey anti chicken coupled to Alexa Fluor 488, goat anti hamster coupled to Alexa Fluor 594 and donkey anti rat coupled to Cy3 were from Jackson Immunoresearch. donkey anti rabbit coupled to Alexa Fluor 647 and SYTOX blue were from ThermoFisher Scientific.

R848 and CpG treatment

Gavage and intraperitoneal injections were performed with 10 µg of R848 (Invivogen) and 125µg of CpG (Integrated DNA Technologies) in 100 µL of sterile PBS. Fingolimod hydrochloride (FTY720, Cayman chemical company) was dissolved in 0.1% NaCl and injected intraperitoneally at 1mg/kg in 200µL twenty-four hours after stimulation.

Immunofluorescence staining and confocal microscopy

PPs were fixed with Antigenfix (Diapath) for 1 h, washed and processed as previously described (Lelouard et al., 2012). Slides were observed with a Zeiss LSM 780 confocal microscope using the spectral imaging mode (Lelouard et al., 2018). Images were analysed using Adobe Photoshop CC 2019.

Cell extraction

PPs were digested with collagenase II/DNase I as previously described (Bonnardel et al., 2015b). $CD11c^+$ cells were sorted using anti-CD11c microbeads and an AutoMACS magnetic cell separator

according to manufacturer's instructions (Miltenyi Biotec). The small intestines devoid of PPs were cut longitudinally in half and washed in a Petri dish with PBS. They were cut into 2mm² pieces in complete medium containing DTT (1mM) and were washed quickly in cold Hank's Balanced Salt Solution (HBSS) containing 2% FCS. Intestinal epithelial cells were removed by incubating tissues in EDTA buffer (HBSS, EDTA 2mM) at 37°C for 20 min in a shaker. This step was repeated once after a quick wash with HBSS buffer. Tissues were then digested with collagenase VIII (1mg/mL) and DNAse I (200µg/mL) at 37°C in a shaker for 15 min. Digestion was stopped by adding 20 mL of cold PEF 2%. Debris were removed by filtration with a 70 µm cell strainer.

Flow cytometry and cell sorting

Cells were preincubated on ice for 5 min with 2.4G2 antibody to block Fc receptors and stained for surface markers. Cell mortality was evaluated using LIVE/DEAD™ Fixable Blue Dead Cell Stain Kit (Life Technologies). Intracellular staining was performed using eBioscience™ Intracellular Fixation & Permeabilization Buffer Set according to manufacturer's instructions (Invitrogen). Multiparametric flow cytometry and cell sorting were performed using a FACS LSRII UV and a FACSAria III (BD Biosciences), respectively. Numbers of sorted cells to be sequenced were adjusted to allow a good representativeness of all subsets as detailed in Table S1. Data were analyzed with Flow Jo software.

Statistical analysis

Results were compared with GraphPad Prism 8 software using nonparametric Kruskal-Wallis with Dunn's multiple comparisons tests.

Single cell RNA-sequencing analysis

Next generation sequencing was performed using the Chromium Single Cell 3' kit from 10X genomics (California, USA) for the library preparation and the NextSeq 500/550 High Output Kit v2 (75 cycles) cartridges from Illumina for the sequencing. FASTQ raw files were processed using Cell Ranger software (v2.1.1, default parameters), which performs alignment, filtering, barcode counting and unique molecular identifier (UMI) counting. Reads were aligned to the mouse mm10 genome. Quality control (QC) was performed to remove poor quality cells thanks to in-house developed R scripts. Using Seurat R package CreateSeuratObject function, cells with less than 200 or more than 5000 (potential doublets) detected genes, cells with low number of UMI (log10 (UMI) < 3.3) and cells with more than 40% mitochondrial gene expression (apoptotic cells) were removed. Dimensionality reduction and clustering was performed using Uniform manifold approximation and projection (UMAP) embedding map colored by Seurat clustering. RNA velocity analysis was performed with scVelo (Bergen et al., 2020).

References

Becker, M., Guttler, S., Bachem, A., Hartung, E., Mora, A., Jakel, A., Hutloff, A., Henn, V., Mages, H.W., Gurka, S., and Kroczek, R.A. (2014). Ontogenic, Phenotypic, and Functional Characterization of XCR1(+) Dendritic Cells Leads to a Consistent Classification of Intestinal Dendritic Cells Based on the Expression of XCR1 and SIRPalpha. Frontiers in immunology *5*, 326.

Bergen, V., Lange, M., Peidli, S., Wolf, F.A., and Theis, F.J. (2020). Generalizing RNA velocity to transient cell states through dynamical modeling. Nat Biotechnol.

Bonnardel, J., Da Silva, C., Henri, S., Tamoutounour, S., Chasson, L., Montanana-Sanchis, F., Gorvel, J.P., and Lelouard, H. (2015a). Innate and Adaptive Immune Functions of Peyer's Patch Monocyte-Derived Cells. Cell reports *11*, 770-784.

Bonnardel, J., Da Silva, C., Masse, M., Montanana-Sanchis, F., Gorvel, J.P., and Lelouard, H. (2015b). Gene expression profiling of the Peyer's patch mononuclear phagocyte system. Genom Data *5*, 21-24.

Bonnardel, J., Da Silva, C., Wagner, C., Bonifay, R., Chasson, L., Masse, M., Pollet, E., Dalod, M., Gorvel, J.P., and Lelouard, H. (2017). Distribution, location, and transcriptional profile of Peyer's patch conventional DC subsets at steady state and under TLR7 ligand stimulation. Mucosal Immunol *10*, 1412-1430.

Bosteels, C., Neyt, K., Vanheerswynghels, M., van Helden, M.J., Sichien, D., Debeuf, N., De Prijck, S., Bosteels, V., Vandamme, N., Martens, L., *et al.* (2020). Inflammatory Type 2 cDCs Acquire Features of cDC1s and Macrophages to Orchestrate Immunity to Respiratory Virus Infection. Immunity *52*, 1039-1056 e1039.

Contractor, N., Louten, J., Kim, L., Biron, C.A., and Kelsall, B.L. (2007). Cutting edge: Peyer's patch plasmacytoid dendritic cells (pDCs) produce low levels of type I interferons: possible role for IL-10, TGFbeta, and prostaglandin E2 in conditioning a unique mucosal pDC phenotype. Journal of immunology *179*, 2690-2694.
Craig, S.W., and Cebra, J.J. (1971). Peyer's patches: an enriched source of precursors for IgA-producing immunocytes in the rabbit. The Journal of experimental medicine *134*, 188-200.
Da Silva, C., Wagner, C., Bonnardel, J., Gorvel, J.P., and Lelouard, H. (2017). The Peyer's Patch Mononuclear Phagocyte System at Steady State and during Infection. Frontiers in immunology *8*, 1254.
Durai, V., Bagadia, P., Briseño, C.G., Theisen, D.J., Iwata, A., Davidson, J.T.t., Gargaro, M., Fremont, D.H., Murphy, T.L., and Murphy, K.M. (2018). Altered compensatory cytokine signaling underlies the discrepancy between Flt3(-/-) and Flt3l(-/-) mice. The Journal of experimental medicine *215*, 1417-1435.
Faust, N., Varas, F., Kelly, L.M., Heck, S., and Graf, T. (2000). Insertion of enhanced green fluorescent protein into the lysozyme gene creates mice with green fluorescent granulocytes and macrophages. Blood *96*, 719-726.
Guendel, F., Kofoed-Branzk, M., Gronke, K., Tizian, C., Witkowski, M., Cheng, H.-W., Heinz, G.A., Heinrich, F., Durek, P., Norris, P.S., *et al.* (2020). Group 3 Innate Lymphoid Cells Program a Distinct Subset of IL-22BP-Producing Dendritic Cells Demarcating Solitary Intestinal Lymphoid Tissues. Immunity *53*, 1015-1032.e1018.
Hanawa-Suetsugu, K., Itoh, Y., Ab Fatah, M., Nishimura, T., Takemura, K., Takeshita, K., Kubota, S., Miyazaki, N., Wan Mohamad Noor, W.N.I., Inaba, T., *et al.* (2019). Phagocytosis is mediated by two-dimensional assemblies of the F-BAR protein GAS7. Nature communications *10*, 4763.
Jinnohara, T., Kanaya, T., Hase, K., Sakakibara, S., Kato, T., Tachibana, N., Sasaki, T., Hashimoto, Y., Sato, T., Watarai, H., *et al.* (2017). IL-22BP dictates characteristics of Peyer's patch follicle-associated epithelium for antigen uptake. The Journal of experimental medicine *214*, 1607-1618.
Jung, C., Hugot, J.P., and Barreau, F. (2010). Peyer's Patches: The Immune Sensors of the Intestine. International journal of inflammation *2010*, 823710.
Jung, S., Aliberti, J., Graemmel, P., Sunshine, M.J., Kreutzberg, G.W., Sher, A., and Littman, D.R. (2000). Analysis of fractalkine receptor CX(3)CR1 function by targeted deletion and green fluorescent protein reporter gene insertion. Molecular and cellular biology *20*, 4106-4114.
Kawaguchi, M., Yamamoto, K., Takeda, N., Fukushima, T., Yamashita, F., Sato, K., Kitamura, K., Hippo, Y., Janetka, J.W., and Kataoka, H. (2019). Hepatocyte growth factor activator inhibitor-2 stabilizes Epcam and maintains epithelial organization in the mouse intestine. Communications biology *2*, 11.
Kim, S.-H., Cho, B.-H., Kim, K.S., and Jang, Y.-S. (2021). Complement C5a promotes antigen cross-presentation by Peyer's patch monocyte-derived dendritic cells and drives a protective CD8+ T cell response. Cell reports *35*, 108995.
Kimura, S., Yamakami-Kimura, M., Obata, Y., Hase, K., Kitamura, H., Ohno, H., and Iwanaga, T. (2015). Visualization of the entire differentiation process of murine M cells: suppression of their maturation in cecal patches. Mucosal Immunol *8*, 650-660.
Kunimura, K., Sakata, D., Tun, X., Uruno, T., Ushijima, M., Katakai, T., Shiraishi, A., Aihara, R., Kamikaseda, Y., Matsubara, K., *et al.* (2019). S100A4 Protein Is Essential for the Development of Mature Microfold Cells in Peyer's Patches. Cell reports *29*, 2823-2834.e2827.
Lelouard, H., Fallet, M., de Bovis, B., Meresse, S., and Gorvel, J.P. (2012). Peyer's patch dendritic cells sample antigens by extending dendrites through M cell-specific transcellular pores. Gastroenterology *142*, 592-601 e593.

Lelouard, H., Henri, S., De Bovis, B., Mugnier, B., Chollat-Namy, A., Malissen, B., Meresse, S., and Gorvel, J.P. (2010). Pathogenic bacteria and dead cells are internalized by a unique subset of Peyer's patch dendritic cells that express lysozyme. Gastroenterology *138*, 173-184 e171-173.
Lelouard, H., Mailfert, S., and Fallet, M. (2018). A ten-color spectral imaging strategy to reveal localization of gut immune cell subsets. Zeiss Application note.
Miller, J.C., Brown, B.D., Shay, T., Gautier, E.L., Jojic, V., Cohain, A., Pandey, G., Leboeuf, M., Elpek, K.G., Helft, J.*, et al.* (2012). Deciphering the transcriptional network of the dendritic cell lineage. Nature immunology *13*, 888-899.
Park, K., Mikulski, Z., Seo, G.Y., Andreyev, A.Y., Marcovecchio, P., Blatchley, A., Kronenberg, M., and Hedrick, C.C. (2016). The transcription factor NR4A3 controls CD103+ dendritic cell migration. The Journal of clinical investigation *126*, 4603-4615.
Reboldi, A., Arnon, T.I., Rodda, L.B., Atakilit, A., Sheppard, D., and Cyster, J.G. (2016). IgA production requires B cell interaction with subepithelial dendritic cells in Peyer's patches. Science *352*, aaf4822.
Reboldi, A., and Cyster, J.G. (2016). Peyer's patches: organizing B-cell responses at the intestinal frontier. Immunological reviews *271*, 230-245.
Schlitzer, A., Sivakamasundari, V., Chen, J., Sumatoh, H.R., Schreuder, J., Lum, J., Malleret, B., Zhang, S., Larbi, A., Zolezzi, F.*, et al.* (2015). Identification of cDC1- and cDC2-committed DC progenitors reveals early lineage priming at the common DC progenitor stage in the bone marrow. Nature immunology *16*, 718-728.
Scott, C.L., Bain, C.C., Wright, P.B., Sichien, D., Kotarsky, K., Persson, E.K., Luda, K., Guilliams, M., Lambrecht, B.N., Agace, W.W.*, et al.* (2015). CCR2(+)CD103(-) intestinal dendritic cells develop from DC-committed precursors and induce interleukin-17 production by T cells. Mucosal Immunol *8*, 327-339.
Szabo, R., Callies, L.K., and Bugge, T.H. (2019). Matriptase drives early-onset intestinal failure in a mouse model of congenital tufting enteropathy. Development (Cambridge, England) *146*.
Wagner, C., Bonnardel, J., Da Silva, C., Martens, L., Gorvel, J.P., and Lelouard, H. (2018). Some news from the unknown soldier, the Peyer's patch macrophage. Cell Immunol *330*, 159-167.
Wagner, C., Bonnardel, J., Da Silva, C., Spinelli, L., Portilla, C.A., Tomas, J., Lagier, M., Chasson, L., Masse, M., Dalod, M.*, et al.* (2020). Differentiation Paths of Peyer's Patch LysoDCs Are Linked to Sampling Site Positioning, Migration, and T Cell Priming. Cell reports *31*.
Waskow, C., Liu, K., Darrasse-Jèze, G., Guermonprez, P., Ginhoux, F., Merad, M., Shengelia, T., Yao, K., and Nussenzweig, M. (2008). The receptor tyrosine kinase Flt3 is required for dendritic cell development in peripheral lymphoid tissues. Nature immunology *9*, 676-683.
Wu, X., Satpathy, A.T., Kc, W., Liu, P., Murphy, T.L., and Murphy, K.M. (2013). Bcl11a Controls Flt3 Expression in Early Hematopoietic Progenitors and Is Required for pDC Development In Vivo. PloS one *8*, e64800.

A-II/ Summary

Using single cell RNA sequencing analysis, spectral confocal microscopy and flow cytometry we highlighted:

- The transcriptional and spatiotemporal landscape of all PP phagocyte populations from their arrival in the tissue to their final maturation state at homeostasis.
- The importance of tissue-specific studies to validate or invalidate so called “universal” markers in the literature.
- The role of the type of stimulus, of the subset identity but also importantly of the initial residence site in the activation profile of dendritic cells.
- The consequences of two different stimuli on the adaptive immune responses initiated in Peyer’s patches.

Altogether, we outlined the importance of targeting not only the right phagocyte subset but also the right place at the right time with the right stimulus to orientate the immune response.

B) Development of a strategy to analyze the gut microbiota composition

B-I/ Introduction

The microbiota is crucial for host immunological, hormonal and metabolic homeostasis. Variations in the composition of the microbiota, both quantitative and qualitative, between and within individuals over time, are associated with a range of health conditions. Deciphering its composition in a fast, semi-quantitative and cost-effective way can therefore be very useful to predict the development of non-communicable diseases such as inflammatory bowel diseases, asthma, obesity and allergies or to identify the causative agents of such diseases (Nagler, 2020).

1) Recent advances in microbiota characterization methods

The methodologies used to classify and determine the composition of the microbiota since the end of the 19th century are summarized in Figure 1. Before the molecular era, the study of intestinal bacteria was first boosted in the 1960s and 1970s by the emergence and utilization of anaerobic cultivation techniques, which identified more than 400 to 500 distinct bacterial species (Dave *et al*., 2012). The morphology, physiology and biochemistry of bacteria were the basis for their taxonomical classification. In 1977, Carl Woese and collaborators described a technique using ribonuclease digestion products of the ribosomal RNA (16S rRNA) as a phylogenetic marker (Woese *et al*., 1977). Bacteria ribosomes consist of a small (30S) and a large (50S) subunit. The 50S subunit contains about thirty-four proteins as well as 5S rRNA (120 bases), and 23S rRNA (about 2900 bases), and the 30S subunit contains about twenty-one proteins and the 16S rRNA (about 1500 bases) (Blaut *et al*., 2002). Because 16S rRNA molecules contain regions with different degrees of variability (varying from conserved to highly variable regions), it is indeed possible to distinguish organisms at different phylogenetic levels (Namsolleck *et al*., 2004). This property has been at the origin of a wide range of applications in microbial taxonomy and microbial ecology (Tindall *et al*., 2010). Then, the first list of validated prokaryotic names was reported in 1980, as an attempt to officially regulate bacterial species names. It initially contained 1791 validated prokaryotic species (Skerman *et al*., 1989). Thereafter, various culture-independent molecular techniques were developed, and during the last decades they have been extensively used to identify bacteria from complex samples. In 2017, 15 448 species were included in the List of Prokaryotic Names with Standing in Nomenclature

(LPSN established in 1997), a key online resource of bacterial and archaeal nomenclature and classification (Parte, 2018).

Culture-independent molecular techniques rely on the isolation of bacterial DNA directly from environmental or biological samples. Quantitative PCR (qPCR) microbiome profiling are based on PCR using oligonucleotide sequences specific to selected microbial clades (Kurina *et al*., 2020). Microbial community profiling or "Fingerprinting" amplifies bacterial DNA by using universal primers that target the 16S rRNA gene. The resulting amplicons contain variable regions that discern the constituent bacteria by electrophoretic or hybridization techniques (Dave *et al*., 2012). A higher-resolution version of this method includes cloning and gene sequencing. Identification of bacteria relies on robust bioinformatics tools, such as the Greengenes database (DeSantis *et al*., 2006), the Ribosomal Database Project (Cole *et al*., 2014), and SILVA (Quast *et al*., 2013).

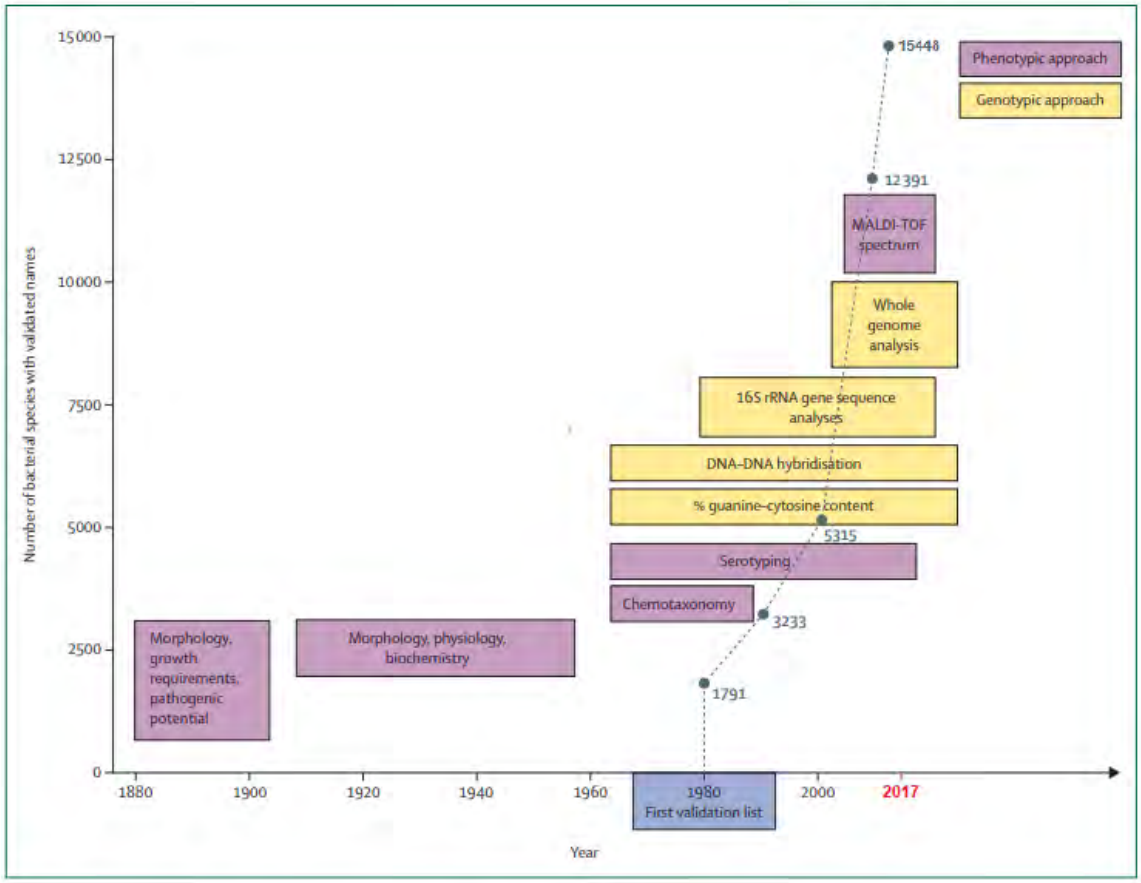

Figure 1: Worldwide changes in bacterial taxonomic methods and the number of described species. Modified from Hugon *et al*., 2015.

Next generation sequencing (NGS) technologies have revolutionized this method by increasing the depth and speed of phylogenetic profiling. Pyrosequencing identifies nucleotides by the amplitude of light signals generated by the luciferin during DNA synthesis. Contrarily to 16S rRNA sequencing techniques, whole genome shotgun sequencing or "Metagenomics" attempts to determine the whole collection of genes within a sample, i.e. microbiome. Generated data are analyzed by assembling the entire genome of microbes with previously characterized genes to build a picture of functional capability of the microbiota (Wooley and Ye, 2009). This very interesting technique allows the extension of the known composition of the gut microbiota. In a recent study, Almeida and collaborators expanded the species repertoire by proposing 1952 uncultured and reference-free candidate bacterial species (Almeida *et al*., 2019).

The different techniques used to characterize the gut microbiota have strengths and weaknesses (Table 1). Molecular techniques also show limitations and biases that may hide the true nature of bacterial biodiversity. The analysis of microbial communities based on multi-template PCR can produce inaccuracies in the abundance and diversity of genes. The basic problems of PCR come from those resulting in sequence artifacts (PCR errors), and those skewing the distribution of PCR products due to unequal amplification (PCR bias) (Peng *et al*., 2018). Most of the techniques are subject of these PCR problems, except for culture, fluorescence *in situ* hybridization (FISH) and metagenomics. There is no clear consensus on what constitutes a bacterial species at a molecular level, so alternative methods of describing ''phylotypes'' are based on operational taxonomic units (OTUs), that are clusters of similar sequence variants of the 16S rRNA gene (Dave *et al*., 2012). Furthermore, OTUs frequencies have low correlation with species frequencies, meaning that the most abundant OTUs usually do not contain the most abundant species (Hamady and Knight, 2009).

The 16S rRNA gene sequences enable to identify and discern taxa; however, their physiological and ecological significance may be missed because a substantial proportion of gut bacteria are unculturable. Even if some major advances have been made by improving culture conditions, only a maximum of 50 % of the OTUs detected by 16S rRNA gene sequencing of fecal samples are cultivable (Lau *et al*., 2016). However, culture using selective media allows for the growth and detection of less abundant bacteria that may be missed by insufficient sequencing depth in culture-independent studies. The cultivation of native strains remains the gold standard of functional studies of the microbiota and their interactions with mammalian hosts until synthetic biology allows a reliable reconstruction of native microorganisms (Hamady and Knight, 2009). A substantial part of the biologic information acquired by high-end sequencers is still not interpretable due to the insufficient quality of databases. Many of the

identified genes do not have a known function. Therefore, most of the data is descriptive and the interpretation remains very often speculative (Lagkouvardos *et al.*, 2017).

Table 1: Advantages and disadvantages of the techniques used to characterize the gut microbiota.

Technique	**Strength**	**Weakness**
Culture	Inexpensive, semi-quantitative	Labor intensive, less than 30% of gut microbiota have been cultured
qPCR	Rapid, quantitative, phylogenetic characterization	PCR bias, unable to identify unknown species
DGGE/TGGE	Rapid, semi-quantitative, bands can be used for further analysis	PCR bias, no phylogenetic characterization
T-RFLP	Inexpensive, rapid, semi-quantitative	PCR bias, no phylogenetic characterization, low resolution
FISH	No PCR bias, semi-quantitative, phylogenetic characterization	Related to probe sequences, incapable of characterizing unknown species
Cloned 16S rRNA gene sequencing	Quantitative, phylogenetic characterization	Labor intensive, PCR bias, expensive, cloning bias
DNA microarrays	Rapid, semi-quantitative, phylogenetic characterization	Cross hybridization, PCR bias, species present in low levels can be difficult to detect
Direct sequencing of 16S rRNA amplicons	Rapid, quantitative, phylogenetic characterization, capable to identify unknown species	Labor intensive, PCR bias, expensive
Shotgun sequencing	Quantitative, phylogenetic characterization	Expensive, analysis of data is computationally intense

Abbreviations: DGGE, denaturing gradient gel electrophoresis; FISH, fluorescence in situ hybridization; qPCR, quantitative PCR; TGGE, temperature gradient gel electrophoresis; T-RFLP, terminal restriction fragment length polymorphism. Adapted from Maccaferri et al., 2011; Fraher et al., 2012 and Rezasoltani et al., 2020.

All these biases suggest that only combination of different techniques allow to gain access to the entire bacterial diversity. For example, absolute quantification of microbial abundances from NGS datasets can be achieved by integrating flow cytometry (Vandeputte *et al.*, 2017). However, only few studies really require this level of resolution. For instance, monitoring changes in the F/B ratio in the gut microbiota of patients requires fingerprinting assay rather than metagenomics as it is much faster and cheaper (Hamady and Knight, 2009).

2) Fluorescence *in situ* hybridization (FISH)

As mentioned above, culture-independent approaches are required to access the uncultivated species. Although metagenomics has emerged as a front-runner technology for this purpose, it does not allow spatial resolution of bacterial communities nor individual identification. Therefore, methods that

fractionate communities into individual cells are valuable complementary approaches to metagenomics. To accomplish this, targeted separation of microorganisms based on the 16S rRNA gene and FISH, emerged in the single-cell genomics field (Haroon *et al*., 2013).

The principle of *in situ* hybridization is the detection of a target DNA or RNA site by a labelled probe molecule. Based on the knowledge of the 16S rRNA sequence information it is possible to design a probe that specifically targets a given organism (Namsolleck *et al*., 2004). In the late 1960s, the earliest *in situ* hybridizations performed were not fluorescent but rather utilized probes labeled with radioisotopes. In the late 1980s, Giovannoni and collaborators were the first to demonstrate the phylogenetic identification of microbial single cells by microscopy with single radiolabeled oligonucleotides (Giovannoni *et al*., 1988). Later, the use of fluorescence for visualization of nucleic acids was developed as an alternative to unstable and less safe radiolabeled probes.

16S rRNA FISH uses fluorescently labeled oligonucleotides that specifically target 16S rRNAs of the ribosome inside of a living cell, thereby causing the cell to fluoresce (Fig. 2) (DeLong et al., 1989). The method takes advantage of a singular property of the rRNAs, the natural amplification of the target site by the presence of hundreds to thousands copies of ribosomes per living cell. For instance, a single *Escherichia coli* cell has between 10^4 and 10^5 ribosomes and, consequently, as many copies of 16S rRNAs (Amman *et al*., 1990). However, sometimes it is impossible to find suitable signature sites on the 16S rRNA making the 23s rRNA an alternative target. The 23s rRNA structure and function are also highly conserved and has twice potential probe target sites than the 16S rRNA. Additionally, there is no significant difference between the hybridization of oligonucleotide probes to 16S and 23S rRNA (Fuchs *et al*., 2001).

The taxonomical Linnaean system categorizes organisms through different levels converging from empire, domain, kingdom, phylum, class, order, family, until it gives them binomial names composed by their genus and species. Ribosomal RNA FISH allows specific targeting of bacteria at resolution levels ranging from phylum to species within the phylogenetic tree and can give *in situ* spatial organization information. Thus, it is now a much-used and important technique (Jovel *et al*., 2016).

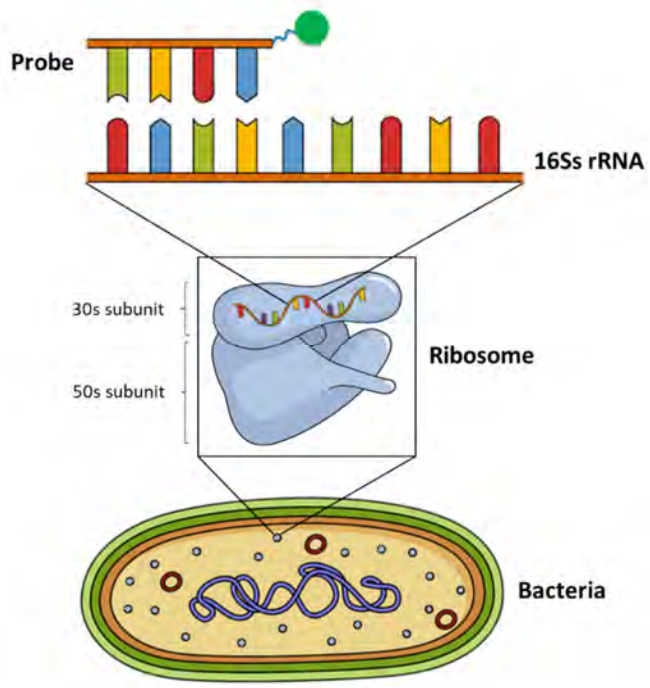

Figure 2: Fluorescence *in situ* hybridization (FISH) using specific 16S rRNA-targeted oligonucleotide probes detects living bacteria.

In principle, bacterial cell wall is permeated and fixed by treatment with lysozyme, paraformaldehyde or/and ethanol to allow the probes to enter into the cell. In stringent and specific conditions, the hybridization between the probe and the complementary targeted 16S rRNA sequence occurs, causing the whole cell to fluoresce (Blaut *et al*, 2002). Generally, these probes are labelled covalently at the 5´ end with a fluorescent dye and have a length of 15-23 nucleotides. After stringent washing, specifically stained cells are detected via epifluorescence microscopy or flow cytometry (Wagner *et al*., 2003).

In our project, we are particularly interested in using the FISH technique to analyze the gut microbiota composition in a fast, semi-quantitative and cost-effective way. To this end, we designed a multiparametric panel including nine specific probes that target main phyla of the gut: Firmicutes, Bacteroidetes, Proteobacteria, Actinobacteria, and Verrucomicrobia.

B-II/ Material and Methods

Bacteria and culture conditions.

All bacteria strains used in this study are listed in Table 2. The strains were obtained from three sources indicated in the table: DSM stands for Deutsche Sammlung von Mikroorganismen und Zellkulturen (Braunschweig, Germany), NCTC for National Collection of Type Cultures, and CSUR for Collection of strains from the Unité des Rickettsies of the IHU Méditerranée Infection (Marseille, France). Bacterial strains were grown in Columbia sheep blood agar plates and hemoculture bottles (BACT/ALERT®) from BioMérieux (Marcy l'Etoile, France) at 37 °C in aerobic or anaerobic condition depending on the strain. Anaerobic condition was achieved using a GasPak generator (Becton Dickinson Microbiology Systems, Sparks, MD, USA). MALDI-TOF MS was used to quickly confirm the identity of the strains. Exponentially grown cells were harvested by centrifugation at 5000 g for 10 min, washed with sterile phosphate-buffered saline (PBS) (Gibco, Life Technologies), and fixed with 4% (wt/vol) paraformaldehyde in PBS for 20 min. After fixation, the bacteria were washed with PBS and stored in 50% ethanol–PBS until FISH procedure.

Table 2. Bacteria used in the FISH studies.

Phylum	*Species*	Origin	Atmosphere
Firmicutes	*Streptococcus gallolyticus*	CSURP715	Aerobic
	Ruminococcus gnavus	CSURP9144	Anaerobic
	Lactobacillus fermentum	CSURP2734	Anaerobic
	Enterococcus faecalis	CSURP2282	Aerobic
	Clostridium butyricum	CSURP295	Anaerobic
	Blautia coccoides	DSM26115	Anaerobic
	Clostridium difficile	CSURP346	Anaerobic
Proteobacteria	*Alcaligenes faecalis*	CSURP580	Aerobic
	Comamonas kerstersii	CSURP849	Aerobic
	Proteus mirabilis	CSURP2711	Aerobic
	Serratia marcescens	CSURP833	Aerobic
	Escherichia coli	CSURP2701	Aerobic
	Salmonella enterica Typhimurium	NCTC 12023	Aerobic
Bacteroidetes	*Bacteroides fragilis*	CSURP4575	Anaerobic
	Bacteroides thetaiotaomicron	CSURP5529	Anaerobic
	Porphyromonas uenonis	CSURP5172	Aerobic
Actinobacteria	*Bifidobacterium adolescentis*	CSURP4050	Anaerobic
	Bifidobacterium longum	CSURP7400	Anaerobic
	Propionibacterium acidipropionici	CSURP2295	Aerobic
Verrucomicrobia	*Akkermansia muciniphila*	DSM 22959	Anaerobic
Fusobacteria	*Fusobacterium necrophorum*	CSURP1016	Anaerobic

Design of oligonucleotide probes

All the probes used in this study are listed in Table 3. Most of them were already published but the one indicated as "This study" were designed by Inmunotech Beckman Coulter (Marseille, France). Based on the 16S rRNA published for all the phyla composing the gut microbiota bacteria (HMP Reference Genomes, NCBI), a first round of alignment was done using Clustal Omega to identify the variable regions allowing to differentiate each phylum. A second round of alignment was performed to identify the conserved region within each phylum. The probes were designed "by hand" using the IUPAC ambiguity codes. Finally, the designed sequences were aligned using NCBI-BLAST against their nucleotide data bank of bacterial and archaeal 16S rRNA to check their phylum-specificity. Fluorophore-labeled probes were commercially synthesized by Eurogentec (Seraing, Belgium) and Integrated DNA Technologies (USA). These probes were linked at their 5' ends with different fluorophores. Non-specific binding was assessed with the complementary sequence of each probe, which corresponds to the target sequence. This probe is referred as the negative one (neg). The probes were tested with the cultured organisms listed in Table 2.

Table 3: rRNA-targeted oligonucleotide probes used.

	Probe	5´-Sequence-3´	Fluorophore	Tm (°C)	Reference
Eubacteria	Eub338	GCTGCCTCCCGTAGGAGT	All	60	Amann *et al*., 1990
	Eub338 neg	ACTCCTACGGGAGGCAGC	All	60	Wallner *et al*., 1993
Bacteroidetes	Bact	ACTTAWCGCTTTCGCTTGGCCGC	A700	62	This study
	Bact neg	GCGGCCAAGCGAAAGCGWTAAGT	A700	62	
	Bac303	CCAATGTGGGGGACCTT	A700	55	Manz *et al*., 1996
	Bacto1080	GCACTTAAGCCGACACCT	A700	55	Doré *et al*., 1998
Actinobacteria	HCG664	AGGAATTCCAGTCTCCCC	A488	54	Glöckner *et al*., 2000
	HCG664 neg	GGGGAGACTGGAATTCCT	A488	54	
Akkermansia muciniphila	MUC 1437	CCTTGCGGTTGGCTTCAGAT	A647	58	Derrien *et al*., 2008
	MUC 1437 neg	ATCTGAAGCCAACCGCAAGG	A647	58	
Proteobacteria	Proteoβγ*	GTGGTAAKCGYCCTCC	Cy3	52	This study
	Proteoβγ neg*	GGAGGRCGMTTACCAC	Cy3	52	
	Proteoε*	GTTARSTGCATTACTG	Cy3	42	
	Proteoε neg*	CAGTAATGCASYTAAC	Cy3	42	
	Alf968*	GGTAAGGTTCTGCGCGTT	Cy3	56	Manz *et al*., 1992
	Alf968 neg*	AACGCGCAGAACCTTACC	Cy3	56	
	Bet42a*	GCCTTCCCACTTCGTTT	Cy3	53	
	Bet42a neg*	AAACGAAGTGGGAAGGC	Cy3	53	
	Gam42a*	GCCTTCCCACATCGTTT	Cy3	53	
	Gam42a neg*	AAACGATGTGGGAAGGC	Cy3	53	
Firmicutes	LGC354A*	TGGAAGATTCCCTACTGC	CF405s	51	Meier *et al*., 1999
	LGC354A neg*	GCAGTAGGGAATCTTCCA	CF405s	51	
	LGC354B*	CGGAAGATTCCCTACTGC	CF405s	52	
	LGC354B neg*	GCAGTAGGGAATCTTCCG	CF405s	52	
	LGC354C*	CCGAAGATTCCCTACTGC	CF405s	52	
	LGC354C neg*	GCAGTAGGGAATCTTCGG	CF405s	52	
	Erec482	GCTTCTTAGTCARGTACCG	CF405s	51	Franks *et al*., 1998
	Erec482 neg	CGGTACYTGACTAAGAAGC	CF405s	51	

* In an equimolar mixture for each group

IUPAC ambiguity codes: R = G or A; Y = C or T; M = A or C; K = G or T; S = G or C; W = A or T; H = A or C or T; B = G or T or C; V = G or C or A; D = G or A or T. Tm: melting temperature. All: A430, Pacific Blue, CF405s, HL405, e393, A488, Cy3, A647, A700, and A750. neg: negative probe. A: AlexaFluor®

Sample preparation and FISH Flow- acquisition

Samples were pelleted by centrifugation (Eppendorf microcentrifuge; 5000g, 5 min, 4°C), washed with PBS, and resuspended in 100 µL of 0.5% Triton-PBS (Sigma-Aldrich Corporation, Burlington, Massachusetts) and 100 µL of lysozyme (10mg/mL in PBS; Sigma L6876). The samples were incubated for 30 min at 37°C in a ThermoMixer (Eppendorf). Pellets were washed in 1 mL of PBS and then resuspended in 50 µL of Hybridization Buffer (HB; 20mM Tris-HCl**,** 3M NaCl, 0.01% SDS, [pH=7.5] filtered with 0.2µm filter), to which were added the appropriate amount of each probe. For total bacterial count, propidium Iodide (PI) was used at 50 ng/µL. Hybridization was conducted 3h at 42°C in darkness with 300 rpm shake. Non-bound probe was removed by adding 1 mL of HB to each tube for an additional 45 min incubation. After centrifugation, pellets were resuspended in PBS (500 µL) for data acquisition. Data acquisition was performed using a Cytoflex flow cytometer (Beckman Coulter) equipped with Violet-Blue-Red lasers. The 405 nm violet laser was used to measure the side angle scatter (V-SSC), and the blue laser to measure the green fluorescence intensity of the Megamix Plus fluorescent beads (BioCytex, Marseille-France) used as reference of size ranging from 0.1 to 1 µm. The results were expressed in percentage following these two formulas: number of cells hybridizing with the specific probe/ total bacteria hybridizing with the EUB 338 probe or number of cells hybridizing with the specific probe/ the total bacteria stained with PI.

Animal model

6–10 weeks-old C57BL/6J mice from Janvier Labs were maintained at our animal house facility in ventilated cages under specific pathogen free conditions at an ambient temperature of 22°C with a 12h light/dark cycle. The French ethical committee approved all animal studies.

Vancomycin protocol: vancomycin hydrochloride (0.5 g/L; Santa Cruz Biotechnology, Dallas, Texas, USA) was administered to mice in autoclaved drinking water for 21 days. The feces of each mouse were collected every day for 5 days before the antibiotic treatment, the first 5 days of treatment, and then once per week for FISH-Flow analyses.

Fecal sample processing

Fecal samples were processed within 30 min after collection. Feces were weighted and fixed with 4% (wt/vol) paraformaldehyde in PBS for 20 min, meanwhile they were homogenized by mechanical kneading and vortexed until all material was dissociated. The dissociated material was washed by adding 1 mL of PBS. All samples were centrifuged at low speed (200g for 2 min, 4°C) to remove large particles. Fecal bacteria in the supernatant were centrifuged at high speed (5000g for 5 min), and resuspended in PBS (100 mg/mL based on the initial fecal weight) for immediate analysis or stored in 50% ethanol–PBS until FISH analysis.

Statistical analysis

The parameters derived from the data included calculation of the staining index (SI) and the signal-to-noise ratio (S/N). The SI was calculated as the difference between the median fluorescence intensity of the positive and negative populations, divided by two times the standard deviation of the negative populations. In our case, the S/N was calculated using the mean or median fluorescence intensity of the positive cells divided by mean or median fluorescence intensity of the negative cells. Different coefficients of variation (CV) (i.e., standard variation divided by the mean) of the FISH method were calculated to assess the precision of the assay and the biologic variability of the samples. In addition, regression analysis of the mean counts for fecal samples taken at different times was performed for each individual. Using MetaboAnalyst 5.0 web server, data were normalized using the mean-centered and divided by the standard deviation of each variable; Partial Least Squares Discriminant Analysis (PLS-DA) and Non-parametric One-way ANOVA were performed to analyze the effects of vancomycin treatment on fecal samples.

B-III/ Results

1) Detection of bacteria by flow cytometry

In flow cytometry, Forward Scatter (FSC) and Side Scatter (SSC) parameters can be used to distinguish cells based on their size and internal complexity. Light scatter intensity strongly depends on the relationship between the size of the particle to the wavelength of the laser. Furthermore, small particles do not preferentially scatter light in the forward direction and the resolution in this detector may not be sufficient to measure or even identify these particles above background. Consequently, SSC is generally used to measure small things like bacteria, microparticles, or microvesicles (Bushnell, 2021).

Megamix Plus fluorescent beads were used in every acquisition as an additional quality control of the Cytoflex functionality and as a size reference. This mix of fluorescent beads possesses varied diameters selected to cover the theoretical size range of 0.1 to 0.9 µm, allowing to get a constant size region. Because the amount of light scattered by any particle is inversely proportional to the wavelength of the light being used to detect it, we used the side scatter of the violet laser (V-SSC) instead of the blue one (SSC) in order to differentiate the size of these small beads. Indeed, the 405 nm wavelength of the violet laser increases the range of resolution at any given particle size compared to the 488 nm wavelength. In addition, the scattered light from any particle is directly proportional to its diameter, meaning that the biggest particles have the higher SSC values.

Because bacteria can be bigger than 1 µm we needed to use the blue laser to acquire them. However, it was possible to see the corresponding size of the beads from the VSSC to the SSC (Fig. 3, upper panel). Pure culture of bacteria can also be used to define a size range (Fig. 3, bottom panel). For example, *Enterococcus faecalis* are cocci with a size range between 0.6 and 2 µm (Oyama *et al*., 2017). *Bifidobacterim adolescentis* are thin, irregular Y- or V-shaped rod about 5 µm in size. The denser core of *E. faecalis* corresponded to the SSC value of the 0.22 µm beads. For *B. adolescentis*, the core was broader on size which was congruent with its rod shape. Also, its SSC values were higher reaching the SSC value of the 0.9 µm beads. There was a clear difference between the size of the bacteria and the theoretical size of the beads; however, the proportions we obtained with the Cytoflex seemed to be appropriate. The difference can be explained because two particles of exactly the same size may have different refractive indices, due to their composition, and will therefore generate scatter signals with different intensities.

Outside the core of these bacteria, there is a population that increases in size and has a higher quantity of DNA. This population formed an arrow shape between the PI fluorescence intensity and the

SSC values, suggesting the presence of agglomerated bacteria. Microorganisms naturally accumulate rather than exist as individual organisms; thus, bacteria clusters were expected.

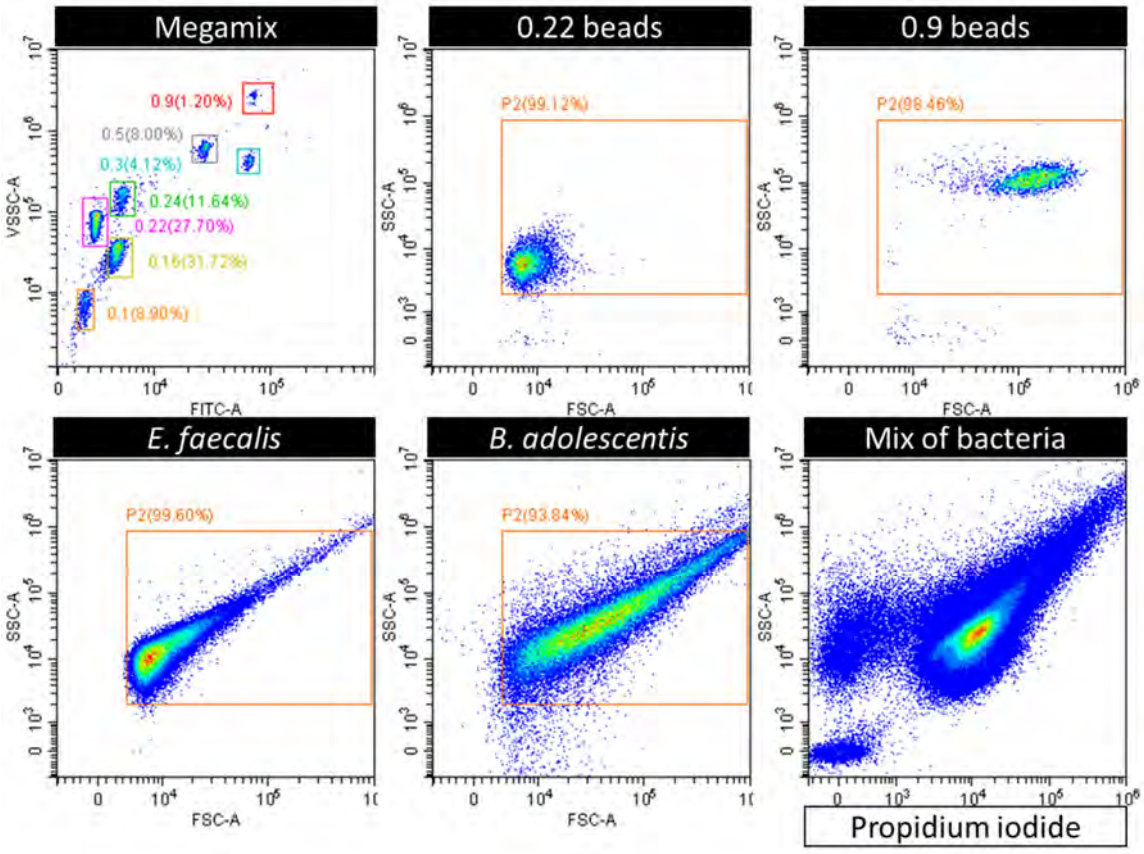

Figure 3: Flow cytometry scatterplots of the side scatter (VSSC: violet laser or SSC: Blue laser) versus Forward Scatter (FSC) or the fluorescence intensity of the propidium iodide (PI).

2) Definition of the phylum panel and hybridization conditions

One of the biggest challenges in multiparametric flow cytometry is the selection of the right combination of fluorochromes. In order to assess which fluorochromes could suit our panel, we tested the universal probe Eub338 in all fluorochromes that were compatible with the configuration of the Cytoflex used (laser and filters) and available for probe-synthesis. Using *E. faecalis,* we incubated the probe Eub338 coupled with all the different fluorochromes incubating at 42°C for 30 min. We calculated the staining index (SI) and the ratio of signal versus noise (S/N) using the mean (X) and the median (Me) fluorescence intensity (Table S1; Annex 2).

Background fluorescence of nonspecific binding of the probe, such as autofluorescence of the bacteria, and instrument noise may affect the ability to resolve between specifically stained bacteria (positive) and unstained bacteria (negative). The S/N ratio measures the sensitivity of an assay and its ability to detect differences between stained and unstained populations. The SI takes into account the intensity distribution spread of the unstained cell population. Both measures are useful for comparing cell populations stained with different fluorescent conjugates of the same probe. In our case, the fluorochromes with less resolving capacity were A430, Pacific Blue, and e393. Consequently, we chose the fluorochromes with the better resolving capacity: CF405s, A488, Cy3, A647, A700, and A750 to design our panel.

Thus, CF405S was the only fluorophore using the violet laser (405nm) excitation. In the blue laser (488nm) we chose A488 and Cy3, and in the red laser (638nm) A647, A700 and A750. The Band Pass filter in the Cytoflex determined the fluorescence channels available for these fluorochromes: FITC (525/40 BP) for A488, PE (585/42 BP) for Cy3, APC (660/10 BP) for A647, APC-700 (712/25 BP) for A700, APC-750 (780/60 BP) for A750 and PB450 (450/45 BP) for CF405s. The chosen fluorochromes had emission curves with a reduced spillover in all the channels (Fig. S1; Annex 2), minimizing the compensation processes while preserving the quality and accuracy of the data.

Given the diversity of genera inside each phylum, finding a single probe to tag a whole phylum was a difficult task. Thus, several probes were needed to cover the phylum diversity of the intestinal microbiota (Fig. 4). In detail, each phylum was cover by the following probes:

- Firmicutes: **LGC354A + LGC354B + LGC354C** for the class Bacilli and **Erec482** for the *Clostridium coccoides* group.
- Proteobacteria: **Proteoβγ + Proteo ε** were designed for this study. In the gut, the most important class of this phylum is the enteric group that represents almost all the Gammaproteobacteria (Rizzatti *et al*., 2017).
- Actinobacteria: **HCG664** is the only probe that targets 23S rRNA instead of the 16S rRNA, they are specific of High C+G Gram positive bacteria corresponding to Actinobacteria.
- Verrucomicrobia: **MUC1437** recognizes specifically *A. muciniphila*, which is the only Verrucomicrobia species present in the gut (Hugon *et al*., 2015).
- Bacteroidetes: **Bact** was designed for this study to recognize the gut microbiota belonging to this phylum.

The stringency of probe hybridization is strongly influenced by the incubation temperature. Some thermodynamic models have been developed to obtain a range of hybridization temperature based on the melting temperatures (Tm) of the probes, but a trial and error optimization is still required (Fontenete *et al*., 2015). Tm can be defined as the temperature at which half of the nucleic-acid strands form a duplex and the other half are single stranded. It does not only depend on the sequence but also on the conjugated fluorochrome.

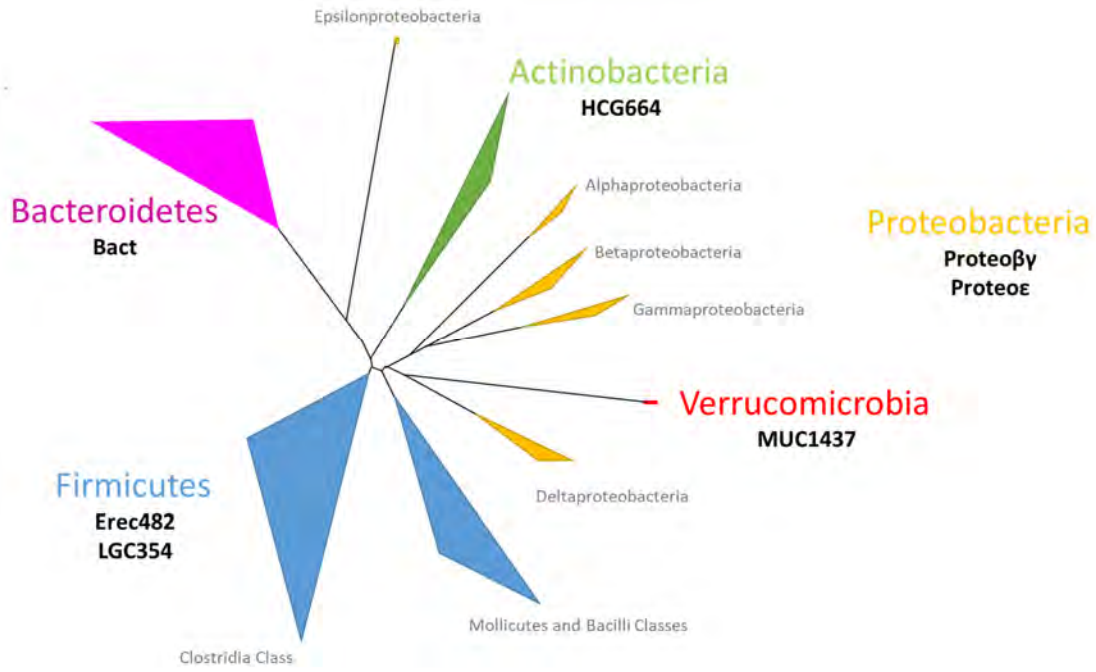

Figure 4: Phylogenetic tree based on the 16S rDNA sequence data set. Different colors are used to represent each phylum and the angle where each triangle joins the tree represents the relative abundance of sequences in the human intestine. Under each phylum name, in bold, are specified the probes included in our panel. Modified from Eckburg *et al*., 2005.

We tested all the probes conjugated with the same fluorochrome (A647) ruling out possible differences due to the brightness of the colors. The Tm for the probes conjugated with A647 ranged between 42-58°C (Table 3). Thus, we chose to test all the probes in two different hybridization temperatures: 42 and 55°C (Table S2; Annex 2). In our case, the majority of the selected probes worked better at 42°C, except the Bacteroidetes probe that worked slightly better at 55°C. Since in a multiplex experiment, probes have to operate at the same temperature and concentrations of denaturing agents, we chose 42°C for the panel.

The next step was to select which probe will be conjugated with which color. For this, we needed to take in consideration the brightness of the fluorochromes, the own probe resolution, and the abundance of the targeted rRNA. Normally, bright fluorochromes are selected for antibodies against low-abundance antigens and dim fluorochromes for antibodies against highly expressed antigens. Thus, we assessed the resolving capacity of all the fluorochromes conjugated to the Eub338 probe (Table S3a; Annex 2). Then, all probes conjugated with A647 were incubated in the same conditions to compare detection ability of the probes (Table S3b; Annex 2).

The most abundant phyla in the intestinal microbiota are Bacteroidetes and Firmicutes (Schroeder and Bäckhed, 2016), and, independently of their phylum, most bacteria are Eubacteria positive (Amann *et al*., 1990). We therefore assigned to Eubacteria and Bacteroidetes the dimmest colors A750 and A700, respectively. In contrast, the brightest colors, Cy3 and A488, were assigned to the less represented phyla: Proteobacteria and Actinobacteria, respectively. Even though Firmicutes is also one of the most abundant phyla, their probes have the lowest resolving capacity. In consequence, we assigned to it one of the brightest color: CF405s. The probe for Verrucomicrobia worked the best, so we assigned it to the dim fluorochrome A647.

Finally, the assignation of fluorochromes to the probes against the different phylum resulted in the following panel:

405nm	**488nm**		**633nm**		
450/45	525/40	585/42	660/10	712/25	780/60
CF405s	**A488**	**Cy3**	**A647**	**A700**	**A750**
Firmicutes	Actinobacteria	Proteobacteria	Verrucomicrobia	Bacteroidetes	Eubacteria

Optimization of the resolving capacity of each probe requires to determine at which concentration each specific probe has to be used. Therefore, we titrated each probe (Table S4 and Figure S2; Annex 2) under the already defined incubation temperature (42°C). Each probe has a S/N ratio that varied differently with the probe concentration. For instance, Eubacteria had a better resolving capacity at low concentration around 0.05 µM. When the probe concentration augmented the unspecific binding increased rapidly. The same observation applied for Bacteroidetes, Verrucomicrobia and Actinobacteria, to which 0.05 µM was chosen as well. For Firmicutes a higher concentration was needed as both probes LCG354 and Erec432 worked better around 0.375 µM. For Proteobacteria the working concentration was increased up to 1 µM, since the resolving capacity was reduced below this concentration.

Since the separation between negative and positive bacteria are not major, it is important to ensure that compensation of fluorescence spillover is not going to affect their separation. To this end, we acquired mixes of positive (specific) and negative (nonspecific) bacteria mono-stained with each conjugated phylum-probe. The need for compensation is due to the emission of photons of multiple energies and wavelengths. The compensations should be more carefully done between colors that emit photons with close wavelength. As explained before, our fluorochrome combination has a reduced spillover between them allowing us to reduce the compensations (Table S5; Annex 2). We observed a minimal spillover in blue and violet laser lines. There was more spillover in the red laser line, a particular attention should be focus in this laser line when analyzing our multicolor panel.

3) Proof of concept of the panel

Until now, each probe was tested individually. Once each condition was defined, we combined all the probes in a mix of bacteria belonging to the five different phyla as a proof of concept. Since probes may require different incubation times to bind their targets we tested 30 min, 3 h (Table S6; Annex 2) and overnight as hybridization times at 42°C. Overnight incubation induced to much noise meaning that the unspecific dye bacteria were really close to specific ones (data not shown). Firmicutes, Actinobacteria and Proteobacteria probes hybridized better with a 3-h incubation. Only Verrucomicrobia probe worked better with 30 min; however, the difference between the two times was not significant allowing us to choose a general 3-h incubation for the whole panel (Table S5; Annex 2).

Using a mix of all bacteria from the five different phyla (Table 2), we tested the panel at the chosen conditions. The combination of all the positive probes incubated for 3 hours at 42°C allowed to distinguish the bacteria of each phylum (Fig. 5). The mix of all negative probes determined the non-specific binding; their fluorescence intensities allow us to delimit accurately the gates for positive populations. The percentage of positive populations was not equal between the phyla, reflecting their different proportion in the initial mix.

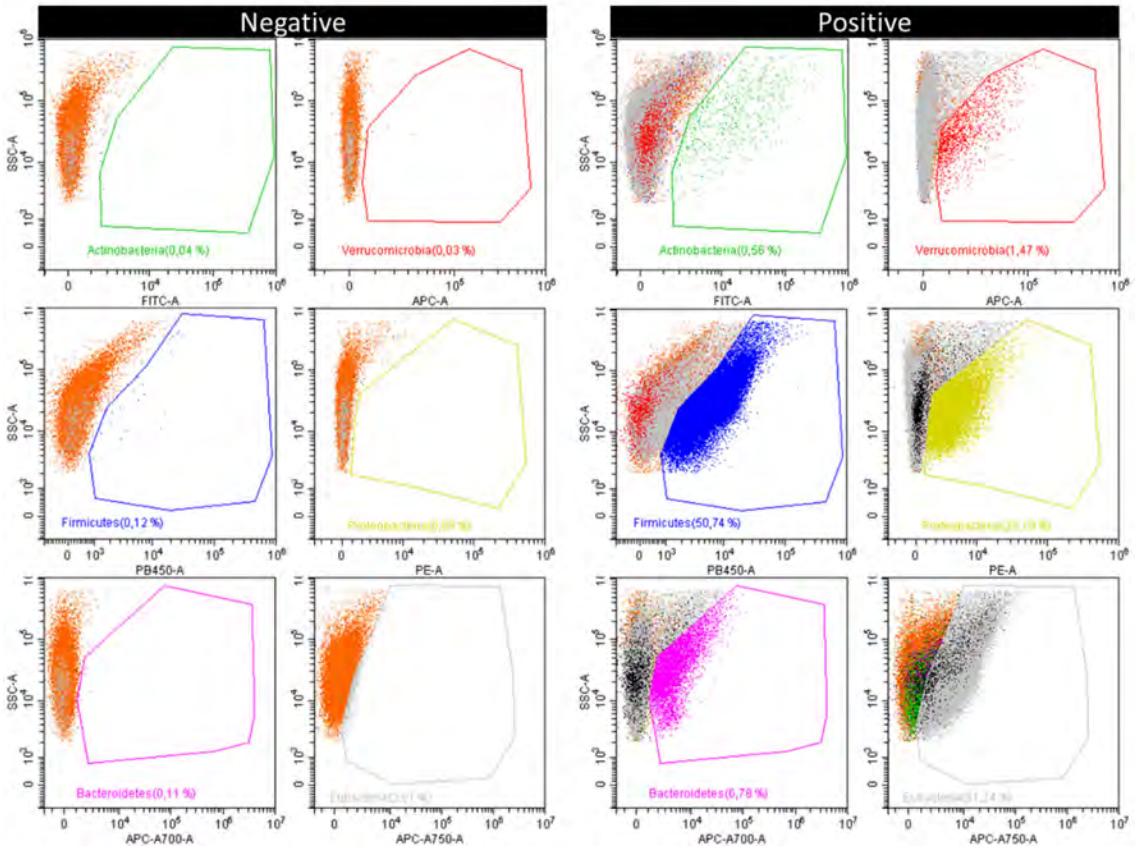

Figure 5: Flow cytometry scatterplots of SSC *versus* the fluorescence intensity of fluorochromes associated to the different probes included in the panel. The negative (left panel) and the positive (right panel) probes were incubated with a mix of bacteria belonging to the five different phyla for 3 h at 42°C.

It was then important to determine the specificity of detection. For this, we elaborated a cross-hybridization plan, in which all the bacteria belonging to a specific phylum were incubated with the whole panel probes. Therefore, for each mix the positive signals were expected to come from the corresponding phylum probe as well as the Eubacteria one which recognizes all phyla. As before, the positive gates were delimited by the fluorescence intensity of the negative probes.

For all the phylum specific bacterial mixes, the corresponding phylum-probe in addition to the Eubacteria probe showed indeed specific strong positive signals whereas other probes showed no or faint recognition (Fig. 6). These results indicate that the panel is specific given that each phylum-probe does not recognize bacteria belonging to other phyla. However, it is important to keep in mind that the number of bacteria species included in each phylum in this study was not exhaustive.

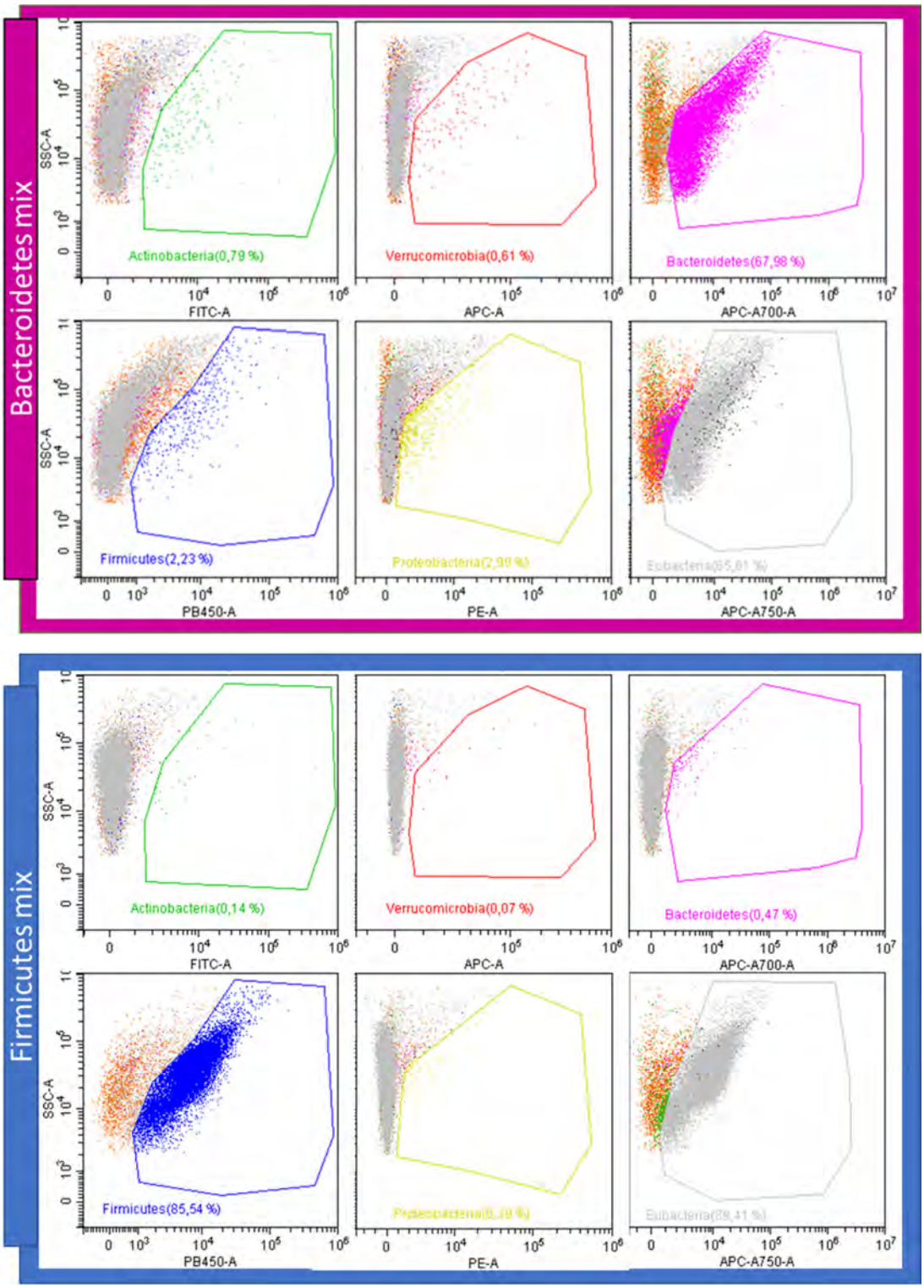

Figure 6: Flow cytometry dot plots of SSC versus the fluorescence intensity of fluorochromes included in the panel. A mix of bacteria belonging to each phylum: Bacteroidetes, Firmicutes, Actinobacteria, Proteobacteria, and *A. muciniphila* were incubated with the panel for 3 h at 42°C.

Figure 6, continuation:

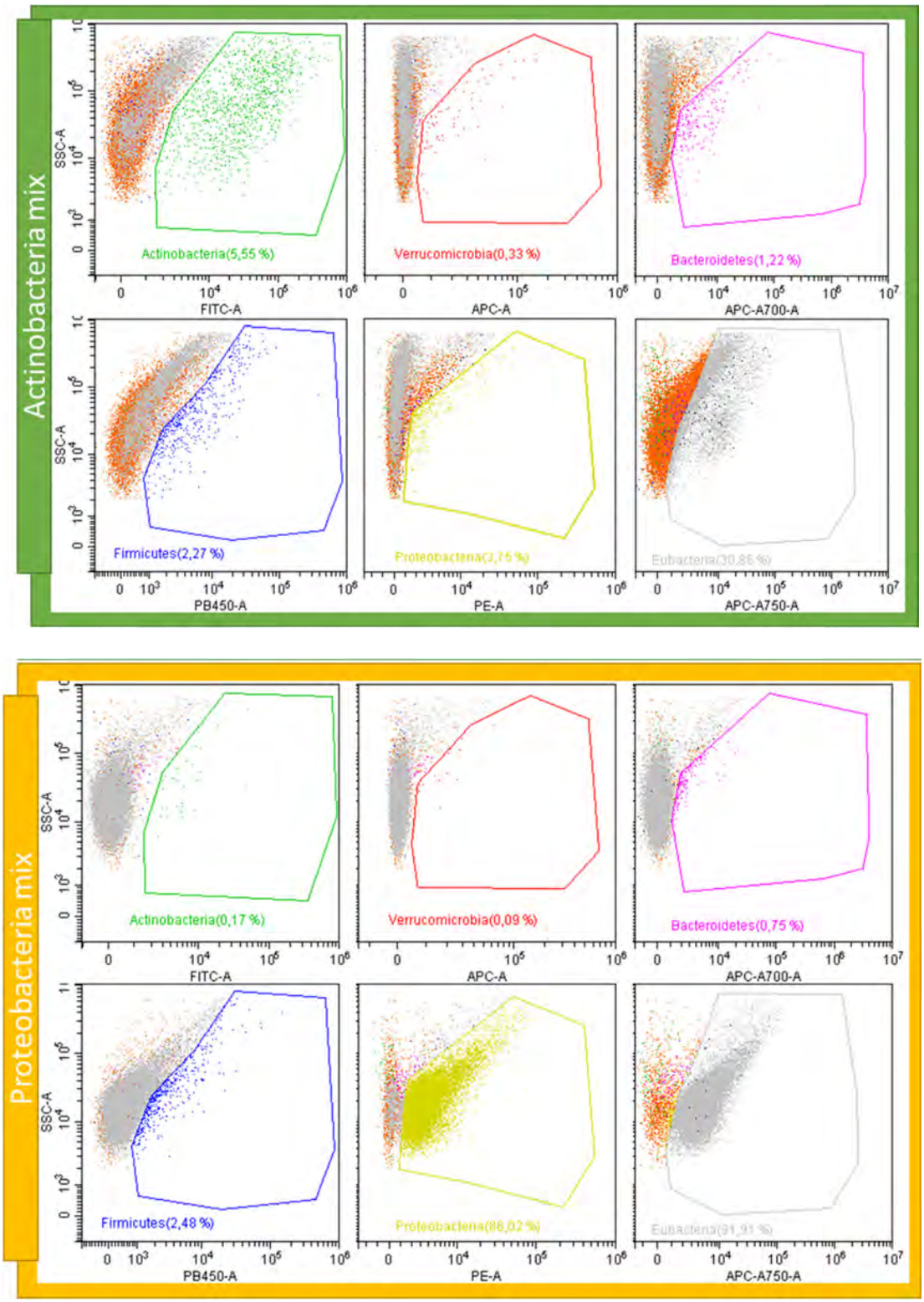

Figure 6, continuation:

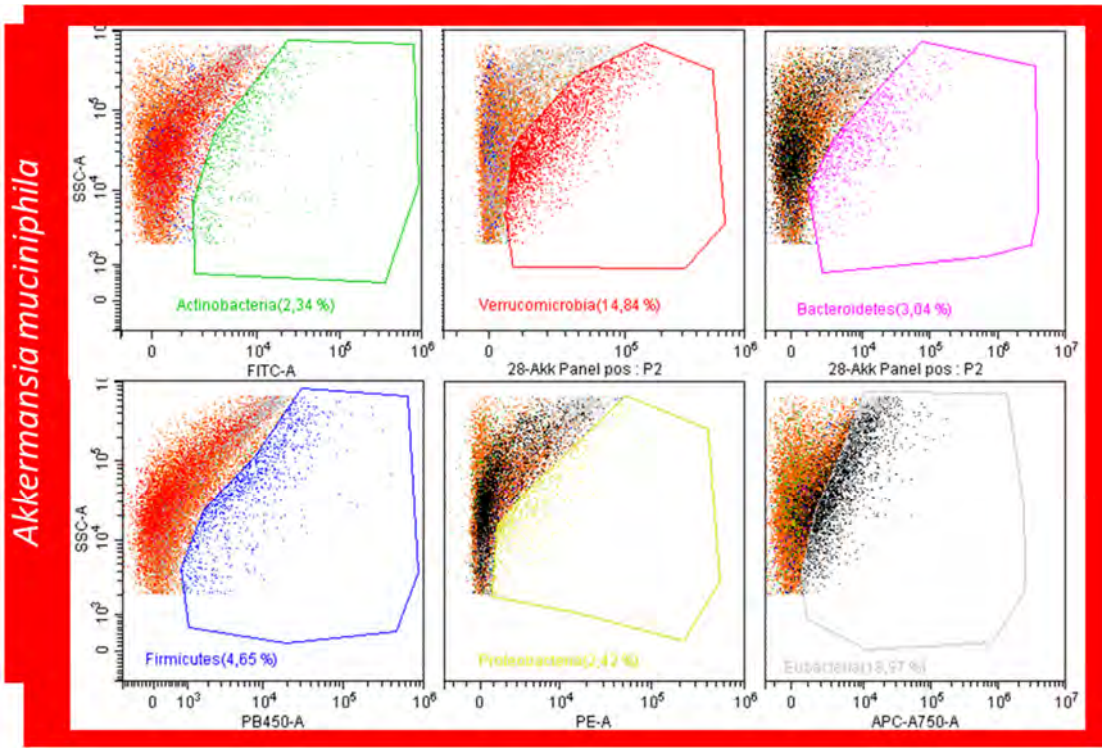

4) Performance of the FISH-Flow method

The precision of a method is the closeness of agreement between independent test results obtained from homogenous test material under stipulated conditions of use. Repeatability and reproducibility define a method precision. The analysis of successive measurements performed under the same condition determines repeatability. Reproducibility can be assessed by measurements performed under changed conditions, such as time, operator or reagent lots (Burtis *et al*., 2012). To define our method precision, we analyzed the same mix of all the bacteria from all the phyla (Table 2) ten times in a same day (intra-assay variation) and once per day for ten days (inter-assay variation). This material was prepared the same day and kept in PBS-ethanol stocks at -20°C. From this data set, coefficients of variation were calculated (Fig. 7).

Precision often depends on the concentration of the analyte being considerate, in this case the percentage of phylum-specific bacteria. The variability was lower in more represented populations on the bacterial mix such as Eubacteria, Firmicutes, Bacteroidetes and Proteobacteria. Congruently, higher variations were observed in less represented populations such as Actinobacteria and Verrucomicrobia. For

both intra-assay and inter-assay variability, we observed a CV decrease when frequency of bacteria increased. This is in accordance with has been described with classical flow cytometry approaches performed in cells from blood samples with CV between 20 and 30% for frequencies below 5% (Streitz *et al*., 2013). As expected, intra-assay variability remains smaller than the inter-assay variability.

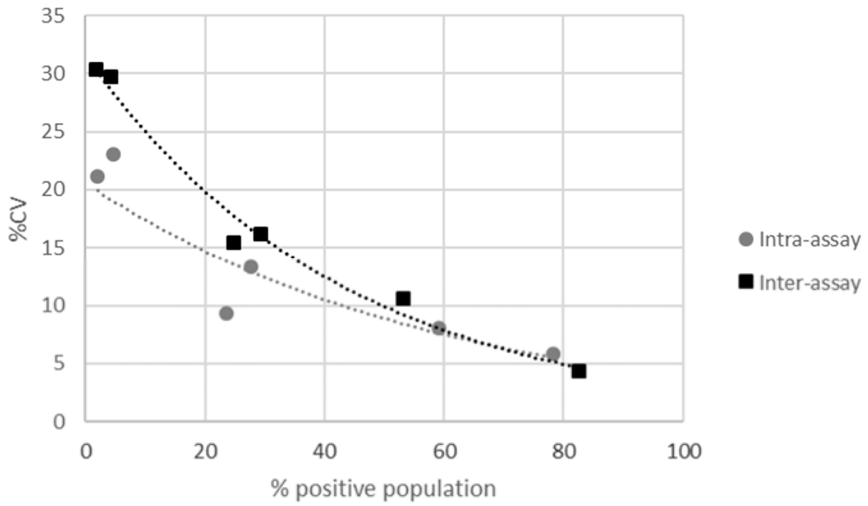

Figure 7: Graphic representation of the Intra and Inter-assay coefficients of variation versus mean percentage of positive bacteria.

5) Sensitivity of the FISH-Flow method: detection of changes in the phyla proportions

One of the intended uses for the FISH-Flow method is the detection of significant changes in the proportion of the five major phyla found in any intestinal samples. Since the cytoflex uses a peristatic pump, the flow is constant which allows to quantify the number of events without the addition of counting beads. We used a slow flow rate (10 µL/ min) and we acquired for 30 s each bacterial mix. In average, in 5µL we had 7.5 $x10^3$ bacteria, meaning that in the total volume (500µL) we had $7.5x10^5$ bacteria (1x). To assess the ability of the method to detect changes in the number of bacteria, we tested each probe with different amounts of bacteria ranging from the already used amount (1x) to one-hundred times this amount (100x) using one bacterial species as target (Table 5, grey rows).

The higher percentages of positive bacteria were obtained with 100X amount of bacteria, except for Bacteroidetes, which was detected better at 10X amount of bacteria. These results meant that increasing the amount of bacteria resulted in more specific labelling of bacteria. A good balance between the number of bacteria and the amount of probes is necessary for the optimal function of our method. We

decided then to adjust the concentration at 10^7 bacteria for further experiments, representing the 100X amount of bacteria.

Table 5: Percentage of positive bacteria detected for each probe. The amount of the targeted bacteria ranged from 1X to 100X, grey rows. Different proportions of specific and unspecific bacteria with a 100X total amount of bacteria, black rows.

		% positive bacteria							Bacterial number
		Eub338	LGC354	Erec482	HCG664	Bact	Proteoβγε	MUC1432	
Amount of bacteria	100x	85.09	98.49	94.23	84.41	42.93	91.03	50.49	10^7
	10x	94.18	93.39	94.83	17.05	77.67	83.38	43.46	10^6
	1x	63.99	49.42	62.60	8.53	53.70	23.28	22.77	10^5
	% of specific bacteria	50	52.69	57.89	51.55	49.81	52.40	21.65	10^7
		10	3.92	36.27	2.52	12.17	2.37	2.95	
		1	0.57	3.80	1.07	4.72	0.87	0.51	

For Verrucomicrobia, the maximum percentage of positive bacteria detected was 50% at 100X amount of bacteria, meaning that the probe did not label half of the *A. muciniphila* present in the mix. We did not manage to grow this bacterium in liquid medium and we needed to several days to have enough bacteria using solid medium. This meant that some of them might not be metabolically active, which is a crucial for this technique.

We also assess the capacity of each probe to detect its specific bacteria when surrounded by unspecific bacteria. For this, we used the 100x amount of bacteria with 50, 10 and 1% of specific bacteria for each probe (Table 5, black rows). At 50-50 ratio all probes, except the Verrucomicrobia probe, were able to detect the theoretical percentage around 50%. However, Verrucomicrobia probe recognized 22% in good agreement with the fact that the probe labeled only half of the present bacteria. For the 10-90 ratio, the percentages decreased but did not correspond to the theoretical 10%, except for Bacteroidetes probe. A further decrease was observed when only 1% of specific bacteria were present in the mix. This result indicates that the panel can detect changes between 100 and 1% for all the phyla but with a lower accuracy in less represented bacteria.

6) Fecal samples analysis

Fecal samples were fixed rapidly after collection to avoid the lysis of strict anaerobic bacteria. Then the fibers and debris were discarded by low-speed centrifugation and the final fecal bacteria pellet was resuspended at 100 mg/mL. We used 10µL of this suspension (equivalent to 1mg of feces) that were in a

final volume of 500 µL of PBS to finally acquired 5 µL of each tube. In a samples collected from 5 different mice (data not shown), we had in average $2.5x10^7$ bacteria / mg of feces. This amount was close to the 100X desired amount defined before. We acquired again at slow flow rate keeping a low abort rate (around 1%), using the already determined range size gate (referred as P2 in Fig. 3).

In 10 mice, an average of 86% of the acquired events in the gate P2 were Eubacteria positive. To know if the rest of events corresponded to non-recognized bacteria or debris we used PI as a DNA dye. From the events in P2, 92% were PI-stained cells meaning that 8% corresponded to debris. Additionally, the discrepancy between the PI and the Eubacteria probe was of 6%, this gap could correspond to the presence of Eub338 negative bacteria (Daims *et al*., 1999), insufficiently permeabilized bacteria or bacteria with a poor metabolic state. However, the majority of bacteria in murine feces were detectable by FISH analysis, which was indicative of the freshness and good condition of the samples.

We evaluated the fecal murine microbial populations from 10 mice every day for 5 days with our panel (Fig. 8A). The two most abundant bacterial phyla in the feces were Firmicutes and Bacteroidetes representing in average 64.7 and 27.3% respectively; Proteobacteria, Verrucomicrobia and Actinobacteria represented in average 1.6, 1.0 and 0.4 % respectively (Fig. 8B). A 4.9% of Eubacteria positive bacteria was not positive for any phyla-probe in our panel.

Individual data for each mouse show that most of results are consistent and form a dense core. However, some results moved away from the core showing some data variability (Fig. 8C). Because the data were pooled from the 10 mice and from all the five days, we wanted to refine our analysis to find from where this variability was coming from. For this, we analyzed the intervariability and the intravariability in the fecal murine microbial populations to assess the biological variability. We calculated the variation within a mouse (CVlong) and between mice (CVtrans) within a day (Table 6, white rows). Changes in bacterial composition within a mouse over time showed a higher CV in less represented bacterial populations. As mentioned before, rare populations have an intrinsic higher variability. Variation over time increased up to 50% for Actinobacteria, Proteobacteria and Verrucomicrobia, which each one accounts for less of 1% of the total Eubacteria population. This high variability has a less general impact because even a 200% of increase will represent only a 2% of the total composition of the sample. Meaning that a slightly increase of less representative phylum can be detected but the exact percentage will be less accurate in comparison with the more representative phyla. Lower variability was observed for Bacteroidetes and Firmicutes probably due to their higher representation in the fecal microbiota. Overall, fecal microbiota composition of an individual mouse seems relatively stable on time.

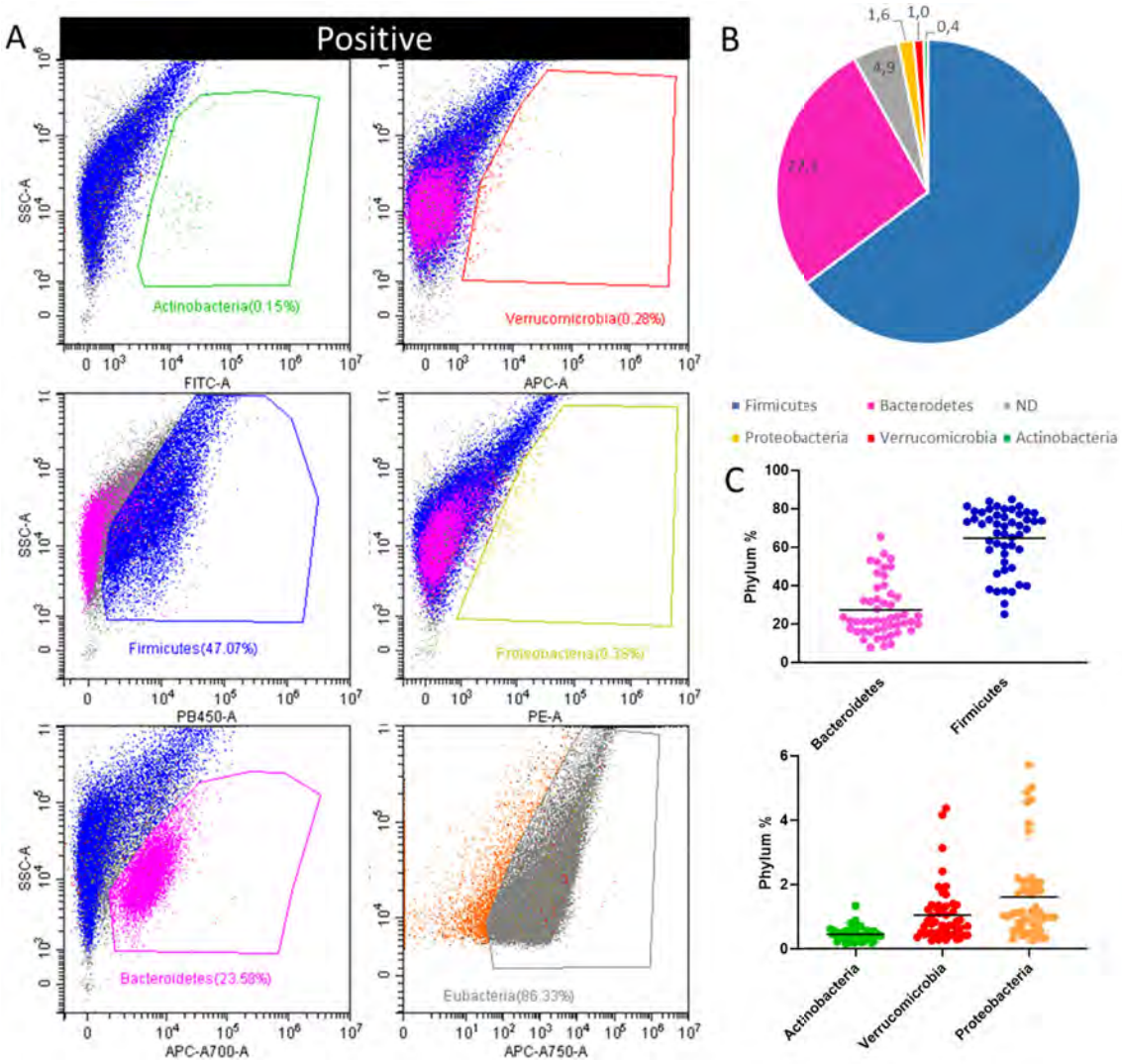

Figure 8: A: Flow cytometry dot plots of SSC versus the fluorescence intensity of fluorochromes included in the panel of a fecal sample from one mouse. Graphic representation of the phylum composition of the fecal samples from 10 mice followed every day for 5 days, for a total of 50 analyzed samples. B: Mean percentage and C: Individual data for each phylum was obtained from the total Eubacteria positive bacteria.

Table 6: Intra and Interindividual coefficients of variation and mean percentage of positive bacteria for each probe.

		Eubacteria	Firmicutes	Actino	Bact	Proteo	Verruco
Longitudinal (%)	Mean	81.3	72.6	0.4	23.7	1.2	1.0
	CV	8.2	16.0	39.1	36.6	52.2	50.8
Transversal (%)	Mean	80.4	64.8	0.5	26.4	1.2	0.9
	CV	5.2	23.8	24.3	55.5	50.0	51.8

Changes in bacterial composition between mice in a same day (CVtrans) showed also a higher CV in less represented bacterial populations (Table 6, grey rows). Variation over time and between mice were similar for Proteobacteria and Verrucomicrobia. Conversely, a lower variability for Actinobacteria and Eubacteria could reflect the reduced variability in measurements made the same day. Interestingly, Firmicutes and Bacteroidetes had a higher variability between mice than overtime. Because these were the main phyla present in the samples, their probe precision was better which allows us to better assess the variability between different individuals. The variability between mice was less than 25%, which shows a low beta diversity.

Figure 9 shows in panel A, the daily phyla percentages, while panel B shows the absolute number of bacteria in 1 mg of feces. Interestingly, the higher percentage variability corresponded to the less concentrated samples (e.g. day 3). As shown before, changes in the amount of bacteria present in the hybridization tube alters the probes resolving capacity (Table 5, grey rows).

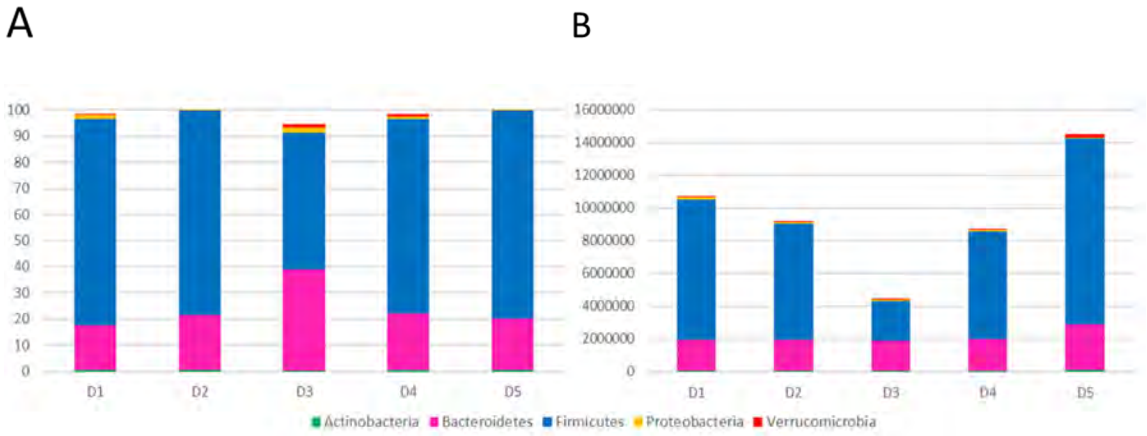

Figure 9: Graphic representation of the phylum composition of the fecal samples from one mouse. A: Daily phyla percentage and B: number of bacteria/mg of feces from day 1 (D1) to day 5 (D5) for each phylum was obtained from the total Eubacteria positive bacteria.

Even though all the samples were freshly recovered from mice, we noticed that the driest samples had the lower bacterial concentration in the same mass of feces. Sample physical properties seems need to be taken in consideration before analysis.

7) Microbiota disruption in clinical dysbiosis

Once the steady-state composition of the murine fecal microbiota was determined, we then put the mice under vancomycin treatment for 4 weeks to assess the microbiota changes due to antibiotic treatment. A weekly follow-up was done for each mouse using our panel to evaluate the changes in each phylum. As stated before, the percentage of Eubacteria positive bacteria at steady state was around 86%. After vancomycin treatment, this percentage drops dramatically around 45% (Fig. 10). The increase of non-labelled particles in P2 could be explained by the presence of dead or the poor metabolic state of vancomycin-targeted bacteria. After treatment the number of total bacteria also dropped dramatically (data non shown), so we needed to increase five times the amount on bacteria in the tubes (from 10 to 50µL) to keep the required amount of bacteria for our titrated panel.

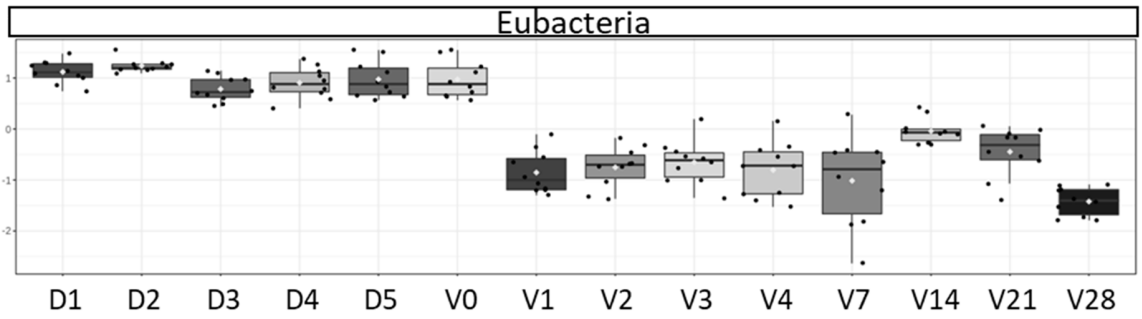

Figure 10: Boxplot representation of the Eubacteria positive bacteria present in fecal samples of 10 mice followed one week prior to vancomycin treatment (D1-D5); just before starting the treatment (V0) and then for several days of treatment (V1-V28). Individual data and interquartile range are shown for each day, the white dot represent the mean value. The x-axis shows the days and the y-axis is the normalized percentages.

The phyla composition over time of the treated mice is shown in Figure 11. An increase frequency of Proteobacteria and Verrucomicrobia was observed, parallel to an important decrease of Bacteroidetes. The increase of Proteobacteria was acute returning to normal levels after 3 days of treatment (Fig. 11, V3). The decrease of Bacteroidetes and the increase of Verrucomicrobia were stable over time. In Actinobacteria there was also a slightly decrease but specially a reduction of its variability evidenced by a reduced interquartile range (IQR) after vancomycin treatment. The IQR describes the middle 50% of values when ordered from lowest to highest to easily evidence dispersion. Firmicutes decreased a bit the first day of treatment (Fig. 11, V1), then it returned to steady state levels until the fourth week (Fig. 11, V28) were it decreased again.

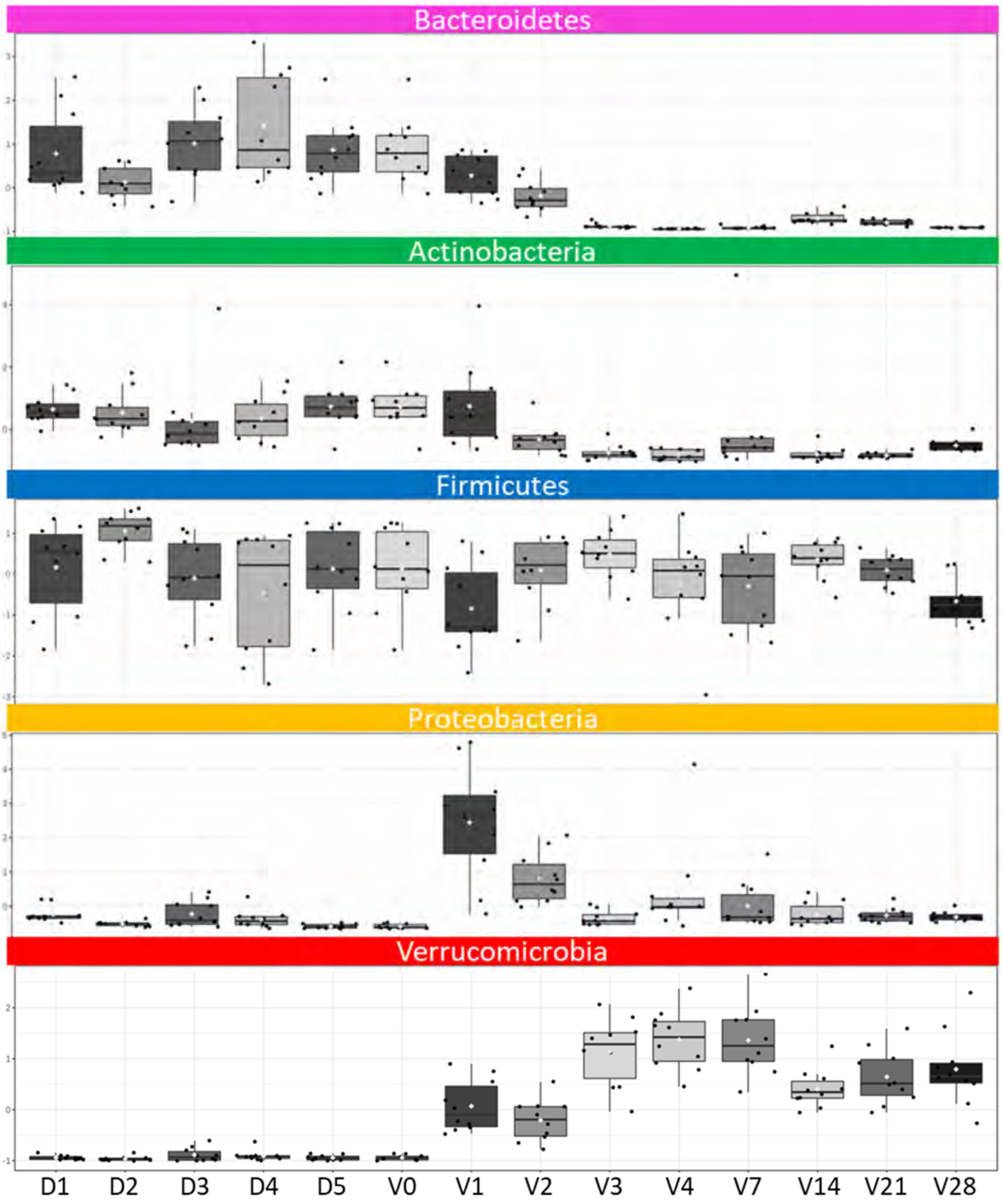

Figure 11: Boxplot representation of the phylum composition of fecal samples from 10 mice followed one week prior to vancomycin treatment (D1-D5); just before starting the treatment (V0) and then for several days of treatment (V1-V28). The percentage of each phylum was obtained from the total Eubacteria positive bacteria. Individual data and interquartile range are shown for each day, the white dot represent the mean value. The x-axis shows the days and the y-axis is the normalized percentages.

To emphasize variation and bring out strong patterns in our dataset we used the principal components (PCA) analysis (Fig. 12A). This technique reduces the variables of the dataset and allows to explore and visualize them easily. All the steady state samples (Fig. 12A, circles) clustered together as well as the latter days of treatment (Fig. 12A, triangles). Interestingly, the first day of treatment (Fig. 12A, violet oval with squares) is in the interphase of both clusters. The second, third and fourth days are surrounding the vancomycin cluster showing clearly their transition. The parameters with the highest impact in the clustering are Verrucomicrobia, Eubacteria and Bacteroidetes (Fig. 12B).

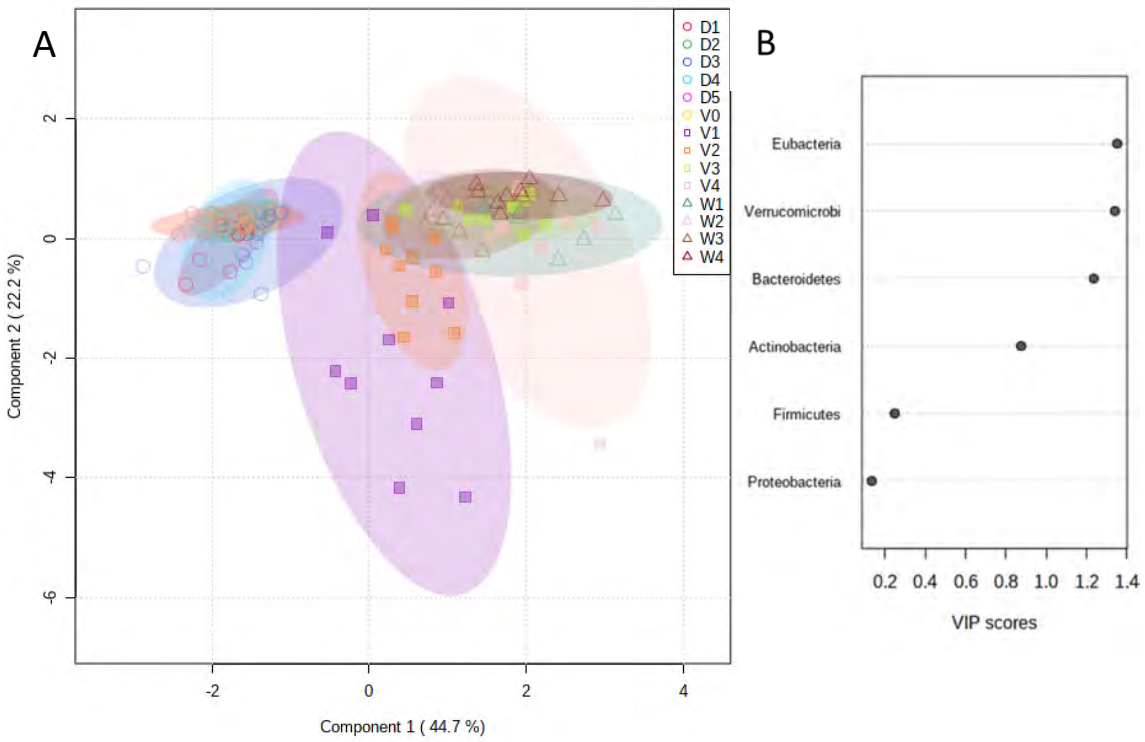

Figure 12. A: Score plot of the principal components analysis (PCA) for the fecal samples at steady state (circles), first days of treatment (squares) and weeks after vancomycin treatment based on all phyla percentages of our panel. B: Score plot of variable importance in projection (VIP), summarizes the contribution of each variable makes to the model.

B-IV/ Discussion

FISH has been used to directly identify microorganisms within complex samples in a few hours having a widespread application in environmental and medical microbiology. Several hundred rRNA-targeted oligonucleotide probes suitable for FISH have been described. A large online database providing an overview of published probes and their characteristics is available (http://www.probebase.net). This database gives detailed information about the probes, including the optimal hybridization conditions and the specificity of the probes (Greuter *et al*., 2016). In principle, the same probes used for the microscopic detection of fluorescent cells can also be used for detection by Flow cytometry. For the first time, Amann and collaborators presented a combination of FISH with Flow cytometry (FISH-Flow) for the analysis of defined mixtures of bacteria (Amann *et al*., 1990). Sensitive flow cytometers allow the classification of many microbial cells according to their cell size, DNA content, and specific staining conferred by fluorescent antibodies or rRNA-targeted oligonucleotide probes (Wallner *et al*., 1997). A method was developed based only on the forward scatter (FSC) and DNA content (DAPI staining) to analyze the heterogeneity but not phylogenetic identity of the fecal microbiota. This fast and inexpensive tool for the analysis of the microbiota and offers the unique opportunity to isolate defined bacterial populations for further molecular and functional analysis (Zimmermman *et al*., 2016).

We designed a multiparametric FISH-Flow panel including nine specific probes that target main phyla of the gut microbiota: Firmicutes, Bacteroidetes, Proteobacteria, Actinobacteria, and Verrucomicrobia. We used the negative of each probe to eliminate their background fluorescence, which allowed us to defined true positive signals. In similar publications, this important control was only considered for Eubacteria probe (Rigotier-Gois *et al*., 2003; Barc *et al*., 2004). In our opinion, this control is essential especially on the technique standardization. The optimal hybridization conditions and properties of the method were determined using a known mix of cultured bacteria belonging to all phyla, as a proof of concept. The panel allowed us to distinguish bacteria of each phylum in a specific manner. The method has a good precision with an acceptable variability even for small populations. It can also detect changes between 100 and 1% for all the phyla but with less accurate results in less represented bacteria.

Then, we tested our panel in complex samples such as murine fecal samples. Less than 10% of events corresponded to debris meaning that the differential centrifugation steps were enough to isolate bacteria from feces. Furthermore, the majority of bacteria were detectable by FISH-Flow analysis, which

was indicative of the optimal fecal preparation. The yield and quality of microbial DNA extracted from fecal samples are considerably affected by the aptness of the fecal sampling method used, e.g. the ratio of Firmicutes to Bacteroidetes is affected by freezing versus fresh samples (Song *et al.*, 2018). Fixating the samples directly after collection and prior to disrupt their protective natural conformation allowed us to prevent the lysis of strict anaerobic bacteria without a deleterious effect for the rest of bacteria.

In general, the most important pre-analytical variable for our method is the number of bacteria. We notice that the driest samples had the lower bacterial concentration in the same mass of feces meaning that fecal physical properties need to be taken in consideration. For all the probes, concentrations around 10^7 bacteria resulted in more specific labelling of bacteria. Because it is not possible to control the physical properties of samples or expect that samples coming from different clinical conditions have similar bacterial loads, one way to control their effect is to quantify the total number the bacteria before performing the hybridization. Using PI or DAPI staining on the already fixed samples it is possible to quantify in a rapid way the concentration and adjust to our desired amount of bacteria. Like this, a good balance between the number of bacteria and the amount of probes can be ensured for the optimal function of our method.

As in humans, the two most abundant bacterial phyla in mice colonic microbiota are Firmicutes and Bacteroidetes. Whereas Proteobacteria and Actinobacteria are present at low levels in the (Ley *et al.*, 2005). Our results were consistent with the literature, just a small percentage of Eubacteria positive bacteria was not positive for any phyla-probe of our panel. These bacteria can belong to other phyla such as TM7, Fusobacteria, Tenericutes or Spirochaetes also present in the fecal microbiota (Ley *et al.*, 2005; The Human Microbiome Project Consortium, 2012). Despite this, our panel was able to classify almost all fecal bacteria present in the samples. The human gut has an intermediate beta diversity, which corresponds to the differences between samples from different people (The Human Microbiome Project Consortium, 2012). The variability between mice was less than 25%, which shows a low inter-individual variation. It is important to recall that these are genetically homogeneous mice that had the same diet and lived under the same conditions, this particular feature could explain this low variability.

Several studies had used FISH-Flow to describe the composition of fecal microbiota with a combination of the following probes: Erec482, Bif164 (*Bifidobacterium)*, Enter1432 (Enterobacteriaceae), and Bacto1080 or Bac303 resulting on a recognition between 50 and 69% of the bacterial cells (Rigotier-Gois *et al.*, 2003; Barc *et al.*, 2004). These probes were chosen because in the gut *Bifidobacterium* is the most important Actinobacteria genus (Binda *et al.*, 2018) and the family Enterobacteriaceae represents

almost all the Gammaproteobacteria, the most important class of Proteobacteria (Rizzatti *et al*., 2017). Bacto1080 recognizes the *Bacteroides* group composed by *Bacteroides-Porphyromonas-Prevotella* and the Bac303 does not recognize *Porphyromonas*, neither recognize the *Rikenellas* genus (Rigotier-Gois *et al*., 2003) also present in the gut microbiota (Forster *et al*., 2019). With our panel we were able to classify up to 95% of Eubacteria positive bacteria, our superior recognition can be explained by the use of a combination of broader phylogenetic probes (Fig. 4). Our combination includes the addition a whole phyla probe for Actinobacteria, more classes for Proteobacteria (βε) and Firmicutes (Bacilli); and the phylum Verrucomicrobia. Furthermore, contrary to our multiparametric panel these previous studies used just two fluorophores (FITC and Cy5) to label the probes using pairs of Eub338 plus another probe in separate tubes, making them more laborious.

It is well known that antibiotics affect both pathogenic and commensal gut bacteria, resulting in drastic modifications of the microbiota composition. The impact of antibiotics on intestinal microbiota has been documented by nonculture-based techniques, demonstrating high intraindividual and interindividual variability, even for similar antimicrobial compounds (Escudero-Sánchez *et al*., 2021). The initial state of the human gut microbiome determines its reshaping by antibiotic treatment (Raymond *et al*., 2016). For all this, it is important to have an easy way method to follow-up the composition of the microbiota. Vancomycin acts by inhibiting proper cell wall synthesis in Gram-positive bacteria. Firmicutes and Actinobacteria are Gram-positive bacteria, both slightly decreased after vancomycin administration. At steady state, Actinobacteria were present in a very low proportion (0.4%) that decrease even more after antibiotic treatment. Firmicutes also decreased slightly in proportion but because it was the major phylum this decrease represented a big loss in absolute number. Several species of *Lactobacillus* (Firmicutes) are intrinsically resistant to vancomycin binding (Gueimonde *et al*., 2013) and can be markedly increased in the vancomycin-treated mice (Xu *et al*., 2019). Proteobacteria, Bacteroidetes and Verrucomicrobia (*A. muciniphila*) are Gram-negative bacteria. As expected and in agreement with the literature, an increase of Proteobacteria and Verrucomicrobia was observed under vancomycin treatment (Hansen *et al*., 2012; Rodrigues *et al*., 2017). Additionally, despite its specificity toward depleting Gram-positive bacteria, vancomycin treatment depleted Bacteroidetes. Singh and collaborators proposed that a possible explanation is that Bacteroidetes are ablated through a nutritional cross-feeding dependency provided by vancomycin-sensitive bacteria (Singh *et al*., 2020).

The proof of concept was successfully achieved and we were able to define, in a non-invasive way, the fecal microbiota composition using a FISH-Flow technique at steady state and in case of clinical

dysbiosis. FISH-Flow is undoubtedly a high throughput, sensitive, fast and inexpensive tool that could be applied to a large number of samples. Considering the probes price and the basic maintenance of the Cytoflex, we could estimate that our method is at least ten times less expensive than metagenomics. One major advantage of FISH is the capability to quantify individual cells without the need to grow them, decreasing the time of analysis and allowing to know the actual number of metabolically active bacteria in a sample. As mentioned before, quantifications are possible with the Cytoflex due to the flow is constant. FISH is not subject of PCR bias and allows phylogenetic characterization at different levels. Amplifying and sequencing DNA as in PCR-related techniques, neither accurately reflect bacterial quantities (varying copy numbers) nor discern microbes as dead or alive (Dave *et al*., 2012; Lau *et al*., 2016). Conversely, FISH as a whole cell technique allows also the differentiation of intact cells from the already lysed ones reflecting the functional microbiota. Advanced sequencing technologies allow us to understand the close association of the gut microbiome with human health and critical illnesses. In the future, analyses of the gut microbiome will provide key information associating with human individual health, which will help provide personalized health care for diseases (Song *et al*., 2018). A broad spectrum of human diseases has been related to changes in the gut microbiota composition, so monitoring or screening them with our fast, semi-quantitive and inexpensive method can be a useful tool in the diagnostic and therapeutic success.

B-V/ Summary

We developed a multiparametric FISH-Flow panel targeting the main phyla of the gut microbiota:

- We designed a good combination of fluorochrome-probes based on their resolving capacity.
- We standardized the analytic conditions for all phylum-specific probes.
- We successfully achieved the proof of concept and evaluated the method specificity, sensibility and precision.
- We tested our panel in murine fecal samples at steady state.
- We were able to detect the alteration of microbiota induced by antibiotic treatment in feces.

Our method allows a fast monitoring of fecal phyla composition in a semi-quantitative and cost-effective way. It can be very useful to detect microbiota dysregulation and potentially predict the development of non-communicable diseases.

DISCUSSION AND PERSPECTIVES

A- Peyer's patch phagocytes characterization and determination of their role in the induction of adaptive immune responses.

Single cell analysis provides a higher resolution of cellular differences and a better understanding of the function of an individual cell in the context of its microenvironment (Eberwine *et al*., 2014). We performed a single cell transcriptional analysis at steady state of all PP phagocytes, which allowed us to determined sets of genes that distinguish cDC from monocyte-derived DC. We rule out the specific expression of some published markers, highlighting how delicate it can be to generalise findings between tissues and emphasises the importance of tissue-specific studies. Importantly, we identified a chronology of the maturation processes for both cDC1 and cDC2 defining their differentiation pathways. Therefore, we described for the first time the transcriptional and spatiotemporal landscape of all PP phagocyte populations from their arrival in the tissue to their final maturation state at homeostasis. It provides us with new tools to study more accurately the PP physiology.

Furthermore, using ligands of the endosomal TLR7 and TLR9, we studied the activation processes of the different PP phagocytes in link with their functions. To complement the transcriptional profiles of PP phagocyte activation, we also evaluated the effect of each agonist on the effector B and T cells. In both conditions of activation, all cDC migrated to the IFR (strong expression of *Ccr7*), with the exception of newly recruited cDC2 that probably seeded the emptied SED (*Ccr6* expression). DAV cDC2 seemed to have an important role in the control of the inflammatory response through expression of immunomodulators, such as the immunosuppressive enzyme Indoleamine 2,3-dioxygenase (IDO). By contrast, in both conditions, late activated dome cDC2 expressed the proinflammatory cytokines *Il12b and Il6.* Therefore, we showed that the initial residence site of cDC2, DAV or dome, shapes their future activation profile. As expected, stimulus type and subset identity also imprint the activation profile, thus orientating the immune response. The activation with CpG caused an important $CD8^+$ T cell response that correlated mostly with a strong recruitment of cDC1, known to indeed efficiently cross-present antigens and prime naïve $CD8^+$ T cells.

The activation of cDC with R848 is known to be indirect and depends on TNF secretion (Bonnardel *et al*., 2017), highlighting the importance of *in vivo* over *in vitro* studies. Indeed, the activation of cDC with R848 cannot be observed *in vitro*. Moreover, synergic or antagonistic effects resulting from the combined

activation profiles of each phagocyte subpopulation is missed in *in vitro* experiments. It is also important to note that microenvironment components such as stromal cells and systemic signals are also important in the inflammatory processes. Finally, local inflammation increases lymphoid organ cellularity and cause lymphoid organ hypertrophy. This hypertrophy is considered to facilitate encounter of antigen-presenting cells and antigen-specific naive lymphocytes enabling the efficient induction of adaptive immune responses. Thus, it is important to consider stimulation of TLR *in vivo* as a complex process with both direct and indirect effects involving many different partners. After stimulation with TLR7, LysoDC but not LysoMac migrate to the IFR to present antigens to naive T cells (Bonnardel *et al*., 2017; Wagner *et al*., 2020). TLR7 stimulation produced a more profound activation effect in monocyte-derived cells than TLR9 stimulation. Furthermore, R848-stimulated monocyte-derived cells expressed strong levels of *Cxcl9* known to mediate T-cell migration. Interestingly, during DSS-induced colitis PP B cells through their expression of CXCL9 actively recruit Treg, which in turn facilitate IgA isotype switch (Wang *et al*., 2018). Thus, expression of *Cxcl9* by LysoDC could be involved in the increase of Treg and the B cell response observed after R848 stimulation. However, it is not clear if this increase of Treg would be a consequence of the CXCL9 release or of antigen presentation and priming activity of LysoDC.

In the future, *in vivo* assessment of cDC and LysoDC contribution to the immune response initiation could be dissected by the depletion of each population. cDC differentiate from pre-DCs and express the transcription factor Zbtb46 (Satpathy *et al*., 2012; Meredith *et al*., 2012). For elucidating the contribution of cDC, we could use mouse chimeras transferred with BM from Zbtb46-DTR donor mice. This system would allow us to specifically deplete cDC after administration of diphtheria toxin (DT). Chimeras are necessary because a single injection of DT is lethal in Zbtb46-DTR mice within 24-48h, probably due to the expression of Zbtb46 in other cell types such as stromal cells (Rombouts *et al*., 2016). Until now, a transgenic mouse model to specifically deplete LysoDC is lacking. However, we recently found that embigin is expressed by most LysoDC but not LysoMac (Wagner *et al*., 2020). Moreover, LysoDC that do not express embigin are the ones that reside in the follicle and do not acquire the DC gene signature. Therefore, an embigin-based model of LysoDC depletion could allow to deplete specifically subepithelial LysoDC. Alternatively, the number of LysoDC in the PP can be diminished with intravenous injection of clodronate-containing liposomes. These liposomes are phagocyted by blood monocytes, which are then killed by their clodronate content, avoiding the arrival of these LysoDC precursors in the PP. Following depletion of each specific phagocyte subset, stimulation with CpG and R848 could be performed to evaluate its role in the B and T responses.

Another approach to specifically address the antigen presentation function of each phagocytes could involved mixed bone-marrow mouse chimera. Indeed, using a mix of BM cells from $CCR2^{-/-}$ and $MHCII^{-/-}$ mice to reconstitute irradiated mice, would give LysoDC unable to present antigens in an MHCII context, since these cells would all derived from the $MHCII^{-/-}$ mice that express CCR2 necessary for the recruitment of LysoDC in PP (Bonnardel *et al*., 2015). By contrast, cDC derived from the $CCR2^{-/-}$ BM would keep their antigen presentation ability. With this system, we could elucidate the importance of LysoDC antigen presentation *in vivo*. Following the same strategy, we could also explore the role of other key molecules, such as CCR7 that could impair LysoDC migration to the IFR.

LysoDC are specific of PP, and maybe of ILF, in several species including humans (Lelouard *et al*., 2010; Wagner *et al*, 2020), their functions in immune responses *in vivo* are still incompletely understood. With single-cell RNA sequencing technology, their differentiation pathways (Wagner *et al*., 2020) and now their activation profile have been obtained, showing a strong link between their location and functions. We saw that R848 stimulation leads to an increase in the B cell response. Intact antigens displayed on the surface of LysoDC or LysoMac could be presented to B cells in the SED to undergo CSR (Reboldi *et al*., 2016). Alternatively, LysoDC or LysoMac could also transfer those antigens to FDC or cDC to support B and T cells responses, respectively. To test this hypothesis, antigen transfer to cDC could be evaluated *in vitro* using sorted $MHCII^{-/-}$ LysoDC cultured in presence of OVA for antigen uptake before co-culture with sorted $MHCII^{+/+}$ cDC and OVA-specific naïve helper T cells.

Rotavirus is a virus that infects Peyer's patches through M cells. It has been shown that shortly after rotavirus infection, DC are mobilized to the SED and increase the expression of surface activation markers, as well as mRNA expression of IL-10, IFN, IL-12/23p40, and TNF genes (Lopez-Guerrero *et al*., 2010). Actually, activation of endosomal TLR can mimic viral infection and may show some common features with this viral infection. Correlating with our results, this mitigated immune response suggests indeed that DC play an important role in controlling the infection and, at the same time, avoiding an excessive inflammatory immune response. Viral particles are shed into the lumen of the intestine and intestinal IgA levels correlate with protection from rotavirus infection. Within 48 hours, an early T cell independent antibody response to rotavirus is generated *in vivo* (Blutt *et al*., 2002). Additionally, CTL are needed for timely virus clearance while antibodies are critical for protection from reinfection. These $CD8^+$ T cells peak in PP 7 days after oral infection (Jiang *et al*., 2008). Unlike agonist activation, *in vivo* infections imply the presence of several antigens and sustained stimuli. However, with our simpler model (one agonist, one pulse) we managed to elicit immune responses that give us a hint of the phagocyte

populations and processes involved. Altogether, our study underscores the importance of targeting not only the right phagocyte subset but also the right place at the right time to orientate the immune response. This information is key for the treatment of intestinal diseases but also for the design of enteric vaccines.

B- Peyer's patch and the gut microbiota

LysoDC and LysoMac are key in the innate defense of the SED as unlike cDC they have a strong antibacterial and antiviral gene signature (Bonnardel *et al*., 2015). Additionally, LysoDC sample actively luminal antigens by TMD and are enriched in the upper part of the SED (Da Silva *et al*., 2017); therefore, they more in contact with antigens than cDC. Detection of some microbiota species by Mincle/Clec4e expressed by LysoDC fosters their IL-6 production and their ability to generate Th17 cells, thereby promoting the production of IL-17 and IL-22 known to contribute to intestinal barrier integrity (Martinez-Lopez *et al*., 2019).

IgA regulates commensal community composition, which is required for gut homeostasis and health. In addition to contributing to immune exclusion at mucosal surfaces, SIgA is able to selectively reenter via M cells into PP and to associate with phagocytes in the SED. It has been reported that the SIgA receptors Dectin-1 and SIGNR3 in DC mediate a non-inflammatory type of response reflected by decreased secretion of IL-12p70, CXCL-1, and IL-6 and by increased production of TGF-β (Mikulic *et al*., 2017). Thus, the type of receptor by which the microbiota is detected modulates mucosal phagocytes conditioning.

As part of my thesis, we successfully designed a multiparametric FISH-Flow panel including nine specific probes that target main phyla of the gut microbiota: Firmicutes, Bacteroidetes, Proteobacteria, Actinobacteria, and Verrucomicrobia. This method allowed us to know the fecal composition at the phylum level in a fast, semi-quantitative and cost-effective way. In addition, we could add an anti-IgA antibody to the panel in order to identify IgA-coated bacteria as it has been done previously to perform 16S rRNA sequencing and identify each of the bacteria that are coated with IgAs (Palm *et al*., 2014; Bunker *et al*., 2015; Kau *et al*., 2015).

Furthermore, bacteria can survive a modified version of FISH allowing to sort specific taxonomic groups of bacteria and subsequently culture them (Batani *et al*., 2019). This technique could be useful for the identification and sorting of live bacteria from healthy donors for fecal microbiota transplantation. For example, fecal transplantation is to date the best available treatment for recurrent *Clostridium difficile*

infection (Schroeder and Bäckhed, 2016). Additionally, probiotics have also been used as treatment or prophylaxis for dysbiosis. It would be then possible to study the beneficial or deleterious effect of different bacteria on the immune response through specific colonization.

PP are colonized with a specific microbiota (Jepson *et al*., 1993; Obata *et al*., 2010; Sonnenberg *et al*., 2012). In principle, we could use the same probes for detection of phyla by spectral confocal microscopy. Thus, the use of our FISH probes together with immune cell markers could provide important information on the organizational structure of regional microbial communities in the PP and on potential interaction between phagocyte subsets and the microbiota. Recently, a high-phylogenetic-resolution microbiome mapping by FISH (HiPR-FISH) has indeed been published, allowing creating maps of the location and identity of hundreds of microbial species in complex communities (Shi *et al*., 2020).

Finally, the analysis of fecal microbiota composition is a valuable tool that could be used to detect anomalies in the distribution of microbiota in relation to non-communicable disease susceptibilities. . Moreover, other probes could be standardized to detect more specifically other bacteria at any phylogenetic level (species, genus, family, etc.). An overview of published probes and their characteristics is indeed available in an online database (Greuter *et al*., 2016).

REFERENCES

Agace, W. W. and McCoy, K. D. (2017) 'Regionalized Development and Maintenance of the Intestinal Adaptive Immune Landscape', Immunity, 46(4), pp. 532–548. doi: 10.1016/j.immuni.2017.04.004.

Aguzzi, A., Kranich, J. and Krautler, N. J. (2014) 'Follicular dendritic cells: origin, phenotype, and function in health and disease', Trends in Immunology, 35(3), pp. 105–113. doi: 10.1016/j.it.2013.11.001.

Al Nabhani, Z. et al. (2019) 'A Weaning Reaction to Microbiota Is Required for Resistance to Immunopathologies in the Adult', Immunity, 50(5), pp. 1276-1288.e5. doi: 10.1016/j.immuni.2019.02.014.

Al Nabhani, Z. and Eberl, G. (2020) 'Imprinting of the immune system by the microbiota early in life', Mucosal Immunology, 13(2), pp. 183–189. doi: 10.1038/s41385-020-0257-y.

Allaire, J. M. et al. (2018) 'The Intestinal Epithelium: Central Coordinator of Mucosal Immunity', Trends in Immunology, 39(9), pp. 677–696. doi: 10.1016/j.it.2018.04.002.

Almeida, A. et al. (2019) 'A new genomic blueprint of the human gut microbiota', Nature, 568(7753), pp. 499–504. doi: 10.1038/s41586-019-0965-1.

Amann, R. I. et al. (1990) 'Combination of 16S rRNA-targeted oligonucleotide probes with flow cytometry for analyzing mixed microbial populations.', Applied and Environmental Microbiology, 56(6), pp. 1919–1925. doi: 10.1128/AEM.56.6.1919-1925.1990.

Anagnostou, K. and Clark, A. (2016) 'What do we mean by oral tolerance?', Clinical & Experimental Allergy, 46(6), pp. 782–784. doi: 10.1111/cea.12751.

Anosova, N. G. et al. (2008) 'Cholera toxin, E. coli heat-labile toxin, and non-toxic derivatives induce dendritic cell migration into the follicle-associated epithelium of Peyer's patches', Mucosal Immunology, 1(1), pp. 59–67. doi: 10.1038/mi.2007.7.

Arpaia, N. et al. (2013) 'Metabolites produced by commensal bacteria promote peripheral regulatory T-cell generation', Nature, 504(7480), pp. 451–455. doi: 10.1038/nature12726.

Arroyo Portilla, C. et al. (2021) 'From Species to Regional and Local Specialization of Intestinal Macrophages', Frontiers in Cell and Developmental Biology, 8, p. 19.

Baaten, B. J. G. et al. (2012) 'Regulation of Antigen-Experienced T Cells: Lessons from the Quintessential Memory Marker CD44', Frontiers in Immunology, 3. doi: 10.3389/fimmu.2012.00023.

Bain, C. C. et al. (2013) 'Resident and pro-inflammatory macrophages in the colon represent alternative context-dependent fates of the same Ly6Chi monocyte precursors', Mucosal Immunology, 6(3), pp. 498–510. doi: 10.1038/mi.2012.89.

Bain, C. C. et al. (2014) 'Constant replenishment from circulating monocytes maintains the macrophage pool in the intestine of adult mice', Nature Immunology, 15(10), pp. 929–937. doi: 10.1038/ni.2967.

Bain, C. C. et al. (2017) 'TGFβR signalling controls CD103 + CD11b + dendritic cell development in the intestine', Nature Communications, 8(1), p. 620. doi: 10.1038/s41467-017-00658-6.

Bain, C. C. and Schridde, A. (2018) 'Origin, Differentiation, and Function of Intestinal Macrophages', Frontiers in Immunology, 9, p. 2733. doi: 10.3389/fimmu.2018.02733.

Barc, M. C. et al. (2004) 'Effect of Amoxicillin-Clavulanic Acid on Human Fecal Flora in a Gnotobiotic Mouse Model Assessed with Fluorescence Hybridization Using Group-Specific 16S rRNA Probes in Combination with Flow Cytometry', Antimicrobial Agents and Chemotherapy, 48(4), pp. 1365–1368. doi: 10.1128/AAC.48.4.1365-1368.2004.

Batani, G. et al. (2019) 'Fluorescence in situ hybridization (FISH) and cell sorting of living bacteria', Scientific Reports, 9(1), p. 18618. doi: 10.1038/s41598-019-55049-2.

Batista, F. D. and Harwood, N. E. (2009) 'The who, how and where of antigen presentation to B cells', Nature Reviews Immunology, 9(1), pp. 15–27. doi: 10.1038/nri2454.

Becker, M. et al. (2014) 'Ontogenic, phenotypic, and functional characterization of XCR1+ dendritic cells leads to a consistent classification of intestinal dendritic cells based on the expression of XCR1 and SIRP', Frontiers in Immunology, p. 12.

Bemark, M., Boysen, P. and Lycke, N. Y. (2012) 'Induction of gut IgA production through T cell-dependent and T cell-independent pathways: Bemark et al .', Annals of the New York Academy of Sciences, 1247(1), pp. 97–116. doi: 10.1111/j.1749-6632.2011.06378.x.

Benckert, J. et al. (2011) 'The majority of intestinal IgA+ and IgG+ plasmablasts in the human gut are antigen-specific', Journal of Clinical Investigation, 121(5), pp. 1946–1955. doi: 10.1172/JCI44447.

Bennett, K. M. et al. (2016) 'Induction of Colonic M Cells during Intestinal Inflammation', The American Journal of Pathology, 186(5), pp. 1166–1179. doi: 10.1016/j.ajpath.2015.12.015.

Bergqvist, P. et al. (2006) 'Gut IgA Class Switch Recombination in the Absence of CD40 Does Not Occur in the Lamina Propria and Is Independent of Germinal Centers', The Journal of Immunology, 177(11), pp. 7772–7783. doi: 10.4049/jimmunol.177.11.7772.

Binda, C. et al. (2018) 'Actinobacteria: A relevant minority for the maintenance of gut homeostasis', Digestive and Liver Disease, 50(5), pp. 421–428. doi: 10.1016/j.dld.2018.02.012.

Biram, A. et al. (2019) 'BCR affinity differentially regulates colonization of the subepithelial dome and infiltration into germinal centers within Peyer's patches', Nature Immunology, 20(4), pp. 482–492. doi: 10.1038/s41590-019-0325-1.

Blaut, M. et al. (2002) 'Molecular biological methods for studying the gut microbiota: the EU human gut flora project', British Journal of Nutrition, 87(S2), pp. S203–S211. doi: 10.1079/BJN/2002539.

Blutt, S. E. et al. (2002) 'Early Response to Rotavirus Infection Involves Massive B Cell Activation', The Journal of Immunology, 168(11), pp. 5716–5721. doi: 10.4049/jimmunol.168.11.5716.

Bogunovic, M. et al. (2009) 'Origin of the Lamina Propria Dendritic Cell Network', Immunity, 31(3), pp. 513–525. doi: 10.1016/j.immuni.2009.08.010.

Bonnardel, J. et al. (2015) 'Innate and Adaptive Immune Functions of Peyer's Patch Monocyte-Derived Cells', Cell Reports, 11(5), pp. 770–784. doi: 10.1016/j.celrep.2015.03.067.

Bonnardel, J. et al. (2017) 'Distribution, location, and transcriptional profile of Peyer's patch conventional DC subsets at steady state and under TLR7 ligand stimulation', Mucosal Immunology, 10(6), pp. 1412–1430. doi: 10.1038/mi.2017.30.

Boyaka, P. N. and Fujihashi, K. (2019) '20 - Host Defenses at Mucosal Surfaces', in Rich, R. R. et al. (eds) Clinical Immunology (Fifth Edition). London: Elsevier, pp. 285-298.e1. doi: 10.1016/B978-0-7020-6896-6.00020-X.

Buettner, M. and Lochner, M. (2016) 'Development and Function of Secondary and Tertiary Lymphoid Organs in the Small Intestine and the Colon', Frontiers in Immunology, 7, p. 11.

Bunker, J. J. et al. (2015) 'Innate and Adaptive Humoral Responses Coat Distinct Commensal Bacteria with Immunoglobulin A', Immunity, 43(3), pp. 541–553. doi: 10.1016/j.immuni.2015.08.007.

Bunker, J. J. and Bendelac, A. (2018) 'IgA Responses to Microbiota', Immunity, 49(2), pp. 211–224. doi: 10.1016/j.immuni.2018.08.011.

Burtis, C. A., Ashwood, E. R. and Bruns, D. E. (2012) Tietz Textbook of Clinical Chemistry and Molecular Diagnostics - E-Book. Elsevier Health Sciences. Available at: https://books.google.fr/books?id=BBLRUI4aHhkC.

Bushnell, T. (2021) What Is Flow Cytometry Light Scatter And How Cell Size And Particle Size Affects It - Cheeky Scientist. Available at: https://expert.cheekyscientist.com/whats-flow-cytometry-light-scatter-how-cell-size-particle-size-affects-it/ (Accessed: 26 April 2021).

Castigli, E. et al. (2004) 'Impaired IgA class switching in APRIL-deficient mice', Proceedings of the National Academy of Sciences, 101(11), pp. 3903–3908. doi: 10.1073/pnas.0307348101.

Castigli, E. and Geha, R. S. (2007) 'TACI, isotype switching, CVID and IgAD', Immunologic Research, 38(1–3), pp. 102–111. doi: 10.1007/s12026-007-8000-2.

Cazac, B. B. and Roes, J. (2000) 'TGF-β Receptor Controls B Cell Responsiveness and Induction of IgA In Vivo', Immunity, 13(4), pp. 443–451. doi: 10.1016/S1074-7613(00)00044-3.

Cerovic, V. et al. (2013) 'Intestinal CD103 − dendritic cells migrate in lymph and prime effector T cells', Mucosal Immunology, 6(1), pp. 104–113. doi: 10.1038/mi.2012.53.

Cerovic, V. et al. (2015) 'Lymph-borne CD8α+ dendritic cells are uniquely able to cross-prime CD8+ T cells with antigen acquired from intestinal epithelial cells', Mucosal Immunology, 8(1), pp. 38–48. doi: 10.1038/mi.2014.40.

Chabot, S. et al. (2006) 'TLRs Regulate the Gatekeeping Functions of the Intestinal Follicle-Associated Epithelium', The Journal of Immunology, 176(7), pp. 4275–4283. doi: 10.4049/jimmunol.176.7.4275.

Chabot, S. M. et al. (2008) 'Effects of Flagellin on the Functions of Follicle-Associated Epithelium', The Journal of Infectious Diseases, 198(6), pp. 907–910. doi: 10.1086/591056.

Chen, H. et al. (2020) 'BCR selection and affinity maturation in Peyer's patch germinal centres', Nature, 582(7812), pp. 421–425. doi: 10.1038/s41586-020-2262-4.

Chieppa, M. et al. (2006) 'Dynamic imaging of dendritic cell extension into the small bowel lumen in response to epithelial cell TLR engagement', Journal of Experimental Medicine, 203(13), pp. 2841–2852. doi: 10.1084/jem.20061884.

Choi, Y. S. et al. (2011) 'ICOS Receptor Instructs T Follicular Helper Cell versus Effector Cell Differentiation via Induction of the Transcriptional Repressor Bcl6', Immunity, 34(6), pp. 932–946. doi: 10.1016/j.immuni.2011.03.023.

Chung, Y. et al. (2011) 'Follicular regulatory T cells expressing Foxp3 and Bcl-6 suppress germinal center reactions', Nature Medicine, 17(8), pp. 983–988. doi: 10.1038/nm.2426.

Clemente, J. C. et al. (2012) 'The Impact of the Gut Microbiota on Human Health: An Integrative View', Cell, 148(6), pp. 1258–1270. doi: 10.1016/j.cell.2012.01.035.

Cole, J. R. et al. (2014) 'Ribosomal Database Project: data and tools for high throughput rRNA analysis', Nucleic Acids Research, 42(D1), pp. D633–D642. doi: 10.1093/nar/gkt1244.

Coombes, J. L. et al. (2007) 'A functionally specialized population of mucosal CD103+ DCs induces Foxp3+ regulatory T cells via a TGF-β– and retinoic acid–dependent mechanism', Journal of Experimental Medicine, 204(8), pp. 1757–1764. doi: 10.1084/jem.20070590.

Cornes, J. S. (1965) 'Number, size, and distribution of Peyer's patches in the human small intestine: Part I The development of Peyer's patches', Gut, 6(3), pp. 225–229. doi: 10.1136/gut.6.3.225.

Craig, S. W. and Cebra, J. J. (1971) 'PEYER'S PATCHES: AN ENRICHED SOURCE OF PRECURSORS FOR IGA-PRODUCING IMMUNOCYTES IN THE RABBIT', Journal of Experimental Medicine, 134(1), pp. 188–200. doi: 10.1084/jem.134.1.188.

Cunningham, M. et al. (2021) 'Shaping the Future of Probiotics and Prebiotics', Trends in Microbiology, p. S0966842X21000056. doi: 10.1016/j.tim.2021.01.003.

Cyster, J. G. and Schwab, S. R. (2012) 'Sphingosine-1-Phosphate and Lymphocyte Egress from Lymphoid Organs', Annual Review of Immunology, 30(1), pp. 69–94. doi: 10.1146/annurev-immunol-020711-075011.

Cyster, J. G. and Von Andrian, U. H. (2004) 'Dynamics of B Cell Migration to and within Secondary Lymphoid Organs', in Molecular Biology of B Cells. Elsevier, pp. 203–221. doi: 10.1016/B978-012053641-2/50015-0.

Da Silva, C. et al. (2017) 'The Peyer's Patch Mononuclear Phagocyte System at Steady State and during Infection', Frontiers in Immunology, 8, p. 1254. doi: 10.3389/fimmu.2017.01254.

Daims, H. et al. (1999) 'The Domain-specific Probe EUB338 is Insufficient for the Detection of all Bacteria: Development and Evaluation of a more Comprehensive Probe Set', Systematic and Applied Microbiology, 22(3), pp. 434–444. doi: 10.1016/S0723-2020(99)80053-8.

Dave, M. et al. (2012) 'The human gut microbiome: current knowledge, challenges, and future directions', Translational Research, 160(4), pp. 246–257. doi: 10.1016/j.trsl.2012.05.003.

Delong, E. F. and Pace, N. R. (2001) 'Environmental Diversity of Bacteria and Archaea', S YSTEMATIC BIOLOGY, 50, p. 9.

DeLong, E., Wickham, G. and Pace, N. (1989) 'Phylogenetic stains: ribosomal RNA-based probes for the identification of single cells', Science, 243(4896), pp. 1360–1363. doi: 10.1126/science.2466341.

Derrien, M. et al. (2008) 'The Mucin Degrader Akkermansia muciniphila Is an Abundant Resident of the Human Intestinal Tract', Applied and Environmental Microbiology, 74(5), pp. 1646–1648. doi: 10.1128/AEM.01226-07.

DeSantis, T. Z. et al. (2006) 'Greengenes, a Chimera-Checked 16S rRNA Gene Database and Workbench Compatible with ARB', Applied and Environmental Microbiology, 72(7), pp. 5069–5072. doi: 10.1128/AEM.03006-05.

Disson, O. et al. (2018) ‘Peyer’s patch myeloid cells infection by Listeria signals through gp38+ stromal cells and locks intestinal villus invasion’, Journal of Experimental Medicine, 215(11), pp. 2936–2954. doi: 10.1084/jem.20181210.

DiToro, D. et al. (2018) ‘Differential IL-2 expression defines developmental fates of follicular versus nonfollicular helper T cells’, Science, 361(6407), p. eaao2933. doi: 10.1126/science.aao2933.

Donaldson, G. P., Lee, S. M. and Mazmanian, S. K. (2016) ‘Gut biogeography of the bacterial microbiota’, Nature Reviews Microbiology, 14(1), pp. 20–32. doi: 10.1038/nrmicro3552.

Doré, J. et al. (1998) ‘Design and Evaluation of a 16S rRNA-Targeted Oligonucleotide Probe for Specific Detection and Quantitation of Human Faecal Bacteroides Populations’, Systematic and Applied Microbiology, 21(1), pp. 65–71. doi: 10.1016/S0723-2020(98)80009-X.

Eberwine, J. et al. (2014) ‘The promise of single-cell sequencing’, Nature Methods, 11(1), pp. 25–27. doi: 10.1038/nmeth.2769.

Eckburg, P. B. et al. (2005) ‘Diversity of the Human Intestinal Microbial Flora’, Science, 308(5728), pp. 1635–1638. doi: 10.1126/science.1110591.

Escudero-Sánchez, R. et al. (2020) ‘Long-Term Impact of Suppressive Antibiotic Therapy on Intestinal Microbiota’, Genes, 12(1), p. 41. doi: 10.3390/genes12010041.

Esterházy, D. et al. (2019) ‘Compartmentalized gut lymph node drainage dictates adaptive immune responses’, Nature, 569(7754), pp. 126–130. doi: 10.1038/s41586-019-1125-3.

Fagarasan, S. et al. (2010) ‘Adaptive Immune Regulation in the Gut: T Cell–Dependent and T Cell–Independent IgA Synthesis’, Annual Review of Immunology, 28(1), pp. 243–273. doi: 10.1146/annurev-immunol-030409-101314.

Fenton, T. M. et al. (2020) ‘Immune Profiling of Human Gut-Associated Lymphoid Tissue Identifies a Role for Isolated Lymphoid Follicles in Priming of Region-Specific Immunity’, Immunity, 52(3), pp. 557-570.e6. doi: 10.1016/j.immuni.2020.02.001.

Flannigan, K. L. and Denning, T. L. (2018) ‘Segmented filamentous bacteria-induced immune responses: a balancing act between host protection and autoimmunity’, Immunology, 154(4), pp. 537–546. doi: 10.1111/imm.12950.

Fontenete, S. et al. (2015) ‘Prediction of melting temperatures in fluorescence in situ hybridization (FISH) procedures using thermodynamic models’, Critical Reviews in Biotechnology, pp. 1–12. doi: 10.3109/07388551.2014.993589.

Forster, S. C. et al. (2019) ‘A human gut bacterial genome and culture collection for improved metagenomic analyses’, Nature Biotechnology, 37(2), pp. 186–192. doi: 10.1038/s41587-018-0009-7.

Fraher, M. H., O’Toole, P. W. and Quigley, E. M. M. (2012) ‘Techniques used to characterize the gut microbiota: a guide for the clinician’, Nature Reviews Gastroenterology & Hepatology, 9(6), pp. 312–322. doi: 10.1038/nrgastro.2012.44.

Franks, A. H. et al. (1998) ‘Variations of Bacterial Populations in Human Feces Measured by Fluorescent In Situ Hybridization with Group-Specific 16S rRNA-Targeted Oligonucleotide Probes’, Applied and Environmental Microbiology, 64(9), pp. 3336–3345. doi: 10.1128/AEM.64.9.3336-3345.1998.

Frey, A. et al. (1996) 'Role of the glycocalyx in regulating access of microparticles to apical plasma membranes of intestinal epithelial cells: implications for microbial attachment and oral vaccine targeting.', Journal of Experimental Medicine, 184(3), pp. 1045–1059. doi: 10.1084/jem.184.3.1045.

Fuchs, B. M. et al. (1998) 'Flow Cytometric Analysis of the In Situ Accessibility of Escherichia coli 16S rRNA for Fluorescently Labeled Oligonucleotide Probes', Applied and Environmental Microbiology, 64(12), pp. 4973–4982. doi: 10.1128/AEM.64.12.4973-4982.1998.

Gaboriau-Routhiau, V. et al. (2009) 'The Key Role of Segmented Filamentous Bacteria in the Coordinated Maturation of Gut Helper T Cell Responses', Immunity, 31(4), pp. 677–689. doi: 10.1016/j.immuni.2009.08.020.

Gebert, A., Rothkötter, H.-J. and Pabst, R. (1996) 'M Cells in Peyer's Patches of the Intestine', in International Review of Cytology. Elsevier, pp. 91–159. doi: 10.1016/S0074-7696(08)61346-7.

Geerlings, S. et al. (2018) 'Akkermansia muciniphila in the Human Gastrointestinal Tract: When, Where, and How?', Microorganisms, 6(3), p. 75. doi: 10.3390/microorganisms6030075.

Giovannoni, S. J. et al. (1988) 'Phylogenetic Group-Specific Oligodeoxynucleotide Probes for Identification of Single Microbial Cells', 170, p. 7.

Glöckner, F. O. et al. (2000) 'Comparative 16S rRNA Analysis of Lake Bacterioplankton Reveals Globally Distributed Phylogenetic Clusters Including an Abundant Group of Actinobacteria', Applied and Environmental Microbiology, 66(11), pp. 5053–5065. doi: 10.1128/AEM.66.11.5053-5065.2000.

Greuter, D. et al. (2016) 'probeBase—an online resource for rRNA-targeted oligonucleotide probes and primers: new features 2016', Nucleic Acids Research, 44(D1), pp. D586–D589. doi: 10.1093/nar/gkv1232.

Gribonika, I. et al. (2019) 'Class-switch recombination to IgA in the Peyer's patches requires natural thymus-derived Tregs and appears to be antigen independent', Mucosal Immunology, 12(6), pp. 1268–1279. doi: 10.1038/s41385-019-0202-0.

Gros, M. J., Naquet, P. and Guinamard, R. R. (2008) 'Cell Intrinsic TGF-β1 Regulation of B Cells', The Journal of Immunology, 180(12), pp. 8153–8158. doi: 10.4049/jimmunol.180.12.8153.

Gueimonde, M. et al. (2013) 'Antibiotic resistance in probiotic bacteria', Frontiers in Microbiology, 4. doi: 10.3389/fmicb.2013.00202.

Guilliams, M. et al. (2016) 'Unsupervised High-Dimensional Analysis Aligns Dendritic Cells across Tissues and Species', Immunity, 45(3), pp. 669–684. doi: 10.1016/j.immuni.2016.08.015.

Hadis, U. et al. (2011) 'Intestinal Tolerance Requires Gut Homing and Expansion of FoxP3+ Regulatory T Cells in the Lamina Propria', Immunity, 34(2), pp. 237–246. doi: 10.1016/j.immuni.2011.01.016.

Hamada, H. et al. (2002) 'Identification of Multiple Isolated Lymphoid Follicles on the Antimesenteric Wall of the Mouse Small Intestine', p. 9.

Hamady, M. and Knight, R. (2009) 'Microbial community profiling for human microbiome projects: Tools, techniques, and challenges', Genome Research, 19(7), pp. 1141–1152. doi: 10.1101/gr.085464.108.

Hanayama, R. et al. (2002) 'Identification of a factor that links apoptotic cells to phagocytes', Nature, 417(6885), pp. 182–187. doi: 10.1038/417182a.

Hansen, C. H. F. et al. (2012) 'Early life treatment with vancomycin propagates Akkermansia muciniphila and reduces diabetes incidence in the NOD mouse', Diabetologia, 55(8), pp. 2285–2294. doi: 10.1007/s00125-012-2564-7.

Haroon, M. F. et al. (2013) 'In-Solution Fluorescence In Situ Hybridization and Fluorescence-Activated Cell Sorting for Single Cell and Population Genome Recovery', in Methods in Enzymology. Elsevier, pp. 3–19. doi: 10.1016/B978-0-12-407863-5.00001-0.

Hase, K. et al. (2006) 'The Membrane-Bound Chemokine CXCL16 Expressed on Follicle-Associated Epithelium and M Cells Mediates Lympho-Epithelial Interaction in GALT', The Journal of Immunology, 176(1), pp. 43–51. doi: 10.4049/jimmunol.176.1.43.

Haynes, N. M. et al. (2007) 'Role of CXCR5 and CCR7 in Follicular Th Cell Positioning and Appearance of a Programmed Cell Death Gene-1 High Germinal Center-Associated Subpopulation', The Journal of Immunology, 179(8), pp. 5099–5108. doi: 10.4049/jimmunol.179.8.5099.

Heesters, B. A., Myers, R. C. and Carroll, M. C. (2014) 'Follicular dendritic cells: dynamic antigen libraries', Nature Reviews Immunology, 14(7), pp. 495–504. doi: 10.1038/nri3689.

Hirota, K. et al. (2013) 'Plasticity of TH17 cells in Peyer's patches is responsible for the induction of T cell–dependent IgA responses', Nature Immunology, 14(4), pp. 372–379. doi: 10.1038/ni.2552.

Hoces, D. et al. (2020) 'Growing, evolving and sticking in a flowing environment: understanding IgA interactions with bacteria in the gut', Immunology, 159(1), pp. 52–62. doi: 10.1111/imm.13156.

Hornef, M. W. and Torow, N. (2020) '"Layered immunity" and the "neonatal window of opportunity" – timed succession of non-redundant phases to establish mucosal host–microbial homeostasis after birth', Immunology, 159(1), pp. 15–25. doi: 10.1111/imm.13149.

Houston, S. A. et al. (2016) 'The lymph nodes draining the small intestine and colon are anatomically separate and immunologically distinct', Mucosal Immunology, 9(2), pp. 468–478. doi: 10.1038/mi.2015.77.

Huang, F.-P. et al. (2000) 'A Discrete Subpopulation of Dendritic Cells Transports Apoptotic Intestinal Epithelial Cells to T Cell Areas of Mesenteric Lymph Nodes', Journal of Experimental Medicine, 191(3), pp. 435–444. doi: 10.1084/jem.191.3.435.

Hugon, P. et al. (2015) 'A comprehensive repertoire of prokaryotic species identified in human beings', The Lancet Infectious Diseases, 15(10), pp. 1211–1219. doi: 10.1016/S1473-3099(15)00293-5.

Huus, K. E., Petersen, C. and Finlay, B. B. (2021) 'Diversity and dynamism of IgA−microbiota interactions', Nature Reviews Immunology. doi: 10.1038/s41577-021-00506-1.

Iglesias-Vázquez, L. et al. (2020) 'Composition of Gut Microbiota in Children with Autism Spectrum Disorder: A Systematic Review and Meta-Analysis', Nutrients, 12(3), p. 792. doi: 10.3390/nu12030792.

Ivanov, I. I. et al. (2009) 'Induction of Intestinal Th17 Cells by Segmented Filamentous Bacteria', Cell, 139(3), pp. 485–498. doi: 10.1016/j.cell.2009.09.033.

Iwasaki, A. and Kelsall, B. L. (2000) 'Localization of Distinct Peyer's Patch Dendritic Cell Subsets and Their Recruitment by Chemokines Macrophage Inflammatory Protein (Mip)-3α, Mip-3β, and Secondary Lymphoid Organ Chemokine', Journal of Experimental Medicine, 191(8), pp. 1381–1394. doi: 10.1084/jem.191.8.1381.

Jepson, M. A. et al. (1993) 'Actin accumulation at sites of attachment of indigenous apathogenic segmented filamentous bacteria to mouse ileal epithelial cells.', Infection and Immunity, 61(9), pp. 4001–4004. doi: 10.1128/IAI.61.9.4001-4004.1993.

Jiang, J. Q. et al. (2008) 'Qualitative and Quantitative Characteristics of Rotavirus-Specific CD8 T Cells Vary Depending on the Route of Infection', Journal of Virology, 82(14), pp. 6812–6819. doi: 10.1128/JVI.00450-08.

Jinnohara, T. et al. (2017) 'IL-22BP dictates characteristics of Peyer's patch follicle-associated epithelium for antigen uptake', Journal of Experimental Medicine, 214(6), pp. 1607–1618. doi: 10.1084/jem.20160770.

Joeris, T. et al. (2017) 'Diversity and functions of intestinal mononuclear phagocytes', Mucosal Immunology, 10(4), pp. 845–864. doi: 10.1038/mi.2017.22.

Jovel, J. et al. (2016) 'Characterization of the Gut Microbiome Using 16S or Shotgun Metagenomics', Frontiers in Microbiology, 7. doi: 10.3389/fmicb.2016.00459.

Jung, C., Hugot, J.-P. and Barreau, F. (2010) 'Peyer's Patches: The Immune Sensors of the Intestine', International Journal of Inflammation, p. 12.

Kaetzel, C. S. (2005) 'The polymeric immunoglobulin receptor: bridging innate and adaptive immune responses at mucosal surfaces', Immunological Reviews, 206(1), pp. 83–99. doi: 10.1111/j.0105-2896.2005.00278.x.

Kasubuchi, M. et al. (2015) 'Dietary Gut Microbial Metabolites, Short-chain Fatty Acids, and Host Metabolic Regulation', Nutrients, 7(4), pp. 2839–2849. doi: 10.3390/nu7042839.

Kato, L. M. et al. (2014) 'Gut T FH and IgA: key players for regulation of bacterial communities and immune homeostasis', Immunology & Cell Biology, 92(1), pp. 49–56. doi: 10.1038/icb.2013.54.

Kau, A. L. et al. (2015) 'Functional characterization of IgA-targeted bacterial taxa from malnourished Malawian children that produce diet-dependent enteropathy', p. 32.

Kawamoto, S. et al. (2014) 'Foxp3+ T Cells Regulate Immunoglobulin A Selection and Facilitate Diversification of Bacterial Species Responsible for Immune Homeostasis', Immunity, 41(1), pp. 152–165. doi: 10.1016/j.immuni.2014.05.016.

Kho, Z. Y. and Lal, S. K. (2018) 'The Human Gut Microbiome – A Potential Controller of Wellness and Disease', Frontiers in Microbiology, 9, p. 1835. doi: 10.3389/fmicb.2018.01835.

Khoruts, A. et al. (2010) 'Changes in the Composition of the Human Fecal Microbiome After Bacteriotherapy for Recurrent Clostridium difficile-associated Diarrhea', Journal of Clinical Gastroenterology, 44(5), pp. 354–360. doi: 10.1097/MCG.0b013e3181c87e02.

Knoop, K. A. et al. (2009) 'RANKL is necessary and sufficient to initiate development of antigen-sampling M cells in the intestinal epithelium', p. 25.

Knoop, K. A. and Newberry, R. D. (2012) 'Isolated Lymphoid Follicles are Dynamic Reservoirs for the Induction of Intestinal IgA', Frontiers in Immunology, 3. doi: 10.3389/fimmu.2012.00084.

Kobayashi, N. et al. (2019) 'The Roles of Peyer's Patches and Microfold Cells in the Gut Immune System: Relevance to Autoimmune Diseases', Frontiers in Immunology, 10, p. 2345. doi: 10.3389/fimmu.2019.02345.

Kolesnikov, M. et al. (2020) 'Intravital visualization of interactions of murine Peyer's patch-resident dendritic cells with M cells', European Journal of Immunology, 50(4), pp. 537–547. doi: 10.1002/eji.201948332.

Komban, R. J. et al. (2019) 'Activated Peyer's patch B cells sample antigen directly from M cells in the subepithelial dome', Nature Communications, 10(1), p. 2423. doi: 10.1038/s41467-019-10144-w.

Kurina, I. et al. (2020) 'Development of qPCR platform with probes for quantifying prevalent and biomedically relevant human gut microbial taxa', Molecular and Cellular Probes, 52, p. 101570. doi: 10.1016/j.mcp.2020.101570.

Lagkouvardos, I., Overmann, J. and Clavel, T. (2017) 'Cultured microbes represent a substantial fraction of the human and mouse gut microbiota', Gut Microbes, 8(5), pp. 493–503. doi: 10.1080/19490976.2017.1320468.

Larsen, N. et al. (2010) 'Gut Microbiota in Human Adults with Type 2 Diabetes Differs from Non-Diabetic Adults', PLoS ONE. Edited by S. Bereswill, 5(2), p. e9085. doi: 10.1371/journal.pone.0009085.

Lau, J. T. et al. (2016) 'Capturing the diversity of the human gut microbiota through culture-enriched molecular profiling', Genome Medicine, 8(1), p. 72. doi: 10.1186/s13073-016-0327-7.

Lebwohl, B., Sanders, D. S. and Green, P. H. R. (2018) 'Coeliac disease', The Lancet, 391(10115), pp. 70–81. doi: 10.1016/S0140-6736(17)31796-8.

Lécuyer, E. et al. (2014) 'Segmented Filamentous Bacterium Uses Secondary and Tertiary Lymphoid Tissues to Induce Gut IgA and Specific T Helper 17 Cell Responses', Immunity, 40(4), pp. 608–620. doi: 10.1016/j.immuni.2014.03.009.

Lederberg, J. and McCray, A. T. (no date) ''Ome Sweet 'Omics-- A Genealogical Treasury of Words', p. 2.

Leiva-Gea, I. et al. (2018) 'Gut Microbiota Differs in Composition and Functionality Between Children With Type 1 Diabetes and MODY2 and Healthy Control Subjects: A Case-Control Study', Diabetes Care, 41(11), pp. 2385–2395. doi: 10.2337/dc18-0253.

Lelouard, H. et al. (2010) 'Pathogenic Bacteria and Dead Cells Are Internalized by a Unique Subset of Peyer's Patch Dendritic Cells That Express Lysozyme', Gastroenterology, 138(1), pp. 173-184.e3. doi: 10.1053/j.gastro.2009.09.051.

Lelouard, H. et al. (2012) 'Peyer's Patch Dendritic Cells Sample Antigens by Extending Dendrites Through M Cell-Specific Transcellular Pores', Gastroenterology, 142(3), pp. 592-601.e3. doi: 10.1053/j.gastro.2011.11.039.

Lemke, G. (2019) 'How macrophages deal with death', Nature Reviews Immunology, 19(9), pp. 539–549. doi: 10.1038/s41577-019-0167-y.

Ley, R. E. et al. (2005) 'Obesity alters gut microbial ecology', Proceedings of the National Academy of Sciences, 102(31), pp. 11070–11075. doi: 10.1073/pnas.0504978102.

Li, H. et al. (2020) 'Mucosal or systemic microbiota exposures shape the B cell repertoire', Nature, 584(7820), pp. 274–278. doi: 10.1038/s41586-020-2564-6.

Li, H. S. et al. (2011) 'Cell-intrinsic role for IFN-α–STAT1 signals in regulating murine Peyer patch plasmacytoid dendritic cells and conditioning an inflammatory response', Blood, 118(14), pp. 3879–3889. doi: 10.1182/blood-2011-04-349761.

Liang, D. et al. (2018) 'Involvement of gut microbiome in human health and disease: brief overview, knowledge gaps and research opportunities', Gut Pathogens, 10(1), p. 3. doi: 10.1186/s13099-018-0230-4.

Litvak, Y. et al. (2017) 'Dysbiotic Proteobacteria expansion: a microbial signature of epithelial dysfunction', Current Opinion in Microbiology, 39, pp. 1–6. doi: 10.1016/j.mib.2017.07.003.

Lopez-Guerrero, D. V. et al. (2010) 'Rotavirus Infection Activates Dendritic Cells from Peyer's Patches in Adult Mice', Journal of Virology, 84(4), pp. 1856–1866. doi: 10.1128/JVI.02640-08.

Maccaferri, S., Biagi, E. and Brigidi, P. (2011) 'Metagenomics: Key to Human Gut Microbiota', Digestive Diseases, 29(6), pp. 525–530. doi: 10.1159/000332966.

Mackay, F. and Browning, J. L. (2002) 'BAFF: A fundamental survival factor for B cells', Nature Reviews Immunology, 2(7), pp. 465–475. doi: 10.1038/nri844.

Macpherson, A. J. and Uhr, T. (2004) 'Induction of Protective IgA by Intestinal Dendritic Cells Carrying Commensal Bacteria', 303, p. 5.

Manz, W. et al. (1992) 'Phylogenetic Oligodeoxynucleotide Probes for the Major Subclasses of Proteobacteria: Problems and Solutions', Systematic and Applied Microbiology, 15(4), pp. 593–600. doi: 10.1016/S0723-2020(11)80121-9.

Manz, W. et al. (1996) 'Application of a suite of 16S rRNA-specific oligonucleotide probes designed to investigate bacteria of the phylum cytophaga-flavobacter-bacteroides in the natural environment', Microbiology, 142(5), pp. 1097–1106. doi: 10.1099/13500872-142-5-1097.

Martinez-Guryn, K., Leone, V. and Chang, E. B. (2019) 'Regional Diversity of the Gastrointestinal Microbiome', Cell Host & Microbe, 26(3), pp. 314–324. doi: 10.1016/j.chom.2019.08.011.

Martínez-López, M. et al. (2019) 'Microbiota Sensing by Mincle-Syk Axis in Dendritic Cells Regulates Interleukin-17 and -22 Production and Promotes Intestinal Barrier Integrity', Immunity, 50(2), pp. 446-461.e9. doi: 10.1016/j.immuni.2018.12.020.

Masahata, K. et al. (2014) 'Generation of colonic IgA-secreting cells in the caecal patch', NATURE COMMUNICATIONS, p. 13.

Mazzini, E. et al. (2014) 'Oral Tolerance Can Be Established via Gap Junction Transfer of Fed Antigens from CX3CR1+ Macrophages to CD103+ Dendritic Cells', Immunity, 40(2), pp. 248–261. doi: 10.1016/j.immuni.2013.12.012.

Meier, H. et al. (1999) 'Specific Oligonucleotide Probes for in situ Detection of a Major Group of Gram-positive Bacteria with low DNA G+C Content', Systematic and Applied Microbiology, 22(2), pp. 186–196. doi: 10.1016/S0723-2020(99)80065-4.

Merad, M. et al. (2013) 'The Dendritic Cell Lineage: Ontogeny and Function of Dendritic Cells and Their Subsets in the Steady State and the Inflamed Setting', Annual Review of Immunology, 31(1), pp. 563–604. doi: 10.1146/annurev-immunol-020711-074950.

Meredith, M. M. et al. (2012) 'Expression of the zinc finger transcription factor zDC (Zbtb46, Btbd4) defines the classical dendritic cell lineage', Journal of Experimental Medicine, 209(6), pp. 1153–1165. doi: 10.1084/jem.20112675.

Mescher, A. L. (2018) 'Digestive Tract', in Junqueira's Basic Histology: Text and Atlas. 15th edn. New York, NY: McGraw-Hill Education. Available at: accessmedicine.mhmedical.com/content.aspx?aid=1160662697 (Accessed: 26 April 2021).

MetaHIT Consortium et al. (2010) 'A human gut microbial gene catalogue established by metagenomic sequencing', Nature, 464(7285), pp. 59–65. doi: 10.1038/nature08821.

MetaHIT Consortium et al. (2014) 'An integrated catalog of reference genes in the human gut microbiome', Nature Biotechnology, 32(8), pp. 834–841. doi: 10.1038/nbt.2942.

Mikulic, J., Bioley, G. and Corthésy, B. (2017) 'SIgA–Shigella Immune Complexes Interact with Dectin-1 and SIGNR3 to Differentially Regulate Mouse Peyer's Patch and Mesenteric Lymph Node Dendritic Cell's Responsiveness', Journal of Molecular Biology, 429(15), pp. 2387–2400. doi: 10.1016/j.jmb.2017.05.024.

Miyanishi, M. et al. (2007) 'Identification of Tim4 as a phosphatidylserine receptor', Nature, 450(7168), pp. 435–439. doi: 10.1038/nature06307.

Moghaddami, M., Cummins, A. and Mayrhofer, G. (1998) 'Lymphocyte-Filled Villi: Comparison With Other Lymphoid Aggregations in the Mucosa of the Human Small Intestine', 115(6), p. 12.

Moro-Sibilot, L. et al. (2016) 'Plasmacytoid dendritic cells are dispensable for noninfectious intestinal IgA responses in vivo: Cellular immune response', European Journal of Immunology, 46(2), pp. 354–359. doi: 10.1002/eji.201545977.

Mowat, A. M. and Agace, W. W. (2014) 'Regional specialization within the intestinal immune system', Nature Reviews Immunology, 14(10), pp. 667–685. doi: 10.1038/nri3738.

Mowat, A. McI. (2018) 'To respond or not to respond — a personal perspective of intestinal tolerance', Nature Reviews Immunology, 18(6), pp. 405–415. doi: 10.1038/s41577-018-0002-x.

Moya, A. and Ferrer, M. (2016) 'Functional Redundancy-Induced Stability of Gut Microbiota Subjected to Disturbance', Trends in Microbiology, 24(5), pp. 402–413. doi: 10.1016/j.tim.2016.02.002.

Mueller, S. N. et al. (2013) 'Memory T Cell Subsets, Migration Patterns, and Tissue Residence', Annual Review of Immunology, 31(1), pp. 137–161. doi: 10.1146/annurev-immunol-032712-095954.

Muramatsu, M. et al. (2000) 'Class Switch Recombination and Hypermutation Require Activation-Induced Cytidine Deaminase (AID), a Potential RNA Editing Enzyme', Cell, 102(5), pp. 553–563. doi: 10.1016/S0092-8674(00)00078-7.

Murphy, K. M. and Weaver, C. (2017) Janeway's Immunobiology. Garland Science/Taylor & Francis Group, LLC. Available at: https://books.google.fr/books?id=YH1djwEACAAJ.

Murri, M. et al. (2013) 'Gut microbiota in children with type 1 diabetes differs from that in healthy children: a case-control study', BMC Medicine, 11(1), p. 46. doi: 10.1186/1741-7015-11-46.

Nagao-Kitamoto, H. et al. (2016) 'Functional Characterization of Inflammatory Bowel Disease–Associated Gut Dysbiosis in Gnotobiotic Mice', Cellular and Molecular Gastroenterology and Hepatology, 2(4), pp. 468–481. doi: 10.1016/j.jcmgh.2016.02.003.

Nagashima, K. et al. (2017) 'Targeted deletion of RANKL in M cell inducer cells by the Col6a1-Cre driver', Biochemical and Biophysical Research Communications, p. 7.

Nagler, C. R. (2020) ‘Drugging the microbiome’, Journal of Experimental Medicine, 217(4), p. e20191642. doi: 10.1084/jem.20191642.

Nakajima, A. et al. (2018) ‘IgA regulates the composition and metabolic function of gut microbiota by promoting symbiosis between bacteria’, Journal of Experimental Medicine, 215(8), pp. 2019–2034. doi: 10.1084/jem.20180427.

Nakamura, Y., Kimura, S. and Hase, K. (2018) ‘M cell-dependent antigen uptake on follicle-associated epithelium for mucosal immune surveillance’, Inflammation and Regeneration, 38(1), p. 15. doi: 10.1186/s41232-018-0072-y.

Namsolleck, P. et al. (2004) ‘Molecular methods for the analysis of gut microbiota’, Microbial Ecology in Health and Disease, 16(2–3), pp. 71–85. doi: 10.1080/08910600410032367.

Neutra, M. R., Mantis, N. J. and Kraehenbuhl, J.-P. (2001) ‘Collaboration of epithelial cells with organized mucosal lymphoid tissues’, Nature Immunology, 2(11), pp. 1004–1009. doi: 10.1038/ni1101-1004.

Niess, J. H. (2005) ‘CX3CR1-Mediated Dendritic Cell Access to the Intestinal Lumen and Bacterial Clearance’, Science, 307(5707), pp. 254–258. doi: 10.1126/science.1102901.

Niess, J. H. et al. (2008) ‘Commensal Gut Flora Drives the Expansion of Proinflammatory CD4 T Cells in the Colonic Lamina Propria under Normal and Inflammatory Conditions’, The Journal of Immunology, 180(1), pp. 559–568. doi: 10.4049/jimmunol.180.1.559.

Obata, T. et al. (2010) ‘Indigenous opportunistic bacteria inhabit mammalian gut-associated lymphoid tissues and share a mucosal antibody-mediated symbiosis’, Proceedings of the National Academy of Sciences, 107(16), p. 7419. doi: 10.1073/pnas.1001061107.

Ohno, H. (2015) ‘Intestinal M cells’, Journal of Biochemistry, 159(2), pp. 151–160. doi: 10.1093/jb/mvv121.

Owen, R. L. (1977) ‘Sequential Uptake of Horseradish Peroxidase by Lymphoid Follicle Epithelium of Peyer’s Patches in the Normal Unobstructed Mouse Intestine: An Ultrastructural Study’, Gastroenterology, 72(3), pp. 440–451. doi: 10.1016/S0016-5085(77)80254-0.

Oyama, L. B. et al. (2017) ‘Buwchitin: A Ruminal Peptide with Antimicrobial Potential against Enterococcus faecalis’, Frontiers in Chemistry, 5, p. 51. doi: 10.3389/fchem.2017.00051.

Pabst, O. and Slack, E. (2020) ‘IgA and the intestinal microbiota: the importance of being specific’, Mucosal Immunology, 13(1), pp. 12–21. doi: 10.1038/s41385-019-0227-4.

Païdassi, H. et al. (2011) ‘Preferential Expression of Integrin αvβ8 Promotes Generation of Regulatory T Cells by Mouse CD103+ Dendritic Cells’, Gastroenterology, 141(5), pp. 1813–1820. doi: 10.1053/j.gastro.2011.06.076.

Palm, N. W. et al. (2014) ‘Immunoglobulin A Coating Identifies Colitogenic Bacteria in Inflammatory Bowel Disease’, Cell, 158(5), pp. 1000–1010. doi: 10.1016/j.cell.2014.08.006.

Parker, A. et al. (2018) ‘Host-microbe interaction in the gastrointestinal tract’, Environmental Microbiology, 20(7), pp. 2337–2353. doi: 10.1111/1462-2920.13926.

Parte, A. C. (2018) ‘LPSN – List of Prokaryotic names with Standing in Nomenclature (bacterio.net), 20 years on’, International Journal of Systematic and Evolutionary Microbiology, 68(6), pp. 1825–1829. doi: 10.1099/ijsem.0.002786.

Peng, W. et al. (2018) 'Metagenome complexity and template length are the main causes of bias in PCR-based bacteria community analysis', Journal of Basic Microbiology, 58(11), pp. 987–997. doi: https://doi.org/10.1002/jobm.201800265.

Pérez-Cobas, A. E. et al. (2013) 'Gut microbiota disturbance during antibiotic therapy: a multi-omic approach', Gut, 62(11), pp. 1591–1601. doi: 10.1136/gutjnl-2012-303184.

Peterson, D. A. et al. (2008) 'Metagenomic Approaches for Defining the Pathogenesis of Inflammatory Bowel Diseases', Cell Host & Microbe, 3(6), pp. 417–427. doi: 10.1016/j.chom.2008.05.001.

Peterson, L. W. and Artis, D. (2014) 'Intestinal epithelial cells: regulators of barrier function and immune homeostasis', Nature Reviews Immunology, 14(3), pp. 141–153. doi: 10.1038/nri3608.

Prados, A. et al. (2021) 'Fibroblastic reticular cell lineage convergence in Peyer's patches governs intestinal immunity', Nature Immunology. doi: 10.1038/s41590-021-00894-5.

Quast, C. et al. (2012) 'The SILVA ribosomal RNA gene database project: improved data processing and web-based tools', Nucleic Acids Research, 41(D1), pp. D590–D596. doi: 10.1093/nar/gks1219.

Raymond, F. et al. (2016) 'The initial state of the human gut microbiome determines its reshaping by antibiotics', The ISME Journal, 10(3), pp. 707–720. doi: 10.1038/ismej.2015.148.

Reboldi, A. and Cyster, J. G. (2016) 'Peyer's patches: organizing B-cell responses at the intestinal frontier', Immunological Reviews, 271(1), pp. 230–245. doi: 10.1111/imr.12400.

Reboldi, A. et al. (2016) 'IgA production requires B cell interaction with subepithelial dendritic cells in Peyers patches', Science, 352(6287), pp. aaf4822–aaf4822. doi: 10.1126/science.aaf4822.

Rezasoltani, S. et al. (2019) 'Signature of Gut Microbiome by Conventional and Advanced Analysis Techniques: Advantages and Disadvantages', Middle East Journal of Digestive Diseases, 12(1), pp. 5–11. doi: 10.15171/mejdd.2020.157.

Rigottier-Gois, L. et al. (2003) 'Fluorescent hybridisation combined with flow cytometry and hybridisation of total RNA to analyse the composition of microbial communities in human faeces using 16S rRNA probes', FEMS Microbiology Ecology, 43(2), pp. 237–245. doi: 10.1111/j.1574-6941.2003.tb01063.x.

Rivollier, A. et al. (2012) 'Inflammation switches the differentiation program of Ly6Chi monocytes from antiinflammatory macrophages to inflammatory dendritic cells in the colon', Journal of Experimental Medicine, 209(1), pp. 139–155. doi: 10.1084/jem.20101387.

Rizzatti, G. et al. (2017) 'Proteobacteria: A Common Factor in Human Diseases', BioMed Research International, 2017, pp. 1–7. doi: 10.1155/2017/9351507.

Rochereau, N. et al. (2013) 'Dectin-1 Is Essential for Reverse Transcytosis of Glycosylated SIgA-Antigen Complexes by Intestinal M Cells', PLoS Biology. Edited by D. Nemazee, 11(9), p. e1001658. doi: 10.1371/journal.pbio.1001658.

Rodrigues, R. R. et al. (2017) 'Antibiotic-Induced Alterations in Gut Microbiota Are Associated with Changes in Glucose Metabolism in Healthy Mice', Frontiers in Microbiology, 8, p. 2306. doi: 10.3389/fmicb.2017.02306.

Rodriguez-Manzanet, R. et al. (2010) 'T and B cell hyperactivity and autoimmunity associated with niche-specific defects in apoptotic body clearance in TIM-4-deficient mice', Proceedings of the National Academy of Sciences, 107(19), pp. 8706–8711. doi: 10.1073/pnas.0910359107.

Rombouts, M., Cools, N. and Grootaert, M. O. J. (2017) 'Long-Term Depletion of Conventional Dendritic Cells Cannot Be Maintained in an Atherosclerotic Zbtb46-DTR Mouse Model', PLOS ONE, p. 16.

Russell, M. W. et al. (2015) 'Overview', in Mucosal Immunology. Elsevier, pp. 3–8. doi: 10.1016/B978-0-12-415847-4.00001-X.

Saffarian, A. et al. (2019) 'Crypt- and Mucosa-Associated Core Microbiotas in Humans and Their Alteration in Colon Cancer Patients', mBio. Edited by J. Parkhill, 10(4), pp. e01315-19, /mbio/10/4/mBio.01315-19.atom. doi: 10.1128/mBio.01315-19.

Sakhon, O. S. et al. (2015) 'M cell-derived vesicles suggest a unique pathway for trans-epithelial antigen delivery', Tissue Barriers, 3(1–2), p. e1004975. doi: 10.1080/21688370.2015.1004975.

Sartor, R. B. and Wu, G. D. (2017) 'Roles for Intestinal Bacteria, Viruses, and Fungi in Pathogenesis of Inflammatory Bowel Diseases and Therapeutic Approaches', Gastroenterology, 152(2), pp. 327-339.e4. doi: 10.1053/j.gastro.2016.10.012.

Satpathy, A. T. et al. (2012) 'Zbtb46 expression distinguishes classical dendritic cells and their committed progenitors from other immune lineages', Journal of Experimental Medicine, 209(6), pp. 1135–1152. doi: 10.1084/jem.20120030.

Schroeder, B. O. and Bäckhed, F. (2016) 'Signals from the gut microbiota to distant organs in physiology and disease', Nature Medicine, 22(10), pp. 1079–1089. doi: 10.1038/nm.4185.

Scott, C. L. et al. (2015) 'CCR2+CD103− intestinal dendritic cells develop from DC-committed precursors and induce interleukin-17 production by T cells', Mucosal Immunology, 8(2), pp. 327–339. doi: 10.1038/mi.2014.70.

Sender, R., Fuchs, S. and Milo, R. (2016) 'Revised Estimates for the Number of Human and Bacteria Cells in the Body', PLOS Biology, 14(8), p. e1002533. doi: 10.1371/journal.pbio.1002533.

Serbina, N. V. and Pamer, E. G. (2006) 'Monocyte emigration from bone marrow during bacterial infection requires signals mediated by chemokine receptor CCR2', Nature Immunology, 7(3), pp. 311–317. doi: 10.1038/ni1309.

Shi, H. et al. (2020) 'Highly multiplexed spatial mapping of microbial communities', Nature, 588(7839), pp. 676–681. doi: 10.1038/s41586-020-2983-4.

Shi, J. et al. (2018) 'PD-1 Controls Follicular T Helper Cell Positioning and Function', Immunity, 49(2), pp. 264-274.e4. doi: 10.1016/j.immuni.2018.06.012.

Shin, N.-R., Whon, T. W. and Bae, J.-W. (2015) 'Proteobacteria: microbial signature of dysbiosis in gut microbiota', Trends in Biotechnology, 33(9), pp. 496–503. doi: 10.1016/j.tibtech.2015.06.011.

Sichien, D. et al. (2017) 'Development of conventional dendritic cells: from common bone marrow progenitors to multiple subsets in peripheral tissues', Mucosal Immunology, 10(4), pp. 831–844. doi: 10.1038/mi.2017.8.

Singh, V. et al. (2020) 'Vancomycin prevents fermentable fiber-induced liver cancer in mice with dysbiotic gut microbiota', Gut Microbes, 11(4), pp. 1077–1091. doi: 10.1080/19490976.2020.1743492.

Skerman, V. B. D., McGowan, V. and Sneath, P. H. A. (eds) (1989) Approved Lists of Bacterial Names (Amended). Washington (DC): ASM Press. Available at: http://www.ncbi.nlm.nih.gov/books/NBK814/.

Sobhon, P. (1971) 'The light and the electron microscopic studies of Peyer's patches in non germ-free adult mice', Journal of Morphology, 135(4), pp. 457–481. doi: 10.1002/jmor.1051350404.

Song, E.-J., Lee, E.-S. and Nam, Y.-D. (2018) 'Progress of analytical tools and techniques for human gut microbiome research', Journal of Microbiology, 56(10), pp. 693–705. doi: 10.1007/s12275-018-8238-5.

Sonnenberg, G. F. and Artis, D. (2012) 'Innate lymphoid cell interactions with the microbiota: implications for intestinal health and disease', p. 19.

Sonnenberg, G. F. et al. (2012) 'Innate Lymphoid Cells Promote Anatomical Containment of Lymphoid-Resident Commensal Bacteria', Science, 336(6086), pp. 1321–1325. doi: 10.1126/science.1222551.

Spiljar, M., Merkler, D. and Trajkovski, M. (2017) 'The Immune System Bridges the Gut Microbiota with Systemic Energy Homeostasis: Focus on TLRs, Mucosal Barrier, and SCFAs', Frontiers in Immunology, 8, p. 1353. doi: 10.3389/fimmu.2017.01353.

Spor, A., Koren, O. and Ley, R. (2011) 'Unravelling the effects of the environment and host genotype on the gut microbiome', Nature Reviews Microbiology, 9(4), pp. 279–290. doi: 10.1038/nrmicro2540.

Stagg, A. J. (2018) 'Intestinal Dendritic Cells in Health and Gut Inflammation', Frontiers in Immunology, 9, p. 2883. doi: 10.3389/fimmu.2018.02883.

Stebegg, M. et al. (2018) 'Regulation of the Germinal Center Response', Frontiers in Immunology, 9, p. 2469. doi: 10.3389/fimmu.2018.02469.

Sterlin, D. et al. (2019) 'Human IgA binds a diverse array of commensal bacteria', Journal of Experimental Medicine, 217(3), p. e20181635. doi: 10.1084/jem.20181635.

Streitz, M. et al. (2013) 'Standardization of whole blood immune phenotype monitoring for clinical trials: panels and methods from the ONE study', Transplantation Research, 2(1), p. 17. doi: 10.1186/2047-1440-2-17.

Sun, C.-M. et al. (2007) 'Small intestine lamina propria dendritic cells promote de novo generation of Foxp3 T reg cells via retinoic acid', Journal of Experimental Medicine, 204(8), pp. 1775–1785. doi: 10.1084/jem.20070602.

Sun, T., Nguyen, A. and Gommerman, J. L. (2020) 'Dendritic Cell Subsets in Intestinal Immunity and Inflammation', The Journal of Immunology, 204(5), pp. 1075–1083. doi: 10.4049/jimmunol.1900710.

Suzuki, K. et al. (2010) 'The Sensing of Environmental Stimuli by Follicular Dendritic Cells Promotes Immunoglobulin A Generation in the Gut', Immunity, 33(1), pp. 71–83. doi: 10.1016/j.immuni.2010.07.003.

Tamoutounour, S. et al. (2012) 'CD64 distinguishes macrophages from dendritic cells in the gut and reveals the Th1-inducing role of mesenteric lymph node macrophages during colitis: HIGHLIGHTS', European Journal of Immunology, 42(12), pp. 3150–3166. doi: 10.1002/eji.201242847.

Teng, F. et al. (2016) 'Gut Microbiota Drive Autoimmune Arthritis by Promoting Differentiation and Migration of Peyer's Patch T Follicular Helper Cells', Immunity, 44(4), pp. 875–888. doi: 10.1016/j.immuni.2016.03.013.

Tezuka, H. and Ohteki, T. (2019) 'Regulation of IgA Production by Intestinal Dendritic Cells and Related Cells', Frontiers in Immunology, 10, p. 1891. doi: 10.3389/fimmu.2019.01891.

The Human Microbiome Project Consortium (2012) 'Structure, function and diversity of the healthy human microbiome', Nature, 486(7402), pp. 207–214. doi: 10.1038/nature11234.

Thursby, E. and Juge, N. (2017) 'Introduction to the human gut microbiota', Biochemical Journal, 474(11), pp. 1823–1836. doi: 10.1042/BCJ20160510.

Tindall, B. J. et al. (2010) 'Notes on the characterization of prokaryote strains for taxonomic purposes', International Journal of Systematic and Evolutionary Microbiology, 60(1), pp. 249–266. doi: 10.1099/ijs.0.016949-0.

Tropini, C. et al. (2017) 'The Gut Microbiome: Connecting Spatial Organization to Function', Cell Host & Microbe, 21(4), pp. 433–442. doi: 10.1016/j.chom.2017.03.010.

Tsuji, M. et al. (2009) 'Preferential Generation of Follicular B Helper T Cells from Foxp3+ T Cells in Gut Peyer's Patches', Science, 323(5920), pp. 1488–1492. doi: 10.1126/science.1169152.

Vance, R. E. (2015) 'The NAIP/NLRC4 inflammasomes', Current Opinion in Immunology, 32, pp. 84–89. doi: 10.1016/j.coi.2015.01.010.

Vandeputte, D. et al. (2017) 'Quantitative microbiome profiling links gut community variation to microbial load', Nature, 551(7681), pp. 507–511. doi: 10.1038/nature24460.

Varol, C. et al. (2009) 'Intestinal Lamina Propria Dendritic Cell Subsets Have Different Origin and Functions', Immunity, 31(3), pp. 502–512. doi: 10.1016/j.immuni.2009.06.025.

Vaziri, N. D. et al. (2013) 'Chronic kidney disease alters intestinal microbial flora', Kidney International, 83(2), pp. 308–315. doi: 10.1038/ki.2012.345.

Victora, G. D. and Nussenzweig, M. C. (2012) 'Germinal Centers', Annual Review of Immunology, 30(1), pp. 429–457. doi: 10.1146/annurev-immunol-020711-075032.

Wagner, C. et al. (2018) 'Some news from the unknown soldier, the Peyer's patch macrophage', Cellular Immunology, 330, pp. 159–167. doi: 10.1016/j.cellimm.2018.01.012.

Wagner, C. et al. (2020) 'Differentiation Paths of Peyer's Patch LysoDCs Are Linked to Sampling Site Positioning, Migration, and T Cell Priming', Cell Reports, 31(1), p. 107479. doi: 10.1016/j.celrep.2020.03.043.

Wagner, M., Horn, M. and Daims, H. (2003) 'Fluorescence in situ hybridisation for the identification and characterisation of prokaryotes', Current Opinion in Microbiology, 6(3), pp. 302–309. doi: 10.1016/S1369-5274(03)00054-7.

Wallner, G., Amann, R. and Beisker, W. (1993) 'Optimizing fluorescent in situ hybridization with rRNA-targeted oligonucleotide probes for flow cytometric identification of microorganisms', Cytometry, 14(2), pp. 136–143. doi: 10.1002/cyto.990140205.

Wang, Y. et al. (2009) '16S rRNA gene-based analysis of fecal microbiota from preterm infants with and without necrotizing enterocolitis', The ISME Journal, 3(8), pp. 944–954. doi: 10.1038/ismej.2009.37.

Wang, Z. et al. (2018) 'Peyer's patches-derived CD11b+ B cells recruit regulatory T cells through CXCL9 in dextran sulphate sodium-induced colitis', Immunology, 155(3), pp. 356–366. doi: https://doi.org/10.1111/imm.12977.

Welty, N. E. et al. (2013) 'Intestinal lamina propria dendritic cells maintain T cell homeostasis but do not affect commensalism', Journal of Experimental Medicine, 210(10), pp. 2011–2024. doi: 10.1084/jem.20130728.

Woese, C. R., Fox, G. E. and Pechman, K. R. (1977) 'Comparative Cataloging of 16S Ribosomal Ribonucleic Acid: Molecular Approach to Procaryotic Systematics', International Journal of Systematic and Evolutionary Microbiology, 27(1), pp. 44–57. doi: 10.1099/00207713-27-1-44.

Wooley, J. C. and Ye, Y. (2009) 'Metagenomics: Facts and Artifacts, and Computational Challenges', Journal of Computer Science and Technology, 25(1), pp. 71–81. doi: 10.1007/s11390-010-9306-4.

Worthington, J. J. et al. (2011) 'Intestinal Dendritic Cells Specialize to Activate Transforming Growth Factor-β and Induce Foxp3+ Regulatory T Cells via Integrin αvβ8', Gastroenterology, 141(5), pp. 1802–1812. doi: 10.1053/j.gastro.2011.06.057.

Xu, X. et al. (2019) 'Alteration of GLP-1/GPR43 expression and gastrointestinal motility in dysbiotic mice treated with vancomycin', Scientific Reports, 9(1), p. 4381. doi: 10.1038/s41598-019-40978-9.

Yang, T. et al. (2015) 'Gut Dysbiosis Is Linked to Hypertension', Hypertension, 65(6), pp. 1331–1340. doi: 10.1161/HYPERTENSIONAHA.115.05315.

Zhao, X. et al. (2003) 'CCL9 Is Secreted by the Follicle-Associated Epithelium and Recruits Dome Region Peyer's Patch CD11b + Dendritic Cells', The Journal of Immunology, 171(6), pp. 2797–2803. doi: 10.4049/jimmunol.171.6.2797.

Zimmermann, J. et al. (2016) 'High-resolution microbiota flow cytometry reveals dynamic colitis-associated changes in fecal bacterial composition', European Journal of Immunology, 46(5), pp. 1300–1303. doi: 10.1002/eji.201646297.

Annex 1: From species to regional and local specialization of intestinal macrophages

frontiers in Cell and Developmental Biology

REVIEW
published: 18 February 2021
doi: 10.3389/fcell.2020.624213

From Species to Regional and Local Specialization of Intestinal Macrophages

Cynthia Arroyo Portilla[1,2], *Julie Tomas*[1], *Jean-Pierre Gorvel*[1] *and Hugues Lelouard*[1]*

[1] Aix Marseille Univ, CNRS, INSERM, CIML, Marseille, France, [2] Departamento de Análisis Clínicos, Facultad de Microbiología, Universidad de Costa Rica, San José, Costa Rica

Initially intended for nutrient uptake, phagocytosis represents a central mechanism of debris removal and host defense against invading pathogens through the entire animal kingdom. In vertebrates and also many invertebrates, macrophages (MFs) and MF-like cells (e.g., coelomocytes and hemocytes) are professional phagocytic cells that seed tissues to maintain homeostasis through pathogen killing, efferocytosis and tissue shaping, repair, and remodeling. Some MF functions are common to all species and tissues, whereas others are specific to their homing tissue. Indeed, shaped by their microenvironment, MFs become adapted to perform particular functions, highlighting their great plasticity and giving rise to high population diversity. Interestingly, the gut displays several anatomic and functional compartments with large pools of strikingly diversified MF populations. This review focuses on recent advances on intestinal MFs in several species, which have allowed to infer their specificity and functions.

Keywords: intestinal immunity, macrophages, microbiota, phagocytosis, stromal microenvironment, dietary antigens, metabolites, antigen sampling

OPEN ACCESS

Edited by:
Katrin Kierdorf,
University of Freiburg, Germany

Reviewed by:
Stephen J. Jenkins,
University of Edinburgh,
United Kingdom
Guy E. Boeckxstaens,
KU Leuven, Belgium

***Correspondence:**
Hugues Lelouard
lelouard@ciml.univ-mrs.fr

Specialty section:
This article was submitted to Cell Death and Survival, a section of the journal Frontiers in Cell and Developmental Biology

Received: *30 October 2020*
Accepted: *30 December 2020*
Published: *18 February 2021*

Citation:
Arroyo Portilla C, Tomas J, Gorvel J-P and Lelouard H (2021) From Species to Regional and Local Specialization of Intestinal Macrophages. Front. Cell Dev. Biol. 8:624213. doi: 10.3389/fcell.2020.624213

INTRODUCTION

The innate immune system encompasses different defense mechanisms selected over evolutionary time and encoded in the germline, hence passed to offspring with only minor refinements. Genome sequencing has established that much of these defense systems are conserved across animal phyla, reflecting their remarkable effectiveness and versatility (Litman and Cooper, 2007). These conserved defense mechanisms include the complement system, pattern recognition receptors (PRRs), and phagocytosis. The complement system is an ancient component of immunity that likely evolved from protection of the unicellular protists to essential defense functions in the blood of vertebrates (Elvington et al., 2016). Classical PRRs, such as Toll-like receptors (TLRs), C-type lectins, NOD-like receptors (NLRs), and perforin-2/MPEG-1, are already identified in non-bilaterian animals (Traylor-Knowles et al., 2019). Phagocytosis, from ancient Greek meaning "cell eating," is typically an eukaryote-specific process that consists in the ingestion of particulate matters larger than 0.4 μm by a cell through invagination of its membrane (Mills, 2020). Inside the Eukaryota domain, plant cells are not able to phagocyte due to their rigid cell wall. In addition, no phagocytosis has been reported in fungi, with the exception of the parasitic fungus *Rozella allomycis* (Yutin et al., 2009). By contrast, protists use phagocytosis for the intake of nutrients from the environment where these unicellular organisms reside. In parasitic infections, such as

trichomoniasis, the protozoan *Trichomonas vaginalis* uses phagocytosis to ingest *Saccharomyces cerevisiae* cells, vaginal epithelial cells, leucocytes, and erythrocytes (Pereira-Neves and Benchimol, 2007). Phagocytosis involves cell membrane receptors for target recognition. Thus, the scavenger receptor cysteine-rich (SRCR) domain family of receptors is encoded in the genomes from the most primitive sponges to mammals (Dzik, 2010). Receptors for phagocytosis bind the particles either directly or via opsonins (antibodies or complement components) that enhance phagocytosis (Richards and Endres, 2017). The specialized compartment resulting from membrane invagination around the targeted material is termed phagosome (Niedergang and Grinstein, 2018). Interestingly, the soil-living amoeba *Dictyostelium discoideum* uses molecular mechanisms of phagosome maturation very similar to higher eukaryotic cells, such as macrophages (MFs) (Gotthardt et al., 2002). This efficient "digestive" system of ingested material defines the primary function around which phagocytosis extends its functional ability throughout evolution (Desjardins et al., 2005). However, despite that phagocytosis is often proposed as an evolutionarily conserved mechanism, the diversity and variability of proteins associated with phagosomes across the different eukaryotic species suggest that phagocytosis may have evolved independently several times (Yutin et al., 2009; Mills, 2020).

The kingdom Animalia is composed of multicellular eukaryotic organisms. This cellular scaling has required the acquisition of cell–cell adhesion, communication, cooperation, and specialization (Niklas, 2014). Organism size has always been considered an important factor for the evolution of multicellularity. The advantages of increased size include predator evasion, increased motility, and an increased capacity to store nutrients. Interestingly, the organism size has an impact in cellular specialization, which may evolve more easily in larger organisms (Willensdorfer, 2008). In animals, phagocytosis has extended from the nutritional function to key roles in homeostasis, such as apoptotic cell removal, tissue remodeling, and immune defense (Desjardins et al., 2005). Hartenstein and Martinez have recently reviewed the role of phagocytosis in nutrition and have compared this function of invertebrate enteric phagocytes/enterocytes with MF ability to eliminate pathogens and damaged cells (Hartenstein and Martinez, 2019). Endodermal-derived enterocytes play indeed a prominent role in the invertebrate digestive system by taking up the extracellularly pre-digested material and completing the digestive process intracellularly. By contrast, MFs are mesodermally derived motile cells that engulf and digest foreign materials and cellular detritus that threaten the integrity of the organism. Thus, phagocytosis is an ancient process that likely evolved from the feeding of phagotrophic unicellular organisms to the defense against pathogens in complex organisms. Non-nutritional-related phagocytic cells observed in invertebrate species bear different names (e.g., amoebocytes, coelomocytes, or hemocytes) depending on the hosting species, but basically they have a MF-like appearance and have, to a certain extent, comparable functions as part of the innate immune system (**Table 1**) (Buchmann, 2014). The hypothesis of a common origin for immunity and digestion is mainly based on the existence of shared components such as enzymes, receptors, signaling pathways, and cellular processes (Broderick, 2015). Thus, many of the enzymes involved in immunity play also a role in digestion (e.g., lysozymes and proteases), with specific contexts for which these functions cannot be distinguished, e.g., for animals that capture and feed on bacteria. However, an extensive transcriptomic analysis done in different phagocytic cell types across widely divergent clades was inconclusive for homology assessments (Hartenstein and Martinez, 2019). Anyhow, in immunity, bacteria internalized via phagocytosis are typically sequestered within phagolysosomes where several antibacterial strategies are used to kill and degrade them, such as compartment acidification, enzyme production and activation, and generation of reactive oxygen species (ROS). Many types of eukaryotes produce ROS, which likely represent an ancient antimicrobial strategy for targeting intracellular bacteria (Richter and Levin, 2019).

Interestingly, phagocytosis shares molecular mechanisms with autophagy, a degradative cellular process in which eukaryotic cells digest their own components (Birgisdottir and Johansen, 2020). Like phagocytosis, autophagy is an ancient highly conserved process likely to date back to the common ancestor of all eukaryotes (Duszenko et al., 2011). Like phagocytosis, autophagy likely evolved from a cellular nutrition mechanism to become a key player in cellular homeostasis and defense against pathogens. Although autophagy and phagocytosis are activated by different mechanisms, they converge on similar pathways that are regulated by shared molecules. Thus, LC3-associated phagocytosis (LAP) involves engulfment of large extracellular particles through the engagement of components of the autophagy machinery among which Beclin 1, the phosphatidylinositol 3-kinase Vps34, ATG (autophagy) family proteins, and finally LC3 (Sanjuan et al., 2007; Martinez et al., 2011, 2015). LC3 recruitment to the phagosome favors phagosome fusion with lysosomes, acidification, and ingested material degradation. LAP is involved in several phagocyte functions, such as pathogen clearance, antigen presentation by major histocompatibility complex (MHC) class II molecules, regulation of proinflammatory cytokine production and efferocytosis (Martinez, 2018).

From its earliest beginnings, the study of innate immunity has greatly benefited from works carried out on simple organisms, starting from the discovery of phagocytosis significance in starfish larva by Elie Metchnikoff to the more recent discovery of PRRs in the fruit fly by Jules Hoffman (Lemaitre et al., 1996; Hoffmann and Reichhart, 2002; Buchmann, 2014; Gordon, 2016). Indeed, these organisms combine easy genetic manipulations and phenotypic analyses with fast generation renewal and simplified cell diversity and signaling pathways including key elements conserved across species. It is therefore important to appreciate the diversity of MFs across species to have a complete picture of them. With the tissue organization of complex organisms, MFs have acquired new functions within their residence niche where they maintain strong relationships with their neighboring cells, allowing their resident tissue to function properly. In this review, we describe the nature of MFs and MF-like cells across the animal kingdom with a special focus on the intestinal tissue of

TABLE 1 | Main features of MF-like cells across species.

	Diploblastic	Platyhelminths	Nematoda	Arthropoda	Echinodermata	Vertebrates		
						Zebrafish	Birds	Mouse	Human
Representative organism	Cnidaria, Porifera	Planarian	*Caenorhabditis elegans*	*Drosophila melanogaster*	Sea urchin	Zebrafish	Birds	Mouse	Human
Body cavity	No	Acoelomates	Pseudocoelomates	Coelomates					
Gut formation	No	Protostomia			Deuterostomia				
Adaptive immunity		No				Yes			
Phagocyte name	Amoebocytes	Reticular cells	Coelomocytes	Plasmatocytes (different subsets)	Hemocytes/Filopodial cells/Ovoid cells	Macrophages			
Gut-specific population		No		Proventriculus	No	Yes			
Main known functions	Digestive phagocytosis Nutrient transport	Digestive and immune phagocytosis Nutrient transport MORN2-mediated antimicrobial activity	Digestive phagocytosis Fat consumption Life span extension upon starvation Metal detoxification	**Exclusive immune phagocytosis** Efferocytosis Wound healing Antimicrobial signaling IESCs proliferation Glucose homeostasis	Digestive and immune phagocytosis Encapsulation Syncytia formation	**Exclusive immune phagocytosis** Protection against infection and inflammation Microbiota shaping Th17 cells/Tregs regulation Intestinal inflammatory lymphangiogenesis	**Exclusive immune phagocytosis** Antigen uptake Protection Against invading pathogens Antimicrobial activities	**Exclusive immune phagocytosis** Multiple functions depending on their location (see **Table 2**)	

IESCs: intestinal epithelial stem cells; Tregs, regulatory T cells.

each species when data are available. We consider more precisely the local and regional specialization of MFs in the mammalian intestine and discuss recent findings highlighting their great diversity of functions from one location to another.

MACROPHAGE-LIKE CELLS OF THE DIPLOBLASTS

Living cells depend on a constant supply of energy-rich organic molecules from the environment, making the emergence of a specialized system for food digestion and nutrient absorption a crucial innovation for multicellular organisms. The most ancient division within the animal kingdom is between diploblasts and triploblasts (**Figure 1**). Diploblasts are radially symmetrical animals with two distinct germ layers: an inner layer or endoderm/gut and an outer layer or ectoderm/skin. In between these two layers, triploblasts have an additional layer: the mesoderm (Telford et al., 2015). Because of the lack of this intermediate layer, mesodermal MFs *per se* are not found in diploblasts. Instead, the gelatinous matrix (mesoglea) between both layers contains large numbers of motile amoebocytes that carry out multiple functions, the most primitive being digestion (**Table 1**). Amoebocytes ingest and digest food caught by enterocytes and transport nutrients to the other cells. Amoebocytes have been reported in the different diploblastic phyla: Cnidaria (Menzel et al., 2015), Ctenophora (Traylor-Knowles et al., 2019), and Porifera (Adamska, 2016). However, in Placozoa, a sister phylum of Cnidaria, amoebocytes have not been described, probably because these animals are mostly composed of epithelial cells (Mayorova et al., 2019). The ability to phagocyte and move in the mesoglea makes the amoebocytes very similar to mesodermal MFs. Additionally, the presence in these animals of conserved innate defense mechanisms, such as PRRs and pore-forming proteins (e.g., the MF-expressed gene 1 protein, Mpeg1), supports the participation of these amoebocytes in innate immunity (Brennan and Gilmore, 2018; Walters et al., 2020).

MACROPHAGE-LIKE CELLS IN ACOELOMATE AND PSEUDOCOELOMATE PROTOSTOMES

The triploblasts have two major branches, the Protostomia and Deuterostomia (**Figure 1**). Their names reflect the fundamentally different fates of the blastopore, the primary embryonic gut opening (Nielsen et al., 2018). In protostomes, the blastopore forms the mouth with the anus forming secondarily (protostomy = mouth first); in the deuterostomes, it is the other way around (deuterostomy = mouth second). The presence of a mouth creates an asymmetry with an anterior–posterior axis making the triploblastic condition a synonym of Bilateria. The gastrointestinal tract (GIT) displays diversified levels of complexity according to species, with the endoderm-derived one-way gut of most bilaterians being the prevailing and more specialized form (Annunziata et al., 2019).

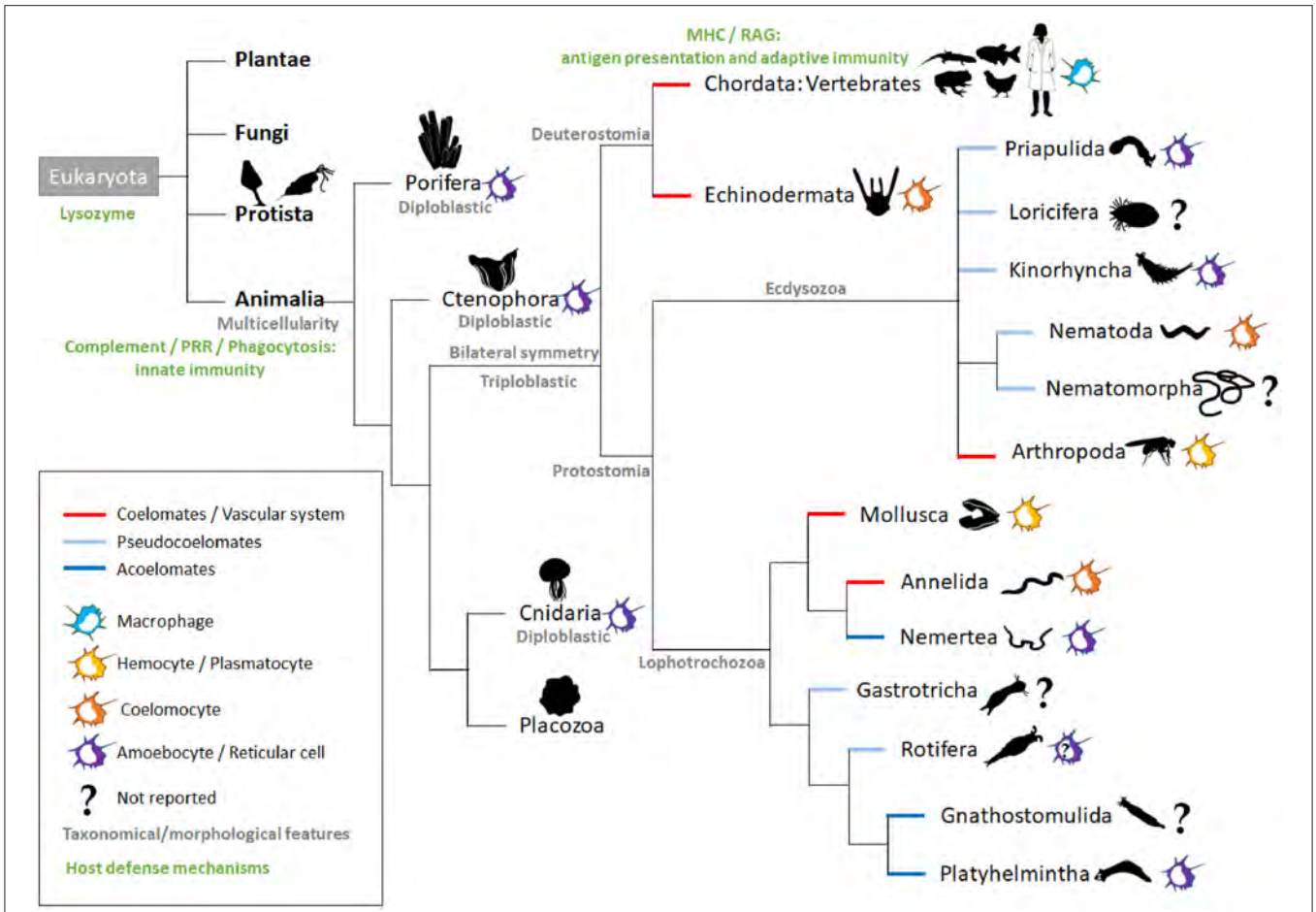

FIGURE 1 | Intestinal macrophage-like cell types across animal species. The main kingdoms (bold black) of the Eukaryota domain are listed. In animals, the representative phyla are named and ordered according to currently used phylogenetic trees (Peterson and Eernisse, 2016; Giribet and Edgecombe, 2017; Kocot et al., 2017). Additional information is added in gray (taxonomical or morphological) in green (host defense mechanisms; nutritional phagocytosis not taken into account) and by the colored lines (embryological development). For each phylum, colored icons on the right symbolize the macrophage-like cell type; the question marks indicate a lack of literature for the phylum. In Rotifera, amoebocytes have been described, but their function is more related to their motility, and there are no reports related to their immunological role (Baumann et al., 2000). MHC, Major Histocompatibility complex; PRR, pattern recognition receptors; RAG, recombination-activating gene.

The majority of invertebrates belong to Protostomia, whereas all vertebrates and few invertebrates belong to Deuterostomia (**Figure 1**). During embryonic development, if a split in the mesoderm forms a fluid-filled body cavity termed coelom, the animal is referred to as coelomate. When the space between the ectoderm and endoderm tissue layers is filled with a meshwork of mesodermal cells (or parenchyma), the animal is referred to as acoelomate. When the mesoderm has fluid-filled clefts in this meshwork, the animal is then termed pseudocoelomate (Monahan-Earley et al., 2013). Acoelomates and pseudocoelomates are found only in Protostomia (**Figure 1**). By contrast, coelomates are found in both lineages. In several invertebrate phyla, motile MF-like cells in the parenchyma or coelom take up cellular debris resulting from dying cells and actively distribute digested foodstuffs, receiving this material from enteric phagocytes lining the gut (Hartenstein and Martinez, 2019).

The acoelomate protostomes obtain their oxygen and food by simple diffusion across the skin and gut and throughout the intercellular medium. Freely moving reticular cells have been observed in the parenchyma of the platyhelminths (flatworms) (Morita, 1995). These reticular cells are mesenchymal cells that play an important role in nutrient transportation and phagocytosis of foreign material, acting as an immune surveillance system (**Table 1**). Planarian platyhelminth antimicrobial activities involve an orthologous protein for MORN2, which has been associated with LAP and resistance to bacterial infection in human MFs (Abnave et al., 2014). In Nemertea, amebocytes arising from the intestinal segment were reported to play a central role in graft rejection (Langlet and Bierne, 1984). To our knowledge, there are no reports on the presence of MF-like cells in gnathostomulids.

In pseudocoelomates, the pseudocoelomic fluid serves as the circulatory system for nutrients that are taken up, ingested,

degraded, and secreted into the pseudocoelom by the intestinal cells. We did not find any report of MF-like cells in the phyla Gastrotricha, Nematomorpha, and Loricifera. However, in Rotifera, the pseudocoelom of several taxa contains free motile amoeboid cells, but so far, no immune function has been reported for these cells (Baumann et al., 2000). By contrast, phagocytically active amoebocytes have been observed in Priapulida (Mattisson and Fänge, 1973) and Kinorhyncha (Neuhaus and Higgins, 2002). For Nematoda, the cells contained in the pseudocoelomic fluid are termed coelomocytes. *Caenorhabditis elegans* is a simple and genetically tractable nematode model that has enabled key advances in immunity (Willis et al., 2020). However, there is no evidence that their coelomocytes provide a potent defense against bacterial infection (**Table 1**). These six oblong MF-like scavenger cells located in the *C. elegans* body cavity are indeed dispensable to the viability and survival of the worm (Fares and Greenwald, 2001). Nevertheless, studies of *C. elegans* coelomocytes identified novel components of the endocytic machinery that are conserved in mammals (Fares and Greenwald, 2001; Sato et al., 2014). Moreover, *C. elegans* coelomocytes have been shown to regulate fat consumption and life span extension upon starvation (Buis et al., 2019). Finally, they participate in metal detoxification (Tang et al., 2020). Interestingly, old studies performed in another nematode, *Ascaris suum*, have documented the encapsulation of bacteria by coelomocytes (Bolla et al., 1972).

MACROPHAGE-LIKE CELLS IN COELOMATE PROTOSTOMES WITH AN OPEN CIRCULATORY SYSTEM

The advantage of a true coelom is the ability of the inner mesenteric layer to suspend the central gut in the middle of the animals, allowing them to increase their body size. In addition, a circulatory system helps size increase by reducing the functional diffusion distance of nutrients, gases, and metabolic waste products. In animals that have evolved coelom along with a vascular system, cells with the characteristics of MFs are prominent among the circulating cells, commonly referred to as coelomocytes or hemocytes (Hartenstein, 2006). During development, they represent the professional MFs that eliminate apoptotic cells. In addition, they cooperate with humoral factors to battle invading parasites and microbes, many of which enter through the digestive tract.

Blood vascular systems follow one of two principal designs: open or closed. In open circulatory system, the blood, referred to as hemolymph, empties from a contractile heart and major supply vessels into the body cavity termed hemocoel, where it directly bathes the organs. This occurs in arthropods and non-cephalopod molluscs.

In Arthropoda, the fruit fly *Drosophila melanogaster* has been widely used as a suitable model to study innate immunity and has provided invaluable contributions to the knowledge of innate immune system signaling pathways (Hoffmann and Reichhart, 2002). In *D. melanogaster*, hematopoiesis does not occur in adult but only during development through two waves (Wood and Martin, 2017; Banerjee et al., 2019; Sanchez Bosch et al., 2019). The first wave occurs in the embryo and gives rise to hemocytes that proliferate during the larval stages. The second wave of hematopoiesis occurs at the larval stage in an organ called the larval lymph gland. MF-like cells termed plasmatocytes represent about 95% of the total hemocyte population in adult. A single-cell transcriptome of hemocytes made it possible to characterize different subsets of plasmatocytes (ranging from 4 to 12 depending on the study), showing an interesting parallel with the great diversity of MFs in mammals (Cattenoz et al., 2020; Cho et al., 2020; Fu et al., 2020; Tattikota et al., 2020). Although the precise functions of each of these subsets remain to be established, plasmatocytes globally serve essential roles in immune response to infection and wound healing (**Table 1**). While lack of plasmatocytes does not impair fruit fly development, it indeed induces a strong susceptibility to infections by various microorganisms, due notably to an absence of phagocytosis in deficient fruit flies (Charroux and Royet, 2009). Plasmatocytes do not only patrol the body in the circulation but also associate with specific tissues, such as the intestinal epithelium. In the *D. melanogaster* model, the intestine is composed of three main parts: the foregut, the midgut, and the hindgut. The fore- and hindgut have an ectodermal origin, whereas the midgut, which is the functional equivalent of the mammalian small intestine (SI), has an endodermal origin. Plasmatocytes of embryonic origin specifically colonize a region at the foregut/midgut junction known as the proventriculus, where they form a discrete group of functional MFs able to phagocytose both apoptotic bodies and bacterial intruders (Charroux and Royet, 2009; Zaidman-Rémy et al., 2012). Plasmatocytes circulating in the hemolymph can also infiltrate the midgut when necessary (Ayyaz et al., 2015). In addition to their phagocytic activity, plasmatocytes relay intestinal infection-induced oxidative stress signal and nitric oxide production to the fat body, an organ equivalent to the vertebrate liver, which produces an antimicrobial peptide response (Wu et al., 2012). Like mammal MFs, plasmatocytes switch their metabolic program to aerobic glycolysis in order to mount an efficient antibacterial response (Krejčová et al., 2019). Upon injury, circulating plasmatocytes release the cytokines of the unpaired (Upd) family Upd2 and Upd3, which by retrospective alignments of type I cytokines and functional analogies are most closely related to the vertebrate leptins (Rajan and Perrimon, 2012; Beshel et al., 2017). These cytokines bind to the receptor Domeless that activates the JAK-STAT pathway in the fat body and in the gut, where it stimulates intestinal stem cell proliferation, thereby contributing to fly survival (Chakrabarti et al., 2016).

In bivalve molluscs, the distribution of blast-like cells suggests that hematopoiesis may be widespread in connective tissue, with further development of hemocytes in the hemolymph (Hine, 1999). Two main sub-populations of hemocytes have been identified: granulocytes containing many cytoplasmic granules and hyalinocytes containing few or no granules (Girón-Pérez, 2010). Granulocytes are the main cell type involved in the cellular immune defense of bivalves (Rolton et al., 2020). They are also involved in other physiological functions, such as wound healing and shell repair, digestion, and transport of nutrients. Indeed, in the gut lumen, hemocytes ingest and digest foreign materials and

transport the digested materials to the gut lining or other tissues. In addition to this digestive function, hemocytes can engulf and phagocytize foreign pathogens present on the mucosal surfaces of oysters as part of their innate immune functions. Hemocytes routinely traffic between the hemolymph and the outer surfaces of oysters (Provost et al., 2011).

MACROPHAGE-LIKE CELLS IN COELOMATE PROTOSTOMES WITH A CLOSED CIRCULATORY SYSTEM

Closed circulatory systems occur in a wide variety of invertebrates including annelids, cephalopods, and non-vertebrate chordates. Earthworms, which are the best known of all annelids, belong to the class Oligochaeta. Their gut surface is in permanent contact with ingested soil. Moreover, the nephridia and dorsal pores enable microorganisms to enter the coelomic cavity. Hence, both coelom and gut interact with naturally occurring soil microorganisms and have to face strong antigenic environment (Prochazkova et al., 2020). The free circulating immune cells of the coelomic cavity, termed coelomocytes, can be subdivided into two subpopulations, the eleocytes and the amoebocytes (Engelmann et al., 2016). Eleocytes are highly autofluorescent cells due to their large granules termed chloragosomes that contain riboflavin. Eleocytes originate from the chloragogen tissue surrounding the gut and are considered as the terminal differentiation stage of sessile chloragocytes released from this tissue. They have mainly accessory functions such as maintenance of pH and storage of glycogen and lipids. By contrast, amoebocytes are MF-like cells with a broad range of defense functions, including phagocytosis (Engelmann et al., 2016). Two types of amoebocytes have been described, hyaline and granular amoebocytes, without clear separate functions. PRRs [coelomic cytolytic factor (CCF) and lipopolysaccharide (LPS)-binding protein (LBP)] and the TLR signaling pathway molecule Myd88 genes are typically expressed by amoebocytes but not eleocytes, supporting the role of amoebocytes in pathogen detection and neutralization (Bodó et al., 2018). Moreover, amoebocytes express higher levels of the oxidative stress-related super oxide dismutase and antimicrobial lysozyme and lumbricin genes (Bodó et al., 2018). Dermal contact with immunostimulants decreases coelomocyte total number but increases the proportion of granular amoebocytes among them and induces ROS production (Homa et al., 2013, 2016). Experimental microbial challenge triggers the release of phagocytic coelomocytes from the mesenchymal lining of the coelom and thus increases the defense reaction in the coelomic cavity of earthworms (Dvorák et al., 2016).

MACROPHAGE-LIKE CELLS IN INVERTEBRATE DEUTEROSTOMES

Deuterostomes include two main phyla: Echinodermata and Chordata (**Figure 1**). In echinoderms, the circulating immune cells, i.e., the coelomocytes, are heterogeneous in morphology, size, relative abundance, and functions. This makes a single standard classification for all echinoderms a difficult task. The distribution of these cell types is also highly variable among species and even at the individual level (Smith et al., 2018). Nevertheless, phagocytes are present in all echinoderm classes and are the main effectors of the echinoderm immune system. These phagocytes respond to immune challenges through phagocytosis, encapsulation, syncytia formation, and expression of complement components (Golconda et al., 2019).

The sea urchin larva has five major types of immune cells that populate the body cavity (blastocoel), including two phagocytic cell types termed filopodial and ovoid cells (**Table 1**) (Ho et al., 2017). Filopodial cells extend long filopodia that form a reticular network in the blastocoel (Buckley and Rast, 2019). They are likely the MF-like cells observed by Elie Metchnikoff in his seminal works on phagocytosis. Ovoid cells are rarely present at steady state but rapidly appear upon immune challenge and could therefore represent an activation state of some of the filopodial cells. Upon sea urchin larva gut disturbance through the presence of pathogenic bacteria in the seawater, a coordinated immune response takes place (Ho et al., 2017). A subset of immune cells termed pigment cells rapidly migrates from the ectoderm to the gut epithelium where they secrete their antibacterial iron chelator pigment echinochrome A (Ho et al., 2017; Coates et al., 2018). Then, the number and duration of cell–cell interactions among immune cells and with the gut epithelium increase (Ho et al., 2017). Finally, filopodial cells quickly phagocytose bacteria that penetrate the blastocoel of larvae. This coordinated immune response is at least in part launched by secretion of IL-17 family members by gut epithelial cells (Buckley et al., 2017).

VERTEBRATE MACROPHAGES

The phylum Chordata consists of three subphyla: Urochordata, Cephalochordata, and Vertebrata. Vertebrates possess non-phagocytic enterocytes, and a clear dichotomy is made at this level between the digestive and immune function of phagocytosis (Hartenstein and Martinez, 2019). Moreover, vertebrates have evolved adaptive immunity that can recognize and respond to specific antigen determinants thanks to the somatic DNA rearrangement of segmental elements encoding the antigen binding regions of their T and B cell receptors (Cooper and Alder, 2006). Together with adaptive immunity appears a new type of mononuclear phagocytes termed dendritic cells (DCs). DCs make the link between innate and adaptive immunity by initiating and controlling antigen-specific immunity through presentation of antigenic epitopes on MHC class I and class II molecules (Banchereau and Steinman, 1998). Therefore, the vertebrate mononuclear phagocyte system comprises monocytes, MFs, and DCs, as well as their lineage-committed progenitors (Guilliams et al., 2014). The intestinal immune system of vertebrates comprises a unique array of innate and adaptive immune cells. Along the intestinal tract, immune cells are either disseminated throughout the mucosa forming a diffuse distribution or clustered in organized lymphoid tissues. The latter, termed organized gut-associated lymphoid tissues (GALT), initiate the intestinal immune response. Organized GALT have

been reported in their simplest forms in all classes of vertebrates but are especially well-developed in the endotherms, mainly mammals and birds.

The bone marrow is the hematopoietic organ in all vertebrates except some amphibians in which hematopoiesis can also occur in the liver and fishes in which hematopoiesis occurs only in the kidney. Fishes are the most primitive animals in which an adaptive immunity is present. In zebrafish, the first embryonic MFs originate from the mesoderm and migrate over the yolk ball before colonizing other tissues, whereas in adults, myeloid-lineage progenitors arise from the kidney (Stachura and Traver, 2011). MFs and DCs are especially abundant in the spleen and gut (Wittamer et al., 2011). In the adult zebrafish, the gut can be divided following the anterior–posterior axis into seven segments, from the proximal S1 to the most distal S7 (Wang et al., 2010). Each segment exhibits functional differences and also similarities to the mammalian GIT; e.g., the S7 represents the colon-like region (Wang et al., 2010; Lickwar et al., 2017). Distribution of MFs and DCs along these segments and the ability of these phagocytes to sample luminal antigens depending on their location have not been determined so far. Interestingly, Interferon Regulatory Factor 8 (IRF8) depletion leads to a lack of MFs during embryonic development with only partial recovery in adults (Li et al., 2011; Shiau et al., 2015; Ferrero et al., 2020). Thus, brain and gut resident MFs remain strongly impacted by IRF8 deficiency (Earley et al., 2018). Importantly, like in mammals, intestinal MFs are required for shaping the gut microbiota, and dysbiosis occurs in MF-deficient zebrafish (**Table 1**) (Earley et al., 2018). In addition, IRF8-dependent MFs are the main producers of the complement C1q genes in the intestine (Earley et al., 2018). Zebrafish intestinal MFs show other similarities with their mammal counterparts. Thus, like in mouse and human, $CD4^+$ MFs and regulatory T (Treg) cells reside in the zebrafish gut mucosa (Dee et al., 2016). Moreover, microbiota and inflammation promote G-protein-coupled receptor 35 expression in mouse and zebrafish intestinal MFs, which have a protective role during intestinal inflammation by inducing TNF synthesis upon lysophosphatidic acid binding (Kaya et al., 2020). Finally, like in mammals, intestinal inflammation entails infiltration into the gut mucosa of inflammatory MFs, which elicit a Th17 cell response together with a decrease of Treg cells (Coronado et al., 2019). Moreover, in a zebrafish colitis model, MFs promote intestinal inflammatory lymphangiogenesis via their vascular endothelial growth factor gene expression (*vegfa*, *vegfc*, and *vegfd*), highlighting the potential of the zebrafish model to investigate the mechanism of lymphangiogenesis in inflammatory bowel diseases (IBDs) (Okuda et al., 2015).

Amphibians rely heavily on MFs not only for immune defense but also for homeostasis and tissue remodeling/resorption. Most of the literature on amphibian MFs is related to programmed cell death and tissue remodeling during metamorphosis (Grayfer and Robert, 2016). Hematopoiesis of primitive and mainly aquatic amphibian species occurs in the liver, whereas hematopoiesis of more terrestrial amphibian species occurs in the bone marrow (Grayfer and Robert, 2016). In the frog *Xenopus laevis*, the principal site of hematopoiesis is still the liver subcapsular region, but myelopoiesis, i.e., the differentiation of the granulocyte MF precursor (GMP) into granulocytes and MFs, occurs in the bone marrow (Grayfer and Robert, 2013; Yaparla et al., 2016). Precursors with GMP potential migrate from the liver to the bone marrow under the influence of chemokines enriched in the bone marrow, such as CXCL12 (Yaparla et al., 2019). MF differentiation is controlled through binding of the main MF growth factor, colony-stimulating factor-1 (CSF1) to its CSF1 receptor (CSF1R), which is almost exclusively expressed on committed MF precursors (Grayfer and Robert, 2016). IL-34 is as an alternative CSF1R ligand, giving rise to morphologically and functionally distinct MFs (Yaparla et al., 2020). Unfortunately, to our knowledge, the literature on amphibian intestinal MFs consists mainly of old descriptive studies. Lymphoid aggregates resembling mammalian isolated lymphoid follicles (ILFs) have been observed in the urodele amphibians (Ardavín et al., 1982). In these structures, the number of goblet cells decreases, and lymphoid cells, including MFs, penetrate the intestinal epithelium. In the gut lamina propria of toads, MFs tend to cluster and interact with lymphocytes and plasma cells (Chin and Wong, 1977).

Most studies on reptile immune function have focused on systemic immune responses, leaving an important knowledge gap in the mucosal immune responses. Indeed, literature on reptile intestinal immunity consists mainly of descriptive studies (Borysenko and Cooper, 1972; Zapata and Solas, 1979; Solas and Zapata, 1980; Ashford et al., 2019). Reptiles possess primary lymphoid organs such as bone marrow and thymus but lack secondary lymphoid tissues such as Peyer's patches (PPs) or mesenteric lymph nodes (MLNs). Instead, numerous ILF-like lymphoid aggregates are located throughout the small and large intestines. These aggregates are enriched in small lymphocytes and MFs (Borysenko and Cooper, 1972; Zapata and Solas, 1979; Solas and Zapata, 1980; Ashford et al., 2019). MFs are dispersed in the lamina propria but can migrate to the intestinal epithelium in these lymphoid aggregates (Solas and Zapata, 1980). Interestingly, the number of lymphoid aggregates in the SI of poikilothermic snakes depends on the season, diminishing in spring and summer (Solomon et al., 1981). Moreover, temperature can affect functions of lizard MFs, which have an optimal phagocytic activity at 25°C (Mondal and Rai, 2001). In reptiles, the enteropathogenic bacteria *Salmonella enterica* colonize the intestinal tract without any signs of disease, but MFs seem not to be involved in this protection since *S. enterica* is able to kill turtle MFs (Pasmans et al., 2002).

Like mammals, birds have a well-developed mucosal immune system, with several organized GALT. They include the primary lymphoid organ termed bursa of Fabricius and several secondary lymphoid organs, namely, PPs, cecal tonsils, and Meckel's diverticulum (Casteleyn et al., 2010). The chicken gut lamina propria contains various innate immune cells such as heterophils (the avian polymorphonuclear cells), natural killer cells, DCs and MFs, although the differences between the latter two have not been carefully assessed (Broom and Kogut, 2018). Chicken MFs/DCs display a range of PRRs, expression of MHC class II, and phagocytic and antimicrobial activities. Like in mammals, early-life microbial colonization is critical for the immunological maturation of the avian gut, and short early-life antibiotic

treatment induces alteration of mucosal gene expression and a decrease of MF number in the gut lamina propria for at least 2 weeks (Schokker et al., 2017). In chicken duodenum, jejunum, and ileum, MFs/DCs are involved in antigen uptake and provide protection against invading pathogens (**Table 1**) (Taha-Abdelaziz et al., 2020). During coccidiosis, MFs are the principal cell type involved in the clearance of the sporozoites by phagocytosis (de Geus and Vervelde, 2013). During *Salmonella* infection, resistance depends on a genetic locus *SAL1* and has been linked to MFs with better oxidative killing activity and greater and faster expression of proinflammatory cytokines (Wigley, 2014). During dextran sulfate sodium (DSS)-induced intestinal inflammation, increased monocyte/MF infiltration occurs in all segments of laying hen intestine (Nii et al., 2020).

In mammals, embryonic MFs initially originate from yolk sac erythro-myeloid progenitors (Hoeffel and Ginhoux, 2018). Subsequently, early hematopoietic stem cells (HSCs) settle first in the fetal liver and later in bone marrow to form a permanent, self-renewing source of monocytes. Monocytes infiltrate tissues and can replace and differentiate into tissue-resident MFs to varying degrees depending on the organs and the encountered immune challenges, with most MFs keeping an embryonic origin and self-renewal (Hoeffel and Ginhoux, 2018; Liu et al., 2019). Importantly, MF renewal by monocytes is especially prevalent in the intestine, which is always subject to antigenic stimulation whether through food, drink, or microbiota (Bain et al., 2014). In rodents and in human, the GIT is complex and divided longitudinally from the duodenum to the rectum, with functional and morphological distinctions between the small (duodenum, jejunum, and ileum) and large (cecum and proximal and distal colon) intestines (Mowat and Agace, 2014). The SI is specialized in the absorption of nutrients, whereas the primary function of colon is the absorption of water and electrolytes. The SI has villi that increase its surface of exposure to the intestinal lumen content, a thinner and less well-organized mucus layer, and reduced microbial communities than the colon. Mammalian MFs can fulfill the auxiliary functions necessary for the homeostasis of each tissue of residence, such as peristaltic movements and tolerance induction toward dietary and microbiota-derived antigens in the intestine. In the recent years, single-cell RNA sequencing associated with high-resolution confocal microscopy, multiparameter flow cytometry, and functional assay analyses have allowed to reveal unsuspected aspects of the local and regional specialization of MFs in mouse and human intestine as discussed below and shown in **Table 2**.

TELL ME WHERE YOU LIVE AND I WILL TELL YOU WHAT KIND OF MACROPHAGE YOU ARE

We have seen that across species, specialized cells assume at least one of the main activities of what we call MF in vertebrates: phagocytosis. These cells show a remarkable plasticity according to their local microenvironment, i.e., the network of factors and cells with which they interact. With the increasing complexity of tissue functions occurring during the metazoan evolution, these cells have diversified even more and have acquired dedicated functions to offer protection and to sustain activity of their tissue of residence.

The specific stromal microenvironment that surrounds HSCs in the bone marrow has been identified decades ago as niches indispensable for the maintenance and differentiation of HSCs (Morrison and Scadden, 2014). However, it is only very recently that this concept of niche has been fully appreciated for peripheral tissues, especially for MF identity imprinting (Gosselin et al., 2014; Lavin et al., 2014; van de Laar et al., 2016). Two recent reviews have described how this local microenvironment is now crucial to be considered in order to better characterize and understand the functions of tissue-resident MFs (Blériot et al., 2020; Guilliams et al., 2020). Nowadays, studies dedicated to the conditioning of MFs by their local microenvironment are mainly developed in human and mouse in which a unique MF transcriptional program seems to correspond to each specific niche of the intestine (Bujko et al., 2018; De Schepper et al., 2018; Kang et al., 2020). Since phagocytic cells interact with and react to external factors and neighboring stromal and immune cells whatever the species considered, we however assume that this concept can be widely extended to other species.

In the following parts, we detail how intestinal MF identity and functions are impacted by their niche of residence. We particularly focus on the (re)categorization of the MFs according to their anatomical location within the intestinal mucosa (**Table 2**). We also consider the strong influence of two exogenous factors inseparable from the intestine, the intestinal microbiota and the dietary antigens.

A (Re)Categorization of Intestinal Macrophages by Their Radial Distribution and Local Compartmentalization: Protecting and Supporting Your Immediate Neighbors

Most intestinal MFs along the GIT share some common functions, such as the phagocytosis of microorganisms and dead cells. They also share some common specific markers, such as CX_3CR1 and F4/80 in mouse and CD14 and CD16 in human (Bain et al., 2013; Bujko et al., 2018). In addition, in both species, intestinal MFs express CD64, CD163, and MerTK. At the exception of immune inductive sites such as PPs as discussed later, gut MFs display anti-inflammatory properties at steady state. They indeed weakly respond to many different innate stimulations, constitutively express IL-10 and its receptor, participate in Treg cell expansion, and protect from colitis (Hadis et al., 2011; Bain et al., 2013; Shouval et al., 2014; Zigmond et al., 2014). According to their anatomical location, intestinal MFs interact with specific cells and detect and respond to specific factors that make them crucial support units of their microenvironment. In turn, the latter is decisive for MF recruitment and differentiation in relation to the different anatomic layers of the intestine. Therefore, from the serosa to the epithelium, MFs are territorialized to accomplish specific functions (**Table 2**).

TABLE 2 | Local and regional specialization of intestinal macrophages in human and mouse.

		Location	Name	Main neighbors	Main functions	Species	Key markers	References
Radial specialization	Effector sites: Villus and colonic MFs	Subepithelial SI and colon	LPM	IECs fibroblastic cells Immune cells	Antigen sampling Tissue protection and repair Treg and Th17 cell equilibrium	Mouse Human	CD64, CX_3CR1, F4/80, MerTK CD14, CD16, CD64, MerTK, CD163	Tamoutounour et al., 2012; Bain et al., 2013 Bujko et al., 2018
		Perivascular SI and colon	Perivascular MF	Endothelial cells	Regulation and strengthening of the vasculature Bacterial translocation blockade Systemic antigen uptake	Mouse	CX_3CR1, CD169, CD206	De Schepper et al., 2018; Honda et al., 2020; Kang et al., 2020
		Crypt base SI and colon	Crypt base-associated MF	$Lgr5^+$ epithelial stem cells Paneth cells	Maintain the renewal of the SI crypts Promote the crypt regenerative response Inflammatory monocyte recruitment	Mouse	CSF1R/CD115, CD169, CD206	Pull et al., 2005; Asano et al., 2015; Sehgal et al., 2018; Kang et al., 2020
		Submucosa/muscularis	Muscularis MF	Enteric neurons Smooth muscle cells	Smooth muscle contraction and Peristaltism Tissue-protective	Mouse Human	CX_3CR1, MHC-II, BPM2, β2 AR CD14, CD11b, CD209	Muller et al., 2014; Gabanyi et al., 2016; De Schepper et al., 2018 Bujko et al., 2018
	Inductive sites: Peyer's patch MFs	Subepithelial dome Upper follicle	$TIM\text{-}4^-$ LysoMac	FAE/M cells $RANKL^+$ stromal cells DCs, B and T cells	Uptake of particulate antigens Innate defense Apoptotic IEC removal	Mouse Human	MerTK, CX_3CR1, lysozyme, CD4 Lysozyme, CD11c, SIRPα	Bonnardel et al., 2015 Wagner et al., 2020
		Interfollicular regions Lower follicle	$TIM4^+$ LysoMac	T cells	Apoptotic T cell removal	Mouse Human	MerTK, CX_3CR1, CD4, TIM-4 Lysozyme, TIM-4	Bonnardel et al., 2015 Wagner et al., 2020
		Germinal center	Tingible body MF	B cells	Apoptotic B cell removal	Mouse Human	MerTK, CX_3CR1, CD4, TIM-4 Lysozyme, TIM-4	Bonnardel et al., 2015 Wagner et al., 2020
		Submucosa/muscularis externa	Serosal/muscularis MF	?	?	Mouse Human	MerTK, CX_3CR1, TIM-4 Lysozyme, TIM-4, CD163	Bonnardel et al., 2015 Wagner et al., 2020
Gut segment specialization	Antigen-inducible sampling mechanisms	SI lumen	Luminal MF	IECs	Immune exclusion by pathogen capture (*Salmonella* Typhimurium)	Mouse	CD11c, CX_3CR1, F4/80	Man et al., 2017
		Distal ileum	TED^+ LPM	IECs	Pathogenic bacteria uptake (*Salmonella* Typhimurium)	Mouse	CX_3CR1, CD11c, CD11b	Niess et al., 2005
		Peyer's patches	TMD^+ LysoDC	M cells	Pathogenic bacteria uptake (*Salmonella* Typhimurium)	Mouse	CX_3CR1, lysozyme, CD11c	Lelouard et al., 2012; Bonnardel et al., 2015; Wagner et al., 2020
		Distal colon	$BLPs^+$ LPM	IECs	Fluid sampling and fungus toxin detection IECs protection by regulating fluid absorption	Mouse	CD11c, CD11b, MHCII, F4/80, CX_3CR1, CD64	Chikina et al., 2020
	Adaptive immune responses	Distal ileum	LPM	?	Antigen-specific Th17 cells induction in response to SFB ileum colonization	Mouse	CD64, CSF1R	Panea et al., 2015
		Colon	LPM	?	Induction of Th17 cells and antibodies in response to fungus colon colonization Immune surveillance and maintenance of a balanced colonic fungal community	Mouse Human	CX_3CR1	Leonardi et al., 2018

SI, small intestine; MF, macrophages; LPM, lamina propria MF; DC, dendritic cells; IECs, intestinal epithelial cells; FAE, follicle-associated epithelium; TED, trans-epithelial dendrite; TMD, trans-M cell dendrite; BLP, balloon-like protrusion; SFB, segmented filamentous bacteria; CSF1R, colony-stimulating factor-1 receptor; β2 AR, β2 adrenergic receptor; ?, unknown.

Two main categories of MFs are present in the small and large intestines of mammals: *lamina propria* MFs (LPM) and muscularis MFs (MM) (Hume et al., 1984; Mikkelsen, 1995). LPM can be further subdivided into mucosal and submucosal LPM with different life span, transcriptional program, and functions (De Schepper et al., 2018). Mucosal LPM from the SI to the colon line the intestinal epithelium on the one hand and the vasculature on the other hand (Niess et al., 2005; Chieppa et al., 2006; Chikina et al., 2020; Honda et al., 2020). Mucosal subepithelial LPM are thus strategically positioned to sample luminal antigens and to protect the mucosa from enteropathogens that can penetrate the epithelial barrier. In the mouse SI, the pathogenic bacteria *Salmonella* Typhimurium induce the formation of paracellular transepithelial dendrites by subepithelial LPM, allowing them to capture bacteria directly from the lumen (Niess et al., 2005; Chieppa et al., 2006). In accordance with their bacteria-inducible nature, LPM transepithelial dendrites occur more frequently where bacteria are abundant, i.e., at the tip of villi of the terminal ileum rather than in other parts of the SI (Niess et al., 2005; Chieppa et al., 2006). Whether LPM transepithelial dendrites represent an important mechanism of antigen sampling that could occur in absence of pathogenic bacteria remains under debate (McDole et al., 2012). *Salmonella* Typhimurium induce also the migration of mouse subepithelial LPM into the gut lumen to participate in the immune exclusion of the bacteria from the gut (Arques et al., 2009; Man et al., 2017). Importantly, both transepithelial dendrites and luminal migration are dependent on CX_3CR1 expression by subepithelial LPM and on MyD88-dependent TLR signaling by intestinal epithelial cells (Chieppa et al., 2006; Arques et al., 2009; Man et al., 2017). Whether these partial (dendrites) or complete (luminal migration) transepithelial passages occur in human has yet to be established, especially since CX_3CR1 expression by human intestinal LPM is reduced as compared with that in mice (Bujko et al., 2018). Nevertheless, a missense mutation in the *CX3CR1* gene has been identified in Crohn's disease patients and was linked to an inefficient antifungal response (Leonardi et al., 2018). This suggests that CX_3CR1 is at least important in human for the control of the fungi gut community. Unlike conventional DC, mucosal LPM are unable to migrate into the gut-draining MLNs to present pathogen-derived antigens and prime naïve T cells (Schulz et al., 2009; Bravo-Blas et al., 2019). Nevertheless, they can transfer antigens via gap junctions to neighboring conventional DC that can in turn express CCR7, migrate to the MLNs, and prime naïve T cells (Mazzini et al., 2014). Mucosal conventional DC can also acquire soluble and particulate antigens directly from the lumen through several mechanisms (McDole et al., 2012; Farache et al., 2013), raising the question of the real contribution of MFs to the provision of antigens for antigenic presentation.

Another subpopulation of CX_3CR1^+ mucosal and also submucosal LPM is closely associated to the intestinal vasculature in mice (De Schepper et al., 2018; Honda et al., 2020). Perivascular LPM are either self-maintaining throughout adulthood, especially submucosal ones, or replaced by monocytes on a regular basis, especially mucosal ones (De Schepper et al., 2018). The full maturation of the latter from $Ly6^{hi}$ monocytes is ensured by the microbiota and by the transcription factor NR4A1, a master regulator of the conversion of $CCR2^{hi}CX_3CR1^{int}Ly6C^{hi}$ into $CCR2^{lo}CX_3CR1^{hi}Ly6C^{lo}$ monocytes (Honda et al., 2020). Mucosal perivascular LPM form tight interdigitating connections around all of the vasculature of both SI and colon by which they prevent bacteria translocation into the blood circulation (Honda et al., 2020). Therefore, both subepithelial and perivascular mucosal LPM are fully equipped to prevent penetration of pathogens through epithelial and vascular barriers, offering thus a double defensive line. By contrast, submucosal perivascular LPM are distant from the lumen, the microbiota, and potential pathogens. They acquire a transcriptional profile in relation to their niche, including angiogenesis-related genes, and are necessary for the repair and strengthening of the vasculature since lack of perivascular LPM disturbs the vasculature morphology and induces particle leakage from the blood (De Schepper et al., 2018).

At the base of SI and colonic crypts, a specific subset of submucosal LPM expressing CD169 is tightly associated with the epithelial stem cell niche (Pull et al., 2005; Hiemstra et al., 2014; Asano et al., 2015; Sehgal et al., 2018) (**Table 2**). In the SI, depletion of these stem cell niche-associated LPM following CSF1R blockade induces a defect in Paneth cell differentiation and a reduction in $LGR5^+$ intestinal stem cell numbers (Sehgal et al., 2018). This leads to reduced epithelial proliferation and imbalanced intestinal epithelial cell ratio, notably favoring goblet cells. Therefore, stem cell niche-associated LPM are crucial in the appropriate differentiation of SI epithelial cells. Surprisingly, in the colon, *Csf1*-deficient *op/op* mice with strong LPM depletion show normal colonic crypt morphology, suggesting that unlike SI, colon stem cell niche-associated LPM are not essential to maintain the colonic stem cell niche (Cecchini et al., 1994). Nevertheless, during injury, the colonic stem cell niche-associated LPM are essential to promote the regenerative response, i.e., the proliferation and the survival of colonic epithelial progenitors (Pull et al., 2005). Similarly, in fruit fly, plasmatocytes induce stem cell proliferation in the intestine in response to wounding via their secretion of Upd2 and Upd3 (Chakrabarti et al., 2016). Therefore, as for mouse stem cell niche-associated LPM, fruit fly plasmatocytes can be tightly associated with the intestinal epithelium and can play a major role in tissue repair, highlighting a highly conserved mechanism of cooperation between phagocytes and gut epithelial stem cells.

In mammals, MM display either bipolar (circular muscle and deep muscular plexus MM) or stellate (serosal and myenteric MM) shapes and are closely associated with smooth muscles and enteric neurons of the muscularis externa, distant from any luminal stimulation (Mikkelsen, 1995; Phillips and Powley, 2012). Accordingly, MM display a gene expression profile associated with tissue protection and neuronal development (Gabanyi et al., 2016; De Schepper et al., 2018). MM play a major role in regulating intestinal peristalsis by producing BMP2 and PGE2, which act on enteric neurons and smooth muscles, respectively (Muller et al., 2014; Luo et al., 2018). In addition, MM play a neuroprotective role by limiting infection-induced neuronal loss through an adrenergic/arginase 1/polyamines axis (Matheis et al., 2020). The development of MM is ensured

by CSF1 produced by their associated enteric neurons (Muller et al., 2014). However, other cells (e.g., endothelial cells or interstitial cells of Cajal) can replace enteric neurons since MM are not impacted in mice lacking enteric neurons, as well as in humans in whom the enteric nervous system is absent from the colon (Hirschsprung disease) (Avetisyan et al., 2018). Neuron-associated MFs are also present in the submucosal LP, where they could play a role in the regulation of the intestinal secretion induced by neurons (De Schepper et al., 2018).

From the SI to the colon, from rodents to humans, most mucosal LPM are continuously renewed by blood monocytes (Tamoutounour et al., 2012; Bain et al., 2013, 2014; Bujko et al., 2018). In mice, LPM differentiation from Ly6C^{hi} monocytes is phenotypically characterized by four developmental stages termed monocyte waterfall (Tamoutounour et al., 2012; Bain et al., 2013). Nonetheless, a large part of MM and of the submucosal LPM, especially those associated with neurons and vasculature, appears to be long-lived self-maintained cells and are barely replaced by circulating monocytes (De Schepper et al., 2018; Shaw et al., 2018). These MFs are indeed distant from the gut lumen and thus from microbiota and dietary antigens, the well-known drivers of intestinal MF replacement by circulating monocytes (Bain et al., 2014; Ochi et al., 2016). This may explain their self-maintaining property, which is very similar to that of MFs residing in other tissues (Hashimoto et al., 2013; Yona et al., 2013; Liu et al., 2019). In humans, a recent study went through the characterization of MFs within the upper part of the SI (Bujko et al., 2018). They encompass four well-defined subsets based on marker expression, transcriptional profiles, maturation stage, life span, and location. LPM and MM represent two of these subsets, whereas the other two are related to the monocyte to MF conversion.

(RE)CATEGORIZATION OF INTESTINAL MACROPHAGES BY THEIR GUT SEGMENT LOCATION: INFLUENCE OF DIETARY ANTIGENS AND OF MICROBIOTA

Local compartmentalization of intestinal MFs is broadly similar between the SI and the colon. However, MF numbers are generally higher in the colon than in the SI. Moreover, despite similar differentiation programs and markers, MFs of the SI and of the colon are clearly distinct. Thus, monocytes infiltrating the gut acquire intestinal segment-specific gene expression profiles (Gross-Vered et al., 2020). Their differences are mainly due to the specific functions of each segment of the GIT and to the different exogenous antigens they are exposed to. Thus, ileal MFs display higher expression of genes related to immune reaction and response to challenge than colonic MFs (Gross-Vered et al., 2020). In the following part, we will describe how phenotypically similar MFs can act differently according to their gut segment location.

As mentioned above, the main function of the SI is to absorb nutrients, and its large surface area is continually exposed to important amounts of dietary-derived products. Microbiota density increases drastically from the duodenum to the colon according to gut physico-chemical environment variations (e.g., oxygen and pH levels). Therefore, the colon faces a huge amount of diverse microorganisms (commensal bacteria, archaea, virus, and fungi) and their derived metabolites. The number of goblet cells also increases significantly from the SI to the colon. Consistent with this increased goblet cell frequency, the mammalian colon is protected by thicker and more organized mucus layers than the SI, keeping microorganisms at bay from the epithelium (Johansson et al., 2008; Bergstrom et al., 2020).

Whereas in the colon the microbiota promotes LPM renewal by circulating monocytes and contributes to their functional diversification (Bain et al., 2014; Kang et al., 2020), in the SI, intestinal microbiota is a major factor neither for the control of MF replenishment nor for their IL-10 production (Ochi et al., 2016). Consistently, there is no difference in the number of SI LPM populations between antibiotic-treated and untreated mice. However, dietary factors can directly regulate homeostasis of SI LPM, and a total deficiency in dietary amino acids or the inhibition of the mTOR-mediated amino acid sensing leads to a reduction of IL-10-producing MF number (Ochi et al., 2016). Actually, many other molecules resulting from the degradation of the food, such as vitamins and aryl hydrocarbon receptor (AHR) ligands, are susceptible either directly or indirectly to influence intestinal MF functions in the SI (Mowat and Agace, 2014).

Drosophila melanogaster is a good model to study the impact in the gut of imbalanced diets, such as the high-fat and Western diets, or of potential toxic products, such as fried food-derivatives. In the fruit fly, lipid peroxidation products of fried food induce an increase of ROS production and DNA damages in plasmatocytes (Demir and Marcos, 2017). A similar study was recently performed in mouse and confirmed that dietary peroxidized fats induce proinflammatory responses by peritoneal MFs and resident immune cells in PPs (Keewan et al., 2020). With regard to high-fat diet, Woodcock *et al.* showed that lipid-rich diets reduce the life span of *D. melanogaster* and impair its glucose metabolism (Woodcock et al., 2015). This is due to the activation of the JAK-STAT pathway in response to the Upd3 secreted by the plasmatocytes that become foamy, accumulating neutral triglycerides and other lipids in lipid vacuoles. In mouse, Kawano et al. highlighted that high-fat diet induces CCL2 expression by colonic IEC leading to CCR2-dependent proinflammatory MF infiltration in the colon, which results in inflammasome activation in these newly recruited MF, increased intestinal permeability, and glucose metabolism and insulin resistance impairment (Kawano et al., 2016). The western diet includes a high intake of proteins (mainly from animal-derived sources), saturated fatty acids (SFAs), sugar, processed food, and salt, together with a reduced consumption of vegetables, fruits, vitamins, minerals, and ω-3 polyunsaturated fatty acids (PUFAs). SFAs activate proinflammatory response in MFs through the TLR4-NF-κB pathway (Lee et al., 2003). By contrast, specialized proresolving mediators (SPMs) are a large class of signaling molecules that counteract the effect of proinflammatory dietary antigens on intestinal MFs. SPMs are derived from the metabolism of ω-3 PUFA supplied in the diet, giving rise to protectins, resolvins, and maresins. Alternatively, they are produced as eicosanoids (prostaglandin

D2 and E2 and lipoxin A4) by immune (including MFs) and non-immune cells (Na et al., 2019). SPMs influence MF differentiation toward a proresolving phenotype. Proresolving MFs dampen Th1 and Th17 responses, re-establish breached epithelial barrier, limit entry of neutrophils to the site of injury, and promote monocyte migration (Na et al., 2019). Thus, protectins and resolving D1 promote resolution of inflammation by increasing MF phagocytosis and suppressing inflammatory MFs in inflammatory diseases (Buckley et al., 2014). In summary, diet is a key element to take into account when studying variations in LPM functions. However, it is important to keep in mind that most of the research studying the interplay between the dietary antigens and the intestinal MFs have been performed *in vitro*. Therefore, more *in vivo* studies will be required to fully address the impact of diet on the different populations of intestinal MFs.

The main function of the colon is to absorb electrolytes and water and also to manage undigested foodstuffs. Through saccharolytic and proteolytic fermentations, the colon microbiota is involved in the catabolism of remaining indigestible food and produces a variety of metabolites in the colon including short-chain fatty acids (SCFAs), which are involved in colonic LPM conditioning. Thus, antibiotic treatments cause colonic LPM to express increased levels of proinflammatory cytokines following microbiota recolonization and to become responsive to LPS stimulation (Scott et al., 2018). Interestingly, supplementation of antibiotics with the SCFA butyrate, whose production is reduced under antibiotic treatment, restores the anti-inflammatory profile and hypo-responsiveness of colonic MFs (Scott et al., 2018). Administration of butyrate also promotes colonic LPM antimicrobial activities, such as lysozyme, calprotectin, and ROS production (Schulthess et al., 2019). Anti-inflammatory and anti-microbial effects of butyrate are mediated via inhibition of histone deacetylase 3, thus regulating MF transcriptional and metabolic program (Chang et al., 2014; Schulthess et al., 2019). More generally, microbiota contributes to the functional diversification of colon MFs (Kang et al., 2020). It supports in particular colonic LPM production of IL-10 and limits Th1 cell response while promoting Treg cell expansion (Kim et al., 2018).

Colonic LPM conditioning depends not only on microbiota but also on TGFβ and, above all, IL-10 signaling (Schridde et al., 2017; Biswas et al., 2018). Indeed, IL-10 signaling pathway promotes WASP and DOCK8 interaction leading to STAT3 phosphorylation and anti-inflammatory MF polarization (Biswas et al., 2018). By contrast, lack of IL-10 signaling induces a proinflammatory profile on colonic MFs highlighted by IL-23 and IL-1β production, leading to recruitment of Th17 cells and promoting colitis (Shouval et al., 2016; Bernshtein et al., 2019). Loss of IL-10 receptor signaling in mouse and human MFs indeed induces spontaneous colitis and severe infant-onset IBD, respectively (Shouval et al., 2014; Zigmond et al., 2014). Surprisingly, though more inflammatory, these MFs show defect in *Salmonella* Typhimurium killing due to prostaglandin E2 overproduction (Mukhopadhyay et al., 2020).

Depending on the location of encountered microorganisms, CX_3CR1^+ LPM induce regionalized antigen-specific Th17 responses (**Table 2**). Thus, CX_3CR1^+ LPM are involved in the induction in the SI of a specific and robust Th17 response against segmented filamentous bacteria (SFB) that colonize specifically the ileum (Panea et al., 2015). Unlike pathogen-elicited Th17 cells that are highly glycolytic inflammatory effector cells producing IFNγ, SFB-induced Th17 cells are non-inflammatory homeostatic tissue resident cells (Omenetti et al., 2019). By contrast, colonization with the fungus *Candida albicans* induces a strong Th17 response in the colon where it resides but not in the SI (Leonardi et al., 2018). Actually, colonic LPM are fully equipped to efficiently recognize and respond to the important fungal communities (mycobiota) found in the distal colon, notably via the C-type lectin receptors dectin-1, dectin-2, and mincle (Iliev et al., 2012; Leonardi et al., 2018). Dectin-1 promotes a proinflammatory program in colonic MFs, resulting in inflammasome-dependent IL-1β secretion and inflammatory monocyte recruitment to the inflamed colon (Rahabi et al., 2020). In contrast, Treg cells regulate the inflammatory properties of colonic MFs by inhibiting their IL-1β and IL-23 production (Bauché et al., 2018). This inhibition involves MHC class II engagement by latent activation gene-3 (LAG-3) expressed on Treg cells. Interestingly, the way by which LPM from the distal colon sense their microenvironment is completely different from that performed by SI and proximal colon LPM (**Table 2**). Indeed, distal colon LPM form balloon-like protrusions that insert between colonic epithelial cells but do not extend into the lumen like in the SI (Chikina et al., 2020). They remain instead confined in the intercellular space of the epithelium. These balloon-like protrusions, which are induced by the presence of fungi in the lumen, sample the fluids absorbed by epithelial cells to detect toxins among fungi metabolites. By instructing them to stop absorption, MFs with balloon-like protrusions protect colonic epithelial cells from dying of absorbing too much fungal toxins (Chikina et al., 2020).

SPECIFICITY OF INTESTINAL IMMUNE INDUCTIVE SITE MACROPHAGES

As mentioned above, the gastrointestinal mucosa of vertebrates has specialized sites dedicated to the detection of pathogens in contaminated food and water. Indeed, in reptiles, amphibians, and lungfishes, the gut contains lymphoid aggregates resembling the ILFs found in mammals (Borysenko and Cooper, 1972; Zapata and Solas, 1979; Solas and Zapata, 1980; Tacchi et al., 2015; Ashford et al., 2019). Like mammal ILFs, the number and size of these aggregates increase with microbial challenges (Tacchi et al., 2015; Ashford et al., 2019). Based on recent observations made on lungfish, it seems however that these lymphoid aggregates lack a well-structured organization, showing no segregation between B and T cells, no germinal center, no AID expression, and no somatic hypermutation (Tacchi et al., 2015). The cellular composition of these primitive aggregates is otherwise poorly described; and MFs, although observed by electron microscopy (Ardavín et al., 1982), have not been well-characterized.

In addition to ILFs, mammals and also birds have PPs that are distributed along the SI, especially in the last part of the

ileum (Jung et al., 2010). PPs consist of clustered B cell follicles forming domes on the surface of the mucosa. These domes are separated from each other by dome-associated villi (DAV) over interfollicular regions (IFRs) enriched in T cells. A specialized follicle-associated epithelium (FAE) separates the subepithelial dome (SED) above the follicle from the gut lumen. This FAE provides a permissive environment for pathogen entry. Indeed, it secretes no or few IgA and antimicrobial proteins and is covered by a reduced mucus layer. This is due to lack of polymeric Ig receptor expression, inhibition of IL-22 signaling, and diminished number of goblet cells (Bhalla and Owen, 1982; Pappo and Owen, 1988; Jinnohara et al., 2017). Moreover, the glycocalyx is attenuated over the FAE favoring interaction of luminal antigens with the mucosal surface (Frey et al., 1996; Mantis et al., 2000). Finally, the specialized FAE cell termed M cell efficiently binds and transports all kind of antigens from the lumen to the SED (Ohno, 2016; Kobayashi et al., 2019). Therefore, PP MFs are continually exposed to much more threatening elements than other intestinal MFs. They are accordingly equipped with a whole arsenal against pathogens and prone to promote an inflammatory response (Bonnardel et al., 2015; Wagner et al., 2018). Until now, these MFs have been mainly characterized in mice and to a much lesser extent in humans (**Table 2**). At the exception of DAV MFs that closely resemble LPM of standard villi, other PP MFs are profoundly different from all other MF populations (Wagner et al., 2018). This is exemplified by their lack of F4/80 and CD64 expression in mice and of CD163 in humans (Bonnardel et al., 2015; Wagner et al., 2018, 2020). Nevertheless, they share with most, if not all, mouse MFs the expression of the apoptotic receptor MerTK and high levels of the chemokine receptor CX_3CR1, both markers enabling their distinction from conventional DC (Bonnardel et al., 2015, 2017; Wagner et al., 2020). In relation to their important role in innate defense, PP MFs express very large amounts of the antibacterial protein lysozyme, which was the first reliable marker to identify monocyte-derived cells in PPs of mice, rats, and humans (Lelouard et al., 2010). This has given rise to their LysoMac nickname for lysozyme-expressing MFs (Bonnardel et al., 2015). Interestingly, monocytes give also rise in PPs to the unique lysozyme-expressing DC termed LysoDC. LysoDC have a transcriptional program close but not identical to that of PP MFs as they display additional functions, notably in terms of antigen presentation (Bonnardel et al., 2015; Martinez-Lopez et al., 2019; Wagner et al., 2020). Like conventional DC, mature LysoDC are indeed able to prime naïve T cells at least *in vitro* for IFNγ and IL-17 production (Bonnardel et al., 2015; Martinez-Lopez et al., 2019). This ability is strengthened by stimulation with a TLR7 ligand. In addition, TLR7 stimulation induces expression of CCR7 by subepithelial LysoDC and promotes their migration to the periphery of the IFR where they encounter naïve T cells and where they interact tightly with newly activated proliferative T cells (Wagner et al., 2020). At steady state, very few if any LysoDC are in the IFR, and only few of them are located in the follicle, with most of them being in the SED where they excel in antigen capture. Conversely, MFs have been observed in all regions of PPs (Bonnardel et al., 2015). In addition to LysoMac, mainly located in the SED, the follicle, and the IFR, there are indeed muscularis and serosal MFs, and germinal center tingible body MFs (TBM). Interestingly, these different anatomic locations are tightly linked to phenotypic distinctions between PP MFs (**Table 2**). Thus, muscularis and serosal MFs below the IFR express CD169, whereas other PP MFs do not. As well, TBM and interfollicular and lower follicular LysoMac express the phosphatidylserine receptor TIM-4, whereas subepithelial and upper follicular LysoMac do not. This suggests that an important regional specialization of MF functions exists inside the PPs itself (Wagner et al., 2018). Thus, TIM-4 mainly expressed by MFs in the regions of T cell priming and B cell selection belongs to the family of apoptotic cell receptors and is known to be involved in the regulation of the adaptive immune response and prevention of autoimmunity through removal of both B and T cells (Albacker et al., 2010, 2013; Rodriguez-Manzanet et al., 2010). Therefore, TIM-4^+ MFs could protect PPs from an exaggerated inflammatory reaction by regulating both T and B cell numbers.

As mentioned above, TIM-4^- LysoMac as well as LysoDC are close to the FAE, and they play key role in the uptake of particulate antigens and pathogenic bacteria (Lelouard et al., 2010, 2012; Disson et al., 2018). The mechanisms by which LysoDC and TIM-4^- LysoMac sample luminal antigens are different from either SI or colonic LPM. Indeed, phagocytosis of antigens by LysoDC and TIM-4^- LysoMac either follows M cell transcytosis or occurs through LysoDC dendrite extension into the lumen through M cell-specific transcellular pores (Lelouard et al., 2012; Bonnardel et al., 2015). Therefore, M cells tightly control both mechanisms. Accordingly, absence of M cells is associated with a strong downregulation of antigen uptake in PPs and of IgA production in villi (Rios et al., 2016). Unlike villus paracellular transepithelial dendrites, these LysoDC trans-M cell dendrites do not depend on CX_3CR1 expression (Bonnardel et al., 2015). LysoDC and TIM-4^- LysoMac also influence FAE properties to favor contact with exogenous antigens. Thus, they express *Il22ra2*, which encodes IL-22BP, an inhibitor of Il-22 (Da Silva et al., 2017). IL-22BP promotes microbial sampling by influencing the FAE transcriptional program, notably by inhibiting genes encoding antimicrobial proteins and also genes involved in surface glycosylation and mucus production (Jinnohara et al., 2017). PP MFs are also likely involved in M cell differentiation as long-term blockade of CSF1R, which is known to deplete MFs, impairs M cell differentiation (Sehgal et al., 2018). Finally, together with other immune cells, they could be involved in M cell maturation via the expression of the S100 family member S100a4 (Kunimura et al., 2019).

More globally, in relation to the fact that PPs are a permissive entry site for a large number of pathogens, PP MFs display a strong antiviral and antibacterial transcriptional program (Bonnardel et al., 2015). Moreover, PP MFs lack the typical anti-inflammatory properties of other intestinal MFs (Wagner et al., 2018). Thus, they do not produce IL-10 or express its receptor but instead secrete TNF and IL-6 upon stimulation (Bonnardel et al., 2015; Wagner et al., 2018). Therefore, unlike most intestinal MFs, they retain a strong ability to promote inflammation.

CONCLUSIONS AND PERSPECTIVES

There has been incredible progress in recent years in the appreciation of intestinal MF heterogeneity (**Table 2**). This obviously raises great hope for targeted therapies that would render possible to alter a defective population without disturbing the others or to promote one population over the others and thus restore homeostasis. However, much more work is needed to understand the signaling between MFs and their direct neighbors and how this can be used to remodel MF properties. As suggested by Guilliams et al. (2020), manipulation of the neighboring cells that imprint the MF with its functional properties instead of the MF itself could represent alternative and interesting strategies for deciphering the mechanisms that dictate the fate of intestinal MFs on the one hand and modifying key instructing factors according to pathologies on the other hand. Nutritional- and microbial-based intervention strategies to modulate intestinal MF properties have also become a promising therapeutic approach to treat and prevent intestinal diseases. A great challenge for all these approaches will be to deal with the complexity of the structure and diversity of potentially simultaneous signals (food, microbiota, pathogen, stromal, and immune cell-derived factors) that make the intestine such a special and diversified organ.

AUTHOR CONTRIBUTIONS

CAP, JT, and HL: writing—original draft. CAP, JT, HL, and J-PG: writing—revision. CAP: figure design. HL and J-PG: funding acquisition. All authors contributed to the article and approved the submitted version.

FUNDING

This work was supported by institutional funding from Center National de la Recherche Scientifique and Institut National de la Santé et de la Recherche Médicale, and by the Fondation pour la Recherche Médicale (FRM), Grant No. DEQ20170336745. CAP was supported by the University of Costa Rica.

ACKNOWLEDGMENTS

We thank Camille Wagner for her help in figure drawing.

REFERENCES

Abnave, P., Mottola, G., Gimenez, G., Boucherit, N., Trouplin, V., Torre, C., et al. (2014). Screening in planarians identifies MORN2 as a key component in LC3-associated phagocytosis and resistance to bacterial infection. *Cell Host Microbe* 16, 338–350. doi: 10.1016/j.chom.2014.08.002

Adamska, M. (2016). Sponges as models to study emergence of complex animals. *Curr. Opin. Genet. Dev* 39, 21–28. doi: 10.1016/j.gde.2016.05.026

Albacker, L. A., Karisola, P., Chang, Y. J., Umetsu, S. E., Zhou, M., Akbari, O., et al. (2010). TIM-4, a receptor for phosphatidylserine, controls adaptive immunity by regulating the removal of antigen-specific T cells. *J. Immunol.* 185, 6839–6849. doi: 10.4049/jimmunol.1001360

Albacker, L. A., Yu, S., Bedoret, D., Lee, W. L., Umetsu, S. E., Monahan, S., et al. (2013). TIM-4, expressed by medullary macrophages, regulates respiratory tolerance by mediating phagocytosis of antigen-specific T cells. *Mucosal Immunol.* 6, 580–590. doi: 10.1038/mi.2012.100

Annunziata, R., Andrikou, C., Perillo, M., Cuomo, C., and Arnone, M. I. (2019). Development and evolution of gut structures: from molecules to function. *Cell Tissue Res.* 377, 445–458. doi: 10.1007/s00441-019-03093-9

Ardavín, C. F., Zapata, A., Garrido, E., and Villena, A. (1982). Ultrastructure of gut-associated lymphoid tissue (GALT) in the amphibian urodele, Pleurodeles waltlii. *Cell Tissue Res.* 224, 663–671. doi: 10.1007/BF00213761

Arques, J. L., Hautefort, I., Ivory, K., Bertelli, E., Regoli, M., Clare, S., et al. (2009). Salmonella induces flagellin- and MyD88-dependent migration of bacteria-capturing dendritic cells into the gut lumen. *Gastroenterology* 137, 579–587, 87 e1–2. doi: 10.1053/j.gastro.2009.04.010

Asano, K., Takahashi, N., Ushiki, M., Monya, M., Aihara, F., Kuboki, E., et al. (2015). Intestinal CD169(+) macrophages initiate mucosal inflammation by secreting CCL8 that recruits inflammatory monocytes. *Nat. Commun.* 6:7802. doi: 10.1038/ncomms8802

Ashford, M. A., Palackdharry, S. M., Sadd, B. M., Bowden, R. M., and Vogel, L. A. (2019). Intestinal B cells in the red-eared slider turtle, *Trachemys scripta*: anatomical distribution and implications for ecological interactions with pathogenic microbes. *J. Exp. Zool.* 331, 407–415. doi: 10.1002/jez.2307

Avetisyan, M., Rood, J. E., Huerta Lopez, S., Sengupta, R., Wright-Jin, E., Dougherty, J. D., et al. (2018). Muscularis macrophage development in the absence of an enteric nervous system. *Proc. Natl. Acad. Sci. U.S.A.* 115, 4696–4701. doi: 10.1073/pnas.1802490115

Ayyaz, A., Li, H., and Jasper, H. (2015). Haemocytes control stem cell activity in the Drosophila intestine. *Nat. Cell Biol.* 17, 736–748. doi: 10.1038/ncb3174

Bain, C. C., Bravo-Blas, A., Scott, C. L., Gomez Perdiguero, E., Geissmann, F., Henri, S., et al. (2014). Constant replenishment from circulating monocytes maintains the macrophage pool in the intestine of adult mice. *Nat. Immunol.* 15, 929–937. doi: 10.1038/ni.2967

Bain, C. C., Scott, C. L., Uronen-Hansson, H., Gudjonsson, S., Jansson, O., Grip, O., et al. (2013). Resident and pro-inflammatory macrophages in the colon represent alternative context-dependent fates of the same Ly6Chi monocyte precursors. *Mucosal Immunol.* 6, 498–510. doi: 10.1038/mi.2012.89

Banchereau, J., and Steinman, R. M. (1998). Dendritic cells and the control of immunity. *Nature* 392, 245–252. doi: 10.1038/32588

Banerjee, U., Girard, J. R., Goins, L. M., and Spratford, C. M. (2019). Drosophila as a genetic model for hematopoiesis. *Genetics* 211, 367–417. doi: 10.1534/genetics.118.300223

Bauché, D., Joyce-Shaikh, B., Jain, R., Grein, J., Ku, K. S., Blumenschein, W. M., et al. (2018). LAG3(+) Regulatory T cells restrain interleukin-23-producing CX3CR1(+) gut-resident macrophages during group 3 innate lymphoid cell-driven colitis. *Immunity* 49, 342–352.e5. doi: 10.1016/j.immuni.2018.07.007

Baumann, O., Arlt, K., Römmling, K., Goller, H., and Walz, B. (2000). Characterization of an extremely motile cellular network in the rotifer Asplanchna spp. Structure, kinetics, and the cytoskeleton. *Cell Tissue Res.* 299, 159–172. doi: 10.1007/s004410050014

Bergstrom, K., Shan, X., Casero, D., Batushansky, A., Lagishetty, V., Jacobs, J. P., et al. (2020). Proximal colon-derived O-glycosylated mucus encapsulates and modulates the microbiota. *Science* 370, 467–472. doi: 10.1126/science.aay7367

Bernshtein, B., Curato, C., Ioannou, M., Thaiss, C. A., Gross-Vered, M., Kolesnikov, M., et al. (2019). IL-23-producing IL-10Rα-deficient gut macrophages elicit an IL-22-driven proinflammatory epithelial cell response. *Sci. Immunol* 4:eaau6571. doi: 10.1126/sciimmunol.aau6571

Beshel, J., Dubnau, J., and Zhong, Y. (2017). A leptin analog locally produced in the brain acts via a conserved neural circuit to modulate obesity-linked behaviors in drosophila. *Cell Metab.* 25, 208–217. doi: 10.1016/j.cmet.2016.12.013

Bhalla, D. K., and Owen, R. L. (1982). Cell renewal and migration in lymphoid follicles of Peyer's patches and cecum–an autoradiographic study in mice. *Gastroenterology* 82, 232–242. doi: 10.1016/0016-5085(82)90010-5

Birgisdottir, Å. B., and Johansen, T. (2020). Autophagy and endocytosis - interconnections and interdependencies. *J. Cell Sci.* 133:jcs228114. doi: 10.1242/jcs.228114

Biswas, A., Shouval, D. S., Griffith, A., Goettel, J. A., Field, M., Kang, Y. H., et al. (2018). WASP-mediated regulation of anti-inflammatory macrophages is IL-10 dependent and is critical for intestinal homeostasis. *Nat. Commun.* 9:1779. doi: 10.1038/s41467-018-03670-6

Blériot, C., Chakarov, S., and Ginhoux, F. (2020). Determinants of resident tissue macrophage identity and function. *Immunity* 52, 957–970. doi: 10.1016/j.immuni.2020.05.014

Bodó, K., Ernszt, D., Németh, P., and Engelmann, P. (2018). Distinct immune- and defense-related molecular fingerprints in sepatated coelomocyte subsets of *Eisenia andrei* earthworms. *Invertebrate Survival J.* 15, 338–345. doi: 10.25431/1824-307X/isj.v15i1.338-345

Bolla, R. I., Weinstein, P. P., and Cain, G. D. (1972). Fine structure of the coelomocyte of adult *Ascaris suum*. *J. Parasitol.* 58, 1025–1036. doi: 10.2307/3278127

Bonnardel, J., Da Silva, C., Henri, S., Tamoutounour, S., Chasson, L., Montanana-Sanchis, F., et al. (2015). Innate and adaptive immune functions of peyer's patch monocyte-derived cells. *Cell Rep.* 11, 770–784. doi: 10.1016/j.celrep.2015.03.067

Bonnardel, J., Da Silva, C., Wagner, C., Bonifay, R., Chasson, L., Masse, M., et al. (2017). Distribution, location, and transcriptional profile of Peyer's patch conventional DC subsets at steady state and under TLR7 ligand stimulation. *Mucosal Immunol.* 10, 1412–1430. doi: 10.1038/mi.2017.30

Borysenko, M., and Cooper, E. L. (1972). Lymphoid tissue in the snapping turtle, *Chelydra serpentina*. *J. Morphol.* 138, 487–497. doi: 10.1002/jmor.1051380408

Bravo-Blas, A., Utriainen, L., Clay, S. L., Kästele, V., Cerovic, V., Cunningham, A. F., et al. (2019). Salmonella enterica Serovar typhimurium travels to mesenteric lymph nodes both with host cells and autonomously. *J. Immunol.* 202, 260–267. doi: 10.4049/jimmunol.1701254

Brennan, J. J., and Gilmore, T. D. (2018). Evolutionary origins of toll-like receptor signaling. *Mol. Biol. Evol.* 35, 1576–1587. doi: 10.1093/molbev/msy050

Broderick, N. A. (2015). A common origin for immunity and digestion. *Front. Immunol.* 6:72. doi: 10.3389/fimmu.2015.00072

Broom, L. J., and Kogut, M. H. (2018). The role of the gut microbiome in shaping the immune system of chickens. *Vet. Immunol. Immunopathol.* 204, 44–51. doi: 10.1016/j.vetimm.2018.10.002

Buchmann, K. (2014). Evolution of innate immunity: clues from invertebrates via fish to mammals. *Front. Immunol.* 5:459. doi: 10.3389/fimmu.2014.00459

Buckley, C. D., Gilroy, D. W., and Serhan, C. N. (2014). Proresolving lipid mediators and mechanisms in the resolution of acute inflammation. *Immunity* 40, 315–327. doi: 10.1016/j.immuni.2014.02.009

Buckley, K. M., Ho, E. C. H., Hibino, T., Schrankel, C. S., Schuh, N. W., Wang, G., et al. (2017). IL17 factors are early regulators in the gut epithelium during inflammatory response to Vibrio in the sea urchin larva. *Elife* 6:e23481. doi: 10.7554/eLife.23481.025

Buckley, K. M., and Rast, J. P. (2019). Immune activity at the gut epithelium in the larval sea urchin. *Cell Tissue Res.* 377, 469–474. doi: 10.1007/s00441-019-03095-7

Buis, A., Bellemin, S., Goudeau, J., Monnier, L., Loiseau, N., Guillou, H., et al. (2019). Coelomocytes regulate starvation-induced fat catabolism and lifespan extension through the lipase LIPL-5 in *Caenorhabditis elegans*. *Cell Rep.* 28, 1041–1049.e4. doi: 10.1016/j.celrep.2019.06.064

Bujko, A., Atlasy, N., Landsverk, O. J. B., Richter, L., Yaqub, S., Horneland, R., et al. (2018). Transcriptional and functional profiling defines human small intestinal macrophage subsets. *J. Exp. Med.* 215, 441–458. doi: 10.1084/jem.20170057

Casteleyn, C., Doom, M., Lambrechts, E., Van den Broeck, W., Simoens, P., and Cornillie, P. (2010). Locations of gut-associated lymphoid tissue in the 3-month-old chicken: a review. *Avian Pathol.* 39, 143–150. doi: 10.1080/03079451003786105

Cattenoz, P. B., Sakr, R., Pavlidaki, A., Delaporte, C., Riba, A., Molina, N., et al. (2020). Temporal specificity and heterogeneity of Drosophila immune cells. *EMBO J.* 39:e104486. doi: 10.15252/embj.2020104486

Cecchini, M. G., Dominguez, M. G., Mocci, S., Wetterwald, A., Felix, R., Fleisch, H., et al. (1994). Role of colony stimulating factor-1 in the establishment and regulation of tissue macrophages during postnatal development of the mouse. *Development* 120, 1357–1372.

Chakrabarti, S., Dudzic, J. P., Li, X., Collas, E. J., Boquete, J. P., and Lemaitre, B. (2016). Remote control of intestinal stem cell activity by haemocytes in drosophila. *PLoS Genet.* 12:e1006089. doi: 10.1371/journal.pgen.1006089

Chang, P. V., Hao, L., Offermanns, S., and Medzhitov, R. (2014). The microbial metabolite butyrate regulates intestinal macrophage function via histone deacetylase inhibition. *Proc. Natl. Acad. Sci. U.S.A.* 111, 2247–2252. doi: 10.1073/pnas.1322269111

Charroux, B., and Royet, J. (2009). Elimination of plasmatocytes by targeted apoptosis reveals their role in multiple aspects of the Drosophila immune response. *Proc. Natl. Acad. Sci. U.S.A.* 106, 9797–9802. doi: 10.1073/pnas.0903971106

Chieppa, M., Rescigno, M., Huang, A. Y., and Germain, R. N. (2006). Dynamic imaging of dendritic cell extension into the small bowel lumen in response to epithelial cell TLR engagement. *J. Exp. Med.* 203, 2841–2852. doi: 10.1084/jem.20061884

Chikina, A. S., Nadalin, F., Maurin, M., San-Roman, M., Thomas-Bonafos, T., Li, X. V., et al. (2020). Macrophages maintain epithelium integrity by limiting fungal product absorption. *Cell* 183, 411–428.e16. doi: 10.1016/j.cell.2020.08.048

Chin, K. N., and Wong, W. C. (1977). Some ultrastructural observations on the intestinal mucosa of the toad (Bufo melanostictus). *J. Anatomy* 123, 331–339.

Cho, B., Yoon, S. H., Lee, D., Koranteng, F., Tattikota, S. G., Cha, N., et al. (2020). Single-cell transcriptome maps of myeloid blood cell lineages in Drosophila. *Nat. Commun.* 11:4483. doi: 10.1038/s41467-020-18135-y

Coates, C. J., McCulloch, C., Betts, J., and Whalley, T. (2018). Echinochrome a release by red spherule cells is an iron-withholding strategy of sea urchin innate immunity. *J. Innate Immun.* 10, 119–130. doi: 10.1159/000484722

Cooper, M. D., and Alder, M. N. (2006). The evolution of adaptive immune systems. *Cell* 124, 815–822. doi: 10.1016/j.cell.2006.02.001

Coronado, M., Solis, C. J., Hernandez, P. P., and Feijóo, C. G. (2019). Soybean meal-induced intestinal inflammation in zebrafish Is T cell-dependent and has a Th17 cytokine profile. *Front. Immunol.* 10:610. doi: 10.3389/fimmu.2019.00610

Da Silva, C., Wagner, C., Bonnardel, J., Gorvel, J. P., and Lelouard, H. (2017). The Peyer's patch mononuclear phagocyte system at steady state and during infection. *Front. Immunol.* 8:1254. doi: 10.3389/fimmu.2017.01254

de Geus, E. D., and Vervelde, L. (2013). Regulation of macrophage and dendritic cell function by pathogens and through immunomodulation in the avian mucosa. *Dev. Comp. Immunol.* 41, 341–351. doi: 10.1016/j.dci.2013.03.008

De Schepper, S., Verheijden, S., Aguilera-Lizarraga, J., Viola, M. F., Boesmans, W., Stakenborg, N., et al. (2018). Self-maintaining gut macrophages are essential for intestinal homeostasis. *Cell* 175, 400–415.e13. doi: 10.1016/j.cell.2018.07.048

Dee, C. T., Nagaraju, R. T., Athanasiadis, E. I., Gray, C., Fernandez Del Ama, L., Johnston, S. A., et al. (2016). CD4-transgenic zebrafish reveal tissue-resident Th2- and regulatory T cell-like populations and diverse mononuclear phagocytes. *J. Immunol.* 197, 3520–3530. doi: 10.4049/jimmunol.1600959

Demir, E., and Marcos, R. (2017). Assessing the genotoxic effects of two lipid peroxidation products (4-oxo-2-nonenal and 4-hydroxy-hexenal) in haemocytes and midgut cells of *Drosophila melanogaster* larvae. *Food Chem. Toxicol.* 105, 1–7. doi: 10.1016/j.fct.2017.03.036

Desjardins, M., Houde, M., and Gagnon, E. (2005). Phagocytosis: the convoluted way from nutrition to adaptive immunity. *Immunol. Rev.* 207, 158–165. doi: 10.1111/j.0105-2896.2005.00319.x

Disson, O., Bleriot, C., Jacob, J. M., Serafini, N., Dulauroy, S., Jouvion, G., et al. (2018). Peyer's patch myeloid cells infection by Listeria signals through gp38(+) stromal cells and locks intestinal villus invasion. *J. Exp. Med.* 215, 2936–2954. doi: 10.1084/jem.20181210

Duszenko, M., Ginger, M. L., Brennand, A., Gualdrón-López, M., Colombo, M. I., Coombs, G. H., et al. (2011). Autophagy in protists. *Autophagy* 7, 127–158. doi: 10.4161/auto.7.2.13310

Dvorák, J., Roubalov,á R., Procházková, P., Rossmann, P., Škanta, F., and Bilej, M. (2016). Sensing microorganisms in the gut triggers the immune response in *Eisenia andrei* earthworms. *Dev. Comp. Immunol.* 57, 67–74. doi: 10.1016/j.dci.2015.12.001

Dzik, J. M. (2010). The ancestry and cumulative evolution of immune reactions. *Acta Biochim. Pol.* 57, 443–466. doi: 10.18388/abp.2010_2431

Earley, A. M., Graves, C. L., and Shiau, C. E. (2018). Critical role for a subset of intestinal macrophages in shaping gut microbiota in adult zebrafish. *Cell Rep.* 25, 424–436. doi: 10.1016/j.celrep.2018.09.025

Elvington, M., Liszewski, M. K., and Atkinson, J. P. (2016). Evolution of the complement system: from defense of the single cell to guardian of the intravascular space. *Immunol. Rev.* 274, 9–15. doi: 10.1111/imr.12474

Engelmann, P., Hayashi, Y., Bodó, K., Ernszt, D., Somogyi, I., Steib, A., et al. (2016). Phenotypic and functional characterization of earthworm coelomocyte subsets: Linking light scatter-based cell typing and imaging of the sorted populations. *Dev. Comp. Immunol.* 65, 41–52. doi: 10.1016/j.dci.2016.06.017

Farache, J., Koren, I., Milo, I., Gurevich, I., Kim, K. W., Zigmond, E., et al. (2013). Luminal bacteria recruit CD103+ dendritic cells into the intestinal epithelium to sample bacterial antigens for presentation. *Immunity* 38, 581–595. doi: 10.1016/j.immuni.2013.01.009

Fares, H., and Greenwald, I. (2001). Genetic analysis of endocytosis in *Caenorhabditis elegans*: coelomocyte uptake defective mutants. *Genetics* 159, 133–145.

Ferrero, G., Gomez, E., Lyer, S., Rovira, M., Miserocchi, M., Langenau, D. M., et al. (2020). The macrophage-expressed gene (mpeg) 1 identifies a subpopulation of B cells in the adult zebrafish. *J. Leukoc. Biol.* 107, 431–443. doi: 10.1002/JLB.1A1119-223R

Frey, A., Giannasca, K. T., Weltzin, R., Giannasca, P. J., Reggio, H., Lencer, W. I., et al. (1996). Role of the glycocalyx in regulating access of microparticles to apical plasma membranes of intestinal epithelial cells: implications for microbial attachment and oral vaccine targeting. *J. Exp. Med.* 184, 1045–1059. doi: 10.1084/jem.184.3.1045

Fu, Y., Huang, X., Zhang, P., van de Leemput, J., and Han, Z. (2020). Single-cell RNA sequencing identifies novel cell types in Drosophila blood. *J. Genet. Genomics* 47, 175–186. doi: 10.1016/j.jgg.2020.02.004

Gabanyi, I., Muller, P. A., Feighery, L., Oliveira, T. Y., Costa-Pinto, F. A., and Mucida, D. (2016). Neuro-immune interactions drive tissue programming in intestinal macrophages. *Cell* 164, 378–391. doi: 10.1016/j.cell.2015.12.023

Giribet, G., and Edgecombe, G. D. (2017). Current understanding of ecdysozoa and its internal phylogenetic relationships. *Integr. Comp. Biol.* 57, 455–466. doi: 10.1093/icb/icx072

Girón-Pérez, M. I. (2010). Relationships between innate immunity in bivalve molluscs and environmental pollution. *Invertebrate Survival J.* 7:149–156.

Golconda, P., Buckley, K. M., Reynolds, C. R., Romanello, J. P., and Smith, L. C. (2019). The axial organ and the pharynx are sites of hematopoiesis in the Sea Urchin. *Front. Immunol.* 10:870. doi: 10.3389/fimmu.2019.00870

Gordon, S. (2016). Phagocytosis: the legacy of metchnikoff. *Cell* 166, 1065–1068. doi: 10.1016/j.cell.2016.08.017

Gosselin, D., Link, V. M., Romanoski, C. E., Fonseca, G. J., Eichenfield, D. Z., Spann, N. J., et al. (2014). Environment drives selection and function of enhancers controlling tissue-specific macrophage identities. *Cell* 159, 1327–1340. doi: 10.1016/j.cell.2014.11.023

Gotthardt, D., Warnatz, H. J., Henschel, O., Brückert, F., Schleicher, M., and Soldati, T. (2002). High-resolution dissection of phagosome maturation reveals distinct membrane trafficking phases. *Mol. Biol. Cell* 13, 3508–3520. doi: 10.1091/mbc.e02-04-0206

Grayfer, L., and Robert, J. (2013). Colony-stimulating factor-1-responsive macrophage precursors reside in the amphibian (Xenopus laevis) bone marrow rather than the hematopoietic subcapsular liver. *J. Innate Immun.* 5, 531–542. doi: 10.1159/000346928

Grayfer, L., and Robert, J. (2016). Amphibian macrophage development and antiviral defenses. *Dev. Comp. Immunol.* 58, 60–67. doi: 10.1016/j.dci.2015.12.008

Gross-Vered, M., Trzebanski, S., Shemer, A., Bernshtein, B., Curato, C., Stelzer, G., et al. (2020). Defining murine monocyte differentiation into colonic and ileal macrophages. *Elife* 9:e49998. doi: 10.7554/eLife.49998

Guilliams, M., Ginhoux, F., Jakubzick, C., Naik, S. H., Onai, N., Schraml, B. U., et al. (2014). Dendritic cells, monocytes and macrophages: a unified nomenclature based on ontogeny. *Nat. Rev. Immunol.*14, 571–578. doi: 10.1038/nri3712

Guilliams, M., Thierry, G. R., Bonnardel, J., and Bajenoff, M. (2020). Establishment and maintenance of the macrophage niche. *Immunity* 52, 434–451. doi: 10.1016/j.immuni.2020.02.015

Hadis, U., Wahl, B., Schulz, O., Hardtke-Wolenski, M., Schippers, A., Wagner, N., et al. (2011). Intestinal tolerance requires gut homing and expansion of FoxP3+ regulatory T cells in the lamina propria. *Immunity* 34, 237–246. doi: 10.1016/j.immuni.2011.01.016

Hartenstein, V. (2006). Blood cells and blood cell development in the animal kingdom. *Annu. Rev. Cell Dev. Biol.* 22, 677–712. doi: 10.1146/annurev.cellbio.22.010605.093317

Hartenstein, V., and Martinez, P. (2019). Phagocytosis in cellular defense and nutrition: a food-centered approach to the evolution of macrophages. *Cell Tissue Res.* 377, 527–547. doi: 10.1007/s00441-019-03096-6

Hashimoto, D., Chow, A., Noizat, C., Teo, P., Beasley, M. B., Leboeuf, M., et al. (2013). Tissue-resident macrophages self-maintain locally throughout adult life with minimal contribution from circulating monocytes. *Immunity* 38, 792–804. doi: 10.1016/j.immuni.2013.04.004

Hiemstra, I. H., Beijer, M. R., Veninga, H., Vrijland, K., Borg, E. G., Olivier, B. J., et al. (2014). The identification and developmental requirements of colonic CD169^{+} macrophages. *Immunology* 142, 269–278. doi: 10.1111/imm.12251

Hine, P. M. (1999). The inter-relationships of bivalve haemocytes. *Fish Shellfish Immunol.* 9, 367–385. doi: 10.1006/fsim.1998.0205

Ho, E. C., Buckley, K. M., Schrankel, C. S., Schuh, N. W., Hibino, T., Solek, C. M., et al. (2017). Perturbation of gut bacteria induces a coordinated cellular immune response in the purple sea urchin larva. *Immunol. Cell Biol.* 95:647. doi: 10.1038/icb.2017.40

Hoeffel, G., and Ginhoux, F. (2018). Fetal monocytes and the origins of tissue-resident macrophages. *Cell. Immunol.* 330, 5–15. doi: 10.1016/j.cellimm.2018.01.001

Hoffmann, J. A., and Reichhart, J. M. (2002). Drosophila innate immunity: an evolutionary perspective. *Nat. Immunol* 3, 121–126. doi: 10.1038/ni0202-121

Homa, J., Stalmach, M., Wilczek, G., and Kolaczkowska, E. (2016). Effective activation of antioxidant system by immune-relevant factors reversely correlates with apoptosis of *Eisenia andrei* coelomocytes. *J. Comp. Physiol. B* 186, 417–430. doi: 10.1007/s00360-016-0973-5

Homa, J., Zorska, A., Wesolowski, D., and Chadzinska, M. (2013). Dermal exposure to immunostimulants induces changes in activity and proliferation of coelomocytes of *Eisenia andrei*. *J. Comp. Physiol.* 183, 313–322. doi: 10.1007/s00360-012-0710-7

Honda, M., Surewaard, B. G. J., Watanabe, M., Hedrick, C. C., Lee, W. Y., Brown, K., et al. (2020). Perivascular localization of macrophages in the intestinal mucosa is regulated by Nr4a1 and the microbiome. *Nat. Commun.* 11:1329. doi: 10.1038/s41467-020-15068-4

Hume, D. A., Perry, V. H., and Gordon, S. (1984). The mononuclear phagocyte system of the mouse defined by immunohistochemical localisation of antigen F4/80: macrophages associated with epithelia. *Anat. Rec.* 210, 503–512. doi: 10.1002/ar.1092100311

Iliev, I. D., Funari, V. A., Taylor, K. D., Nguyen, Q., Reyes, C. N., Strom, S. P., et al. (2012). Interactions between commensal fungi and the C-type lectin receptor Dectin-1 influence colitis. *Science* 336, 1314–1317. doi: 10.1126/science.1221789

Jinnohara, T., Kanaya, T., Hase, K., Sakakibara, S., Kato, T., Tachibana, N., et al. (2017). IL-22BP dictates characteristics of Peyer's patch follicle-associated epithelium for antigen uptake. *J. Exp. Med.* 214, 1607–1618. doi: 10.1084/jem.20160770

Johansson, M. E. V., Phillipson, M., Petersson, J., Velcich, A., Holm, L., and Hansson, G. C. (2008). The inner of the two Muc2 mucin-dependent mucus layers in colon is devoid of bacteria. *Proc. Natl. Acad. Sci. U.S.A.* 105:15064. doi: 10.1073/pnas.0803124105

Jung, C., Hugot, J. P., and Barreau, F. (2010). Peyer's patches: the immune sensors of the intestine. *Int. J. Inflam.* 2010:823710. doi: 10.4061/2010/823710

Kang, B., Alvarado, L. J., Kim, T., Lehmann, M. L., Cho, H., He, J., et al. (2020). Commensal microbiota drive the functional diversification of colon macrophages. *Mucosal Immunol.* 13, 216–229. doi: 10.1038/s41385-019-0228-3

Kawano, Y., Nakae, J., Watanabe, N., Kikuchi, T., Tateya, S., Tamori, Y., et al. (2016). Colonic pro-inflammatory macrophages cause insulin resistance in an intestinal Ccl2/Ccr2-dependent manner. *Cell Metab.* 24, 295–310. doi: 10.1016/j.cmet.2016.07.009

Kaya, B., Doñas, C., Wuggenig, P., Diaz, O. E., Morales, R. A., Melhem, H., et al. (2020). Lysophosphatidic acid-mediated GPR35 signaling in CX3CR1(+) macrophages regulates intestinal homeostasis. *Cell Rep.* 32:107979. doi: 10.1016/j.celrep.2020.107979

Keewan, E., Narasimhulu, C. A., Rohr, M., Hamid, S., and Parthasarathy, S. (2020). Are fried foods unhealthy? the dietary peroxidized fatty acid, 13-HPODE, induces intestinal inflammation *in vitro* and *in vivo*. *Antioxidants* 9:926. doi: 10.3390/antiox9100926

Kim, M., Galan, C., Hill, A. A., Wu, W. J., Fehlner-Peach, H., Song, H. W., et al. (2018). Critical role for the microbiota in CX(3)CR1(+) intestinal mononuclear phagocyte regulation of intestinal T Cell responses. *Immunity* 49, 151–163.e5. doi: 10.1016/j.immuni.2018.05.009

Kobayashi, N., Takahashi, D., Takano, S., Kimura, S., and Hase, K. (2019). The roles of Peyer's patches and microfold cells in the gut immune system: relevance to autoimmune diseases. *Front. Immunol.* 10:2345. doi: 10.3389/fimmu.2019.02345

Kocot, K. M., Struck, T. H., Merkel, J., Waits, D. S., Todt, C., Brannock, P. M., et al. (2017). Phylogenomics of lophotrochozoa with consideration of systematic error. *Syst. Biol.* 66, 256–282. doi: 10.1093/sysbio/syw079

Krejčová, G., Danielová, A., Nedbalová, P., Kazek, M., Strych, L., Chawla, G., et al. (2019). Drosophila macrophages switch to aerobic glycolysis to mount effective antibacterial defense. *Elife* 8:e50414. doi: 10.7554/eLife.50414

Kunimura, K., Sakata, D., Tun, X., Uruno, T., Ushijima, M., Katakai, T., et al. (2019). S100A4 protein is essential for the development of mature microfold cells in Peyer's Patches. *Cell Rep.* 29, 2823-34.e7. doi: 10.1016/j.celrep.2019.10.091

Langlet, C., and Bierne, J. (1984). Immunocompetent cells requisite for graft rejection in Lineus (Invertebrata, Nemertea). *Dev. Comp. Immunol.* 8, 547–557. doi: 10.1016/0145-305X(84)90087-9

Lavin, Y., Winter, D., Blecher-Gonen, R., David, E., Keren-Shaul, H., Merad, M., et al. (2014). Tissue-resident macrophage enhancer landscapes are shaped by the local microenvironment. *Cell* 159, 1312–1326. doi: 10.1016/j.cell.2014.11.018

Lee, J. Y., Ye, J., Gao, Z., Youn, H. S., Lee, W. H., Zhao, L., et al. (2003). Reciprocal modulation of Toll-like receptor-4 signaling pathways involving MyD88 and phosphatidylinositol 3-kinase/AKT by saturated and polyunsaturated fatty acids. *J. Biol. Chem.* 278, 37041–37051. doi: 10.1074/jbc.M305213200

Lelouard, H., Fallet, M., de Bovis, B., Meresse, S., and Gorvel, J. P. (2012). Peyer's patch dendritic cells sample antigens by extending dendrites through M cell-specific transcellular pores. *Gastroenterology* 142, 592–601 e3. doi: 10.1053/j.gastro.2011.11.039

Lelouard, H., Henri, S., De Bovis, B., Mugnier, B., Chollat-Namy, A., Malissen, B., et al. (2010). Pathogenic bacteria and dead cells are internalized by a unique subset of Peyer's patch dendritic cells that express lysozyme. *Gastroenterology* 138, 173–184 e1–3. doi: 10.1053/j.gastro.2009.09.051

Lemaitre, B., Nicolas, E., Michaut, L., Reichhart, J. M., and Hoffmann, J. A. (1996). The dorsoventral regulatory gene cassette spätzle/Toll/cactus controls the potent antifungal response in Drosophila adults. *Cell* 86, 973–983. doi: 10.1016/S0092-8674(00)80172-5

Leonardi, I., Li, X., Semon, A., Li, D., Doron, I., Putzel, G., et al. (2018). CX3CR1(+) mononuclear phagocytes control immunity to intestinal fungi. *Science* 359, 232–236. doi: 10.1126/science.aao1503

Li, L., Jin, H., Xu, J., Shi, Y., and Wen, Z. (2011). Irf8 regulates macrophage versus neutrophil fate during zebrafish primitive myelopoiesis. *Blood* 117, 1359–1369. doi: 10.1182/blood-2010-06-290700

Lickwar, C. R., Camp, J. G., Weiser, M., Cocchiaro, J. L., Kingsley, D. M., Furey, T. S., et al. (2017). Genomic dissection of conserved transcriptional regulation in intestinal epithelial cells. *PLoS Biol.* 15:e2002054. doi: 10.1371/journal.pbio.2002054

Litman, G. W., and Cooper, M. D. (2007). Why study the evolution of immunity? *Nat. Immunol.* 8, 547–548. doi: 10.1038/ni0607-547

Liu, Z., Gu, Y., Chakarov, S., Bleriot, C., Kwok, I., Chen, X., et al. (2019). Fate mapping via Ms4a3-expression history traces monocyte-derived cells. *Cell* 178, 1509–1525.e19. doi: 10.1016/j.cell.2019.08.009

Luo, J., Qian, A., Oetjen, L. K., Yu, W., Yang, P., Feng, J., et al. (2018). TRPV4 Channel signaling in macrophages promotes gastrointestinal motility via direct effects on smooth muscle cells. *Immunity* 49, 107–119.e4. doi: 10.1016/j.immuni.2018.04.021

Man, A. L., Gicheva, N., Regoli, M., Rowley, G., De Cunto, G., Wellner, N., et al. (2017). CX3CR1+ cell-mediated salmonella exclusion protects the intestinal mucosa during the initial stage of infection. *J. Immunol.* 198, 335–343. doi: 10.4049/jimmunol.1502559

Mantis, N. J., Frey, A., and Neutra, M. R. (2000). Accessibility of glycolipid and oligosaccharide epitopes on rabbit villus and follicle-associated epithelium. *Am. J. Physiol. Gastrointest. Liver Physiol.* 278, G915–G923. doi: 10.1152/ajpgi.2000.278.6.G915

Martinez, J. (2018). LAP it up, fuzz ball: a short history of LC3-associated phagocytosis. *Curr. Opin. Immunol.* 55, 54–61. doi: 10.1016/j.coi.2018.09.011

Martinez, J., Almendinger, J., Oberst, A., Ness, R., Dillon, C. P., Fitzgerald, P., et al. (2011). Microtubule-associated protein 1 light chain 3 alpha (LC3)-associated phagocytosis is required for the efficient clearance of dead cells. *Proc. Natl. Acad. Sci. U.S.A.* 108, 17396–17401. doi: 10.1073/pnas.1113421108

Martinez, J., Malireddi, R. K., Lu, Q., Cunha, L. D., Pelletier, S., Gingras, S., et al. (2015). Molecular characterization of LC3-associated phagocytosis reveals distinct roles for Rubicon, NOX2 and autophagy proteins. *Nat. Cell Biol.* 17, 893–906. doi: 10.1038/ncb3192

Martinez-Lopez, M., Iborra, S., Conde-Garrosa, R., Mastrangelo, A., Danne, C., Mann, E. R., et al. (2019). Microbiota sensing by mincle-syk axis in dendritic cells regulates interleukin-17 and−22 production and promotes intestinal barrier integrity. *Immunity* 50, 446–461 e9. doi: 10.1016/j.immuni.2018.12.020

Matheis, F., Muller, P. A., Graves, C. L., Gabanyi, I., Kerner, Z. J., Costa-Borges, D., et al. (2020). Adrenergic signaling in muscularis macrophages limits infection-induced neuronal loss. *Cell* 180, 64–78.e16. doi: 10.1016/j.cell.2019.12.002

Mattisson, A., and Fänge, R. (1973). Ultrastructure of erythrocytes and leucocytes of *Priapulus caudatus* (de Lamarck) (Priapulida). *J. Morphol.* 140, 367–379. doi: 10.1002/jmor.1051400309

Mayorova, T. D., Hammar, K., Winters, C. A., Reese, T. S., and Smith, C. L. (2019). The ventral epithelium of *Trichoplax adhaerens* deploys in distinct patterns cells that secrete digestive enzymes, mucus or diverse neuropeptides. *Biol. Open* 8:bio045674. doi: 10.1242/bio.045674

Mazzini, E., Massimiliano, L., Penna, G., and Rescigno, M. (2014). Oral tolerance can be established via gap junction transfer of fed antigens from $CX3CR1^{+}$ macrophages to $CD103^{+}$ dendritic cells. *Immunity* 40, 248–261. doi: 10.1016/j.immuni.2013.12.012

McDole, J. R., Wheeler, L. W., McDonald, K. G., Wang, B., Konjufca, V., Knoop, K. A., et al. (2012). Goblet cells deliver luminal antigen to CD103+ dendritic cells in the small intestine. *Nature* 483, 345–349. doi: 10.1038/nature10863

Menzel, L. P., Tondo, C., Stein, B., and Bigger, C. H. (2015). Histology and ultrastructure of the coenenchyme of the octocoral Swiftia exserta, a model organism for innate immunity/graft rejection. *Zoology* 118, 115–124. doi: 10.1016/j.zool.2014.09.002

Mikkelsen, H. B. (1995). Macrophages in the external muscle layers of mammalian intestines. *Histol. Histopathol* 10, 719–736.

Mills, D. B. (2020). The origin of phagocytosis in Earth history. *Interface Focus* 10:20200019. doi: 10.1098/rsfs.2020.0019

Monahan-Earley, R., Dvorak, A. M., and Aird, W. C. (2013). Evolutionary origins of the blood vascular system and endothelium. *J. Thrombosis Haemostasis* 11(Suppl 1):46–66. doi: 10.1111/jth.12253

Mondal, S., and Rai, U. (2001). *In vitro* effect of temperature on phagocytic and cytotoxic activities of splenic phagocytes of the wall lizard, *Hemidactylus flaviviridis*. *Comparative Biochem. Physiol. A* 129, 391–398. doi: 10.1016/S1095-6433(00)00356-1

Morita, M. (1995). Structure and function of the reticular cell in the planarian Dugesia dorotocephala. *Hydrobiologia* 305, 189–196. doi: 10.1007/978-94-011-0045-8_32

Morrison, S. J., and Scadden, D. T. (2014). The bone marrow niche for haematopoietic stem cells. *Nature* 505, 327–334. doi: 10.1038/nature12984

Mowat, A. M., and Agace, W. W. (2014). Regional specialization within the intestinal immune system. *Nat. Rev. Immunol.* 14, 667–685. doi: 10.1038/nri3738

Mukhopadhyay, S., Heinz, E., Porreca, I., Alasoo, K., Yeung, A., Yang, H. T., et al. (2020). Loss of IL-10 signaling in macrophages limits bacterial killing driven by prostaglandin E2. *J. Exp. Med.* 217:e20180649. doi: 10.1084/jem.20180649

Muller, P. A., Koscs,ó B., Rajani, G. M., Stevanovic, K., Berres, M. L., Hashimoto, D., et al. (2014). Crosstalk between muscularis macrophages and enteric neurons regulates gastrointestinal motility. *Cell* 158, 300–313. doi: 10.1016/j.cell.2014.04.050

Na, Y. R., Stakenborg, M., Seok, S. H., and Matteoli, G. (2019). Macrophages in intestinal inflammation and resolution: a potential therapeutic target in IBD. *Nat. Rev. Gastroenterol. Hepatol.* 16, 531–543. doi: 10.1038/s41575-019-0172-4

Neuhaus, B., and Higgins, R. P. (2002). Ultrastructure, biology, and phylogenetic relationships of kinorhyncha. *Integr. Comp. Biol.* 42, 619–632. doi: 10.1093/icb/42.3.619

Niedergang, F., and Grinstein, S. (2018). How to build a phagosome: new concepts for an old process. *Curr. Opin. Cell Biol.* 50, 57–63. doi: 10.1016/j.ceb.2018.01.009

Nielsen, C., Brunet, T., and Arendt, D. (2018). Evolution of the bilaterian mouth and anus. *Nat. Ecol. Evolution* 2, 1358–1376. doi: 10.1038/s41559-018-0641-0

Niess, J. H., Brand, S., Gu, X., Landsman, L., Jung, S., McCormick, B. A., et al. (2005). CX3CR1-mediated dendritic cell access to the intestinal lumen and bacterial clearance. *Science* 307, 254–258. doi: 10.1126/science.1102901

Nii, T., Bungo, T., Isobe, N., and Yoshimura, Y. (2020). Intestinal inflammation induced by dextran sodium sulphate causes liver inflammation and lipid metabolism disfunction in laying hens. *Poult. Sci.* 99, 1663–1677. doi: 10.1016/j.psj.2019.11.028

Niklas, K. J. (2014). The evolutionary-developmental origins of multicellularity. *Am. J. Bot.* 101, 6–25. doi: 10.3732/ajb.1300314

Ochi, T., Feng, Y., Kitamoto, S., Nagao-Kitamoto, H., Kuffa, P., Atarashi, K., et al. (2016). Diet-dependent, microbiota-independent regulation of IL-10-producing lamina propria macrophages in the small intestine. *Sci. Rep.* 6:27634. doi: 10.1038/srep27634

Ohno, H. (2016). Intestinal M cells. *J. Biochem.* 159, 151–160. doi: 10.1093/jb/mvv121

Okuda, K. S., Misa, J. P., Oehlers, S. H., Hall, C. J., Ellett, F., Alasmari, S., et al. (2015). A zebrafish model of inflammatory lymphangiogenesis. *Biol. Open* 4, 1270–1280. doi: 10.1242/bio.013540

Omenetti, S., Bussi, C., Metidji, A., Iseppon, A., Lee, S., Tolaini, M., et al. (2019). The intestine harbors functionally distinct homeostatic tissue-resident and inflammatory Th17 cells. *Immunity* 51, 77–89.e6. doi: 10.1016/j.immuni.2019.05.004

Panea, C., Farkas, A. M., Goto, Y., Abdollahi-Roodsaz, S., Lee, C., Koscso, B., et al. (2015). Intestinal monocyte-derived macrophages control commensal-specific Th17 responses. *Cell Rep.* 12, 1314–1324. doi: 10.1016/j.celrep.2015.07.040

Pappo, J., and Owen, R. L. (1988). Absence of secretory component expression by epithelial cells overlying rabbit gut-associated lymphoid tissue. *Gastroenterology* 95, 1173–1177. doi: 10.1016/0016-5085(88)90347-2

Pasmans, F., De Herdt, P., and Haesebrouck, F. (2002). Interactions of Salmonella enterica serovar Muenchen with macrophages of the turtle *Trachemys scripta* scripta. *Dev. Comp. Immunol.* 26, 295–304. doi: 10.1016/S0145-305X(01)00075-1

Pereira-Neves, A., and Benchimol, M. (2007). Phagocytosis by Trichomonas vaginalis: new insights. *Biol. Cell* 99, 87–101. doi: 10.1042/BC20060084

Peterson, K. J., and Eernisse, D. J. (2016). The phylogeny, evolutionary developmental biology, and paleobiology of the Deuterostomia: 25 years of new techniques, new discoveries, and new ideas. *Organisms Diversity Evol.* 16, 401–418. doi: 10.1007/s13127-016-0270-x

Phillips, R. J., and Powley, T. L. (2012). Macrophages associated with the intrinsic and extrinsic autonomic innervation of the rat gastrointestinal tract. *Autonomic Neurosci.* 169, 12–27. doi: 10.1016/j.autneu.2012.02.004

Prochazkova, P., Roubalova, R., Dvorak, J., Navarro Pacheco, N. I., and Bilej, M. (2020). Pattern recognition receptors in annelids. *Dev. Comp. Immunol.* 102:103493. doi: 10.1016/j.dci.2019.103493

Provost, K., Dancho, B. A., Ozbay, G., Anderson, R. S., Richards, G. P., and Kingsley, D. H. (2011). Hemocytes are sites of enteric virus persistence within oysters. *Appl. Environ. Microbiol.* 77, 8360–8369. doi: 10.1128/AEM.06887-11

Pull, S. L., Doherty, J. M., Mills, J. C., Gordon, J. I., and Stappenbeck, T. S. (2005). Activated macrophages are an adaptive element of the colonic epithelial progenitor niche necessary for regenerative responses to injury. *Proc. Natl. Acad. Sci. U.S.A.* 102, 99–104. doi: 10.1073/pnas.0405979102

Rahabi, M., Jacquemin, G., Prat, M., Meunier, E., AlaEddine, M., Bertrand, B., et al. (2020). Divergent roles for macrophage C-type lectin receptors, dectin-1 and mannose receptors, in the intestinal inflammatory response. *Cell Rep.* 30, 4386–4398.e5. doi: 10.1016/j.celrep.2020.03.018

Rajan, A., and Perrimon, N. (2012). Drosophila cytokine unpaired 2 regulates physiological homeostasis by remotely controlling insulin secretion. *Cell* 151, 123–137. doi: 10.1016/j.cell.2012.08.019

Richards, D. M., and Endres, R. G. (2017). How cells engulf: a review of theoretical approaches to phagocytosis. *Rep. Prog. Phys.* 80:126601. doi: 10.1088/1361-6633/aa8730

Richter, D. J., and Levin, T. C. (2019). The origin and evolution of cell-intrinsic antibacterial defenses in eukaryotes. *Curr. Opin. Genet. Dev.* 58-59, 111–122. doi: 10.1016/j.gde.2019.09.002

Rios, D., Wood, M. B., Li, J., Chassaing, B., Gewirtz, A. T., and Williams, I. R. (2016). Antigen sampling by intestinal M cells is the principal pathway initiating mucosal IgA production to commensal enteric bacteria. *Mucosal Immunol.* 9, 907–916. doi: 10.1038/mi.2015.121

Rodriguez-Manzanet, R., Sanjuan, M. A., Wu, H. Y., Quintana, F. J., Xiao, S., Anderson, A. C., et al. (2010). T and B cell hyperactivity and autoimmunity associated with niche-specific defects in apoptotic body clearance in TIM-4-deficient mice. *Proc. Natl. Acad. Sci. U.S.A.* 107, 8706–8711. doi: 10.1073/pnas.0910359107

Rolton, A., Delisle, L., Berry, J., Venter, L., Webb, S. C., Adams, S., et al. (2020). Flow cytometric characterization of hemocytes of the flat oyster, *Ostrea chilensis*. *Fish Shellfish Immunol.* 97, 411–420. doi: 10.1016/j.fsi.2019.12.071

Sanchez Bosch, P., Makhijani, K., Herboso, L., Gold, K. S., Baginsky, R., Woodcock, K. J., et al. (2019). Adult drosophila lack hematopoiesis but rely on a blood cell reservoir at the respiratory epithelia to relay infection signals to surrounding tissues. *Dev. Cell* 51, 787–803.e5. doi: 10.1016/j.devcel.2019.10.017

Sanjuan, M. A., Dillon, C. P., Tait, S. W., Moshiach, S., Dorsey, F., Connell, S., et al. (2007). Toll-like receptor signalling in macrophages links the autophagy pathway to phagocytosis. *Nature* 450, 1253–1257. doi: 10.1038/nature06421

Sato, K., Norris, A., Sato, M., and Grant, B. D. (2014). "*C. elegans* as a model for membrane traffic". in *WormBook*, ed. The *C. elegans* Research Community. doi: 10.1895/wormbook.1.77.2

Schokker, D., Jansman, A. J., Veninga, G., de Bruin, N., Vastenhouw, S. A., de Bree, F. M., et al. (2017). Perturbation of microbiota in one-day old broiler chickens with antibiotic for 24 hours negatively affects intestinal immune development. *BMC Genomics* 18:241. doi: 10.1186/s12864-017-3625-6

Schridde, A., Bain, C. C., Mayer, J. U., Montgomery, J., Pollet, E., Denecke, B., et al. (2017). Tissue-specific differentiation of colonic macrophages requires TGFbeta receptor-mediated signaling. *Mucosal Immunol.* 10, 1387–1399. doi: 10.1038/mi.2016.142

Schulthess, J., Pandey, S., Capitani, M., Rue-Albrecht, K. C., Arnold, I., Franchini, F., et al. (2019). The short chain fatty acid butyrate imprints an antimicrobial program in macrophages. *Immunity* 50, 432–445.e7. doi: 10.1016/j.immuni.2018.12.018

Schulz, O., Jaensson, E., Persson, E. K., Liu, X., Worbs, T., Agace, W. W., et al. (2009). Intestinal CD103+, but not CX3CR1+, antigen sampling cells migrate in lymph and serve classical dendritic cell functions. *J. Exp. Med.* 206, 3101–3114. doi: 10.1084/jem.20091925

Scott, N. A., Andrusaite, A., Andersen, P., Lawson, M., Alcon-Giner, C., Leclaire, C., et al. (2018). Antibiotics induce sustained dysregulation of intestinal T cell immunity by perturbing macrophage homeostasis. *Sci. Transl. Med.* 10:eaao4755. doi: 10.1126/scitranslmed.aao4755

Sehgal, A., Donaldson, D. S., Pridans, C., Sauter, K. A., Hume, D. A., and Mabbott, N. A. (2018). The role of CSF1R-dependent macrophages in control of the intestinal stem-cell niche. *Nat. Commun.* 9:1272. doi: 10.1038/s41467-018-03638-6

Shaw, T. N., Houston, S. A., Wemyss, K., Bridgeman, H. M., Barbera, T. A., Zangerle-Murray, T., et al. (2018). Tissue-resident macrophages in the intestine are long lived and defined by Tim-4 and CD4 expression. *J. Exp. Med.* 215, 1507–1518. doi: 10.1084/jem.20180019

Shiau, C. E., Kaufman, Z., Meireles, A. M., and Talbot, W. S. (2015). Differential requirement for irf8 in formation of embryonic and adult macrophages in zebrafish. *PLoS ONE* 10:e0117513. doi: 10.1371/journal.pone.0117513

Shouval, D. S., Biswas, A., Goettel, J. A., McCann, K., Conaway, E., Redhu, N. S., et al. (2014). Interleukin-10 receptor signaling in innate immune cells regulates mucosal immune tolerance and anti-inflammatory macrophage function. *Immunity* 40, 706–719. doi: 10.1016/j.immuni.2014.03.011

Shouval, D. S., Biswas, A., Kang, Y. H., Griffith, A. E., Konnikova, L., Mascanfroni, I. D., et al. (2016). Interleukin 1β mediates intestinal inflammation in mice and patients with interleukin 10 receptor deficiency. *Gastroenterology* 151, 1100–1104. doi: 10.1053/j.gastro.2016.08.055

Smith, L. C., Arizza, V., Barela Hudgell, M. A., Barone, G., Bodnar, A. G., Buckley, K. M., et al. (2018). "Echinodermata: the complex immune system in echinoderms," In *Advances in Comparative Immunology* ed. E. L. Cooper. (Cham: Springer International Publishing). p. 409–501. doi: 10.1007/978-3-319-76768-0_13

Solas, M. T., and Zapata, A. (1980). Gut-associated lymphoid tissue (GALT) in reptiles: intraepithelial cells. *Dev. Comp. Immunol.* 4, 87–97. doi: 10.1016/S0145-305X(80)80011-5

Solomon, J. B., Developmental ISo., and Immunology C. (1981). *Aspects of Developmental and Comparative Immunology: Proceedings of the 1st Congress of Developmental and Comparative Immunology, 27 July-1 August 1980*, Aberdeen: Pergamon Press.

Stachura, D. L., and Traver, D. (2011). "Chapter 4 - cellular dissection of zebrafish hematopoiesis," in *Methods in Cell Biology*. eds H. W. Detrich, M. Westerfield, L. I. Zon. (Academic Press). 101, *p*. 75–110. doi: 10.1016/B978-0-12-387036-0.00004-9

Tacchi, L., Larragoite, E. T., Muñoz, P., Amemiya, C. T., and Salinas, I. (2015). African lungfish reveal the evolutionary origins of organized mucosal lymphoid tissue in vertebrates. *Curr. Biol.* 25, 2417–2424. doi: 10.1016/j.cub.2015.07.066

Taha-Abdelaziz, K., Astill, J., Shojadoost, B., Borrelli, S., M. A. M., and Sharif, S. (2020). Campylobacter-derived ligands induce cytokine and chemokine expression in chicken macrophages and cecal tonsil mononuclear cells. *Vet. Microbiol.* 246:108732. doi: 10.1016/j.vetmic.2020.108732

Tamoutounour, S., Henri, S., Lelouard, H., de Bovis, B., de Haar, C., van der Woude, C. J., et al. (2012). CD64 distinguishes macrophages from dendritic cells in the gut and reveals the Th1-inducing role of mesenteric lymph node macrophages during colitis. *Eur. J. Immunol.* 42, 3150–3166. doi: 10.1002/eji.201242847

Tang, B., Williams, P. L., Xue, K. S., Wang, J. S., and Tang, L. (2020). Detoxification mechanisms of nickel sulfate in nematode *Caenorhabditis elegans*. *Chemosphere* 260:127627. doi: 10.1016/j.chemosphere.2020.127627

Tattikota, S. G., Cho, B., Liu, Y., Hu, Y., Barrera, V., Steinbaugh, M. J., et al. (2020). A single-cell survey of Drosophila blood. *Elife* 9:e54818. doi: 10.7554/eLife.54818.sa2

Telford, M. J., Budd, G. E., and Philippe, H. (2015). Phylogenomic insights into animal evolution. *Curr. Biol.* 25, R876–R887. doi: 10.1016/j.cub.2015.07.060

Traylor-Knowles, N., Vandepas, L. E., and Browne, W. E. (2019). Still enigmatic: innate immunity in the ctenophore *Mnemiopsis leidyi*. *Integr. Comp. Biol.* 59, 811–818. doi: 10.1093/icb/icz116

van de Laar, L., Saelens, W., De Prijck, S., Martens, L., Scott, C. L., Van Isterdael, G., et al. (2016). Yolk sac macrophages, fetal liver, and adult monocytes can colonize an empty niche and develop into functional tissue-resident macrophages. *Immunity* 44, 755–768. doi: 10.1016/j.immuni.2016.02.017

Wagner, C., Bonnardel, J., Da Silva, C., Martens, L., Gorvel, J. P., and Lelouard, H. (2018). Some news from the unknown soldier, the Peyer's patch macrophage. *Cell. Immunol.* 330, 159–167. doi: 10.1016/j.cellimm.2018.01.012

Wagner, C., Bonnardel, J., Da Silva, C., Spinelli, L., Portilla, C. A., Tomas, J., et al. (2020). Differentiation paths of Peyer's patch LysoDCs are linked to sampling site positioning, migration, and T cell priming. *Cell Rep* 31:107479. doi: 10.1016/j.celrep.2020.03.043

Walters, B. M., Connelly, M. T., Young, B., and Traylor-Knowles, N. (2020). The complicated evolutionary diversification of the Mpeg-1/Perforin-2 family in cnidarians. *Front. Immunol.* 11:1690. doi: 10.3389/fimmu.2020.01690

Wang, Z., Du, J., Lam, S. H., Mathavan, S., Matsudaira, P., and Gong, Z. (2010). Morphological and molecular evidence for functional organization along the rostrocaudal axis of the adult zebrafish intestine. *BMC Genomics* 11:392. doi: 10.1186/1471-2164-11-392

Wigley, P. (2014). *Salmonella enterica* in the chicken: how it has helped our understanding of immunology in a non-biomedical model species. *Front. Immunol.* 5:482. doi: 10.3389/fimmu.2014.00482

Willensdorfer, M. (2008). Organism size promotes the evolution of specialized cells in multicellular digital organisms. *J. Evol. Biol.* 21, 104–110. doi: 10.1111/j.1420-9101.2007.01466.x

Willis, A. R., Sukhdeo, R., and Reinke, A. W. (2020). Remembering your enemies: mechanisms of within-generation and multigenerational immune priming in *Caenorhabditis elegans*. *FEBS J.* doi: 10.1111/febs.15509

Wittamer, V., Bertrand, J. Y., Gutschow, P. W., and Traver, D. (2011). Characterization of the mononuclear phagocyte system in zebrafish. *Blood* 117, 7126–7135. doi: 10.1182/blood-2010-11-321448

Wood, W., and Martin, P. (2017). Macrophage functions in tissue patterning and disease: new insights from the fly. *Dev. Cell* 40, 221–233. doi: 10.1016/j.devcel.2017.01.001

Woodcock, K. J., Kierdorf, K., Pouchelon, C. A., Vivancos, V., Dionne, M. S., and Geissmann, F. (2015). Macrophage-derived upd3 cytokine causes impaired glucose homeostasis and reduced lifespan in Drosophila fed a lipid-rich diet. *Immunity* 42, 133–144. doi: 10.1016/j.immuni.2014.12.023

Wu, S. C., Liao, C. W., Pan, R. L., and Juang, J. L. (2012). Infection-induced intestinal oxidative stress triggers organ-to-organ immunological communication in Drosophila. *Cell Host Microbe* 11, 410–417. doi: 10.1016/j.chom.2012.03.004

Yaparla, A., Koubourli, D. V., Popovic, M., and Grayfer, L. (2020). Exploring the relationships between amphibian (*Xenopus laevis*) myeloid cell subsets. *Dev. Comp. Immunol.* 113:103798. doi: 10.1016/j.dci.2020.103798

Yaparla, A., Reeves, P., and Grayfer, L. (2019). Myelopoiesis of the Amphibian *Xenopus laevis* is segregated to the bone marrow, away from their hematopoietic peripheral liver. *Front. Immunol.* 10:3015. doi: 10.3389/fimmu.2019.03015

Yaparla, A., Wendel, E. S., and Grayfer, L. (2016). The unique myelopoiesis strategy of the amphibian *Xenopus laevis*. *Dev. Comp. Immunol.* 63, 136–143. doi: 10.1016/j.dci.2016.05.014

Yona, S., Kim, K. W., Wolf, Y., Mildner, A., Varol, D., Breker, M., et al. (2013). Fate mapping reveals origins and dynamics of monocytes and tissue macrophages under homeostasis. *Immunity* 38, 79–91. doi: 10.1016/j.immuni.2012.12.001

Yutin, N., Wolf, M. Y., Wolf, Y. I., and Koonin, E. V. (2009). The origins of phagocytosis and eukaryogenesis. *Biol. Direct* 4:9. doi: 10.1186/1745-6150-4-9

Zaidman-Rémy, A., Regan, J. C., Brandão, A. S., and Jacinto, A. (2012). The Drosophila larva as a tool to study gut-associated macrophages: PI3K regulates a discrete hemocyte population at the proventriculus. *Dev. Comp. Immunol.* 36, 638–647. doi: 10.1016/j.dci.2011.10.013

Zapata, A., and Solas, M. T. (1979). Gut-associated lymphoid tissue (GALT) in reptilla: structure of mucosal accumulations. *Dev. Comp. Immunol.* 3, 477–487. doi: 10.1016/S0145-305X(79)80043-9

Zigmond, E., Bernshtein, B., Friedlander, G., Walker, C. R., Yona, S., Kim, K. W., et al. (2014). Macrophage-restricted interleukin-10 receptor deficiency, but not IL-10 deficiency, causes severe spontaneous colitis. *Immunity* 40, 720–733. doi: 10.1016/j.immuni.2014.03.012

Conflict of Interest: The authors declare that the research was conducted in the absence of any commercial or financial relationships that could be construed as a potential conflict of interest.

Annex 2: Supplementary data, development of a strategy to analyze the gut microbiota composition

Table S1: Staining Index (SI) and Signal/Noise (S/N) ratio of the hybridization couple Eub338-*E. faecalis*, in all fluorochrome candidates for the Cytoflex.

	SI		**S/N**	
	X	Me	X	Me
A430	0,26	0,22	2,09	2,35
Pacific Blue	0,14	0,11	1,79	2,32
CF405s	0,99	0,87	8,21	15,04
HL405	0,62	0,53	4,37	6,15
e393	0,24	0,22	2,60	3,60
A488	4,47	3,72	9,84	10,00
Cy3	6,75	5,46	17,36	17,77
A647	20,87	17,26	6,45	7,48
A700	7,86	6,40	23,98	28,11
A750	1,10	0,87	6,77	7,70

Table S2: Staining Index (SI) and Signal/Noise (S/N) ratio of all the panel probes incubated at 42°C and 55°C individually using their phylum representatives.

	SI		**S/N**	
	X	Me	X	Me
Proteobacteria 42°C*	1,00	0,46	6,15	6,77
Proteobacteria 55°C	0,63	0,33	4,47	5,22
Eubacteria 42°C*	0,64	0,41	4,66	5,28
Eubacteria 55°C	0,20	0,10	2,49	3,46
Firmicutes 42°C*	0,53	0,32	4,56	4,92
Firmicutes 55°C	0,28	0,06	3,01	1,99
Bacteroidetes 42°C	1,07	0,39	5,73	6,56
Bacteroidetes 55°C*	1,36	0,55	5,90	5,95
Actinobacteria 42°C*	1,03	0,62	7,16	27,53
Actinobacteria 55°C	0,47	0,17	4,34	11,44
Verrucomicrobia 42°C*	3,42	1,60	20,76	22,14
Verrucomicrobia 55°C	0,76	0,35	7,49	20,51

*better resolving capacity

Table S3: a) Staining Index (SI) and Signal/Noise (S/N) ratio of the Eub338 conjugated with all the fluorochromes. b) Staining Index (SI) and Signal/Noise (S/N) ratio of all the panel probes conjugated with A647. Both set of probes were incubated at 42°C. Scale color indicates the resolving capacity.

a)

	SI		S/N	
	X	Me	X	Me
A750	0,61	0,45	2,93	3,05
A700	1,47	0,83	5,92	5,38
A647	1,65	1,36	3,75	3,86
Cy3	6,44	5,05	17,09	17,45
A488	4,91	3,97	10,13	10,25
CF405s	4,68	3,45	13,18	13,60

b)

	SI		S/N	
	X	Me	X	Me
Proteobacteria	1,00	0,46	6,15	6,77
Eubacteria	0,64	0,41	4,66	5,28
Firmicutes	0,53	0,32	4,56	4,92
Bacteroidetes	1,07	0,39	5,73	6,56
Actinobacteria	1,03	0,62	7,16	27,53
Verrucomicrobia	3,42	1,60	20,76	22,14

Table S4: Staining Index (SI) and Signal/Noise (S/N) ratio of all the probes at different concentrations using their phylum representatives. Scale color indicates the resolving capacity.

Eub338		SI		S/N	
A750	µmol/L	X	Me	X	Me
	0.01	2.65	2.16	4.81	4.72
	0.05	5.66	4.47	9.37	9.01
	0.1	5.55	4.38	9.01	8.56
	0.375	2.58	2.24	4.94	5.30
	0.5	2.08	1.70	4.03	4.02
	1	2.28	1.98	4.65	5.06
	1.5	1.83	1.54	3.68	3.74
	3	0.94	0.84	2.48	2.69

Bact		SI		S/N	
A700	µmol/L	X	Me	X	Me
	0.01	43.3	15.3	65.8	29.5
	0.05	26.2	9.16	51.1	25.1
	0.1	29.7	14.9	55.1	37.7
	0.375	25.6	12.6	42.3	27.4
	0.5	24.7	12.4	46.2	33
	1	18.1	10.4	36.4	31.7
	1.5	17	9.85	33.3	28.3
	3	14.2	8.25	29.5	25.8

MUC1437		SI		S/N	
A647	µmol/L	X	Me	X	Me
	0.01	7.8	4.3	26	24.2
	0.05	8.98	4.63	27.5	22.9
	0.1	10.8	5.4	28.5	20.7
	0.375	6.25	3.16	18.2	14.2
	0.5	12.7	8.46	19	15.8
	1	7.92	4.97	12.1	9.39
	1.5	6.61	4.28	10.7	8.9
	3	7.19	4.48	11.3	8.83

HCG664		SI		S/N	
A488	µmol/L	X	Me	X	Me
	0.01	22.58	13.24	87.83	115.1
	0.05	20.65	11.04	87.86	90.68
	0.1	23.66	13.41	99.79	114.6
	0.375	22.02	14.00	97.84	206.8
	0.5	27.44	18.09	66.49	70.00
	1	26.43	17.88	63.49	70.25
	1.5	27.24	19.66	66.23	74.42
	3	30.35	22.04	79.07	86.99

LGC354		SI		S/N	
CF405s	µmol/L	X	Me	X	Me
	0.01	8.79	7.07	12.4	11.7
	0.05	9.39	7.16	14	12.9
	0.1	11.7	9.07	19.1	19
	0.375	13.9	10.9	21.9	21.5
	0.5	9.57	6.88	14.9	13.3
	1	14.3	11.2	22.7	22.1
	1.5	11.6	9.27	17.5	16.9
	3	11.9	9.13	17.4	16.1

Erec482		SI		S/N	
CF405s	µmol/L	X	Me	X	Me
	0.01	7.09	6.28	8.89	8.81
	0.05	6.30	5.49	8.19	8.08
	0.1	6.65	5.98	8.88	9.10
	0.375	9.04	7.88	11.23	11.02
	0.5	13.15	11.77	12.60	12.21
	1	14.23	12.81	14.05	13.71
	1.5	14.46	12.98	14.02	13.64
	3	14.43	13.16	13.74	13.57

Proteoβγε		SI		S/N	
Cy3	µmol/L	X	Me	X	Me
	0.1	1.99	1.38	4.52	4.42
	0.375	5.77	4.07	11.3	11.6
	0.5	5.94	3.89	11.1	10.1
	1	9.46	6.88	16.2	15.5
	1.5	9.47	6.86	18	18.5
	3	8.4	5.98	15.7	15.9

Table S5: Percentage of compensation between all the phyla-probes.

	A488	Cy3	A647	A700	A750	CF405s
A488		3%		1.5%	2%	
Cy3	13%			2%		
A647				2%		
A700			35%			
A750			15%	42%		
CF405s		2%		7%		

Table S6: Staining Index (SI) and Signal/Noise (S/N) ratio of the panel incubated at 42° for 30 minutes and 3 hours.

		SI		**S/N**	
		X	Me	X	Me
Proteobacteria	30m	0,89	0,65	5,32	7,42
	3h*	2,21	1,60	9,52	12,93
Verrucomicrobia	30m*	10,31	6,69	19,03	15,96
	3h	9,36	5,99	18,33	15,48
Bacteroidetes	30m	15,75	9,04	29,38	21,69
	3h	16,54	8,98	30,17	21,05
Firmicutes	30m	3,96	3,06	12,04	15,94
	3h*	6,67	5,01	18,36	21,49
Actinobacteria	30m	5,66	2,57	25,44	33,54
	3h*	16,41	7,83	92,46	133,3
Eubacteria	30m	2,85	0,96	8,30	4,40
	3h	2,76	1,45	10,26	8,89

*better resolving capacity

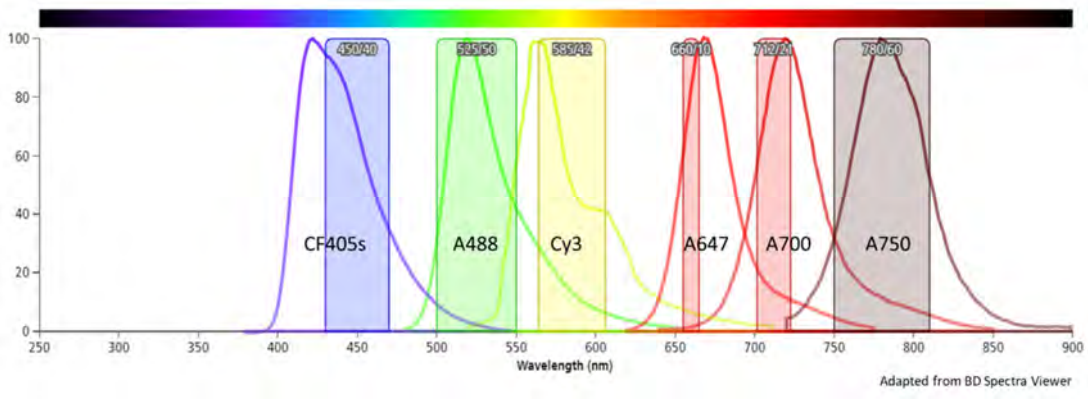

Figure S1: Band Pass filters available in the Cytoflex used and emission spectra of the fluorochromes selected for the panel.

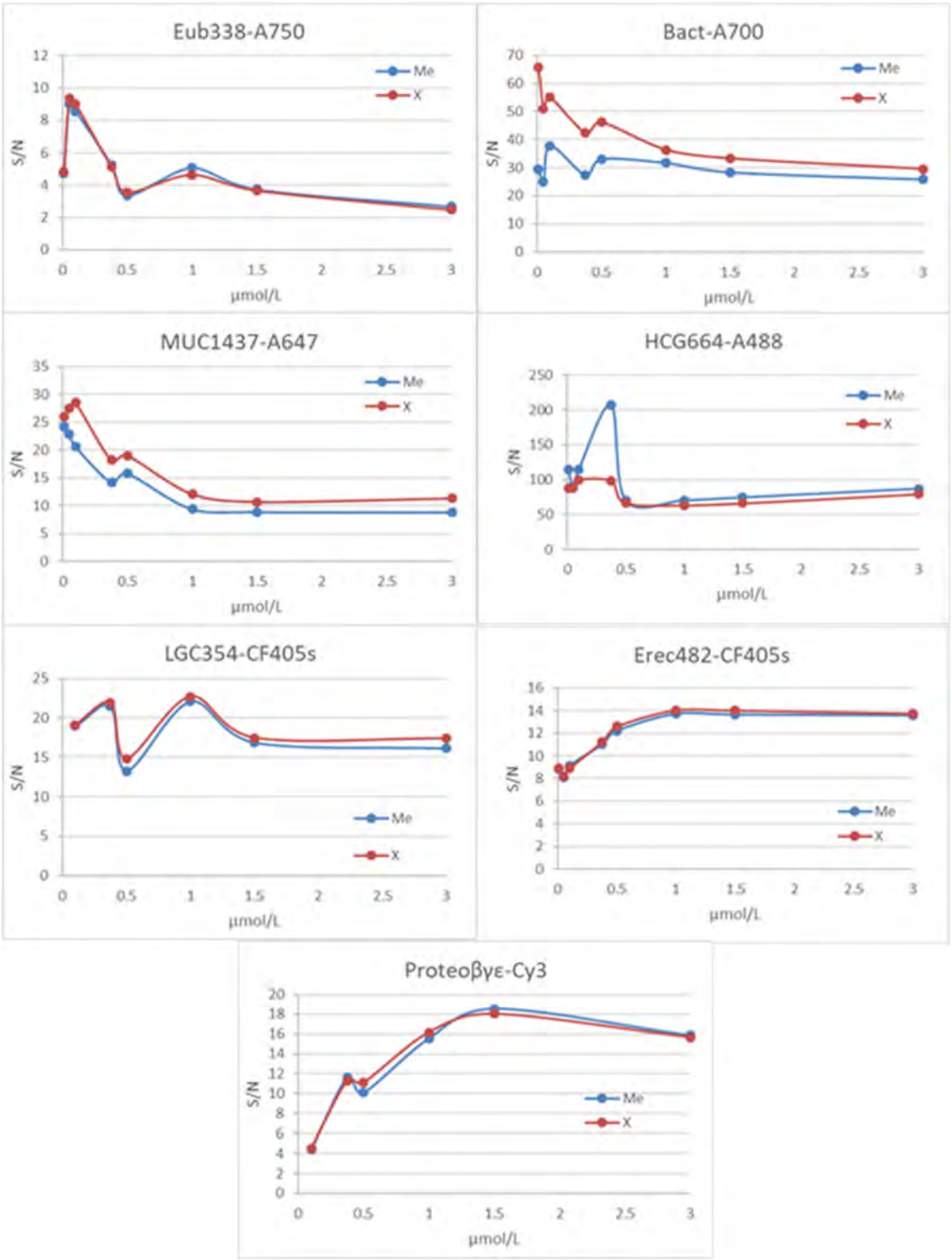

Figure S2: Graphic representation of the S/N ratio *versus* the probe concentration for each phylum-probe included in the panel.

Abstract

Among secondary lymphoid organs, Peyer's patches (PP) have the unique property to combine both antigen sampling and adaptive immune initiation sites. PP phagocytes comprise conventional dendritic cells (cDC) and lysozyme expressing monocyte-derived cells. The latter include dendritic cells (DC) called LysoDC and macrophages termed LysoMac. We deciphered the transcriptional and spatiotemporal landscape of all PP phagocyte populations from their arrival in the tissue to their final maturation state at homeostasis and then compared it with two types of *in vivo* activation, involving the endosomal Toll-like receptors (TLR) 7 and 9. Use of specific agonists helped us to better understand the role of the different phagocytes in the initiation of the immune response. Furthermore, given that PP interfollicular region hosts both villus and subepithelial dome emigrated cDC, we studied their activation profile and showed that the initial residence site shapes their activation profile. These activation profiles were associated with a B and regulatory T cell response upon TLR7 stimulation whereas a strong CD8+ T cell response was elicited upon TLR9 stimulation. Altogether, our study underscores the importance of targeting not only the right phagocyte subset but also the right place at the right time with the right stimulus.

The microbiota is crucial for the development and homeostasis of the mucosal immune system. Furthermore, variations in the composition of the gut microbiota between and within individuals over time are associated with a range of health conditions. We designed a FISH-Flow multiparametric panel including nine specific probes that target the main phyla of the gut: Firmicutes, Bacteroidetes, Proteobacteria, Actinobacteria, and Verrucomicrobia. Once all the different conditions were standardized, we tested our panel in mouse fecal samples including vancomycin-treated animals. As expected, a majority of the fecal bacteria of non-treated mice belonged to Firmicutes and Bacteroidetes, whereas a decrease of both phyla and an important increase of Verrucomicrobia was observed after the antibiotic treatment. This method allowed us to know the fecal composition in a fast, semi-quantitative and cost-effective way. Therefore, it can be very useful to detect a microbiota dysregulation and potentially predict the development of non-communicable diseases.

Résumé

Parmi les organes lymphoïdes secondaires, les plaques de Peyer (PP) ont la propriété unique de combiner à la fois l'échantillonnage d'antigènes et l'initiation de l'immunité adaptative. Les phagocytes des PP comprennent des cellules dendritiques conventionnelles (cDC) et des cellules dérivées de monocytes exprimant le lysozyme. Ces dernières comprennent des cellules dendritiques (CD) appelées LysoDC et des macrophages appelés LysoMac. Nous avons analysé les paysages transcriptionnel et spatio-temporel de toutes les populations de phagocytes des PP depuis leur arrivée dans le tissu jusqu'à leur état final de maturation à l'homéostasie, puis nous l'avons comparé à deux types d'activation in vivo, impliquant les récepteurs endosomiaux Toll-like (TLR) 7 et 9. L'utilisation d'agonistes spécifiques nous a permis de mieux comprendre le rôle des différents phagocytes dans l'initiation de la réponse immunitaire. De plus, étant donné que la région interfolliculaire des PP accueille à la fois des cDC émigrées des villosités et des dômes sous-épithéliaux, nous avons étudié leur profil d'activation et montré que le site de résidence initial façonne leur profil d'activation. Ces profils d'activation ont été associés à une réponse des lymphocytes B et T régulateurs lors de la stimulation par TLR7, tandis qu'une forte réponse des lymphocytes T CD8+ est déclenchée lors de la stimulation par TLR9. Dans l'ensemble, notre étude souligne l'importance de cibler non seulement la population de phagocytes adéquate mais aussi le bon endroit au bon moment avec le bon stimulus.

Le microbiote est crucial pour le développement et l'homéostasie du système immunitaire des muqueuses. En outre, les variations de la composition du microbiote intestinal entre les individus et au sein d'un même individu au fil du temps peuvent fréquemment être associées à des problèmes de santé. Nous avons conçu un panel de neuf sondes FISH pour la cytométrie qui ciblent spécifiquement les principaux phyla de l'intestin : Firmicutes, Bacteroidetes, Proteobacteria, Actinobacteria, et Verrucomicrobia. Une fois les différentes conditions standardisées, nous avons testé notre panel sur des échantillons fécaux de souris, dont certaines avaient été traitées avec l'antibiotique vancomycine. Comme prévu, la majorité des bactéries fécales des souris non traitées appartiennent aux Firmicutes et aux Bacteroidetes, alors qu'une diminution de ces deux phyla et une augmentation importante des Verrucomicrobia sont observées après le traitement antibiotique. Cette méthode nous a permis de connaître la composition fécale d'une manière rapide, semi-quantitative et économique. Elle peut donc être très utile pour détecter un dérèglement du microbiote et potentiellement prédire le développement de maladies non transmissibles.